TERTIARY CONTROL OF HYBRID TUGBOATS

FUEL SAVINGS ASSESSMENT WITH EQUIVALENT CONSUMPTION MINIMIZATION STRATEGY

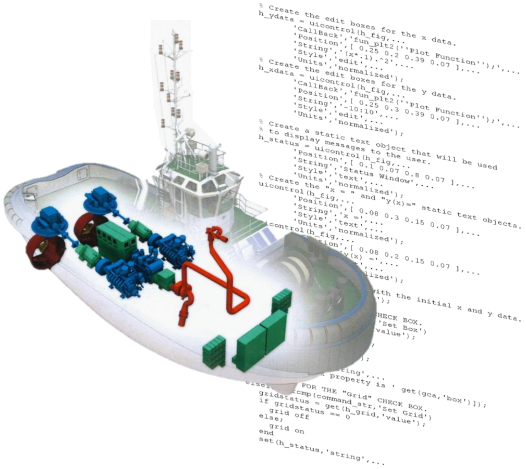

by

Miltiadis KALIKATZARAKIS

Faculty of Mechanical, Maritime & Materials Engineering,
Delft University of Technology, Delft, the Netherlands

TU Delft Delft University of Technology

DAMEN

TERTIARY CONTROL OF HYBRID TUGBOATS

FUEL SAVINGS ASSESSMENT WITH EQUIVALENT CONSUMPTION MINIMIZATION STRATEGY

Thesis

to obtain the degree of Master of Science
at the Delft University of Technology.

by

Miltiadis KALIKATZARAKIS

Faculty of Mechanical, Maritime & Materials Engineering,
Delft University of Technology, Delft, the Netherlands

Student number:	4502973	
Thesis Number:	SDPO.17.019.m	
Project duration:	August 1, 2016 – June 1, 2017	
Thesis committee:	Prof. Dr. Ir. K. Visser,	TU Delft
	Ir. R.D. R. Geertsma	TU Delft, supervisor
	Ir. H.J. Boonen,	Damen Shipyards Group

An electronic version of this thesis is available at http://repository.tudelft.nl/.

Science is a wonderful thing
if one does not have to earn one's living at it.

Albert Einstein

CONTENTS

List of Figures vii

List of Tables xi

Nomenclature xii

Summary xix

1 Introduction 1
- 1.1 The need for energy efficiency in shipping . . . 1
- 1.2 Hybrid Technology . . . 3
- 1.3 Harbor Tugboats . . . 4
- 1.4 Energy Management of Hybrid Powertrains . . . 5
- 1.5 Research Objectives . . . 7
- 1.6 Thesis Outline . . . 8

2 Hybrid Powertrains: Overview 9
- 2.1 Hybrid powertrain Concept . . . 9
- 2.2 Hybrid powertrain Architectures . . . 10
- 2.3 modeling of Hybrid-Electric powertrains . . . 13
- 2.4 Component Modeling . . . 14
- 2.5 Conclusions . . . 22

3 Energy Management Strategies: An Overview 25
- 3.1 Overview . . . 25
- 3.2 Rule-Based Control Strategies . . . 26
- 3.3 Optimization-Based Control Strategies . . . 28
- 3.4 Conclusions . . . 33

4 Tugboat Simulation Model 37
- 4.1 Modeling Approach Overview . . . 37
- 4.2 Diesel Engine . . . 44
- 4.3 Induction Machine . . . 53
- 4.4 Electric Drive . . . 58
- 4.5 Gearbox . . . 63
- 4.6 Propeller . . . 66
- 4.7 Shaft Rotational Dynamics . . . 66
- 4.8 Diesel Generator . . . 67
- 4.9 Battery . . . 70
- 4.10 Power Electronics . . . 72
- 4.11 Switchboard . . . 73
- 4.12 Complete Ship Model Verification . . . 74

5 The Energy Management Problem **81**
5.1 Introduction & General Considerations . . . 81
5.2 Problem Formulation . . . 82
5.3 ECMS-Based Supervisory Control . . . 83
5.4 Constraints . . . 86
5.5 Problem Formulation Summary . . . 87
5.6 Propulsion System Steady-State Model . . . 87
5.7 Analytical Formulation of the optimization Problem . . . 93
5.8 Input & Parameter Determination . . . 96
5.9 Problem Type Identification . . . 103
5.10 Resulting Controller Layout . . . 106

6 Controller Evaluation **109**
6.1 Introduction . . . 109
6.2 Mode selection . . . 110
6.3 Standard Operational Profiles . . . 111
6.4 Sensitivity analysis . . . 120
6.5 Conclusions . . . 127

7 Conclusions & Recommendations **129**
7.1 Conclusions . . . 129
7.2 Recommendations for further work . . . 131

A Dynamic Programming **135**
A.1 Introduction . . . 135
A.2 Application to the Energy Management Problem . . . 136

B Convexity of the Energy Management Problem **139**
B.1 Importance of Convexity . . . 139
B.2 Definitions & Theorems . . . 139
B.3 Convexity of the Problem . . . 140

C Pontryagin's Minimum Principle **147**

D Controller Evaluation: Results **151**
D.1 Quasi-static Maneuvering . . . 151
D.2 Standard Operational Profiles . . . 153
D.3 Sensitivity Analysis . . . 160

References **163**

List of Figures

1.1 Caption for LOF . . . 2
1.2 Typical Operating Profile of a Harbor Tugboat *(Operating Modes by color: Standby, Transit, Assist)*. . . . 5
1.3 Control Layers of a Hybridized Vessel. . . . 6

2.1 Conventional Propulsion System. . . . 10
2.2 Conceptual Hybrid powertrain. . . . 10
2.3 Diesel Electric Propulsion with Hybrid Power Supply . . . 11
2.4 Hybrid Propulsion with Hybrid Power Supply . . . 12
2.5 Time vs. Detail of ICE Models. . . . 14
2.6 Structure of a simple feed-forward ANN. . . . 15
2.7 MVFP Model developed at TU Delft [Stapersma, 2010]. . . . 16
2.8 In-cylinder process concept of an MVFP [Stapersma, 2010]. . . . 16
2.9 Kinetic Battery Model. . . . 18
2.10 Circuit - Oriented Battery Models. . . . 19
2.11 General Ship Propulsion Model. . . . 23

3.1 Overview of Energy Management Strategies . . . 27
3.2 Classification of Energy Management Strategies [Silvas et al., 2016]. . . . 35

4.1 Development cycle of a simulation model [Schlesinger et al., 1979]. . . . 37
4.2 Propulsion System Layout. . . . 39
4.3 Causality Graph: Complete Vessel Model. . . . 40
4.4 Causality Graph: Propulsion System. . . . 41
4.5 Causality Graph: Electrical System. . . . 41
4.6 Validation Quality [Oberkampf et al., 2004]. . . . 43
4.7 Diesel Engine Fuel Consumption. . . . 45
4.8 Caption for LOF . . . 46
4.9 5-point Seiliger Cycle. . . . 46
4.10 Temperature profile from gas via cylinder wall to coolant medium. . . . 48
4.11 Predicted average heat-transfer rate to combustion chamber walls as a function of equivalence ratio (ϕ) and burn rate ($\delta\theta_b$) [Heywood et al., 1988]. . . 50
4.12 Diesel Engine Fuel Consumption - Improved Model. . . . 51
4.13 Diesel Engine Fuel Consumption - Improved Model. . . . 51
4.14 Diesel Engine Fuel Consumption - Improved Model. . . . 52
4.15 Induction Machine per-phase Equivalent Circuit [Ong, 1998]. . . . 53
4.16 Induction Machine dq Equivalent Circuit on the Arbitrary Reference Frame. 54
4.17 No-load and Locked-rotor Tests Equivalent Circuits. . . . 57

4.18 Induction Machine - Electromagnetic Torque and Stator Current. 57
4.19 Block Diagram of a Variable Frequency Drive. 58
4.20 Overview of VFD Control Strategies. 58
4.21 Block Diagram of Indirect FOC Scheme. 60
4.22 Field Weakening. 62
4.23 Induction Machine Efficiency. 62
4.24 Controlled Induction Machine Response. 63
4.25 Gearbox Loss Models - Best Estimations. 65
4.26 Gearbox Model Calibration Results. 65
4.27 Four Quadrants Diagram. 66
4.28 Schematic of the Diesel-generator set. 67
4.29 Synchronous Generator per-phase Equivalent Circuit [Sen, 2007]. 68
4.30 Calibration Results: Diesel-Generator Fuel Consumption at Nominal Speed. 69
4.31 Calibration Results: Synchronous Generator Efficiency. 70
4.32 Equivalent Circuit Model. 70
4.33 Battery Model - Calibration Results. 72
4.34 Simulation Results - Propulsion Chain, Diesel Electric Mode. 74
4.35 Propulsion Chain: Diesel Electric Mode. 75
4.36 Propulsion Chain: Diesel Direct Mode. 76
4.37 Simulation Results - Propulsion Chain, Diesel Direct Mode. 77
4.38 Total Ship Model Validation: Diesel Electric Mode. 77
4.39 Total Ship Model Validation: Diesel Direct Mode. 78
4.40 Dynamic Verification: Vessel Response. 79
4.41 Dynamic Verification: Power Output and Fuel Consumption. 80

5.1 Schematic Overview of the propulsion system. 83
5.2 Main Diesel Engine Fuel Consumption Map. 88
5.3 Main Diesel Engine Fuel Consumption Map - Fitting Errors. 88
5.4 Induction Machine & Drive Efficiency Map. 89
5.5 Induction Machine & Drive Power Loss Map - Fitting Errors. 89
5.6 Diesel Generator Fuel Consumption. 90
5.7 Diesel Generator Fuel Consumption - Fitting Errors. 90
5.8 Battery Efficiency. 91
5.9 Battery Efficiency - Fitting Errors. 91
5.10 Battery Circuit. 91
5.11 Battery System Response: Terminal Voltage. 93
5.12 Propulsive Power Prediction Accuracy. 97
5.13 Measured Power Demand Distribution. 100
5.14 Operating Load Regions. 100
5.15 Comparison between load prediction and actual load demand. 101
5.16 Multiplication factor to correct for SOC deviation. 103
5.17 Schematic overview of the EMS controller. 106

6.1 Fuel Consumption in quasi-static maneuvers. 110
6.2 Simulated Operating Profiles. 111
6.3 Fuel Consumption of ICEs. 114

6.4 Fuel Consumption while towing - Profile 1. 115
6.5 Operational Points of the Diesel engines - Profile 1. 115
6.6 Operational Points of the Diesel engines - Profiles 4 and 5. 116
6.7 DP Solution - Control Decisions. 117
6.8 ECMS - Control Decisions. 118
6.9 A-ECMS - Control Decisions. 119
6.10 Co-state trajectories - Profiles 1 to 5. 119
6.11 Battery energy as a function of achieved fuel savings. 120
6.12 SOC trajectories and fuel consumption for different co-state values. 121
6.13 SOC trajectories and fuel consumption for increased C-rate limitations. . 122
6.14 Co-state trajectories for initial and increased battery limits. 122
6.15 Main engines' operating points for the increased C-rate limitations. 123
6.16 Effect on decision variables obtained with Dynamic Programming. 123
6.17 Operational time in each mode for the three different profiles. 125
6.18 Original, Idle and Busy Operating Profiles. 125
6.19 Co-state trajectories, Busy and Idle profiles. 127

A.1 Dynamic Programming Flowchart. 137

B.1 Left hand-side of Equation (B.1). 145

C.1 Right hand-side of Equation (C.11). 150

D.1 Reference vessel speed and towing force. 151
D.2 Resulting Fuel Consumption. 151
D.3 Power Output of each component. 152
D.4 Reference vessel speed and towing force. 153
D.5 Fuel Consumption and SOC trajectories - Profile 1. 153
D.6 Fuel Consumption and SOC trajectories - Profile 2. 154
D.7 Fuel Consumption and SOC trajectories - Profile 3. 154
D.8 Fuel Consumption and SOC trajectories - Profile 4. 154
D.9 Fuel Consumption and SOC trajectories - Profile 5. 154
D.10 Power Output of each component - Profile 1. 155
D.11 Power Output of each component - Profile 2. 156
D.12 Power Output of each component - Profile 3. 157
D.13 Power Output of each component - Profile 4. 158
D.14 Power Output of each component - Profile 5. 159
D.15 Power output of each component for 2-C rate battery limits - Profile 1. . . 160
D.16 Fuel consumption and SOC trajectory for 2-C rate battery limits - Profile 1. 160
D.17 Power output of each component - Idle Profile. 161
D.18 Fuel consumption and SOC trajectory - Idle Profile. 161
D.19 Power output of each component - Busy Profile. 162
D.20 Fuel consumption and SOC trajectory - Busy Profile. 162

LIST OF TABLES

2.1 Types of HEV Batteries 17

3.1 Main Characteristics of EMS approaches 35

5.1 Continuous Decision Variables - Sign Conventions 87

6.1 Comparative Results - Fuel Consumption, Efficiency, Running Hours. . . . 112
6.2 Comparative Results - Operating Modes. 113
6.3 Increased C-Rate Comparative Results - Fuel Consumption, Efficiency, Running Hours. 124
6.4 Increased C-Rate Comparative Results - Operating Modes. 124
6.5 Comparative Results - Fuel Consumption, Efficiency, Running Hours. . . . 126
6.6 Comparative Results - Operating Modes. 127

7.1 Fuel savings potential of each EMS. 130

B.1 Notation used in this Section. 141

NOMENCLATURE

Abbreviations

Symbol	Description
AC	Alternating Current
ANN	Artificial Neural Network
ASD	Adjustable Speed Drive
ASD	Automatic Voltage Regulator
B	Battery
BA	Bees Algorithm
BP	Bollard Pull
CFD	Computational Fluid Dynamics
CO_2	Carbon Dioxide
CPP	Controllable Pitch Propeller
CPU	Central Processing Unit
DC	Direct Current
DE	Differential Evolution
DIRECT	Dividing Rectangles Algorithm
DOF	Degree of Freedom
DP	Dynamic Programming
ECA	Emission Control Area
ECMS	Equivalent Consumption Minimization Strategy
EEDI	Energy Efficiency Design Index
EEOI	Energy Efficiency Operational Indicator
EM	Electric Machine
EMS	Energy Management Strategy

ENN	Extended Nearest Neighbor
ESC	Extremum Seeking Control
FEA	Finite Element Analysis
FLC	Fuzzy-Logic Controller
FOC	Field Orientation Control
FPP	Fixed Pitch Propeller
G	Generator
GA	Genetic Algorithm
GB	Gearbox
GT	Game Theory
HEV	Hybrid Electric Vehicle
HRR	Heat Release Rate
ICE	Internal Combustion Engine
IMO	International Maritime Organization
KiBaM	Kinetic Battery Model
Li-ion	Lithium-ion
LTV	Linear Time-Varying
MEC	Magnetic Equivalent Circuit
MH	Meta-Heuristics
MINLP	Binary Integer Non-linear Programming
MMF	Magnetomotive Force
MPC	Model Predictive Control
MVFP	Mean Value / First Principle
NiCd	Nickel-Cadmium
NiMH	Nickel-metal Hydrate
NO_x	Nitrogen Oxide and Nitrogen Dioxide
OCT	Optimal Control Theory
PC	Power Converter

PCO	Parallel Chaos Optimization
PI	Proportional - Integral
PID	Proportional - Integral - Derivative
PMP	Pontryagin's Minimum Principle
PSO	Particle Swarm Optimization
PWM	Pulse Width Modulation
RANS	Reynolds Averaged Navier-Stokes
RLS	Regularized Least-Squares
RMS	Root Mean Square
SA	Simulated Annealing
SECA	Sulphur Emission Control Area
SEUMRE	Space Exploration and Uni-Modal Region Elimination
SMPC	Stochastic Model Predictive Control
SMPCL	Stochastic Model Predictive Control with Learning
SoC	State of Charge
SQP	Sequential Quadratic Programming
SVM	Support Vector Machine
VFD	Variable Frequency Drive
VSI	Voltage Source Inverter

Subscripts

Symbol	**Description**
act	Actual
B	Battery
b	Base
b	Bore
e	Engine
el	Electrical
em	Electromagnetic

eqv	Equivalent
fr	Friction
H	Hydraulic
in	Input
lhv	Lower Heating Value
LR	Locked-rotor test
m	Mean
mech	Mechanical
NL	No-load test
nom	Nominal
OC	Open Circuit
out	Output
P	Parallel
p	poles
prop	Propeller
r	Rotor
ress	Rechargeable Energy Storage System
S	Ship
s	Stator
tot	Total

Superscripts

Symbol	Description
e	Synchronously Rotating Reference Frame
r	Rotary Reference Frame
s	Stationary Reference Frame

Greek Symbols

Symbol	Description	Units
α	Heat transfer coefficient	[W/m^2K]

χ	Reactance	Henry
η	Efficiency	-
γ	Heat capacity ratio	-
λ	Thermal Conductivity	[W/mK]
ω	Rotational Speed	rad
ψ	Flux Linkage per second	V
θ	Angle	rad

Roman Symbols

Symbol	**Description**	**Units**
C	Capacitance	Farad
D	Diameter	m
f	Frequency	Hertz
I	Inertia	$kg\ m^2$
I, i	Current	Ampere
L	Inductance	Henry
L	Length	m
M	Torque	Nm
N	Rotational speed	rpm
Nu	Nusselt number	-
P	Power	Watt
Pr	Prandtl number	-
Q	Reactive Power	Var
R,r	Resistance	Ohm
Re	Reynolds number	-
s	slip	-
SFOC	Specific Fuel Oil Consumption	g/kWh
T	Thrust	Newton
t	Thrust Reduction Factor	-

t	thickness	m
U, u	Voltage	Volt
v	Velocity	m/s
w	Wake factor	-

SUMMARY

Oceans have always been of paramount importance to society, as they are a major means of international cargo transportation. As markets became increasingly globalized, shipping volumes soared over the years. Up to the present day, about 90% of global trade by volume is being transported by sea. A direct result of this ever increasing transportation demand is that the industry's annual carbon emissions account for more than 3% of the global anthropogenic CO_2 emissions - comparable to that of a major national economy. Considering the environmental challenges that society faces on the 21st century, a drastic emission reduction and fossil fuel usage is almost mandatory for all major industries, including the maritime sector. Ultimately, near-zero emission levels will be required, pushing the development of electric and fuel-cell vessels. For now, hybrid vessels are a cleaner and more efficient alternative to conventional vessels in certain specific niche markets, without compromising expectations regarding performance and durability.

A major challenge in the operation of hybrid vessels is the powertrain's supervisory or *tertiary* control. The role of a supervisory controller is to optimize the energy flow within the vessel, subject to the components' operational constraints. The algorithms used in these controllers are known as *Energy Management Strategies*, and they are the main research objective of this work. More specifically, the design and assessment of such an integrated control solution for the current generation of Damen's hybrid tugboats which will optimally split the power produced between the various energy sources on board, with the aim to minimize the fuel consumption of the vessel.

Currently, a heuristic strategy is being used in this type of vessels. Although reliable and well-designed, it does not achieve the goal that initiated this work, i.e fuel consumption minimization. As an alternative, a control scheme based on the principles of Equivalent Consumption Minimization Strategy (ECMS) has been developed, tested, and compared to the currently-used heuristic strategy. This is a very interesting comparison as the application of ECMS on a hybrid tugboat with hybrid power supply *and* a Diesel-generator, has not yet been found in the available literature, to the best of the author's knowledge. In order to render the real-time solution of the arising Mixed Integer Optimal Control Problem possible, a novel solution method has been proposed, based on a combination of Convex Programming and the Branch and Bound algorithm, as discussed in Chapter 5. Moreover, an exhaustive-search solution method (Dynamic Programming) has also been applied, in order to benchmark the newly-proposed control strategy. For the purpose of this comparison, a forward-facing simulation model of the vessel has been developed, in which the dynamics of all power sources have been included. Furthermore, the development and validation process of the model led to several useful insights, including the need to extend the Diesel engine model of [Geertsma et al.], and the necessity of modeling and controlling the induction machines in the rotary reference frame to drastically decrease simulation time.

Simulation results demonstrate that the proposed control solutions can achieve av-

erage fuel savings of 4-6% in comparison to the heuristic strategy that is currently being used. The exhaustive-search solutions that were obtained proved useful as well, as they showed that an additional 2-3 % extra fuel reduction (compared to the proposed real-time strategies) can be achieved. Furthermore, it was also revealed that it is possible to devise a new rule-set that can be used in order to reach fuel savings of comparable magnitude.

Finally, through this work, it became evident that the results obtained with ECMS can approach the global optimum (in terms of fuel consumption) only through the proper sizing of battery energy, which can be only estimated by the control designer. It is the conclusion of the author that if further research is conducted in this field, Equivalent Consumption Minimization Strategy has the potential to greatly improve the fuel consumption characteristics of marine-based hybrid vehicles.

1

INTRODUCTION

"Do not call for black power or green power,
call for brain power."

-Barbara Jordan

The aim of this introductory chapter is to present the rationale behind the initiation of this work and to reflect on how the problems and considerations discussed in this text can be embedded in a broader setting. From the existing challenges, the research objectives are defined, and an overview of this work is presented.

1.1. THE NEED FOR ENERGY EFFICIENCY IN SHIPPING

Pondering on the importance of transportation, one can easily reach the conclusion that it constitutes one of mankind's most basic needs. Transportation is a critical component of economic development, with a profound impact on industrial growth, physical mobility and social welfare, both in primitive and advanced societies. Its availability has the potential to accelerate global development patterns and can be a boost - or a barrier - to economic growth within individual nations [Krugman, 1979]. Therefore the search for faster, and less costly (both in terms of people and cargo volume) transportation solutions has continued throughout history, ever since the invention of the wheel.

Oceans have always been of paramount importance to society as they are a major means of international cargo transportation. As markets became increasingly globalized, shipping volumes soared over the years. In the time span between the 1950s up to the latest global economic crisis, shipping transportation has been growing by 5% on average every year [International Council on Clean Transportation, 2007]. As a result, about 90 percent of global trade by volume is being transported by sea [Stopford, 2008, Corbett and Winebrake, 2008], a figure that is expected to rise from 10 billion tonnes to approximately 17 billion tonnes by 2030 [International Chamber of Shipping, 2010].

From an environmental perspective, this increase in transportation demand brings about an increasing necessity in energy saving and emissions regulations. After all, the shipping industry's annual carbon emissions account for more than 3% of the global anthropogenic CO_2 emissions - comparable to that of a major national economy. A rate that can increase up to 8% by 2050 [International Maritime Organization, 2014], without the employment of additional energy-efficiency measures.

The International Maritime Organization (IMO) has been introducing increasingly strict environmental regulations, such as requirements regarding the adoption of the new efficiency indexes EEDI - EEOI [DNV-GL, 2011], progressively tighter emission limits on NO_x and SO_x, and the so-called Emission Control Areas (ECAs). Since 2015, vessels operating in Sulphur Emission Control Areas (SECAs) are required to use fuel with less than 0.1% sulphur content [International Maritime Organization, 2014].

From an economic perspective, low freight rates [Beverelli et al., 2010] and notoriously fluctuating fuel prices (see Figure 1.1) have led to a growing interest in the maritime industry to search into fuel efficient solutions, subdivided between operational and design oriented.

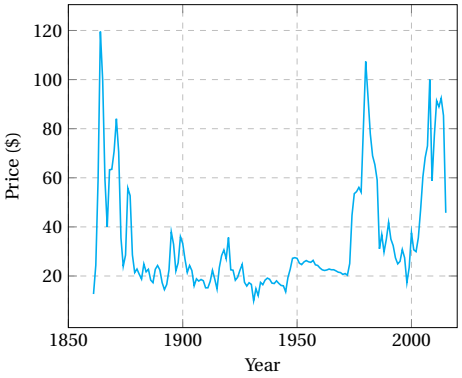

Figure 1.1: Crude Oil Price History Chart [Oil].[1]

Operational measures include optimal voyage planning, by maximizing the volume of cargo being transported while reducing the ballast volume needed [Wen et al., 2016], route adaptation so as to avoid weather conditions with negative impact on fuel consumption [Vettor and Soares, 2016, Shao et al., 2012], the improvement of trim characteristics and draft settings in combination with maintenance schedule optimization, with the ultimate goal of ship resistance reduction [Lu et al., 2015, Galeazzi et al., 2015], and the well-known "slow-steaming" mode of operation, which takes advantage of the propeller law to enhance fuel savings [Guan et al., 2014, Cariou, 2011].

Design oriented measures refer to all the physical solutions that result in more fuel efficient vessels. The majority of the existing approaches so far concentrate on enhancing the performance of individual components of the vessel, most notably the engine block [MAN B & W, 2012, Risse and Buchmann, 2013, Burel et al., 2013], propeller [Xie, 2011, Motley et al., 2012, Nelson et al., 2013], hull form optimization [Huang and Yang, 2016], resistance reduction through air lubrication [Latorre, 1997], or on the addition of waste heat recovery systems on board [Nielsen et al., 2014, Baldi et al., 2015a, Singh and Pedersen, 2016].

[1] Prices adjusted for inflation

1.2. HYBRID TECHNOLOGY

From a historical point of view, marine energy systems have relied upon a relatively simple setup: the main engine, designed to manage the (large) propulsion power demand, and the auxiliary engines, to deal with the electric power demands. The main problem with this approach is that each component fulfills one specific demand [Woud and Stapersma, 2002] which, taking into consideration the large number of combinations of propulsion and electric power demand of a vessel, is not the most energy efficient arrangement.

A solution to this inherent inefficiency of conventional marine energy systems is hybrid propulsion. Such arrangements are popular in the automotive industry [Guzzella et al., 2007, Jager et al., 2013], but only very recently they have been adopted in the shipping sector, namely in naval ships, supply vessels, and few harbor tugs and yachts. Application and challenges of these arrangements are discussed in depth in the work of [Geertsma et al., 2017].

Hybrid electric propulsion systems allow the main engine and the auxiliary engines to contribute both to propulsive and electric power production, thus allowing for additional flexibility on the overall power production [Sciberras et al., 2015]. Additionally, the inclusion of battery packs allows for energy storage, which can further enhance the efficiency of the hybrid power supply system as a whole (hybrid power supply refers to the combination of at least two types of power sources to provide the electrical power) [Sciberras et al., 2015, Grimmelius et al., 2011, Dedes et al., 2012]. In summary, the main advantages of adopting a hybrid propulsion system (mechanical coupling of an Internal Combustion Engine (ICE) and an Electric Machine (EM) to the propulsor) are [Jager et al., 2013]:

- Adaptation to a large variation of operating modes (appropriate for a flexible power demand profile), which results in enhanced operational capability, including fast system response and high plant flexibility.
- High redundancy/reliability due to:
  - Freedom to drive the propulsor either from the ICE or from the EM at any given time.
  - Provision of back-up power from the battery pack, in case of Diesel generator failures.
- Reduction of emissions due to high plant efficiency over a wide range of operating modes.
- Reduction of underwater noise and vibrations, because in electric mode the conductive noise transmission path from the engine can be isolated better.
- Fuel consumption reduction, because at low loads the main engines do not run at part load, but the required power is provided by the generators, which run at their optimum load, due to the shared load from propulsion and hotel loads.

On the other hand, numerous challenges regarding the design and operation processes of such systems arise, including:

- The design of an effective Energy Management Strategy (EMS), as will be explained in detail in the chapters that follow.

- The highly sensitive sizing process, so as to balance the trade-off between reduced fuel consumption and increased capital expenses - a common trait of all systems with such a high degree of integration [Baldi, 2016].

Finally, it should be stressed that there is still much room for improvement when it comes to hybrid schemes, as advancements in other engineering branches can also be incorporated, such as improved battery life, higher energy density of individual components, or by integrated thermal management [Jager et al., 2013].

1.3. HARBOR TUGBOATS

Given that the benefits arising from the adoption of hybrid propulsion have already been identified by the scientific community and such systems are slowly being introduced to commercial vessels, the question that can be raised at this point is the following: Is hybrid technology being exploited to its fullest?

As it seems, the answer lies within the intended operational profile of the vessel. Types of vessels that experience large variations in power demand, accompanied by relatively long periods of low power needs seem to be benefiting the most out of hybrid technology, and thus present the best candidates for further study and analysis. Yachts, dredgers, offshore support vessels and, *most of all*, tugboats present such diverse operating profiles [Grimmelius et al., 2011].

Tugboats are used to tow container-ships, bulk carriers and oil tankers to the harbor, where the waters are too shallow for the vessels to move by themselves. This results in a highly volatile operating profile, as illustrated in Figure 1.2 [2] which includes transit mode: $[200\ s, 300\ s] \cap [500\ s, 700\ s]$, standby mode: $[0, 200\ s] \cap [300\ s, 500\ s]$, and assist mode: $[700\ s, 3500\ s]$.

Nevertheless, to the best of the author's knowledge, not a large number of studies [Grimmelius et al., 2011, Vu et al., 2014, Vu, 2015, Yuan et al., 2016a, Vlaskos et al., 2013, Shiraishi et al., 2013, Boonen, 2016] have addressed quantitatively the merits of hybrid propulsion on harbor tugboats, with equally limited actual applications.

More specifically, the works of [Vu et al., 2014, Vu, 2015, Yuan et al., 2016a] underline the potential of an optimization-based EMS, with a focus on Diesel electric propulsion with hybrid power supply. They reported a 9% and 16% reduction in total energy consumption, when compared to a rule-based control system, thus underlining the potential of an optimization-based EMS. [Vlaskos et al., 2013] provides a comparative analysis of different hybrid architectures and configurations on a harbor tugboat, though operating under the influence of rule-based EMS only - as is the case in the work of [Shiraishi et al., 2013], and [Boonen, 2016] who focuses on the development of a hybrid propulsion tugboat model with hybrid power supply, whose operation is controlled using a rule-based strategy. This strategy however was charge-sustaining, designed in such a way so as to improve the ICEs' operational points.

[2] as measured by Damen Shipyards Group

Thus, both from an environmental and economical perspective, it would be of interest to assess the merits arising from the application of a fully hybridized drivetrain (hybrid propulsion with hybrid power supply). And more so, to a vessel with the operating characteristics of a harbor tugboat. The key point is that a well-designed, fully hybridized drivetrain generally presents fewer losses in comparison to a Diesel-electric propulsion system, therefore its combination with an appropriate EMS is expected to give even better results than the ones reported in the works of [Vu et al., 2014, Vu, 2015, Yuan et al., 2016a].

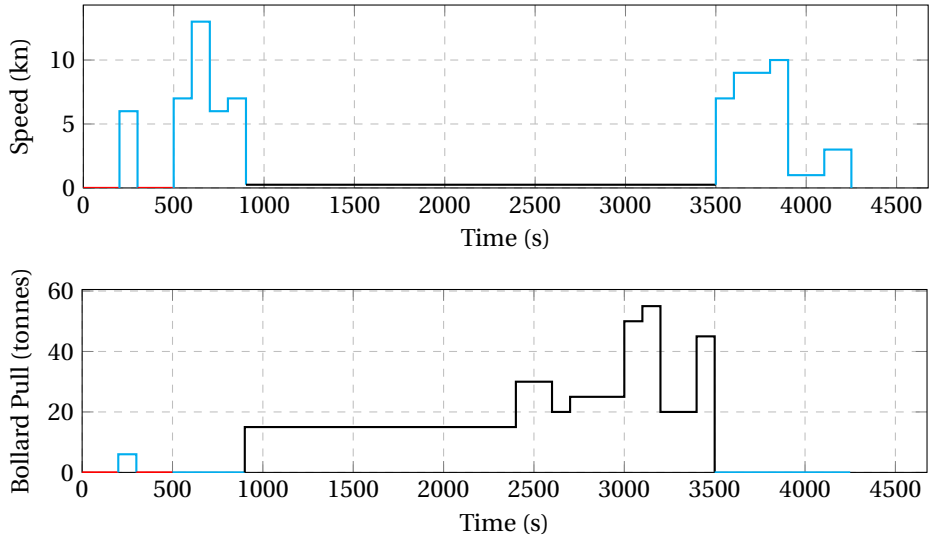

Figure 1.2: Typical Operating Profile of a Harbor Tugboat *(Operating Modes by color: Standby, Transit, Assist).*

1.4. ENERGY MANAGEMENT OF HYBRID POWERTRAINS

In any conventional powertrain, the operator (driver) imposes the wanted power delivery to the vehicle instantly. All his actions, being the inputs to the *component-level* controllers of the drivetrain, are immediately translated into specific actions that need to be taken from each component itself, such as fuel injection to the engine, or a gear shift in the transmission system.

On the other hand, controlling a hybridized vessel, or any other hybrid electric vehicle (HEV), includes two different sets of tasks as shown in Figure 1.3[3], and presented below:

- The *component-level* control task, which consists of [Geertsma et al., 2017]:
  - Governor speed control for the ICE.
  - Combinator curve control with pitch reduction in case of a CPP.

[3] Adjusted accordingly from the work of [Geertsma et al., 2017]

  - Automatic Voltage Regulation (AVR) for the generators.
  - In case of electric propulsion, the motor drive torque is being regulated using the switching signals of PWM converters, coupled with one of the following:
    - Field Orientation Control
    - Direct Torque Control
    - Direct Self Control

- The power management strategy, which regulates the on/off state of each component, making sure that the power demand can be met at any given time.

- The *tertiary control*, whose role is to optimize the energy flow of the drivetrain, while meeting several constraints. This is the control layer that is called *Energy Management Strategy*, as mentioned in Section 1.2 [Sciarretta and Guzzella, 2007].

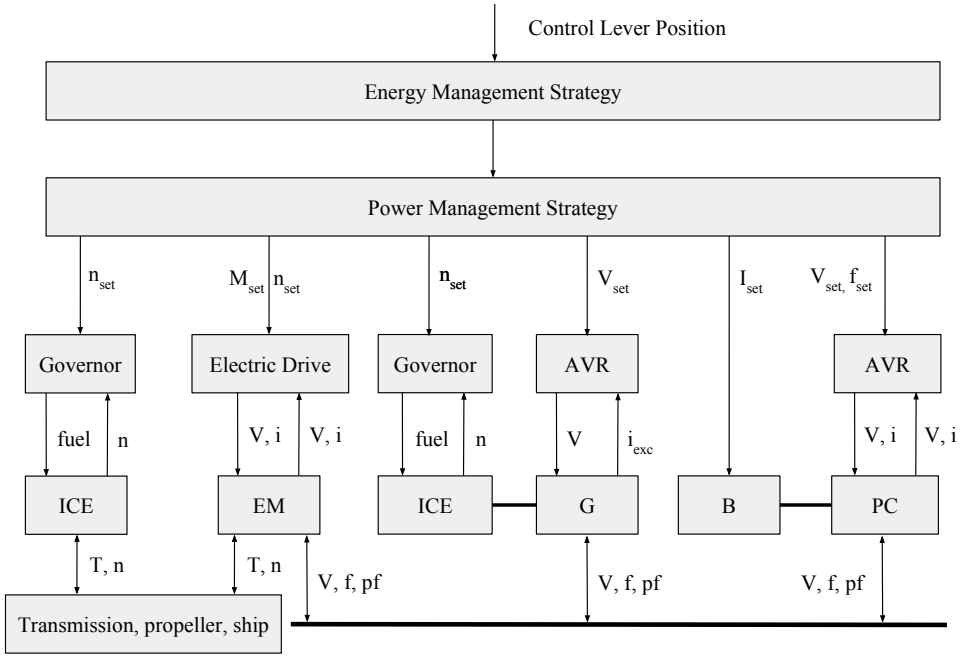

Figure 1.3: Control Layers of a Hybridized Vessel.

The EMS receives information from the HEV as well as its operator, processes this data, and produces the optimal "power-split", i.e. the amount of power produced by each component of the drivetrain so as to meet the power demand in the optimum way (with respect to fuel consumption minimization, pollutant emission minimization, battery life maximization, or any combination of all), while also satisfying all the imposed constraints (which typically include all the physical limitations of the components that

constitute the HEV). An EMS plays a critical role on an HEV, as the fuel savings potential, and emissions, of the hybrid drive-train depend on the optimality of this power distribution. It has been estimated [Sciarretta and Guzzella, 2007] that the achievable fuel economy for an HEV can range between 10% to more than 30%, compared with a conventional drivetrain, provided that a sophisticated controller is present to realize the potential of the hybrid drivetrain. As such, the importance of EMS has sparked a considerable amount of scientific research over the last decade, resulting in an abundance of different approaches, each with its own merits and demerits. The general consensus of the scholars who are active in this field of study has been summarized, in the most articulate way, in the work of [Onori et al., 2016], stating that:

> The adoption of systematic model-based optimization methods using meaningful objective functions to improve the energy management controllers is the pathway to go in order to achieve near-optimal results in designing EMSs.

In spite of this remark, mostly rule-based strategies have been applied to hybrid or electric tugboats so far, except from the works of [Vu et al., 2014, Vu, 2015, Yuan et al., 2016a] focusing on Diesel electric propulsion with hybrid power supply, which generally result in non-optimal system operation, therefore limiting the benefits of a fully hybridized propulsion system. Further enhancements are only possible with the application of optimization-based strategies, as concluded in the works of [Grimmelius et al., 2011, Vu et al., 2014, Vu, 2015, Yuan et al., 2016a, Vlaskos et al., 2013].

1.5. RESEARCH OBJECTIVES

The aim of this work is to provide further insights regarding the fuel savings potential of an optimization-based EMS applied in a hybrid propulsion system with hybrid power supply. Moreover, a quantitative comparison will be given, with respect to the existing rule-based strategy that is thus far being used, as developed by *Damen Shipyards Group*, and the solution obtained by the application of an exhaustive search method.

To address all these considerations, the following questions will be answered throughout this text:

- How can the propulsion plant be modeled to allow for evaluation of energy management strategies?
- Which optimization strategy presents the highest potential and ability to identify the optimal power split between the existing, distinct types of power sources?
- How can operating constraints, such as direct availability of full bollard pull, be taken into account in the EMS?
- How can discrete decisions, such as starting and stopping of engines be implemented in the EMS?
- What is the potential fuel consumption reduction of the proposed control strategy?

1

1.6. THESIS OUTLINE

This work is structured as follows:

- In chapter 2, a review of the different hybrid propulsion architectures of marine vessels is given, along with an overview of their current modeling approaches.
- Chapter 3 provides an extensive analysis of the currently used Energy Management Strategies.
- In chapter 4, the modeling approach followed in this work is presented, and the mathematical models of each component are given, along with validation results.
- In chapter 5 the formulation of the optimization problem is presented.
- Chapter 6 shows detailed results of the simulation and an analysis of the behavior of the proposed supervisory controller.
- Finally, in chapter **??**, the conclusions of this work are drawn, and recommendations for further research in this field are discussed.

2

HYBRID POWERTRAINS: OVERVIEW

"It is not the strongest of the species that survives,
nor the most intelligent,
but the ones most responsive to change."

-Charles Darwin

In this chapter, the concept of the hybrid powertrain will be explained, and different components and architectures will be presented. Finally modeling problems and considerations, typically encountered during the development and testing of new ideas regarding marine propulsion systems, will be touched upon, and an overview of the available modeling approaches will be given.

2.1. HYBRID POWERTRAIN CONCEPT

As discussed in Section 1.2, conventional powertrains utilize only one energy source to deliver propulsive power, the ICE, as shown in Figure 2.1. On the other hand, a hybrid powertrain consists of at least two powertrains capable of generating power. These typically include an ICE to produce mechanical energy and an electrical network responsible for the generation and distribution of electric energy. The main motivation for the development of hybrid powertrains is the possibility to combine the advantages of purely electric propulsion, in particular zero emissions, with the advantages of ICE-based powertrains, namely high energy and power density. Moreover, this hybridization allows for a broad spectrum of topologies that can be generated, depending on the connections between the powertrains, and a wide variety of patterns regarding power delivery. To illustrate the flexibility that a hybrid powertrain is able to provide, a conceptual illustration of such a powertrain, is presented in Figure 2.2. In the most usual case of an ICE working in parallel with an EM & battery combination, indicated as powertrains (1) and (2) respectively, the possible patterns to meet the load requirements include:

1. Power delivery from powertrain (1): Engine-alone propelling mode, used when the batteries are depleted, and the power demand is too high for the engine to recharge the batteries as well, or when the batteries are already fully charged, and the engine is able to meet the complete power demand.

2. Power delivery from powertrain (2), in which the ICE is turned-off. It is used primarily for situations where the ICE cannot operate efficiently (very low speed operation), or in strict emission control areas.

3. Power delivery from both powertrains simultaneously, in cases of high load demand or sharp accelerations.

4. Power delivery from powertrain (1) towards both powertrain (2) and the load, i.e. simultaneous battery charging and power supply to meet load demands.

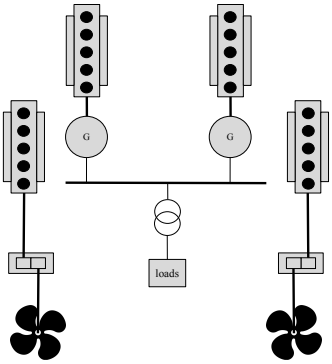

Figure 2.1: Conventional Propulsion System.

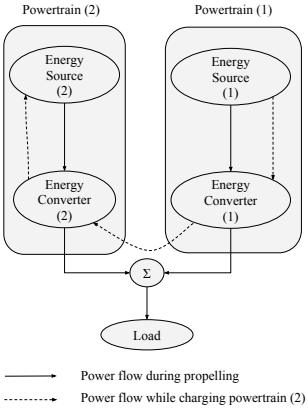

Figure 2.2: Conceptual Hybrid powertrain.

2.2. HYBRID POWERTRAIN ARCHITECTURES

The two basic hybrid configurations with hybrid power supply applied to marine propulsion systems are the following:

2.2.1. DIESEL ELECTRIC PROPULSION WITH HYBRID POWER SUPPLY

In this configuration, two different types of power sources (gen-sets and batteries) provide the propulsive power to the propellers via the electric motors.

The presence of the EM removes the need for a mechanical link between the ICE and the drive shaft, a characteristics which provides the following advantages:

- The ICE's operation is not related to the power requirements of the vessel, so it can be switched-off when running on part load, or operated at any point on its speed-torque map, regardless of the rotational speed of the drive shaft.

- Flexibility regarding the physical location of the various powertrain components is facilitated, making it suitable for application in vehicles with irregularly-shaped machinery spaces [Silvas et al., 2016].

- The battery can enable load leveling and peak shaving, depending on power fluctuations and demands. This results in constant loading of the engines, potentially maintaining an efficient operating point, or even lessen the sizing of the engines [Geertsma et al., 2017].

- Redundancy, as in the case of failure of one generator part of the power can be supplied by the battery pack.

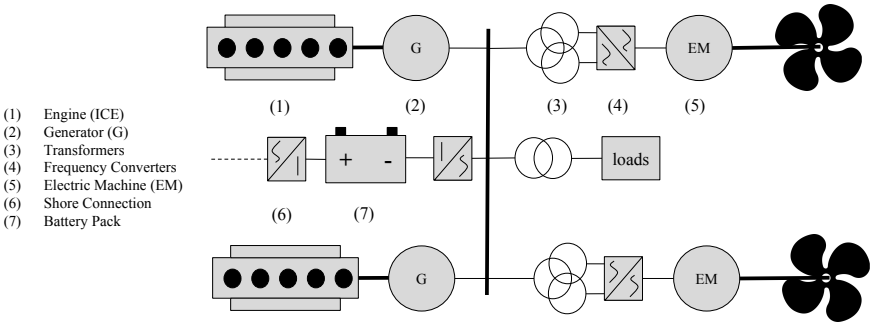

Figure 2.3: Diesel Electric Propulsion with Hybrid Power Supply

On the other hand, in order to transform the brake power of the ICEs to thrust power in the propellers, more energy conversions are needed (mechanical-to-electrical in the generator after the ICE, electrical-to-mechanical in the motor before the load, and twice electrical-to-electrical conversion in transformers and frequency converters), which inadvertently introduce higher transmission losses. Furthermore, the EM has to be sized for the maximum power requirements since it is the primary source of power, increasing capital costs and overall size of the plant.

At this point, it should be stated that a further distinction regarding this propulsion scheme can be made, into AC or DC electric propulsion, each with each own distinct features. However, a comparison between the two is not in the scope of this work, and the interested reader is referred to the survey of [Geertsma et al., 2017], the works of [Zahedi and Norum, 2013, Zahedi et al., 2014] which focus on DC propulsion, or the textbook of [Woud and Stapersma, 2002].

2.2.2. HYBRID PROPULSION WITH HYBRID POWER SUPPLY

The key of this configuration is that two independent power sources (from the ICEs and the EMs) are added together in a mechanical coupling system, able to operate independently from, and assist, each other, as shown in Figure 2.4. In this architecture the ICEs provide thrust in case of high power demand, with the EMs acting as a potential power-booster. For lower load requirements, the EMs can be used either as motors (to prevent the inefficient operation of ICEs at part-load) or as generators (so as to provide electrical power from the ICEs instead of the Diesel generators). Understandably, using this architecture, the vessel combines the benefits of electric (reduced noise & vibrations) and mechanical propulsion (high power density), with an even higher degree of redundancy and efficiency in both design and part-load conditions.

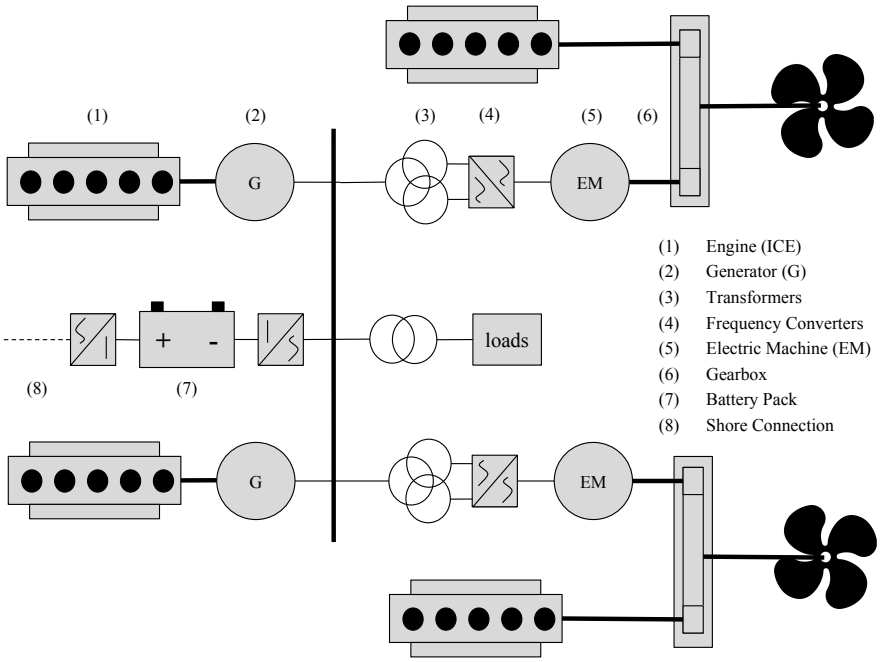

Figure 2.4: Hybrid Propulsion with Hybrid Power Supply

Other advantages of this configuration include that the propulsive power can be delivered to the propellers from the ICE with less conversion stages, in comparison to the topology of Section 2.2.1, which results in fewer transmission losses (since the extra mechanical-to-electrical power conversion observed in the previous powertrain is no longer present). Also, the EMs and ICEs can be sized accordingly so as to deliver jointly the full power demands in the most efficient way (what is also known as the optimal 'power-split').

2.3. MODELING OF HYBRID-ELECTRIC POWERTRAINS

This section contains an overview of the available modeling approaches of the principal components of a hybrid-electric propulsion plant, suitable for control systems design.

2.3.1. GENERAL CONSIDERATIONS

For efficient model-based controlling of HEVs, an "appropriate" mathematical description is of crucial importance. To this end, "appropriate" modeling of a power plant for the development and testing of an EMS, refers to a model whose scope is twofold: The capability of capturing the physics of the powertrain, while also being non-computationally intensive and implementable in real-time situations. Note that, because the focus of EMS is *supervisory* control, and not *component-level* control, only the slower dynamics of the powertrain are of interest, and in most cases only power-based models are usually considered, whereas torque- or current- based models get limited attention.

In the same respect, it is important to realize that it is not sensible to derive a model taking into account all the possible physics effects, primarily because most of these phenomena are not of interest to the main problem. Moreover, such an approach always results into a "heavy", CPU-intensive model, whose validation always needs experimental data that are not readily available, or costly to obtain through experiments [Jager et al., 2013].

This provides us with the freedom to use approximate mathematical models, using reasonable assumptions, which will need to describe only the slower powertrain dynamics, and also represent relevant power losses in nominal conditions, as well as part-load. Moreover, the ability of the model to represent technical, physical, and economic limitations of the powertrain components must be maintained, so as to allow for meaningful simulation results.

2.3.2. MODELING APPROACHES

A lot of research has been conducted on the cyber-physical modeling of hybrid electric powertrains, mainly from the automotive engineering branch, which is arguably at the forefront of hybrid technology. The effort to introduce and develop component models for HEVs has been well documented in literature, and the interested reader is referred to [Chan et al., 2010] for an overview, and in [Guzzella et al., 2007, Ehsani and Emadi, 2009, Mi et al., 2011, Eriksson and Nielsen, 2014, Pistoia, 2010, Husain, 2011, German, 2003] for detailed analysis.

A basic overview of the different approaches used in practice will be presented in this section. In general, three distinct modeling approaches can be identified that are capable of predicting the fuel economy of a hybrid-electric powertrain and are used for the design, and control system optimization of HEVs. In order of increasing complexity:

Average Operating Point Approach: The simplest modeling approach, whose key point is to sum up the full operating profile of the power system to one average point, which is then used to calculate the fuel consumption at that regime. It is well suited to provide a preliminary estimation of the fuel consumption in relatively simple powertrains, but it is not able to yield satisfactorily accurate results when complex propulsion systems have

to be analyzed in a high level of detail.

Quasi-static Approach: In this type of simulation a driver model compares the target operational characteristics of the HEV with the actual ones, and generates a power demand profile in order to follow the target values. As a next step, the generated power demand time series is divided into numerous time intervals, small enough so that the powertrain is required to follow specific, *constant*, operating characteristics, and the average operating point approach is applied at every time interval. In that sense, the model can be regarded as a "quasi-static" model since the behavior of the prime movers within the powertrain is described by means of steady state performance maps. The quasi-static approach can be used to solve the problem of fuel consumption minimization in relatively complex powertrains, and has been applied in supervisory control problems [Jager et al., 2013, Eriksson and Nielsen, 2014].

Dynamic Approach: Finally, in the dynamic approach, the powertrain is formulated using sets of differential equations, so solutions to equations governing conservation of mass, momentum and energy flows can be obtained, thus capturing the dynamic effects of the powertrain. In this way, dynamic events such as abrupt accelerations and maneuvering can be simulated with reasonable accuracy, but at a higher computational burden.
Usually quasi-static methods of modeling are used for the development and analysis of EMS, whereas dynamic methods are only chosen when no other option is available.

2.4. COMPONENT MODELING

Regardless of the chosen modeling approach, the performance of any powertrain model relies upon the methodologies applied to model each of the components. Therefore, in the current section, the most common modeling techniques for each component will be presented.

2.4.1. INTERNAL COMBUSTION ENGINES

One of the most complex tasks in a powertrain simulation is certainly the modeling of the main engine, especially if a good level of fidelity is needed. Many studies exist in literature, dealing with performance prediction and simulation of ICEs, and the choice of a suitable model depends primarily on the requirements of each application and, of course, the available computational tools [Johnson et al., 2010]. It must be pointed out that the analysis and categorization presented here is based on the excellent survey of [Grimmelius et al., 2007].

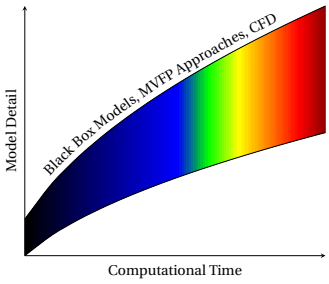

Figure 2.5: Time vs. Detail of ICE Models.

Following, the most-used ICE modeling approaches are presented, in order of increasing

complexity, and therefore computational effort. Figure 2.5 provides a qualitative idea of this trade-off. At this point, it should be noted that for the development of supervisory control algorithms, only the slower, pressure-related dynamic effects of an ICE are relevant to fuel consumption and may have to be taken into account, whereas the relatively fast dynamics can be safely ignored[Guzzella et al., 2007, Kiencke and Nielsen, 2005, Guzzella and Onder, 2009] offer an elaborate analysis.

2.4.1.1. BLACK BOX MODELS

An approach in which the ICE is modeled in terms of its inputs and outputs, based on:

Regression Fits: Which consist of look-up tables or polynomials in which the measured data is stored, (general regression fits are the Willans line approximation [Guzzella et al., 2007, Rizzoni et al., 1999], the Mossel model, and the Strictly Convex Polynomial Equation model [Jager et al., 2013]).

Transfer Function Models: In which the ICE is represent by first, or higher degree order systems capable of capturing only the most basic dynamics.

Artificial Neural Networks (ANNs): ANNs are computational algorithms designed in such a way so as to process information in a similar way to human brain. At their core they are, in essence, simplified models of biological neurons, able to process data in many simple and parallel processing units [Grimmelius et al., 2007]. The structure of an ANN is shown in Figure 2.6.

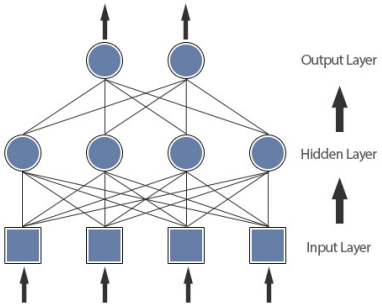

Figure 2.6: Structure of a simple feed-forward ANN.

The black-box modeling approach seems to be the preferred option for control-oriented modeling purposes (where only input-output relations are of interest), due to its superior real time capabilities. A disadvantage is that, in order to capture the ICE behavior accurately, all these methods need a considerable amount of data which is usually not available, hard to come across, or time consuming to obtain through experiments. Moreover, they are all tied to the specific engine whose data is being fitted (or used for training the ANN), thus they are not generic. If one of the engine parameters changes, it is unclear how the measured data should be treated, or how the models should be adjusted.

2.4.1.2. ANALYTICAL MODELS

This category consists of all the models that are, up to some extent, analytical. They consist of a set of algebraic and differential equations solved at each time step, and can be categorized as follows:

Mean Value / First Principle (MVFP) Models: In MVFP approaches, the ICE model is constructed by considering the processes occurring in each of its sub-components. Depending on the complexity of the model, components modeled include cylinders, scavenging and exhaust receivers, the compressor and turbine of the turbocharger, the en-

gine air filter and air cooler and the exhaust pipe. The in-cylinder process is usually approximated by a 6-point Seiliger cycle in order to obtain the work, and thus mean effective pressure and torque. Such models are regarded as a valuable solution to combine low computational requirements with relatively high accuracy, and can be found in abundant in scientific literature, as in the works of [Shamekhi and Shamekhi, 2015, Reb et al., 2015, Sturzebecher et al., 2015, Nikzadfar and Shamekhi, 2015, Baldi et al., 2015b, Maroteaux and Saad, 2015, Theotokatos, 2010, Li et al., 2013, Guardiola et al., 2014] to name a few. MVFP models are mostly used in cases where the ICE model has to be integrated within a larger powertrain system and in which the in-cycle variations are not of primary interest.

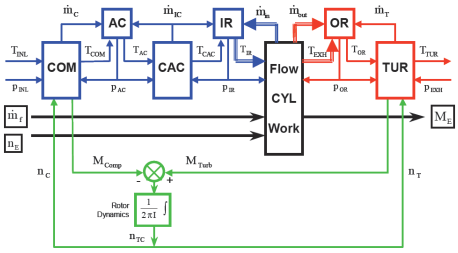

Figure 2.7: MVFP Model developed at TU Delft [Stapersma, 2010].

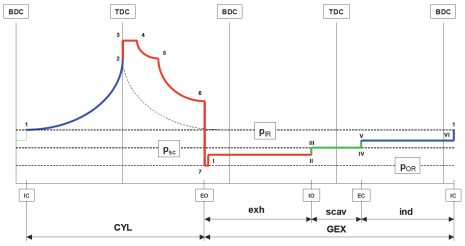

Figure 2.8: In-cylinder process concept of an MVFP [Stapersma, 2010].

Crank-Angle Engine Models: Also known as *filling and emptying* models, the various components of the ICE (cylinders, compressor, air-intake) are modeled as control volumes, in which the mass and energy balance equations are solved, whereas the pipe elements are used to solve mass transfer equations. The in-cylinder process is modeled using the fundamental energy balance, and a fuel burning function (as the coupling of two or more Wiebe equations) for the Heat Release Rate. Because of the fast changes occurring in the cylinder process[1], the differential equations involved are solved in small time steps, per crank angle degree [Grimmelius et al., 2007, Casoli et al., 2014].

Computational Fluid Dynamics (CFD) Models: Finally, the most complete and detailed modeling approach is a CFD model, in which the process of the cylinder is solved by dividing the combustion chamber into small volumes or elements (tens of thousands of them), and in each of these elements the basic equations of fluid dynamics, thermodynamics and chemical reactions (reaction kinetics and equilibrium equations) are solved [Grimmelius et al., 2007]. Understandably, this modeling approach provides extremely detailed information regarding the operation of an ICE, with a high computational burden.

Of course, the number of elements of the combustion chamber can be reduced, therefore reducing the computational time as well. This type of models are known as *Phenomenological multi-zone models*, and usually the number of combustion chamber's elements are in the order of tens.

[1] Of the order of magnitude of a small fraction of the time required for a complete shaft rotation.

2.4.2. BATTERIES

Battery models (mostly analytical ones, as will be discussed in this section) rely on the type of the battery, which is determined by the their electrolyte, according to Table 2.1:

Table 2.1: Types of HEV Batteries

Battery Type	Anode	Cathode	Electrolyte	Cell Voltage
Lithium - ion	C	Li_2O	lithiated solution	3.6 V
Lead - acid	Pb	PbO_2	H_2SO_4	2 V
Nickel - metal hydrate	metal hydrate	$Ni(OH)_2$	KOH	1.2 V
Nickel - cadmium	Cd	$Ni(OH)_2$	KOH	1.2 V

Quantitative comparative studies regarding the different battery types are abundant in scientific literature [Gutmann, 1999, Chau et al., 1999], whereas in [Wang et al., 2016] emerging trends in the subject of HEV batteries are given.

As expected, a variety of models have been proposed to evaluate batteries' interaction with the rest of the powertrain [Rahn and Wang, 2013], all of which recognize that the dynamics of the batteries are rather slow compared to the rest of the components in the powertrain, therefore they have to be accounted for regardless of the modeling approach. Taking that into account, battery modeling can be a gruesome task, since the parameters that influence the battery's properties (mainly the State of Charge (SoC), voltage and current) are dynamically and related to each other, in a highly non-linear fashion.

A complete battery model accounts for electrical, thermal and aging dynamics. The electrical system can be considered as the top of the modeling pyramid, and can be used without the rest of the subsystems. The thermal subsystem requires the electrical subsystem so as to determine the heat produced by the battery pack, whereas the aging subsystem requires the temperature calculated by the thermal subsystem and the SOC, so as to incorporate temperature, storage, and charging/discharging cycles' effects and generate the remaining maximum available capacity of battery as time progresses.

In the modeling of a powertrain for control-oriented purposes usually only the electrical subsystem needs to be modeled [Stanislovaitis, 2015]. This is because, in practice, the battery pack temperature is tightly controlled so as to avoid chemical process instabilities and is kept low to reduce battery wear, thus the influence of the temperature needs not be modeled [Jager et al., 2013]. Nevertheless, regarding the thermal subsystem the reader is referred to [Hu et al., 2012, Jaguemont et al., 2016, Tan et al., 2011, Mi et al., 2007], and for capacity fading effects in [Honkura et al., 2011, Broussely et al., 2001, Bloom et al., 2001, Sarasketa-Zabala et al., 2016, Berecibar et al., 2016, Petit et al., 2016].

In order to correlate the battery current and voltage to the power exchange with the rest of the powertrain, the electrical subsystem can be simulated using the following approaches [Shafiei et al., 2011]:

Fitted Models: One of the most straightforward ways to develop a simplified battery model, based solely on experimental data and simple semi-empirical equations. Of course, in direct relation to the fitted models of ICEs, they suffer from the same drawbacks, and present the same merits.

Example of some simple semi-empirical formulas used for data fitting are:

- Peukert's equation [Rakhmatov and Vrudhula, 2001], which approximates battery lifetime (L) as a function of the discharge current (I), using the simple equation: $L = \int_{t=0}^{t} \frac{\alpha}{I(t)^{\beta}} dt$, with α and β being constant parameters.
- the Shepherd model [Shepherd, 1965a,b], which describes how the voltage of a battery changes with respect to the current load using a formula of similar complexity as Peukert's equation.

Another well-known model is the Kinetic Battery Model (KiBaM), developed in [Manwell and McGowan, 1993, 1994] which simulates the battery's charge as a combination of two connected water reservoirs, according to Figure 2.9. This model was specifically developed to describe the response of large lead-acid storage batteries, which have a distinct (flat) discharge profile. Thus, it can not be used for modern batteries, like Li-ion, due to their sloped discharge profile.

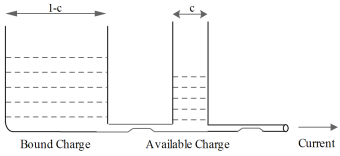

Figure 2.9: Kinetic Battery Model.

More advanced and complicated analytical models, can be found in literature, such as Rakhmatov and Vrudhula's diffusion model, given in [Rakhmatov et al., 2002, 2003], which uses the concentration of active materials in the electrolyte as a key point in the modeling process, to give predictions regarding the battery's lifetime.

Stochastic Models: This approach has not been widely applied in the modeling of batteries despite it's promising results, and it is based on the use of discrete-time Markov chains to describe the charging and discharging effects of the battery (a Markov chain is a stochastic simulation approach used to model randomly changing systems, where it is assumed that future states depend only on the current state and not on the events that occurred before it.)

An interesting application is the stochastic KiBaM, which is an extension of the traditional KiBaM model, with a few modifications so as to model a Ni-MH battery. Interestingly, simulation results showed that the model was sufficiently accurate for predicting battery lifetime, with a maximum error of 2.7% [Rao et al., 2005].

Circuit-oriented Models: In these approaches, electrical components are used to model the behavior of the battery, including constant or controlled voltage sources, connected in series with resistors and resistors with capacitors connected in parallel. By using different connections, several battery effects can be modeled. In general, these models fall under the following categories [Chen and Rincon-Mora, 2006]: Thevenin-based, Impedance based, and Runtime-based, all shown in Figure 2.10.

Electrochemical models: Which represent the most complete modeling approach, and are based on chemical reactions occurring within the battery cells. They mostly consist of six coupled, non-linear differential equations. The most complete electrochemical

model can be found freely online in [University of Berkeley], called 'DualFoil', and it is often used as a benchmark for testing other newly developed battery models. To give an indication on the amount of detail needed for the very highly accurate simulation that this software provides, apart from the load profile more than 50 battery parameters need to be given as inputs.

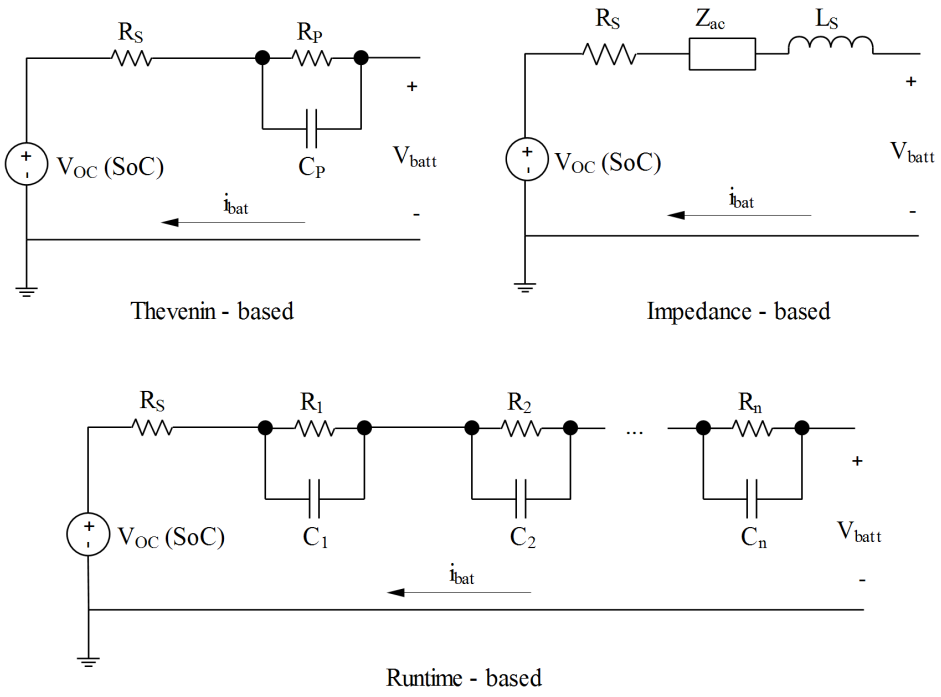

Figure 2.10: Circuit - Oriented Battery Models.

As can be seen, several approaches can be used to simulate battery behavior. The most complete is the use of electrochemical models, however the complexity of solving the six coupled partial differential equations directly reflects on computational time. Moreover, a very detailed knowledge of the battery system is required by the user in order to set up the parameters, which include data that is usually hard to find. Stochastic models are generally somewhat limited, as they are designed only for specific discharge profiles, therefore they can not handle more abstract cases of arbitrary load profiles, with varying discharge currents etc. Circuit-based models are capable of variable complexity (depending on the number of parameters used) and therefore varying levels of accuracy and computational time. This gives the user the freedom to choose freely the time/accuracy trade-off, a characteristic that the other approaches do not have. Moreover, they are the most suitable for simulation purposes, due to their inherent electrical nature, which makes them possible to be connected directly to an electrical network. Finally, fitted models are generally tied to specific types of batteries, or in the case of holis-

tic approaches, like Peukert's equation, they only offer below medium-level accuracy (around 10% error, depending on the simulated conditions, as mentioned in [Rakhmatov and Vrudhula, 2001]).

2.4.3. ELECTRIC MACHINES

Electric Machines are another key component of HEVs, capable of mechanical-to-electrical power conversion and vice versa. EMs used on hybrid propulsion systems typically include synchronous AC generators and induction motors, which are particularly complex systems with a high number of components, therefore the complete modeling of all of them is seldom attempted. Moreover,the spread of their frequency response can also be very broad, making the modeling process even more difficult. The following approaches can be used for simulating EM behavior:

Fitted Models: The simplest modeling technique that can be used, similar to the approaches described for ICEs and batteries. Such models typically use piece-wise quadratic functions in order to describe the conversion characteristics of the EM (including the losses of the power converter) and a simple relation between the input and output power so as to determine the EM efficiency, or torque and efficiency maps, in which desired values of electrical power or torque as used as control inputs [Jager et al., 2013, Guzzella et al., 2007].

Electric-Equivalent Circuit Models: Another modeling technique employed for EM analysis, introduced in the late 1960s [Lwithwaite, 1967, Carpenter, 1968] is the MEC approach. The key characteristic of this modeling approach is that the complex magnetic circuit of the machine is transformed into a much simpler electrical network solved using electric circuit theory, coupled with differential equations to account for the rotational dynamics of the machines when necessary. In this way numerous parameters, for a variety of EM types, can be calculated with relative ease. Such models can be found in most textbooks nowadays [Krause et al., 2013, Gomez-Exposito et al., 2016], their major advantage being computational accuracy, in combination with limited model complexity, easy parametrization and relatively low computational time. As such, this approach is particularly attractive as an analysis and design method. However, in cases for which an accurate estimation of the dynamics of the electric machine are important and their transient behavior has to be taken into consideration, a more advanced approach must be used which includes modeling inductances, flux linkages, etc. One such approach can be found in [Ong, 1998].

Finite Element Analysis (FEA): A more computationally expensive approach for the simulation of EMs. FEA tools incorporate complex geometries, coupled circuits and non-linearities in an EM model, and are typically used when designing efficiency optimized machines, especially for new designs incorporating new shapes and material properties. However, they are not computationally efficient to be used as part of a large-scale dynamic simulation. To give an example, a typical time-domain model of an EM modeled with a typical FEA tool needs hours to reach a steady-state solution, which corresponds to about one second of real time [Yilmaz, 2015]. To overcome this drawback,

several reduced FEA approaches have been proposed, which aim to minimize the computational effort associated with FEA, while maximizing the amount of available information [Sizov et al., 2012].

2.4.4. GEARBOXES

Hybrid powertrain configurations implicate the use of gearboxes capable of switching between diesel and electric drives. The most important characteristic is the loss of torque in a gearbox, which, as shown in [Godjevac et al., 2015], it can be a highly complex calculating procedure when taking into consideration gear losses, losses in the seals and bearings etc. Whereas investigations of the performance of gearboxes are available, the majority of them focus on the automotive industry [Schlegel et al., 2009]. Regarding maritime gearboxes, power loss models have not been investigated in detail, apart from [Godjevac et al., 2015, Stapersma, 1994]. The existing approaches are summarized below. For a comparative analysis the reader is referred to [de Jong et al., 2015].

- Stapersma Model: Developed in [Stapersma, 1994], this simple model proposes a linear equation for the calculation of the nominal power losses, as a function of the shaft speed and the power produced by the prime movers. As stated in [de Jong et al., 2015], the model does not take into account the detailed configuration of each specific gearbox (type, size,lubrication), which can influence the total power loss, however it is sufficient to provide a rough approximation of the gearbox loss behavior at the nominal operating point of the prime mover.

- Drijver Model: Developed in [Drijver, 2013], it can estimate power losses during heavy- and part-load conditions. The total losses are the sum of losses from bearings, teeth, lubrication and seals, which are considered to be a function of shaft speed and load. It can very accurately determine the efficiency of the gearbox in part- or heavy-loading conditions, while requiring very few input parameters [Godjevac et al., 2015].

- Geertsma Model: Which proposes a quadratic fit model for power and torque losses, as functions of shaft rotational speed and torque [Geertsma, 2015].

2.4.5. PROPELLERS

Several propeller models are available which, in combination with data series, are capable of providing an adequately accurate simulation of the propeller. For the scope of this work, of interest is the torque and thrust developed at a certain rotational shaft speed and thrust angle. This can be modeled quite easily with the use of the Open Water Diagram, or the Four Quadrants Diagram, the later having been developed by the Maritime Research Institute Netherlands (MARIN) [Woud and Stapersma, 2002]. Regarding the Open Water Diagram, the performance of the propeller is represented in terms of three non-dimensional coefficients, namely the thrust coefficient K_T, torque coefficient K_Q, and their variation with respect to the advance ratio J. On the other hand, the Four Quadrants Diagram uses thrust and torque coefficients, ($C_T and C_Q$ respectively), as a function of the hydrodynamic pitch angle (β) of the propeller. The Open Water diagram has the limitation of representing stationary forward sailing only ($J > 0$), whereas the

Four Quadrants diagram can provide insight into the whole field of operation for the propeller, including running astern and dynamic behavior, like stopping or abrupt accelerations [Woud and Stapersma, 2002].

Finally, the most complete approach to simulate propeller behavior is the use of Computational Fluid Dynamics (CFD) methods to solve the Reynolds Averaged Navier-Stokes (RANS) equations, which give the most accurate prediction regarding the hull-propeller interaction, maneuvering characteristics, and the flow field around the propeller. As expected, since such models account for highly complex and fundamental physical effects, the increase in computational resources is extremely severe.

2.4.6. POWER ELECTRONICS

For the scope of this work, the only data required from a power electronics component (inverter, rectifier, etc.) simulation is only power losses. The dynamic behavior is not of importance, since the dynamic response of such components is of the order of milliseconds (which results in an even smaller time-step size during the simulation process) [Bacha et al., 2014], therefore not affecting the vessel's fuel consumption characteristics. Once again, the simplest approach to replicate steady-state or dynamic input-output characteristics of power electronic components are fitted models (also known as *behavioral models* among electrical engineers). The power losses are determined with the use of numerical surfaces constructed using manufacturer data, or on the basis of semi-empirical formulas - usually quadratic functions of current load.

Another modeling approach used for the design and optimization process of power electronics, is a *complete circuit model*. Depending on the assumptions used, circuit models can be divided into [Bacha et al., 2014]:

- Switched Models: which describe the converters' behavior *exactly* and as such, they are the most computational-time intensive.
- Sampled-Data Models: Which provide information about the system's state in a periodic manner. In other words, they provide a representation of the component sampled at each complete operating period, and not at switching moments.
- Averaged Models: Able to replicate an average behavior of the system's state over a specific time-window.

2.5. CONCLUSIONS

As stated in section 2.3.1, the most fundamental question in modeling is the objective of the simulation itself and, as such, it should be carefully evaluated. In general, it is not desirable to simulate all aspects of the system in detail, the reason being that the output of the simulation may be overwhelming, therefore obscuring the phenomena that are of primary interest. In this respect, the preferred modeling approach is the one that employs the simplest possible technique so that the simulation meets the immediate objective. As such, it is important to consider which effects influence the parameters that are of immediate interest when it comes to supervisory-control-strategy development and testing. As a first basis, the most important parameters include: Fuel and electrical efficiencies, thermal loading of the engine, and capacity fading effects of the batteries.

2.5.1. MODELING APPROACH OF THIS WORK

Although not the most usual choice [Guzzella et al., 2007] for control systems studies, the dynamic approach will be followed. This is deemed necessary considering that an electric machine used in an adjustable speed applications is capable of significantly faster dynamic response in torque loads compared to a medium speed Diesel engine. This ability can, and should be, exploited in a propulsion system where the two can operate in parallel, provided that their joint operation can be properly controlled. As this aspect will be also considered in this work, the need for a dynamic modeling approach, at least for the prime movers arises. This approach will be based on the general ship modeling approach introduced in [Grimmelius et al., 2007] and generally applied by the marine engineering section of Delft University of Technology, as shown in Figure 2.11.

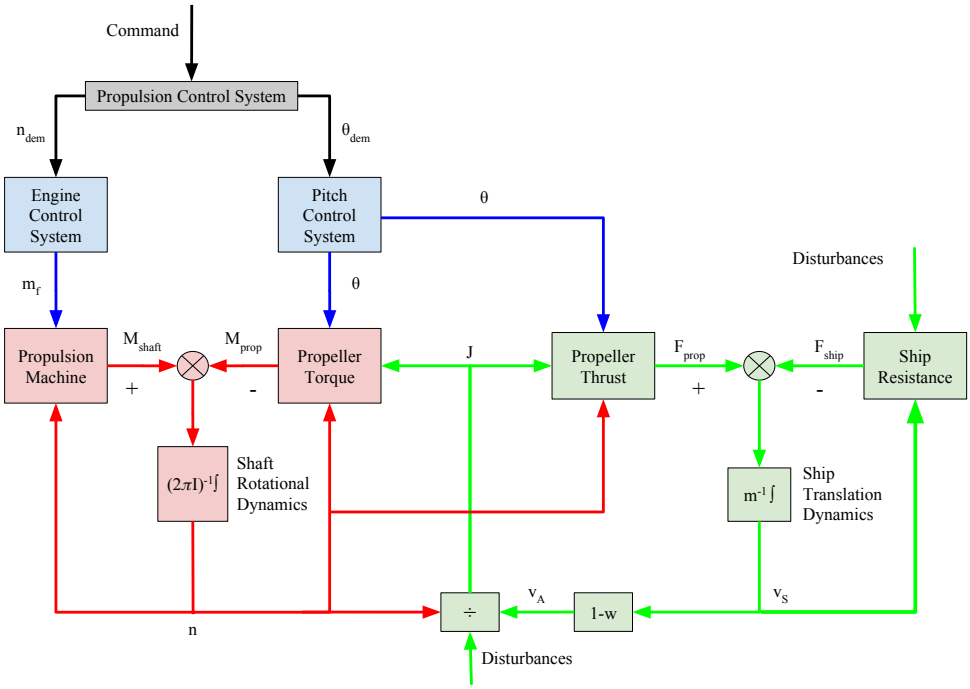

Figure 2.11: General Ship Propulsion Model.

Inputs of the general model are the speed settings of the prime mover, and the pitch setting of the thrusters. The speed setting is processed in the engine control system block, from which the amount of fuel to be injected to the propulsion machine is calculated. Based on that, the propulsion machine block determines the torque produced by the prime mover. The propeller model will determine the required torque and resulting thrust of the propeller based on the input pitch setting, shaft speed, and ship speed. Next, the torque output of the prime movers is compared with the required propeller torque, and their difference results in the rotational speed of the propeller shaft from the shaft rotational dynamics sub-system, according to Newton's second law of rotational motion. In the ship dynamics sub-system, the thrust delivered by the propeller and the

forces resulting from the vessel's movement give the net forces and moments, which are then translated into ship movements using Newton's equations of motions [Grimmelius et al., 2011].

Although further adjustments will be necessary in order to incorporate the components of the specific propulsion system that will be studied in this work (i.e. EMs and batteries), this generic model presents a very good baseline simulation approach to work with, as it provides an accurate representation of all the relevant characteristics of a real vessel and it has been used successfully in the past for the simulation of propulsion systems [Grimmelius et al., 2007, Boonen, 2016] and the evaluation of EMS and their influence on the sailing behavior of a vessel [Grimmelius et al., 2011].

2.5.2. COMPONENT MODELING REQUIREMENTS

Moreover, a first insight into the requirements of the component models that were presented in Section 2.4 can also be provided after the overview of the modeling approach that will be used. Regarding the ICE model, an approach is needed capable of capturing most of the dynamics of the ICE, without going into a detailed crank-angle related calculations, as these will increase the computational time, and the level of detail they provide is not needed. In this respect, an MVFP approach capable of capturing the classic dynamic behavior of an ICE, i.e. the inertias of the engine, and the turbocharger system (2^{nd} order model). As stated in Section 2.4.2, the dynamics of the batteries *must* be taken into consideration, since one of the state parameter that affects the EMS is the SoC of the battery. As such, batteries will be modeled using an equivalent circuit approach, as shown in Figure 2.10, as these have been widely used in the past for control-oriented purposes, are capable of capturing the dynamics of the battery system, and can be incorporated into a wider model with relative ease. In the same respect, electric machines will be modeled using an MEC approach, which presents sufficient accuracy regarding system dynamics. Note that, although the system dynamics (being of the order of magnitude of seconds) are not expected to influence the EMS strategy that will be developed, they still need to be accounted for when an adjustable speed drive is considered, as stated in Section 2.4.3. The gearbox can be modeled using either of the three approaches presented in Section 2.4.4, depending on their accuracy with respect to power and torque losses, as they are the only piece of information that is of interest for the scope of this work. Regarding the modeling approach of the propellers, the Four Quadrants approach will be used, as it is the only one that allows the reverse operation of the shaft. Finally, power electronics will be modeled using fitted models, due to their favorable approach with respect to simulation time, according to the discussion of Section 2.4.6.

3

Energy Management Strategies: An Overview

"We can only see a short distance ahead,
but we can see plenty there that needs to be done."

-Alan Turing

In this chapter, an overview of the different categories of Energy Management Strategies available today will be presented, and a qualitative description and comparison will be given. Based on these remarks, the most appropriate optimization strategy will be chosen.

3.1. Overview

It is generally accepted that the fuel economy potential of hybrid systems can only be achieved with a sophisticated control system [Sciarretta and Guzzella, 2007]. This realization has spurred a considerable amount of research over the last years, which has resulted in a wide variety of control strategies for the optimal performance of hybrid systems. To the best of the author's knowledge, an exhaustive classification of all the contemporary optimization strategies is presented in Figure 3.1, which is based on the review articles [Jager et al., 2013, Sciarretta and Guzzella, 2007, Neffati et al., 2013, Sabri et al., 2016, Silvas et al., 2016, Zhang et al., 2015, Olatomiwa et al., 2016, Chong et al., 2016, Gurkaynak et al., 2009, Wirasingha and Emadi, 2011, Panday and Bansal, 2014].

EMS can be divided into two classes. *Non-causal* methods, which control the drivetrain using exact knowledge of the power trajectory, and *causal*, i.e. real-time implementable strategies, which are able to control the drivetrain without having exact knowledge of the power demand. A different categorization involves optimization-based, and heuristic (or rule-based) strategies. Optimization-based strategies have received more

attention than their rule-based counterparts. Although rule-based strategies cannot obtain the optimum working point of the drivetrain, they are still being used, primarily due to their easy implementation. Regarding global optimization, DP, PMP and some of the stochastic search algorithms present the mostly used approaches, whereas for real-time optimization, ECMS and MPC are the most popular and rapidly developing [Neffati et al., 2013, Panday and Bansal, 2014].

3.2. RULE-BASED CONTROL STRATEGIES

These strategies constitute the first schema to appear in industrial control, in which a set of rules is derived, based on human expertise and intuition. They are based on 'IF-THEN' type of control rules, and require virtually no computational effort or storage capacity. As such, they are easily implementable and have been widely applied in prototypes and commercial HEVs. They can be further divided into deterministic and fuzzy rule-based strategies.

3.2.1. DETERMINISTIC RULE-BASED

In which the rules are derived on the basis of fuel consumption/emission data, operating maps of the ICE, or human expertise for the system to be controlled. More specifically:

- In the thermostat strategy, once the ICE is switched on, it operates on its optimal working point only, whereas the battery is charged/discharged depending on the state of the engine (on/off). Note that the only difference between the thermostat and the power follower strategy is that, in the latter, when the engine is turned on, it operated along its optimal working curve, instead of having just a single operating point.
- The frequency based scheme splits the power demand into high- and low-frequency regions incorporated with load leveling. It is superior than the previous two approaches of this category, as it has been reported to result in better fuel economy, decreased emissions and improved battery life [Sabri et al., 2016].
- The engine optimal efficiency region is also a form of power-balancing strategy, used primarily in series-parallel HEVs, whose primary goal is to keep the ICE running in its most efficient operating region while balancing the operation of the EM as needed, taking advantage of its favorable speed-torque characteristics.
- Finally, the system optimal operational point takes also into consideration the transmission power losses, delivering the optimum point as a trade-off between the optimality of the ICE's operation, and the maximization of the transmission efficiency.

Deterministic rule-based strategies have shown success in commercial HEVs (like Toyota's Prius), however their most severe limitation is lack of flexibility under different operating conditions [Shaohua et al., 2012, Kim et al., 1999, Trovao et al., 2013].

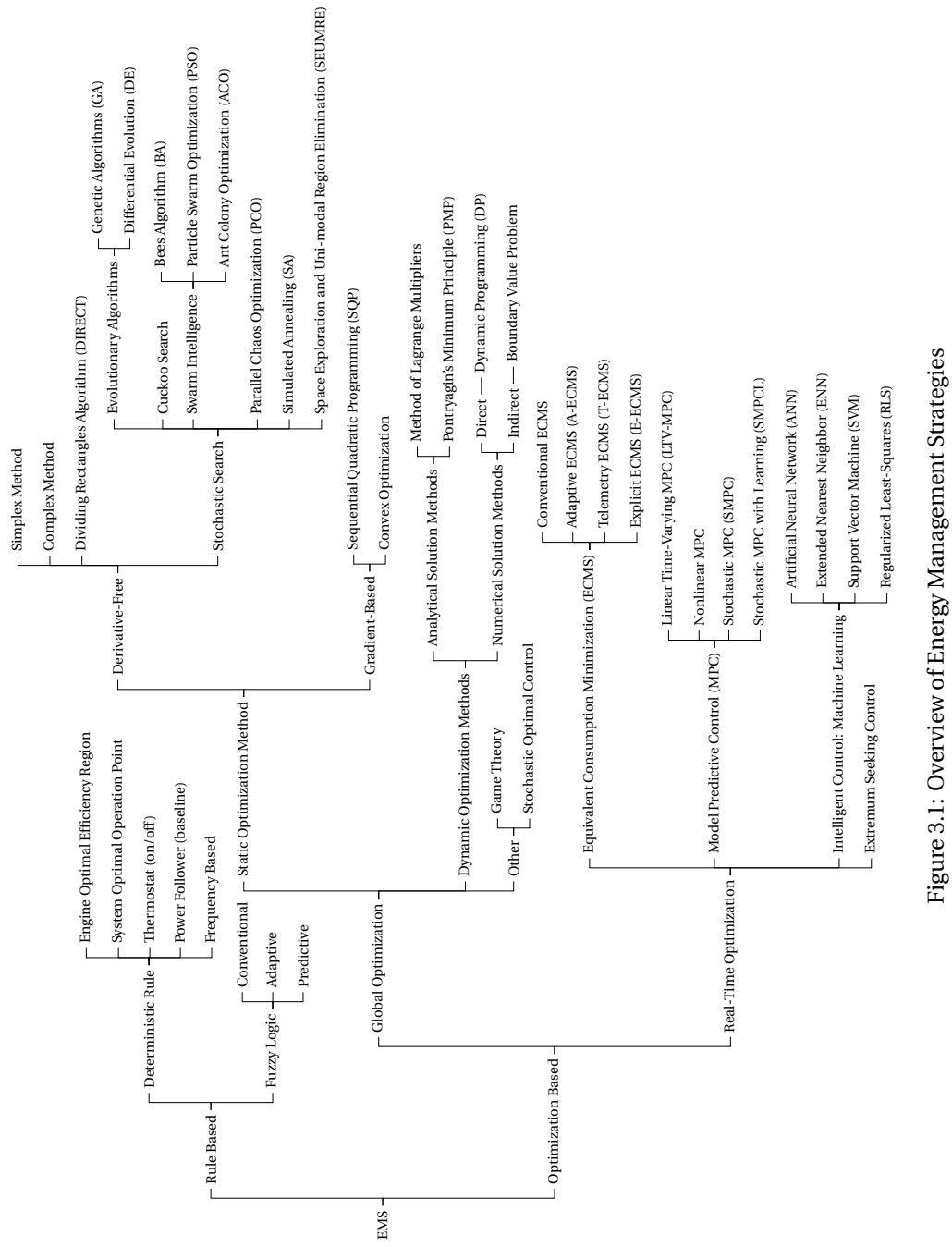

Figure 3.1: Overview of Energy Management Strategies

3.2.2. FUZZY RULE-BASED

This limitation was overcome using Fuzzy Logic controllers (FLC). Fuzzy logic, firstly introduced in [Zadeh, 1965], has a fundamentally different approach when it comes to handling numerical data, which can be used as a tool in intelligent control. According to classical Boolean logic, any statement can be represented as a zero, being false, or one, true. Fuzzy logic introduced another concept, in which the truth of any statement is a matter of degree, interpreting it by any number between zero and one. This idea of approximate reasoning, rather than precise, when applied to controllers can translate the knowledge and experience of the designer in an extensive collection of IF-THEN rules that can be used more efficiently in the decision making process [Arsie et al., 2001, Lee et al., 2000]. In a sense, a fuzzy logic controller is a natural extension of many rule-based controllers implemented (via look-up tables) today [Zhang et al., 2015]. The main advantages of fuzzy logic based controllers over deterministic strategies are robustness against uncertainties and measurements noise, and the ability to be tuned and adapted accordingly, therefore enhancing the degree of freedom of control - highly useful properties as the complexity of the drivetrain increases [Olatomiwa et al., 2016, Baumann et al., 2000, Won and Langari, 2002]. The analysis so far is enough to cover the conventional fuzzy controllers. Without going into much detail, a short introduction about the extended fuzzy logic controllers is presented:

Adaptive-fuzzy Control: It is capable of optimizing conflicting objectives (such as fuel economy and emission reduction) simultaneously, with the optimal operating point being achieved using a weighted-sum approach optimization of conflicting objectives. These weights are adapted according to different driving cycles, achieving tremendous reduction in emissions, with negligible compromise in fuel economy [Panday and Bansal, 2014].

Predictive fuzzy control: The current state is being evaluated based on the available history of the system to be controlled and its variability in the near future, as a look-ahead window. By using rule-based strategies specifically developed for each possible operating condition within this time window, it is possible to obtain a solution closely related to the optimal one, without using any form of optimization. The downside of this approach is that the information used to define the future behavior of the drivetrain, based on known past states, is hard to predict, and it is equally difficult to derive the huge amount of rule sets for each possible operating condition.

3.3. OPTIMIZATION-BASED CONTROL STRATEGIES

In optimization-based strategies, the goal of the controller is to minimize an objective function, usually represented by fuel consumption (or emissions, or both). System optimization takes place as the result of a system-learning-and-adapting approach to the operating conditions, within a given framework of rules and constraints [Wirasingha and Emadi, 2011].

3.3.1. GLOBAL OPTIMIZATION STRATEGIES

Global optimization strategies require an *a priori* knowledge of the operating conditions, so they are also called a-causal control approaches. Understandably, as future conditions can not be predicted *exactly*, this kind of strategies can not be implemented directly for real-time optimization. However, their biggest limitation of this strategy category is heavy computational burden (significantly higher in comparison to rule-based strategies) [Gurkaynak et al., 2009, Wirasingha and Emadi, 2011]. Despite their preview-like nature and computational complexity, they are still studied and used today, mostly for quality comparison and evaluation purposes of all the rest control strategies.

A further subdivision is possible, into two main categories:

3.3.1.1. STATIC OPTIMIZATION

Static Optimization: Which in essence takes as input a rule-based EMS (along with the operating conditions and the drivetrain characteristics) and optimizes its parameters (rules) with respect to minimum fuel consumption. Thus, the energy management problem is converted into a parameter optimization, *static* problem, in which the optimum can be obtained via gradient based and derivative free approaches. The key difference between the two is the use of derivatives in the search of the optimum point - the main characteristic of gradient-based methods. Moreover, due to the multi-modal and discontinuous nature of the functions that describe a complex drivetrain's optimization process, their convexity and differentiability are far from guaranteed. Therefore, gradient-based methods have seen limited use on HEVs, mostly on the simplest of drivetrain configurations [Oh et al., 2007]. On the other hand, derivative-free methods aim for the optimal solution using iterative procedures rather than relying on derivatives [Zhang and Chen, 2001, Shuaiyu et al., 2007], which have been proven to be a more appropriate approach for EMS on HEVs and superior to gradient-based methods in searching for the global optimum over the entire search space[Gurkaynak et al., 2009, Panday and Bansal, 2014].

3.3.1.2. DYNAMIC OPTIMIZATION

In this approach, the EMS problem is formulated as a dynamic, nonlinear, constrained optimization problem, largely known as *optimal control problem*. The main characteristic of this approach is that the dynamic problem is decomposed into a sequence of subproblems, by discretizing it over time [Sundstrom et al., 2008, Sundstrom and Guzzella, 2009], forming an instantaneous cost function at each sample time. By solving the subproblems consecutively, the optimal control schedule can be obtained. Dynamic optimization strategies are further divided into analytical and numerical solution methods, both of which are analyzed in [Jager et al., 2013][1].

3.3.1.3. OTHER METHODS

More unconventional optimization methods used in HEVs' EMS include Game Theory, proposed in [Dextreit and Kolmanovsky, 2014, 2010], and Stochastic Optimal Control [Kolmanovsky et al., 2008, Malikopoulos, 2013, Moura et al., 2011]. These methods have

[1] Interested readers (with a sufficient mathematical background) are also referred to the work of [Bryson, 1996].

not seen wide application (compared to other global optimization strategies) in EMS, due to several, distinct for each approach, reasons.

Game Theory is a mathematical approach to human behavior, used primarily in Economics and Political Sciences. It originates as a mathematical representation of the following concept: A non-cooperative game in which each participant's gain (or loss) is exactly balanced by the losses (or gains) of the other participants. The mathematical solution to such a concept (also known among mathematicians and economists as Nash Equilibrium) has found its application to EMS for HEVs, as it provides the ability to decouple optimal solution of the EMS from the operating cycle. It has seen limited application due to its complex nature and high sensitivity.

Stochastic Optimal Control is a framework for modeling optimization problems that involve uncertainty. The main characteristic of this approach is the formulation of the EMS problem as an infinite-horizon stochastic dynamic optimization problem. It predicts future power demands by generating a probability distribution for them. The optimal control strategy is then obtained using stochastic dynamic programming, which has been known to outperform rule-based strategies [Panday and Bansal, 2014, Malikopoulos, 2013]. The limitations of this approach include sensitivity to calibration parameters and difficulty in the online estimation of probabilities and online reconfiguration of the control law [Zhang et al., 2015].

3.3.2. REAL-TIME IMPLEMENTABLE STRATEGIES

In real-time optimization the global optimal criterion is reduced to an instantaneous optimization approach, by discretizing it over time, as in the dynamic optimization strategies of Section 3.3.1.2, and including a cost function that depends only on the present state of the system parameters. According to Section 3.3.1, when all the information regarding the operating profile is known from the outset, global optimization strategies can be used to provide an optimal solution. The key difference of real-time implementable strategies is their ability to estimate, *with a degree of uncertainty* the future operating conditions of the system, with the latter being already in operation, based only on past and present time information. Of course, the quality of this prediction directly reflects on the optimality of the solution, which will understandably be sub-optimal, i.e. when the implemented strategy is evaluated retrospectively with the offline computed optimal solution, a control sequence that achieves a lower fuel consumption can usually be found.

One of the objectives in the design of a real-time implementable strategy is to achieve a fuel consumption that is close to the off-line computed optimal solution. Additional requirements on such a strategy is imposed by the limited computational requirements that it must exhibit, so as to have a computational burden suitable for real-time implementation, while in the same time not requiring a profound understanding of the complete underlying mathematics of optimal control theory [Ehsani and Emadi, 2009]. Depending on the approach that the strategies employ in order to deal with this degree of uncertainty while satisfying the rest of the requirements, they are further subdivided in the following:

3.3.2.1. EQUIVALENT CONSUMPTION MINIMIZATION STRATEGY

ECMS is arguably the most well-known real time optimization strategy, the concept of which originates from the work of [Paganelli et al., 2000]. In this approach, the instantaneous optimization function is the sum of the actual fuel consumption used by the ICEs and an equivalent fuel consumption related to the SoC variation, thus allowing for a unifying continuous representation of both the energy used in the battery and ICEs. This function is being optimized on a real-time basis, therefore no prior knowledge of the power demand is needed in order to provide an optimal solution. The only disadvantage of this strategy is that it does not guarantee charge sustainability of the plant, [Sciarretta et al., 2004, Won et al., 2005, Pisu and Rizzoni, 2005].

The principle underlying the ECMS approach is that a cost is assigned to the electrical energy, so that the use of electrical stored energy is made equivalent to using (or saving) a certain quantity of fuel. This cost, mostly known as *Equivalence Factor* is obviously unknown, as it depends on future vehicle behavior, but it has been shown that it can be related to driving conditions in a broad sense. Practically speaking, the equivalence factor represents the chain of efficiencies through which fuel is transformed into electrical power and vice - versa. As such, it changes for each operating condition of the drivetrain. In the original formulation of ECMS, the equivalence factor was a vector of constants, one for charge and one for discharge of the battery, both of which can be interpreted as the average overall efficiencies of the electric path for the corresponding operating mode (charging/discharging), and a specific driving cycle. [Onori et al., 2016]

Clearly, the concept of equivalent fuel consumption is tied with the necessity of attributing a meaningful value to the equivalence factor, and as such, it has been the topic of extensive research that involves primarily estimation methods and impact factors. The chosen approach in the estimation of the equivalence factor is the characteristic based on which ECMS can be categorized further into:

- Constant: In which this assumption for the equivalence factor is made (conventional ECMS), for the whole operation of the drivetrain. The optimal constant equivalence factor is based on different optimization methods which, although easy to implement, they require full knowledge of the power demand. Therefore a re-calibration of the factor is necessary for different operating conditions - limiting the generality of ECMS [Zhang et al., 2015].

- Online calculation: Based on the SoC of the battery, direction of electrical current and power demand information (A-ECMS and T-ECMS). According to the level of information, different maps and and relevant factors are constructed so as to update the equivalence factor. This can be done with the use of a P, PI control or adaptive law functions.

3.3.2.2. MODEL PREDICTIVE CONTROL

MPC is a popular real-time optimization strategy, employed to deal with multivariate constrained optimization problems. The main feature of MPC is to allow the current time-slot to be optimized, taking also future time-slots into consideration. This is generally performed in three steps [Yang and Zhu, 2016]:

1. Calculation of the optimal control sequence in a prediction horizon that minimizes the objective function, while satisfying all the constraints.
2. Implementation of the optimal control policy derived in (1).
3. Moving the entire prediction horizon one step forward, so as to repeat the sequence.

In MPC approaches, dealing with future state uncertainties generally involves a prediction method. This prediction method (in automotive engineering) is based on navigation technology and on board sensors, or on mathematical prediction models of two types:

- Deterministic: which provides a deterministic power demand over the prediction horizon.
- Stochastic (SMPC) [Ripaccioli et al., 2010]: which describes the future torque demand with probability distributions, based on the current state of the system or historical data.

As such, MPC can be seen as a receding horizon approach, able to adapt to variations of power demand online, with reduced computational requirements. Since the optimization problem is solved over a future prediction horizon, MPC can be thought of as neither short-sighted, nor sensitive, which is considered as an advantage over ECMS [Zhang et al., 2015]. MPC approaches can also be classified based on the characteristics of the control-oriented model, into linear time-varying MPC (LTV-MPC) and non-linear MPC, with opposing views regarding the time requirements - model complexity trade-off. Non-linear MPC provides higher fuel economy, but at a higher computational cost. A further extension of SMPC is Stochastic MPC with learning (SMPCL), originating from the work of [Cairano et al., 2014]. It has been proposed so as to provide increased robustness and quicker adaptation compared to SMPC, and is proven to have an overall better performance.

3.3.2.3. MACHINE LEARNING

Among intelligent control strategies, machine learning algorithms are mostly used in EMS for HEVs. All machine learning algorithms try to emulate the decisions of human brain, and they are powerful computational methods able to learn and generalize from any training data, which makes them suitable to use for intelligent control strategies in the control of HEVs. Several machine learning techniques have been used for such an application, including Artificial Neural Networks (ANNs) [Murphey et al., 2013, 2012], Support Vector Machines (SVMs) [Wang et al., 2007b], and other machine learning concepts [Park et al., 2009]. The advantage of these approaches is that precise powertrain models are no longer needed, while computational effort is extremely reduced. On the other hand, in order for the control strategy to work satisfactorily, an extensive database is needed for the training of the control algorithm, which is difficult and time consuming to obtain, especially for an optimized drivetrain database obtained, for example with the use of DP, as observed in [Chen et al., 2014].

3.3.2.4. EXTREMUM SEEKING CONTROL

Extremum Seeking Control (ESC) is applicable to non-linear control problems, with the only aim of the policy being to find the operating set-points that minimize or maximize *(extremize)* an objective function. Being a model-free control approach, it can, and has been, used with success in a wide variety of applications [Dochain et al., 2011], one of which being as an EMS for an HEV, originally proposed in the work of [Dinccmen et al., 2010]. It has sufficiently low computational requirements and presents high robustness to uncertainties, however it can only obtain local optima [Dochain et al., 2011]. Although suitable as a real-time control strategy, to the best of the author's knowledge, studies on ESC-based EMS for HEVs still remain under the simulation phase. An excellent primer for ESC can be found in [Ariyur and Krstic, 2003].

3.4. CONCLUSIONS

A summary presenting the most important remarks of all EMS discussed in Chapter 3 is given below:

Deterministic Rule-Based: Easy implementation, exceptionally low computational requirements, however they present inability to optimize energy flow [Shaohua et al., 2012, Kim et al., 1999, Trovao et al., 2013].

Fuzzy Logic Rule-Based: Relatively easy implementation, the controllers are robust and tolerant to imprecise measurements and component variations, and can be easily re-tuned and adapted if necessary. Further improvements have been reported when the rule-set is optimized using stochastic search methods [Arsie et al., 2001, Lee et al., 2000, Baumann et al., 2000, Won and Langari, 2002, Schouten et al., 2002, Khoucha et al., 2010].

Sequential Quadratic Programming: Straightforward implementation and high efficiency in the solution of continuous problems. However, the use of SQP requires the imposing of strong assumptions on the objective function, so as to obtain the derivatives, which can be non-realistic. There is also high possibility of obtaining local optima only [Oh et al., 2007].

Simplex Method: There are no requirements regarding the description of the objective function, or its derivatives, in analytical form and it presents strong capabilities of local search. However, the initial search point affects the quality of the solution, and it has been reported that this approach can easily get trapped in local optima [Zhang and Chen, 2001].

Complex Method: As in the Simplex method, there are no requirements regarding an analytical expression for the objective function and its derivatives. Again the solution relies on a good initial search point, with the danger of getting trapped in local optima. Not suitable for high-dimensional, multi-constraint problems [Shuaiyu et al., 2007].

DIRECT: Does not require neither the derivative of the objective function, nor the specification of the starting point, and it has the ability to cover the entire design space in search of the global optimum. However, it suffers from slow convergence to the true global optimum when reaching the global optima region [Gao and Porandla, 2005].

Stochastic Search Methods: They are capable of finding the global optimum over the entire search space, without requiring any derivatives of the objective function. They present strong robustness and have an extensive application scope. Parallel calculation is possible, and they can be easily combined with other methods. On the other hand, their performance depends on the tuning parameters. Furthermore, they exhibit slow convergence to the true optimum when reaching the global optimal region [Montazeri et al., 2006, Wang et al., 2007a, Wu et al., 2008, Zhang et al., 2009b,a, Long and Nhan, 2012, Wu et al., 2014].

Dynamic Programming: An exhaustive search method, applicable to both linear and non-linear systems, constrained and unconstrained problems. However, it requires *a priori* knowledge of the operating profile, therefore it can not be used on-line, but it is primarily used to benchmark other, real-time implementable strategies [Sundstrom et al., 2008, Lin et al., 2003, Koot et al., 2005, Sundstrom and Guzzella, 2009].

Game Theory: As a method, it has the ability to decouple the optimal solution from the operating conditions, with satisfactory (compared to DP) computational times. Its only advantage is its rather weak robustness [Dextreit and Kolmanovsky, 2014, 2010].

Stochastic Optimal Control: It an be used under a variety of problems and systems, with relatively high computational time (although less than DP methods). Capable of optimizing the control policy over a family of diverse operating profiles with sufficient efficiency. However, the controllers using this approach are highly sensitive to calibration parameters, and also the online reconfiguration of the control law is rather difficult and time consuming [Kolmanovsky et al., 2008, Malikopoulos, 2013, Moura et al., 2011].

Equivalent Consumption Minimization Strategy: It can lead to a system behavior very close to the optimal, with medium computational time requirements. Limited manual tuning of few control parameters is needed, and this approach is adaptable during real-time operation. It fas exhibited the highest potential to be used in future HEVs [Paganelli et al., 2000, Sciarretta et al., 2004, Won et al., 2005, Pisu and Rizzoni, 2005, Musardo et al., 2005].

Model Predictive Control: Also adaptable during real-time operation, neither short-sighted nor sensitive regarding future event anticipation, so it can take control actions accordingly. However, the future power demand must be known in advance by the prediction method. Finally, it has a higher computational cost than ECMS [Tang et al., 2016, Yang and Zhu, 2016, Ripaccioli et al., 2010, Li et al., 2016].

Machine Learning: These methods provide quick adaptation to different operating conditions, they are easily adjustable and consistent in providing high-efficiency operation under various scenarios. On the other hand, they are in need of initial training sets, which require a high amount of data, so as to increase the robustness of the controller [Murphey et al., 2013, 2012, Wang et al., 2007b, Park et al., 2009, Chen et al., 2014].

On the basis of this description and comparison, the following characteristics of each control category can be given as a conclusion:

Table 3.1: Main Characteristics of EMS approaches

Strategy Type	Advantages	Disadvantages
D-RB	Computational Efficiency, easy implementation	Extensive calibration and tuning of parameters
FLC	Robustness to measurement noise and component variability, Low computational requirements	Optimality not guaranteed, calibration of membership function and fuzzy rule set required
Real - Time	Several approaches have the potential to be implemented in HEVs, can obtain sub optimal solutions	Cannot obtain global optimum, some approaches are still difficult to be implemented in current vehicle controllers.
Global	Can obtain optimal solution, no parameter calibration requirements, used to benchmark real-time strategies	*A priori* knowledge of the power demand required, high computational requirements, cannot be implemented directly

Based on Table 3.1, it can be seen that no current EMS is considered to be the absolute best solution, and both rule-based and optimization-based strategies have their own characteristics, advantages and disadvantages. So far, the majority of EMS being applied today, are rule-based strategies due to their simplicity, disregarding their inability to obtain optimal solutions. On the other hand, optimization-based EMS, although new compared to rule-based strategies, have shown thus far very promising results in the available literature.

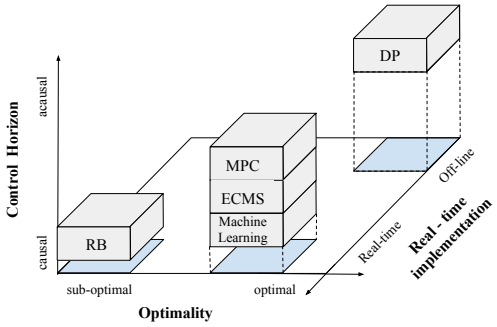

Figure 3.2: Classification of Energy Management Strategies [Silvas et al., 2016].

However, the trade-off between complexity and optimization performance is always present. All the existing approaches reduce computational requirements at the expense of optimization performance. A qualitative comparison is given in Figure 3.2, taken from [Silvas et al., 2016]. In this respect, real-time implementable strategies seem to pro-

vide an overall balance in this time-optimality trade-off, and they are currently the most promising solution, as they can provide us with a solution close to the optimal, with satisfactory computational requirements. Among those, ECMS along with its variations have shown great potential, as they are able to provide solutions of the same quality as the rest of the real-time implementable strategies, while requiring the lowest computational burden among them. Moreover, it does not require any extensive calibrations with respect to control parameters, apart from the equivalence factor. As such, an ECMS-based approach will be implemented in the hybrid tug.

4

TUGBOAT SIMULATION MODEL

"We make ourselves pictures of facts.
The picture is a model of reality.
There is no picture which is a priori true."

-Ludwig Wittgenstein

In this chapter, the process of modeling the constituents of the electric and propulsion subsystems of the hybridized tugboat will be described, and the physical equations used to model the behavior of each component will be presented.

4.1. MODELING APPROACH OVERVIEW

4.1.1. GENERAL CONSIDERATIONS

In order to develop and test a new control strategy a valid simulation model of the propulsion plant is needed. Building the simulation model that will be described in this chapter proved to be a time-consuming task, with relatively difficult choices regarding complexity, structure and desired accuracy. The whole process was based on ideas and considerations presented in the excellent work of [Vrijdag et al., 2009], who propose a systematic approach towards modeling, verification, calibration and validation of a ship propulsion simulation model, quantifying both the validity of static operating points and the system's dynamic behavior. A brief summary of these considerations will be given in this section.

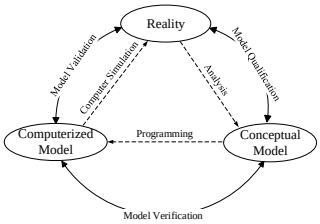

Figure 4.1: Development cycle of a simulation model [Schlesinger et al., 1979].

The basic elements of a credible simulation model are presented in Figure 4.1, taken from [Schlesinger et al., 1979]. The inner arrows describe the processes which relate the elements to each other, and the outer arrows refer to the procedures which evaluate the credibility of these processes. The first step towards the development of a conceptual model is to define the goal of the simulation. This was briefly mentioned in Sections 2.3.1 and 2.5.2, and it could be summarized as follows:

> The ship propulsion simulation model should be capable of capturing the physics of the hybrid propulsion drivetrain accurately enough for the development of a control strategy that minimizes the overall fuel consumption. As such, the prediction of power losses for all the components is of primary importance, both in nominal and part-load conditions, as well as the fuel consumption of the main engines and the Diesel-generator set, and the state of charge of the battery. Furthermore, the model should provide an accurate representation of the dynamic behavior of the induction machines and main engines, in case their difference in dynamic response can be used by the tertiary control system (i.e. fast acceleration requirements, etc.). Finally, (to the degree that this is possible) the model should be non - computationally intensive so as to allow for fast simulations during the development and testing of the control scheme.

Although this summary is somewhat abstract and includes vague terms (the description 'accurately enough' is highly subjective), it provides a first insight regarding the model's complexity, adequacy, and required accuracy. With this in mind, the following specifications for the model can be extracted, which give an adequte starting point for the final model:

- The model has to include mathematical representations of the electrical system (batteries, and Diesel-generator set), prime movers, transmission system, propellers, and maneuvering.
- The models of the main engines and induction motors that drive the shaft should provide accurate results in terms of efficiency and dynamic response, as discussed earlier.
- The accuracy of the electrical system should be confined mostly to power losses for the rest of the components, apart from the battery, for which a more detailed model is needed, capable of predicting accurately its state of charge, as it will ultimately affect the decisions of the control scheme.
- The maneuvering system should be accurate enough with respect to straight line maneuvering behavior of the vessel (the control system will only be tested against straight line maneuvers).

4.1.2. PROPULSION & ELECTRICAL SYSTEM DESCRIPTION

As stated in Section 1.5, one of Damen's hybridized tugboats will be considered for the application of an EMS. The layout of its propulsion system is presented in Figure 4.2.

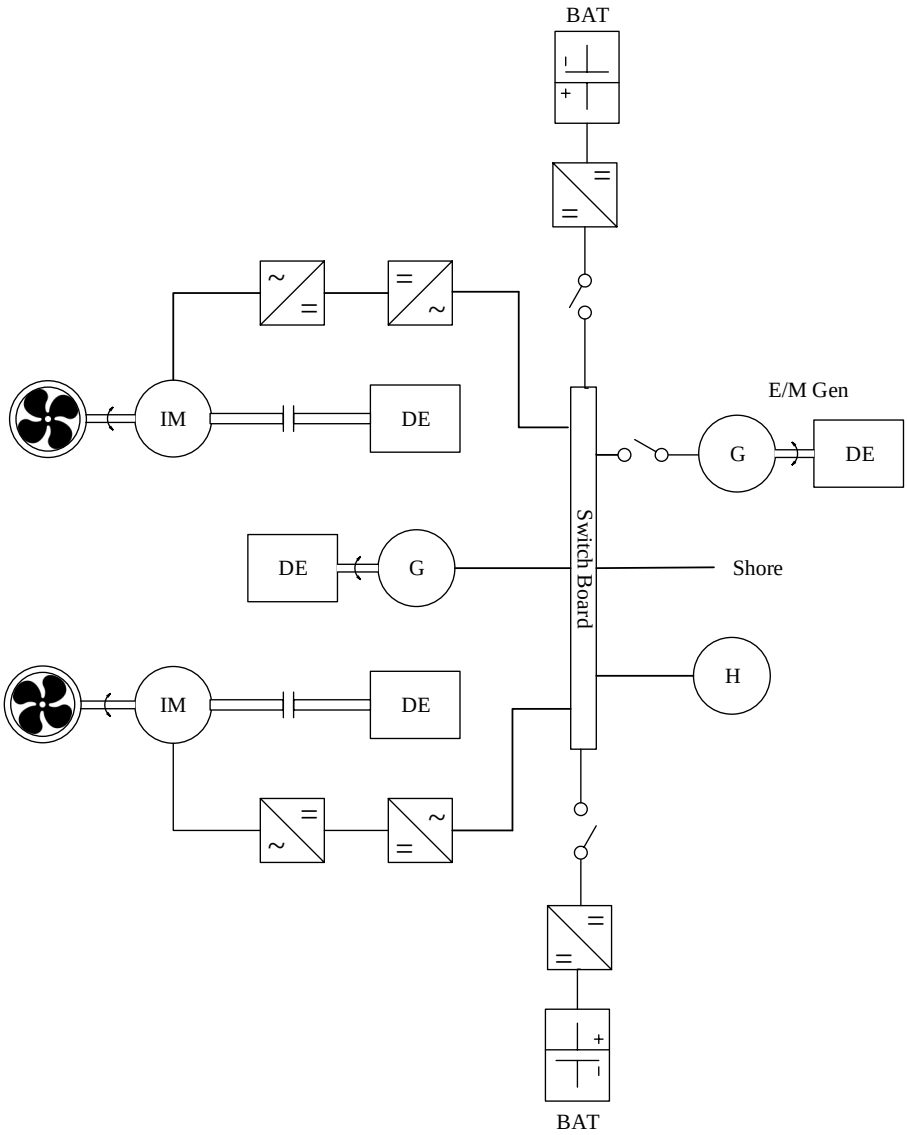

Figure 4.2: Propulsion System Layout.

The tugboat is 28 meters long and 10 meters wide, with a displacement of about 600 tons. As can be seen from Figure 4.2, the system consists of two battery packs of 120 kWh each, an 800kVA Diesel-generator set, two high-speed 4-stroke Diesel engines with a combined power of 3680 kW (4935 hp) at 1600 rpm, and two main electric engines (induction machines) of 230 kW each. The main engines are capable of propelling the

vessel up to 13 knots, with a maximum bollard pull of around 60 tons.

The presence of the induction machines allows for the coupling of both chemical and electric power sources to propel the vessel or to generate power for the consumers of the grid, whereas the presence of the battery packs allows for energy storage and the future use of it. The question that arises is when to use the energy stored in them and when to replenish it, so as to achieve the lowest possible fuel consumption while the system is in operation.

4.1.3. CONCEPTUAL SYSTEM MODELS

The conceptual models that will be used in this work are schematically shown in block diagram form in Figures 4.3 - 4.5. According to Figure 4.3, the EMS controller (the development of which is the main goal of this project) will receive feedback regarding the state of the electrical and propulsion systems, and depending on the power demand from the operator and grid consumers, will distribute the power accordingly among the available power sources. Its structure will be discussed in detail in Chapter 5.

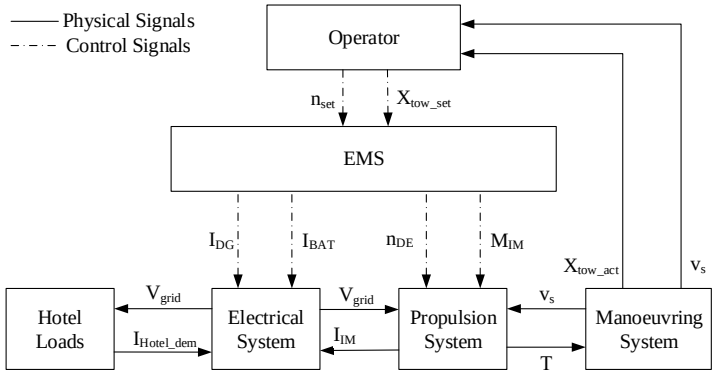

Figure 4.3: Causality Graph: Complete Vessel Model.

The command system block involves the 'simulation' of the operator's behavior. In essence, it consists of two feedback loops with respect to the vessel's speed and towing force, which are translated into shaft rotational speed and the next towing force setpoint. In the 'Hotel Loads' subsystem, a kind of on/off logic for the load steering pumps and the cooling water system has been coded which, in addition to other constant loads, constitute the electric power demand of the vessel. The maneuvering system block is responsible for the translation of the thrust provided by the system to vessel's speed and bollard pull by means of the Kijima maneuvering model [Kijima and Nakiri, 2003], which is a method to determine the hull's hydrodynamic masses and mass moments of inertia of the vessel, based on basic vessel parameters (such as length, beam, draft and block coefficient). Then, the hull forces are determined and translated into vessel speed and bollard pull by means of the motion equations. Note that the model is confined to the longitudinal direction of the vessel only, as only this direction of motion will be considered in this work (the maneuvering system had been already modeled by the Research

& Development department of Damen Shipyards Group prior to the commencement of this project).

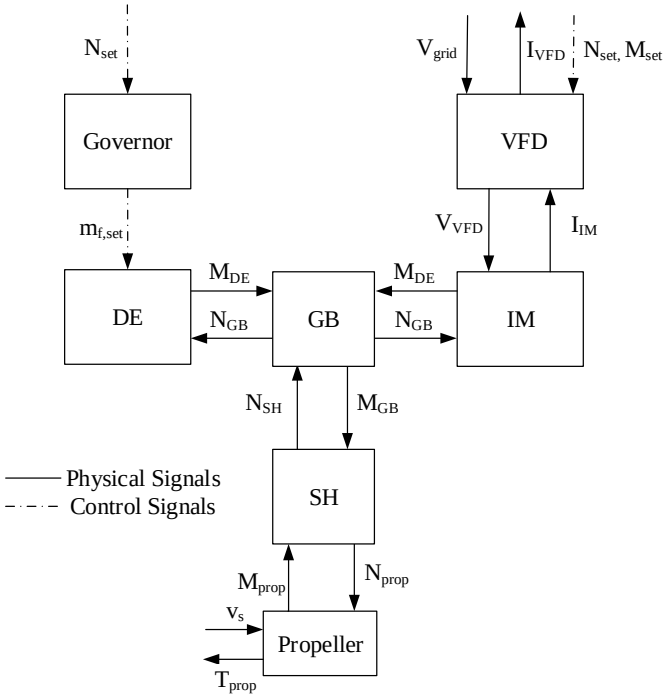

Figure 4.4: Causality Graph: Propulsion System.

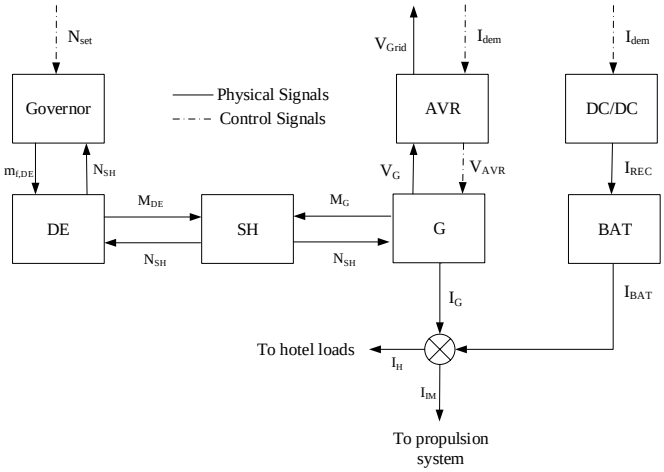

Figure 4.5: Causality Graph: Electrical System.

In Figures 4.4 - 4.5, the block diagrams of the vessel's propulsion and electrical systems are presented, along with the linking variables between the different sub-models. The sub-model boundaries and their input-output relations were chosen based on the functional relations between the models, and in such a way so as to facilitate the analysis of each sub-model individually, without being coupled to the other models. The propulsion system model (Figure 4.2) consists of the models for the prime movers, i.e. Diesel Engines (DE) and Induction Machines (IM) (including low level control systems for those), Shaft (SH) and Gearbox, the Shaft Rotational Dynamics block, and the Propellers. Finally, the electrical system model (Figure 4.5) consists of the Diesel - generator set (D/G), inverter - rectifier models, and the battery packs.

4.1.4. VALIDITY OF THE SIMULATION MODEL

After the development and programming of the conceptual models, the resulting (complete) simulation model must be verified, calibrated and validated.

4.1.4.1. VERIFICATION

The objective here is to show that the model results comply with theoretical process knowledge, i.e. that the simulation produces results that are equal (or similar) to analytical or otherwise known solutions. [Schulten and Stapersma, 2007, Oberkampf et al., 2004]. The problem that occurs at this point is that analytical solutions for complex, non-linear systems are generally hard to derive [Vrijdag et al., 2009], although (as will be shown in the next sections) numerical solutions for individual sub-models of the propulsion and electrical systems could be obtained, due to their limited complexity.

However, considering the difficulty of a formal verification process, and that the scope of this work is not to develop a highly accurate model, but rather to investigate the advantages that a sophisticated propulsion control system entails compared to a baseline model, it could be argued that complete validation is not absolutely necessary. As such, a less formal, simplified, verification was performed, where the results of each individual sub-model were checked against the general expectations of the author (trend-line resemblance etc), before they were connected with each other. As this was an ongoing process throughout the programming phase, specific results will not be shown here. Finally, as the dynamic behavior of the system is also of importance, it was verified against some characteristic accelerations and decelerations. The results are shown in Section 4.12.

4.1.4.2. CALIBRATION

Calibration of the model parameters is necessary to improve the agreement between computational results and experimental data/measurements, or supplier information Thacker et al. [2004]. In this project, the sub-models of all the components of the system were calibrated individually, as will be shown in the rest of this chapter. For each sub-model specific inputs were enforced, and the model's parameters were calibrated so as to get sufficient agreement for the variables that are chosen as outputs. In all the cases, the number of independent variables (parameters) of the models are more than the number of independent output signals. Therefore, the tuning of the parameters could result in an infinite number of combinations that all result in the same output.

As such, the strategy proposed in [Schulten and Stapersma, 2007] was applied: First, all the parameters that are known from an external source are set to their value (the so called *known parameters*. Secondly, from the remaining set of parameters, a few are set to a probable and logical value that may be known from knowledge obtained during the verification phase (*set parameters*) and, finally, the rest of the parameters are used to actually match the model output to a known output (*matched parameters*). If the required agreement cannot be reached for reasonable settings of the parameters, the conceptual models should be reconsidered through re-analysis of reality [Vrijdag et al., 2009]. This might possibly lead to adjustment of the conceptual model and re-programming of parts of the simulation model (In this work, adjustment of the sub-models of the Diesel engines and the induction machines was deemed necessary to obtain satisfactory accuracy).

Although it has not been performed in this project, it should be pointed out that apart from the sub-model calibration, the complete model might also need re-calibration of the parameters. It would be expected that the complete model would give the same level of agreement between simulation and reality as the obtained sub-model calibration results. However, this is not necessarily true due to error propagation between the sub-models. A simple but powerful example on error propagation in simulations can be found in the work of [Vrijdag et al., 2009].

4.1.4.3. VALIDATION

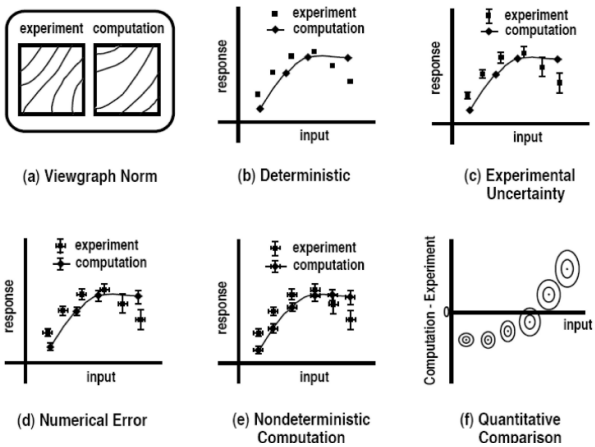

Figure 4.6: Validation Quality [Oberkampf et al., 2004].

A perfectly calibrated model is almost impossible to obtain regardless of the quality of the measurements of the necessary variables, because a simulation model can never capture all the phenomena that are of influence to the propulsion system's performance. The quantification process of this error between simulation predictions and reality is the core of the validation procedure. In this work, focus has been given in the validation of steady state operating points for the complete vessel model.

Figure 4.6 (taken from [Oberkampf et al., 2004]), illustrates different validation procedures of increasing quality, starting (a) from simple side-by-side comparison of contour plots, up to (e) and (f), where validation results include uncertainty information in measurements and simulation results, in both inputs and outputs of the model. In general, quality assessment of steady model behavior lies between levels (c) and (d), however in this work the second (b) type of validation has been performed, known as *deterministic validation*. Simulation results have been compared with measurements or supplier information without showing extra information on the uncertainty intervals. It should be stressed that validation of the dynamic behavior of the model has not been performed, due to lack of measurements (measured time-histories) of the vessel's dynamic response.

4.1.4.4. CONCLUSIONS

As will be seen in the following sections, the simulation model has been partially verified and validated qualitatively, using simplified procedures. When a highly accurate representation of reality is deemed necessary, uncertainty and sensitivity analysis are the next steps, so as to enable an objective quality assessment of the simulation, and a more founded appreciation of model - measurement comparisons. From there, the focus on further model improvements can be determined. For the interested reader, informative examples can be found in the works of [Vrijdag et al., 2009, Schulten and Stapersma, 2007, Vrijdag, 2014, Du and Chen, 2002].

4.2. DIESEL ENGINE

4.2.1. INTRODUCTION

As stated in Section 2.5.2, for the scope of this work focus will be given only on the average dynamic performance of the Diesel engine. As such, a third-order MVFP model will be used to simulate the main engines, developed by [Geertsma et al.], and the interested reader is referred there for a comprehensive analysis and validation results.

4.2.2. MODEL DESCRIPTION & RESULTS ANALYSIS

In brief, a PID controller and a time delay represent the governor and fuel pump of the engine, accounting for the pump's inertia and ignition delay. The six-point Seiliger process is used to determine the work produced per cycle along with the relevant gas properties, and the turbocharger is modeled on the basis of the Büchi balance.

After an extensive calibration of all the model parameters, it was evident that the model could accurately capture the behavior of the engine on the upper half of its operating envelope, however the results for loads lower than that were not satisfactorily accurate. In more detail, simulation results against measurements regarding the specific fuel oil consumption of the engine, demonstrated in Figure 4.7, show absolute errors of the order of magnitude of less than 5% between 50% to 100% of the nominal point, but for lower loads the model increasingly overestimates the specific fuel consumption, with error values ranging between 10% to 45% near the minimum rotational speed of the engine.

For the scope of this work however, equally important is the accurate representation of the engine's operation down to 5% load, as the fuel consumption of the main engines

is one of the primary states of the propulsion system that are going to influence the decisions taken by the EMS controller that will be designed later on. As such, it was deemed necessary to introduce a few modifications to the model, so as to increase its accuracy during part-load conditions.

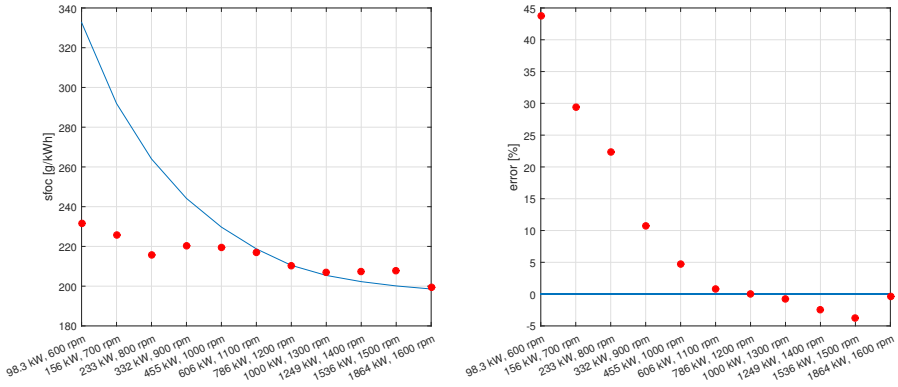

Figure 4.7: Diesel Engine Fuel Consumption.

4.2.3. MODEL EXTENSIONS

As already pointed out in [Geertsma et al.], two limitations of the existing model include (1) the assumption that mechanical losses are linearly dependent on the rotational speed of the engine, and as such are independent of engine load, and (2) that the heat lost to the cylinders which, as discussed in the same work, it could be greater than what the model accounts for. Taking these considerations into account, the following extensions were introduced to the model:

4.2.3.1. MECHANICAL LOSSES

In the work of [Chen and Flynn, 1965] it has been identified that mechanical (friction) losses can be accurately predicted as a function of mean piston speed and mean effective pressure (which is directly related to the engine's load). For practical reasons, more convenient would be the correlation of friction losses to primary parameters of the engine, such as engine's rotational speed and pressure at a distinct point of the Seiliger process.

The correlation with rotational speed is fairly straightforward considering that the mean piston speed is directly proportional to rotational speed:

$$c_m = 2nL_s \propto n \tag{4.1}$$

with:

n : Engine rotational speed [Hz]
L_s : Stroke Length [m]

[1] Courtesy of *Damen Shipyards Group.*

Taking into account available data, a general power-loss-due-to-friction curve was obtained (shown in Figure 4.8), from which it can be deduced that torque losses can be accurately predicted as a quadratic function of the engine's rotational speed.

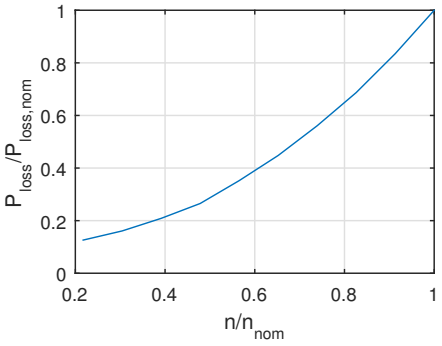

Figure 4.8: Power Loss due to Friction [1].

The connection between friction losses and pressure, on the other hand, is not as simple. In order to identify it, the Seiliger process must be analyzed in more detail. Primarily for reasons of simplicity, the ideal 5-point Seiliger (or dual combustion) cycle will be considered, shown in Figure 4.9. It is a combination of the Otto and the Diesel cycle, as heat is added partly at constant volume and partly at constant pressure, thus allowing for extra time for the fuel to combust.

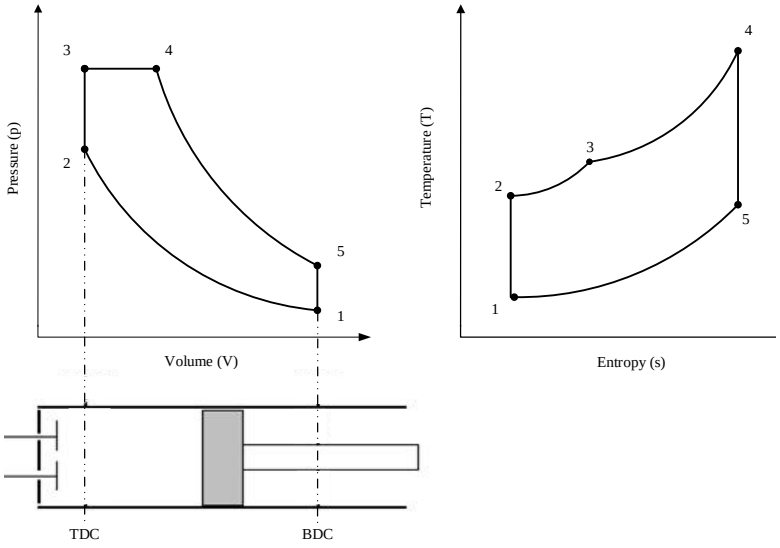

Figure 4.9: 5-point Seiliger Cycle.

The process description is given below:

1 → 2 : Adiabatic compression
2 → 3 : Heat addition at constant volume
3 → 4 : Heat addition at constant pressure
4 → 5 : Adiabatic expansion
5 → 1 : Heat rejection at constant volume

Adiabatic compression (1 → 2):

$$r_c = \frac{v_1}{v_2} = \left(\frac{p_2}{p_1}\right)^{\frac{1}{\gamma}} = \left(\frac{T_2}{T_1}\right)^{\frac{1}{\gamma-1}} \tag{4.2}$$

Heat addition at constant volume (2 → 3):

$$q_{2\to3} = c_v\,(T_3 - T_2) \tag{4.3}$$

$$\alpha = \frac{p_3}{p_2} = \frac{T_3}{T_2} \tag{4.4}$$

Heat addition at constant pressure (3 → 4):

$$q_{3\to4} = c_p\,(T_4 - T_3) \tag{4.5}$$

$$\beta = \frac{v_4}{v_3} = \frac{T_4}{T_3} \tag{4.6}$$

Adiabatic expansion (4 → 5):

$$\left(\frac{T_5}{T_4}\right)^{\frac{1}{\gamma-1}} = \frac{v_4}{v_5} = \frac{v_4}{v_3}\frac{v_3}{v_5} \overset{\text{Fig. 4.9}}{=\!=} \frac{v_4}{v_3}\frac{v_2}{v_1} = \frac{\beta}{r_c} \tag{4.7}$$

Heat rejection at constant volume (5 → 1):

$$q_{5\to1} = c_v\,(T_5 - T_1) \tag{4.8}$$

Net work per cycle:

$$w_{net} = q_{2\to3} + q_{3\to4} - q_{5\to1} \tag{4.9}$$

Mean effective pressure:

$$\begin{aligned} p_{me} &= \frac{w_{net}}{v_s} = \frac{q_{2\to3} + q_{3\to4} - q_{5\to1}}{v_1 - v_2} = \\ &= \frac{p_1 r_c}{(\gamma-1)(r_c-1)}\left(r_c^{\gamma-1}\left((\alpha-1) + \gamma\alpha\left(\beta-1\right)\right) - \left(\alpha\beta^{\gamma}-1\right)\right) \end{aligned} \tag{4.10}$$

From Equation (4.10) it can be seen that the mean effective pressure is directly proportional to the cycle's maximum pressure p_3, through the pressure ratio α. As such, correlating torque losses due to friction to the maximum pressure of the Seiliger process, instead of the mean effective pressure should, in theory, produce the same effect.

As such, mechanical torque losses can be expressed as follows:

$$M_{\text{fr.loss}} = a + bp_3(t) + cn(t) + dn(t)^2 \tag{4.11}$$

4.2.3.2. HEAT LOSS IN THE CYLINDER

According to the primer of [Heywood et al., 1988], several variables affect the magnitude of the heat flux to the different surfaces of the engine combustion chamber, including engine speed, engine load, overall equivalence ratio, compression ratio, spark or injection timing, swirl and squish motion, mixture inlet temperature, coolant temperature and composition, wall material and wall deposits. Of all these variables, engine speed, load and equivalence ratio have the greatest effect, and will be the focus of the analysis that follows:

Neglecting radiative heat, the overall heat transferred to the cylinders over a complete cycle is given by Equation (4.12):

$$\dot{Q}_{\text{loss}} = \int_0^{360\kappa} \sum_{i=1}^{3} \left(h_i\left(\phi, x\right) A_i\left(\phi, x\right) \left(T_{\text{gas}}\left(\phi, x\right) - T_{\text{wall}}\left(\phi, x\right) \right) \right) d\phi \tag{4.12}$$

where:

$i = 1,2,3$: index referring to cylinder wall, piston head, valves
h_i : Heat transfer coefficient $[W/m^2K]$
A_i : Surface exposed to the gas $[m^2]$
ϕ : Crank-angle [deg]
x : Position along the cylinder wall

Assuming that heat is lost only on the cylinder walls, Equation (4.12) can be reduced to:

$$\dot{Q}_{\text{loss}} = \int_0^{360\kappa} h_{\text{wall}}\left(\phi, x\right) A_{\text{wall}}\left(\phi, x\right) \left(T_{\text{gas}}\left(\phi, x\right) - T_{\text{wall}}\left(\phi, x\right) \right) d\phi \tag{4.13}$$

Mean heat flux over a complete cycle:

$$\bar{q}_{\text{loss}} = \frac{\bar{\dot{Q}}_{\text{loss}}}{\bar{A}_{\text{wall}}} = \bar{h}_{\text{wall}}(x) \left(\bar{T}_{\text{gas}}(x) - \bar{T}_{\text{wall}}(x) \right) \tag{4.14}$$

Assuming that the heat transfer coefficient and the temperatures are uniformly distributed along the wall of the cylinder (independent of x):

$$\bar{q}_{\text{loss}} = \bar{h} \left(\bar{T}_{\text{gas}} - \bar{T}_{\text{wall}} \right) \tag{4.15}$$

with:

$$\frac{1}{\bar{h}} = \frac{1}{\bar{\alpha}_{g\to w}} + \frac{t_w}{\lambda_w} + \frac{1}{\bar{\alpha}_{w\to c}} \tag{4.16}$$

where:

t_w : Wall thickness [m]
λ_{wall} : Wall's thermal conductivity [W/mK]
$\bar{\alpha}_{g\to w}$: Convective heat transfer coefficient from gas to wall $[W/m^2K]$
$\bar{\alpha}_{w\to c}$: Convective heat transfer coefficient from wall to coolant medium $[W/m^2K]$

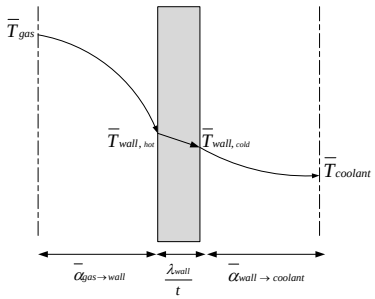

Figure 4.10: Temperature profile from gas via cylinder wall to coolant medium.

Assuming that the major part of the heat transfer takes place from gas to cylinder wall ($\alpha_{g\to w} \gg \bar{\alpha}_{w\to c} + \frac{\lambda_w}{t}$ according to Figure 4.10), it can be stated that $\bar{h} \approx \bar{\alpha}_{g\to w}$.

Following the same path as the works of [Woschni, 1965, Sitkei, 1962], the heat transfer phenomena from exhaust gas to cylinder wall can be thought of as turbulent convective heat transfer in a pipe. In such an analysis, Nusselt (Nu), Prandtl (Pr) and Reynolds (Re) numbers must be introduced:

$$Re = \frac{\rho_{\text{gas}}\, w D_H}{\mu_{\text{gas}}} \tag{4.17}$$

$$Pr = \frac{\mu_{\text{gas}}\, c_{\text{p,gas}}}{\lambda_{\text{gas}}} \tag{4.18}$$

$$Nu = \frac{\bar{\alpha}_{g\to w} D_H}{\lambda_{\text{gas}}} = c_1 Re^m Pr^n \tag{4.19}$$

where:

ρ_{gas} : Density of the gas inside the cylinder $[kg/m^3]$
w : Combustion velocity [m/s]
D_H : Hydraulic diameter of the pipe [m]
μ_{gas} : Dynamic viscosity of the gas in the cylinder [Pa s]
$c_{\text{p,gas}}$: Specific heat capacity at constant pressure of the gas [J/kgK]
λ_{gas} : Thermal conductivity of the gas in the cylinder [W/mK]

As Prandtl is only dependent on fluid properties, which considering the conditions of the gas in the cylinder, do not vary much, it can be assumed as a constant number. Therefore:

$$Nu = c_2\, Re^m \tag{4.20}$$

with m=0.7, considering the works of [Taylor, 1960, Annand et al., 1963].

Under the assumption that $D_H \approx D_b$ (D_b being the bore diameter), $w \approx c_m \propto n$, and perfect gas behavior ($pV = nRT$), it can be stated that:

$$Re \approx \frac{\bar{p}_{\text{gas}}\, c_{me} D_b}{\mu_{\text{gas}}} \overset{p_{\text{gas}} \approx p_3}{\propto} n p_3 \tag{4.21}$$

Considering Equations (4.13 -4.21) in reverse order:

$$Re \propto n p_3 \overset{(4.19)}{\underset{(4.20)}{\Longrightarrow}} \bar{\alpha}_{g\to w} \propto Nu \propto \left(n p_3\right)^{0.7} \overset{(4.15)}{\underset{(4.14)}{\Longrightarrow}} \bar{\dot{Q}}_{\text{loss}} = \bar{q}_{\text{loss}} A \propto \left(n p_3\right)^{0.7}\ [W] \tag{4.22}$$

Taking into account that the time available per cycle is inversely proportional to the rotational speed of the engine ($\frac{1}{n}$), for the heat lost to the cylinders per cycle the following applies:

$$\bar{\dot{Q}}_{\text{loss}} \propto \left(n p_3\right)^{0.7} \frac{1}{n} = p_3^{0.7} n^{-0.3} \Rightarrow \frac{\bar{\dot{Q}}_{\text{loss}}}{\bar{\dot{Q}}_{\text{loss,nom}}} \propto \left(\frac{p_3}{p_{3,\text{nom}}}\right)^{0.7} \left(\frac{n}{n_{\text{nom}}}\right)^{-0.3} \tag{4.23}$$

Equation (4.23) captures the effects of engine speed and load, but the effect of the equivalence ratio is still missing. This effect appears through the gas temperature ($\bar{T}_{\text{gas}}$) of the overall heat transfer and heat flux equations (4.12) - (4.15), which is proportional to the air-excess ratio λ (defined as the inverse of the equivalence ratio ϕ). According to [Heywood et al., 1988]:

> Peak heat flux occurs for mixture equivalence ratio equal to that for maximum power, and decreases as the equivalence ratio is leaned out or enriched from this value.

Considering Figure 4.11, it could be argued that the effect of the air-excess ratio could be approximately captured by a quadratic function, peaking at nominal conditions. As such, the following should apply for the air-excess ratio:

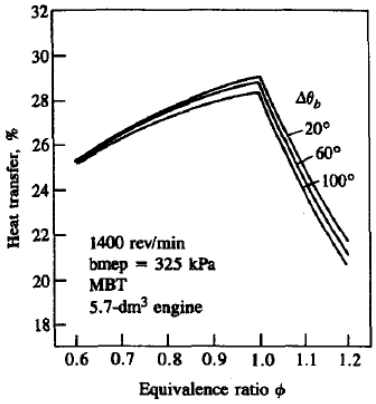

Figure 4.11: Predicted average heat-transfer rate to combustion chamber walls as a function of equivalence ratio (ϕ) and burn rate ($\delta\theta_b$) [Heywood et al., 1988].

$$f(\lambda) = -c_1\left(\frac{\lambda_{\text{nom}}}{\lambda}\right)^2 + c_2\left(\frac{\lambda_{\text{nom}}}{\lambda}\right) + c_3 \quad c_1, c_2, c_3 \in [0, +\infty) \tag{4.24}$$

$$\left.\frac{df(\lambda)}{d\lambda}\right|_{\lambda=\lambda_{\text{nom}}} = 0 \Rightarrow -2c_1 + c_2 = 0 \Rightarrow c_2 = 2c_1 \tag{4.25}$$

Finally:

$$\frac{\bar{\dot{Q}}_{\text{loss}}}{\bar{\dot{Q}}_{\text{loss,nom}}} \propto -c_1\left(\frac{\lambda_{\text{nom}}}{\lambda}\right)^2 + 2c_1\left(\frac{\lambda_{\text{nom}}}{\lambda}\right) + c_3 \quad c_1, c_3 \in [0, +\infty) \tag{4.26}$$

Combining the effects of Equations (4.23), (4.26), the following occurs:

$$\frac{\bar{\dot{Q}}_{\text{loss}}}{\bar{\dot{Q}}_{\text{loss,nom}}} \propto f = w_1\left(-c_1\left(\frac{\lambda_{\text{nom}}}{\lambda}\right)^2 + 2c_1\left(\frac{\lambda_{\text{nom}}}{\lambda}\right) + c_3\right) + w_2\left(\frac{p_3}{p_{3,\text{nom}}}\right)^{0.7}\left(\frac{n}{n_{\text{nom}}}\right)^{-0.3} \tag{4.27}$$

$$\eta_q = 1 - \left(1 - \eta_{\text{q,nom}}\right) f \tag{4.28}$$

with tunable parameters:

$c_1, c_3 \quad : \in (0, +\infty)$
$w_1, w_2 : \sum_{i=1}^{2} w_i = 1, \quad w_i \in [0, 1]$

4.2.4. CALIBRATION RESULTS

The introduction of the above modifications on the model and the calibration of the parameters, results in a considerable improvement in predicting the specific fuel consumption at part-load conditions. From Figure 4.12 it can be seen that the maximum error has a value of 8% and occurs for 5% of the nominal load of the engine. Equally important is the fact that fuel consumption maintained the same accuracy levels for higher loads ($> 50\% P_{\text{nom}}$) as before.

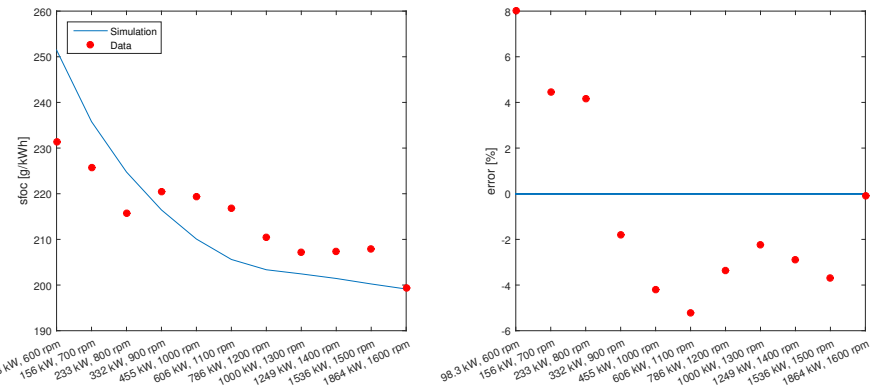

Figure 4.12: Diesel Engine Fuel Consumption - Improved Model.

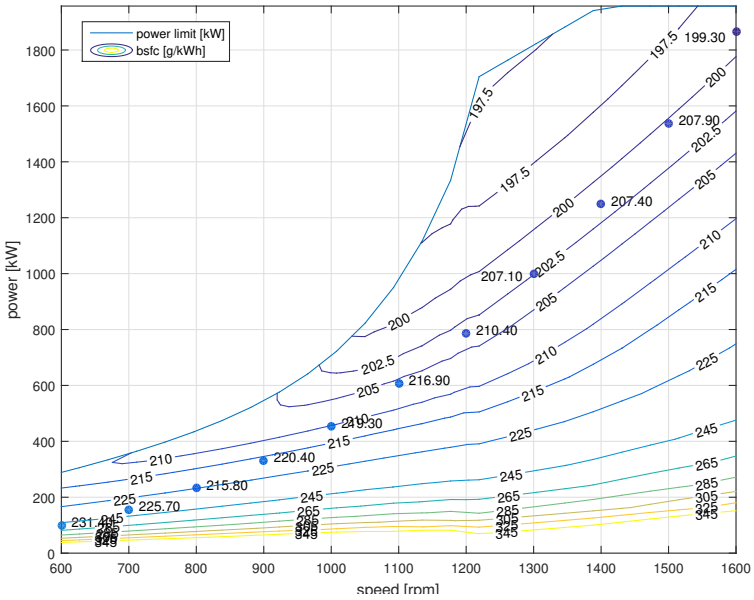

Figure 4.13: Diesel Engine Fuel Consumption - Improved Model.

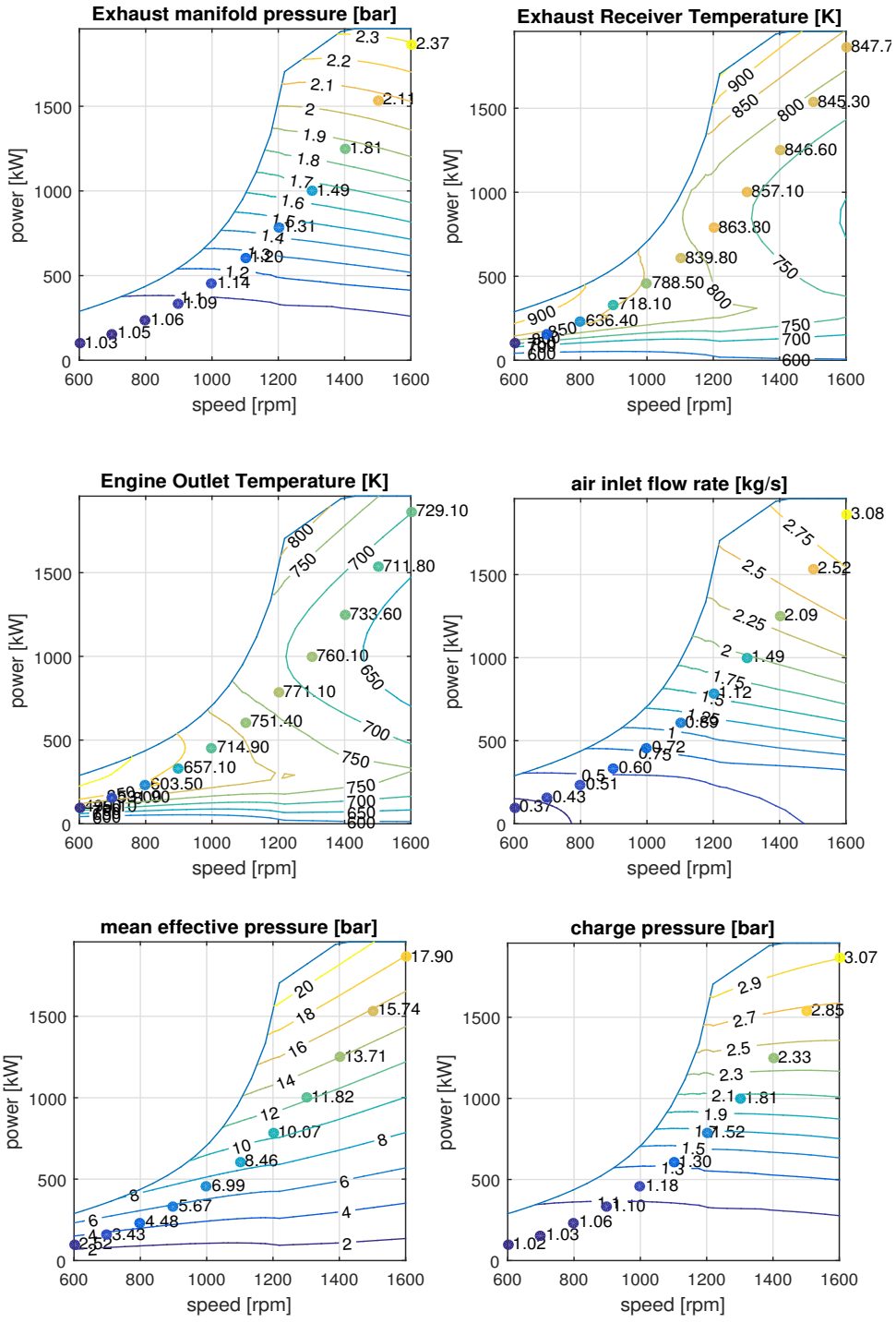

Figure 4.14: Diesel Engine Fuel Consumption - Improved Model.

4.3. INDUCTION MACHINE

4.3.1. INTRODUCTION

Although the traditional per-phase equivalent circuit (shown in Fig. 4.15) has been widely used in the steady-state analysis of induction motors, in adjustable speed drives the transient behavior of the machine is equally important. As such, for the scope of this work, a dynamic model has been developed to accurately represent both transient and steady-state conditions.

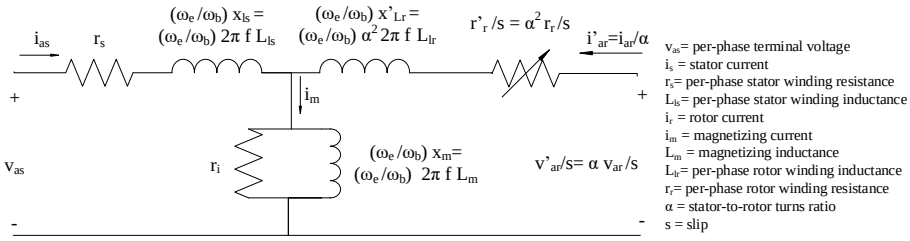

Figure 4.15: Induction Machine per-phase Equivalent Circuit [Ong, 1998].

4.3.2. MACHINE MODEL DESCRIPTION

4.3.2.1. PARK'S TRANSFORMATION

In the study of power systems, mathematical transformations are often used to decouple variables, to facilitate the solution of difficult equations with time-varying coefficients, or to refer all variables to a common reference frame [Sen, 2007]. In this work, a commonly-used transformation will be employed, to allow for the representation of a poly-phase machine in an arbitrary reference frame of two orthogonal phases (called d- and q- axes). Among electrical engineers it is known as Park's transformation, given by Equation (4.29).

$$\begin{bmatrix} \mathscr{F}_{qs} \\ \mathscr{F}_{ds} \\ \mathscr{F}_{0s} \end{bmatrix} = \frac{2}{3} \begin{bmatrix} \cos(\theta) & \cos(\theta - 2\pi/3) & \cos(\theta + 2\pi/3) \\ \sin(\theta) & \sin(\theta - 2\pi/3) & \sin(\theta + 2\pi/3) \\ 1/2 & 1/2 & 1/2 \end{bmatrix} \begin{bmatrix} \mathscr{F}_{as} \\ \mathscr{F}_{bs} \\ \mathscr{F}_{cs} \end{bmatrix} \tag{4.29}$$

In a similar way, inverting Park's transformation, the three-phase variables can be expressed in terms of their qd0 components:

$$\begin{bmatrix} \mathscr{F}_{as} \\ \mathscr{F}_{bs} \\ \mathscr{F}_{cs} \end{bmatrix} = \begin{bmatrix} \cos(\theta) & \sin(\theta) & 1 \\ \cos(\theta - 2\pi/3) & \sin(\theta - 2\pi/3) & 1 \\ \cos(\theta + 2\pi/3) & \sin(\theta + 2\pi/3) & 1 \end{bmatrix} \begin{bmatrix} \mathscr{F}_{ds} \\ \mathscr{F}_{qs} \\ \mathscr{F}_{0s} \end{bmatrix} \tag{4.30}$$

where:

$$\theta(t) = \int_0^t \omega(t)\,dt + \theta(0) \tag{4.31}$$

With θ being the transformation angle between the q-axis of the reference frame rotating at a speed ω and the a-axis of the stationary stator winding. $\mathscr{F}$ denotes any three-phase variable (current, voltage or flux linkage) of the machine. By setting the appro-

priate value for ω in Equation (4.31), the variables of the machine can be transformed into the required reference frame (Reference frames that will be referred to in the following sections include the stationary, rotary, and synchronously rotating, denoted by the superscripts *s,r* and *e* respectively.)

4.3.2.2. MACHINE MODEL ON THE ARBITRARY ROTATING REFERENCE FRAME

The mathematical model of the induction machine, along with its equivalent d and q axis is presented below. Note that, due to lack of data, magnetic saturation effects will not be considered in this work (for the interested reader, this topic is partially covered in the work of [Ong, 1998]).

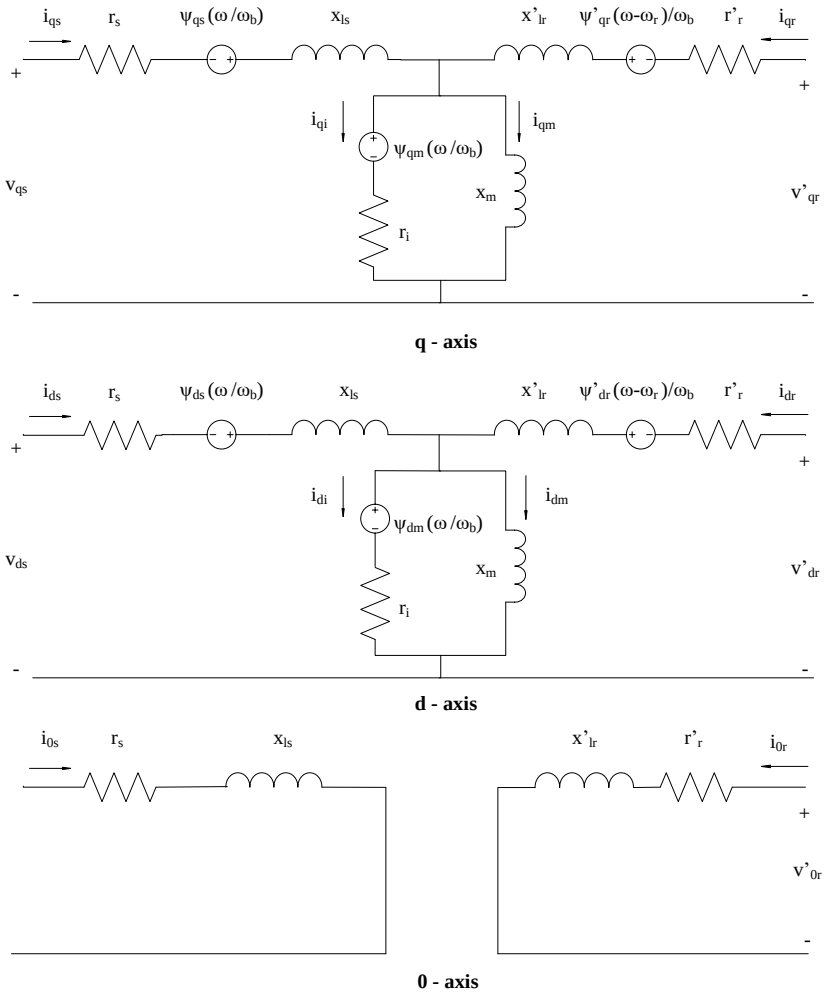

Figure 4.16: Induction Machine dq Equivalent Circuit on the Arbitrary Reference Frame.

Synchronous speed and slip:

$$\omega_{\text{s,mech}} = \frac{2}{P}\omega \tag{4.32}$$

$$N_s = \frac{60\omega_{s,mech}}{2\pi} = \frac{120 f_e}{p_p} \tag{4.33}$$

$$s = \frac{\omega_{s,mech} - \omega_r}{\omega_{\text{s,mech}}} \tag{4.34}$$

Stator and rotor voltage equations:

$$u_{qs} = \frac{d}{dt}\lambda_{qs} + r_s i_{qs} + \omega\lambda_{ds} \tag{4.35}$$

$$u_{ds} = \frac{d}{dt}\lambda_{ds} + r_s i^s_{ds} + \omega\lambda_{qs} \tag{4.36}$$

$$u_{0s} = \frac{d}{dt}\lambda_{0s} + r_s i_{0s} \tag{4.37}$$

$$u_{qr} = 0 = \frac{d}{dt}\lambda'_{qr} + (\omega - \omega_r)\,\lambda'_{dr} + r'_r i'_{qr} \tag{4.38}$$

$$u_{dr} = 0 = \frac{d}{dt}\lambda'_{dr} - (\omega - \omega_r)\,\lambda'_{qr} + r'_r i'_{dr} \tag{4.39}$$

$$u_{0r} = 0 = \frac{d}{dt}\lambda'_{0r} + r'_r i'_{0r} \tag{4.40}$$

Magnetic Branch Voltage Equations:

$$r_i i_{qi} = \frac{d}{dt}\lambda_{qm} + \omega\lambda_{qm} \tag{4.41}$$

$$r_i i_{di} = \frac{d}{dt}\lambda_{dm} + \omega\lambda_m \tag{4.42}$$

Stator and rotor flux linkages:

$$\lambda_{qs} = \lambda_{qm} + L_{ls} i_{qs} \tag{4.43}$$

$$\lambda_{ds} = \lambda_{dm} + L_{ls} i_{qs} \tag{4.44}$$

$$\lambda'_{qr} = \lambda_{qm} + L'_{lr} i'_{qr} \tag{4.45}$$

$$\lambda'_{dr} = \lambda_{dm} + L'_{lr} i'_{dr} \tag{4.46}$$

Mutual flux linkages:

$$\lambda_{dm} = L_m i_{dm} \tag{4.47}$$

$$\lambda_{qm} = L_m i_{qm} \tag{4.48}$$

Current Equations:

$$i_{ds} + i'_{dr} = i_{dm} + i_{di} \tag{4.49}$$

$$i_{qs} + i'_{qr} = i_{qm} + i_{qi} \tag{4.50}$$

Torque equation:

$$M_{em} = \frac{3}{2}\frac{p_p}{2}\left(\lambda_{dr}\left(i_{qs} - i_{qi}\right) - \lambda_{qr}\left(i_{ds} - i_{di}\right)\right) \tag{4.51}$$

where:

ω_r	: Rotor's rotational speed [rad/s]
ω	: Angular speed of the stator's mmf [rad/s]
N_s	: Synchronous speed [rpm]
s	: Slip [-]
p_p	: Number of poles of the machine
$u_{dq0,rs}$	: Stator and rotor voltages in the d- q- and 0- axes [V]
$r_{s,r}$	: Per phase stator and rotor winding resistance [Ω]
r_i	: Resistor that represents iron losses [Ω]
$\lambda_{dq0,rs}$	: Stator and rotor flux linkages in the d- q- and 0- axes [Wb turn]
$\lambda_{dq,m}$	: Mutual flux linkages in the d- q- axes [Wb turn]
L_{ls}, L_{lr}, L_m	: Per phase stator, rotor and mutual winding inductances [H]
$i_{dq0,rs}$	: Currents flowing in the stator and rotor windings in the d- q- and 0- axes [A]
$i_{dq,im}$	: Currents flowing in the iron loss and magnetizing branches [A]

In this work, the synchronously rotating reference frame has been chosen to model the induction machine (by substituting $\omega = \omega_e$ in the above equations), so as to speed up the simulation process. It is interesting to note that the induction machine was modeled in both stationary and synchronously rotating reference frames (purely for comparison purposes), with simulation times (for the complete vessel model) of 3 hours and 14 minutes for the stationary reference frame, and just 18 minutes(!) for the synchronously rotating reference frame. The drastic decrease in simulation time is attributed to the fact that in the synchronously rotating frame sinusoidal signals are not generated (and need not be controlled, as will be explained in the next section), as is the case for the stationary frame.

4.3.3. PARAMETER EXTRACTION

Parameters of the model that need to be identified are the stator and rotor winding resistances ($r_i, r_s, r_r^{'}$) and reactances ($x_m, x_{ls}, x_{lr}^{'}$). These can be easily calculated provided the results of a *no-load test, locked-rotor test* and measurements of the DC resistance of the stator winding are available, as shown in the textbooks of [Sen, 2007, Wildi et al., 2007, Chapman, 2005, Krause et al., 2013]. A brief overview of the tests is given below:

No-load test: Balanced three-phase voltages of rated frequency are applied to the stator windings, whereas the rotor is kept uncoupled from any mechanical load. As such, the machine's slip is exceedingly small and (referring to Figure 4.15) the value of $r_r^{'}/s$ is extremely high, making the value of the current on the rotor windings $i_r^{'}$ negligible.

Locked rotor test: Balanced three-phase voltages of rated frequency are applied to the stator, however the rotor is blocked, so as to prevent any rotation. In this case the slip is equal to one, $r_r^{'}/s = r_r^{'}$, and because $i_s \gg i_m$ the magnetizing branch can be neglected.

The resulting equivalent circuits of the induction machine for each of these tests are given in Figure 4.17 (in the stationary reference frame, and for $\omega_b = \omega_e$).

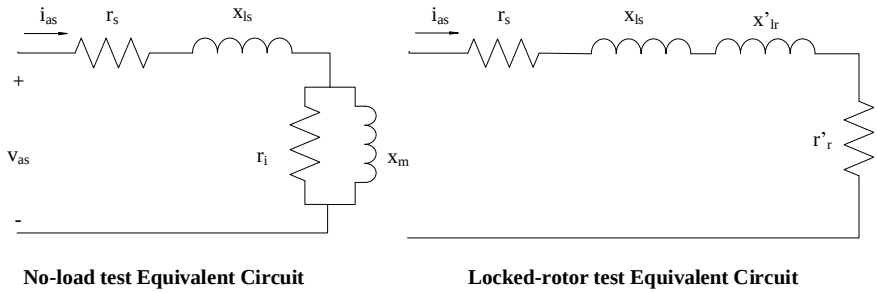

Figure 4.17: No-load and Locked-rotor Tests Equivalent Circuits.

Using the calculated parameters, the model is able capture manufacturer data with satisfactory accuracy, as shown in Figure 4.18. The maximum torque error is around 9% for the rated point, and 5.5% for the stator current. It should be pointed out that the nominal efficiency according to manufacturer data has a value of 95.5%, whereas the calculated one has a value of 95%.

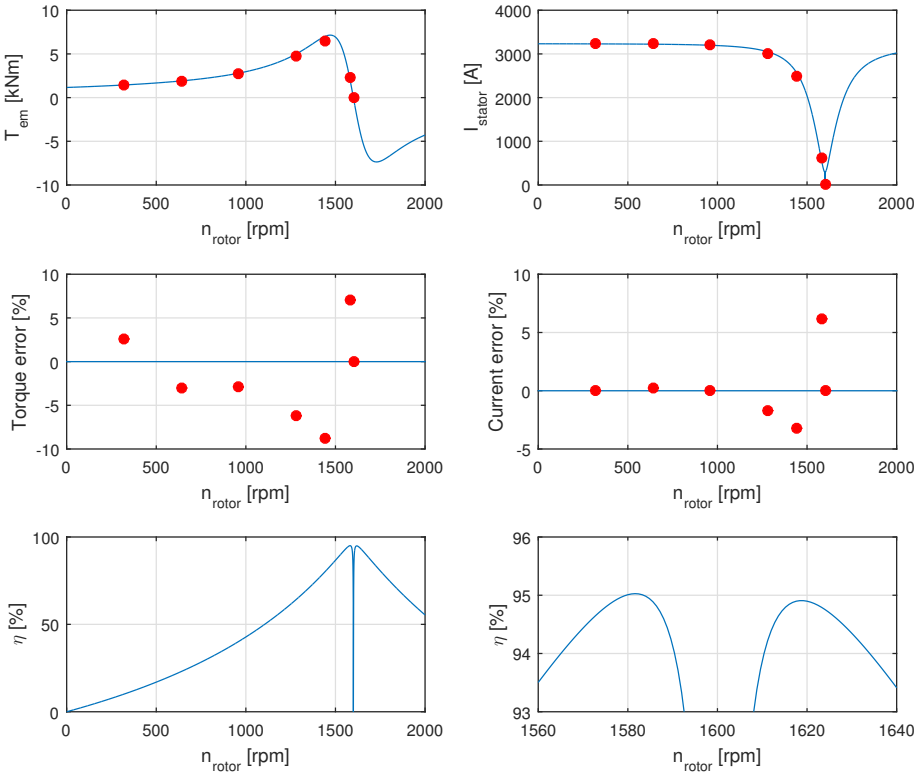

Figure 4.18: Induction Machine - Electromagnetic Torque and Stator Current.

4.4. ELECTRIC DRIVE

4.4.1. INTRODUCTION

An electric motor driving a mechanical load and the associated control equipment such as power converters, switches, relays, sensors and microprocessors, constitute an *electric drive system* [Trzynadlowski, 2000]. In such a system, the motor is being supplied with AC voltage from the grid by means of a variable frequency converter. For induction motors in adjustable speed applications, most commonly employed constituents of the converter are Pulse Width Modulation Voltage Source Inverters (PWM-VSIs) with full-wave (six pulse) diode rectifiers [Mohan and Undeland, 2007], a schematic is shown in Figure 4.19.

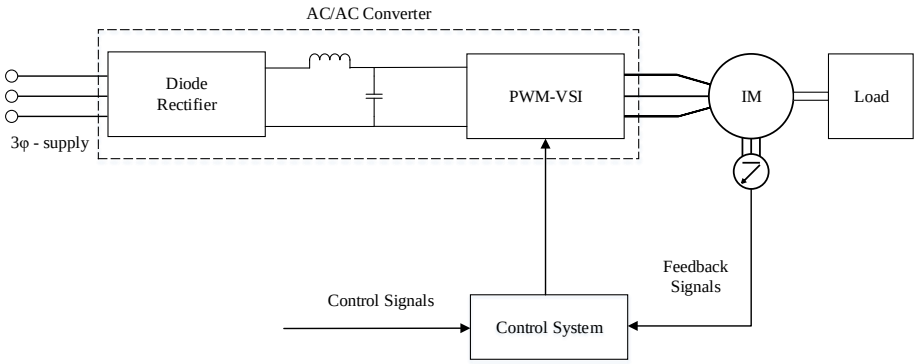

Figure 4.19: Block Diagram of a Variable Frequency Drive.

With a controlled inverter supply, the magnitude, frequency, and phase of the voltages applied to the machine can all be varied electronically. Provided that the inverter can handle bi-directional flow, the induction machine can be made to operate both in motoring and generating modes. The interested reader is referred to the primers of [Mohan and Undeland, 2007] and [Veltman et al., 2007, De Doncker et al., 2010] for detailed information regarding power electronics and electric drives. In general, induction machines can be controlled in many ways. Figure 4.20 presents the key competing VFD control platforms employed nowadays in induction machines, and for an extensive analysis the reader is referred to [Trzynadlowski, 2000].

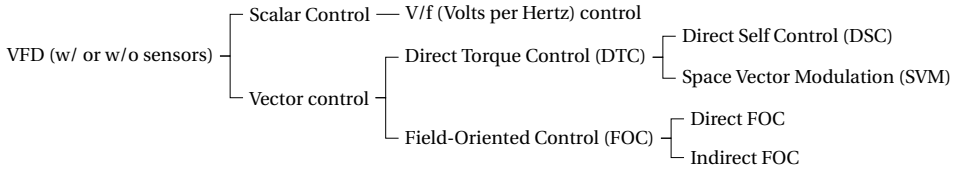

Figure 4.20: Overview of VFD Control Strategies.

In brief, the two main categories include scalar control and vector control methods. Scalar control methods precede vector control but are still used nowadays, mostly because of their simplicity and the small amount of motor data that is needed by the drive, which translate into lower costs and less wiring. On the other hand, scalar techniques present limitations due to the fact that the generation of the three sine wave voltages (by varying magnitude and frequency) are based on an equivalent model for the machine in steady-state. As such, the machine's characteristics are valid in steady-state only, which causes the control scheme to allow for high peak voltage and current transients, thus damaging the dynamic performance and power conversion efficiency of the machine. Moreover, scalar control looks more like three separate single-phase system controls rater than one control method of a three-phase system. This means that there is no consideration of the three-phase interactions (such as imbalance management) [Sen, 2007]. On the other hand, vector control solutions overcome all of these drawbacks, therefore improving the overall efficiency of the machine, along with its dynamic response.

4.4.2. FIELD ORIENTATION CONTROL

For the scope of this work, a control technique that belongs to the class of vector control will be used, known as *field-oriented control* (FOC). It was chosen over Direct Torque Control (DTC) because, although the core principles of the two are the same, DTC requires the modeling of the switches in the inverter, which could cause a substantial increase in simulation time.

The basic concept of FOC, proposed by Hasse in 1969 and Blaschke in 1972 [Trzynadlowski, 2000], is to orient the stationary or 'stator' flux vector to a specific degree relative to the rotor flux vector. The optimal degree of orientation depends upon what characteristic of the motor needs to be maximized. The most common use of FOC is to maximize the motor's *torque-per-ampere ratio*, so as to minimize losses in the motor and supply system for the complete operational profile. For induction machines this is achieved when the stator flux vector is 90 degrees perpendicular to the rotor's flux vector. As will be explained below, this orientation also allows for a completely independent (decoupled) control of the magnetic field and developed torque, which leads to a control structure similar to that of a separately excited DC machine, providing favorable control characteristics (more information on this topic can be found in the books of [Ong, 1998, Trzynadlowski, 2000]).

Furthermore, FOC controls the stator currents represented as vectors by their d- and q- coordinates, using Park's transformation (Section 4.3.2.1). The reliance of the control structure only on these current projections means that it can handle instantaneous electrical quantities, making it accurate under both transient and steady-state operation.

The idea becomes quite clear when one considers the torque equation of the induction machine (4.51), repeated below:

$$M_{em} = \frac{3}{2}\frac{p_p}{2}\left(\lambda_{dr}\left(i_{qs} - i_{qi}\right) - \lambda_{qr}\left(i_{ds} - i_{di}\right)\right)$$

It can be seen that torque includes the difference-of-products terms $\lambda_{dr}\left(i_{qs} - i_{qi}\right)$ and $\lambda_{qr}\left(i_{ds} - i_{di}\right)$. Now, if λ'_{qr} can be reduced to zero, the induction machine's operation would resemble that of a DC motor, where the mmfs established by the currents in the

armature and field windings produce no net interaction effect on one another. In this case torque would be reduced to:

$$M_{em} = \frac{3}{2}\frac{p_p}{2}\frac{L_m}{L_r'}\lambda_{dr}^{'e}\left(i_{qs}^{e} - i_{qi}^{e}\right) \tag{4.52}$$

The principles of field orientation are rather straightforward [Trzynadlowski, 2000] and presented below, along with a block diagram of the adopted control scheme is presented in Figure 4.21:

1. Calculation of the reference values for developed torque M_{em}^{*}, and magnetic flux $\lambda_{dr}^{'e*}$, given the control commands and the state of the induction machine.
2. From these reference values the corresponding reference components i_{qs}^{e*}, i_{ds}^{e*} of the stator current vector in the revolving reference frame can be calculated.
3. Given the stator current vector, the stator voltage vector can be calculated by means of a PI controller for each component of the vector.
4. The angular position, ρ, of the flux vector is determined in order to apply the transformation from the revolving to the stationary reference frame.
5. Finally, the transformation from the stator's vector reference frame (dqs) to the three-phase (abc) is applied in order to obtain the command values of the stator terminal voltages.

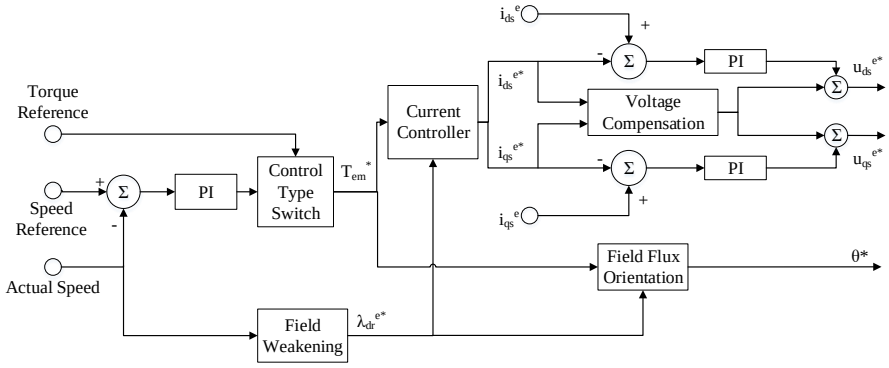

Figure 4.21: Block Diagram of Indirect FOC Scheme.

The new, reduced torque equation (4.52) shows that if $\lambda_{dr}^{'e}$ remains undisturbed, torque can be controlled by only adjusting the stator q- component current i_{qs}^{e} as follows:

$$i_{qs}^{e*} = \frac{M_{em}^{*}}{\frac{3}{2}\frac{p_p}{2}\frac{L_m}{L_r'}\lambda_{dr}^{'e}} + i_{qi}^{e} \tag{4.53}$$

This manipulation is feasible if a synchronously rotating dq0 reference frame is introduced, whose d-axis is aligned with the rotor field [Ong, 1998], so as to allow for λ'^{e}_{dr} to remain constant, via the adjustment of i^{e}_{ds}.

Continuing with $\lambda'_{qr} = 0$, from the rotor flux linkage and mutual flux linkage equations of the q- axis (4.45), (4.48), and the current balance of Equation (4.50), the q-axis rotor current component is determined:

$$i'^{e}_{qr} = \frac{\lambda'^{e}_{qr} - L_m\left(i^{e}_{qs} - i^{e}_{qi}\right)}{L'_r} \xrightarrow{\lambda'^{e}_{qr}=0} i'^{e}_{qr} = -\frac{L_m}{L'_r}\left(i^{e}_{qs} - i^{e}_{qi}\right) \tag{4.54}$$

Similarly, using the same equations for the d-axis (4.46), (4.47), (4.49), the d-axis rotor current component can be calculated:

$$i'^{e}_{dr} = \frac{\lambda'^{e}_{dr} - L_m\left(i^{e}_{ds} - i^{e}_{di}\right)}{L'_r} \tag{4.55}$$

With $\lambda'^{e}_{qr} = 0$ and $\lambda'^{e}_{dr} = \text{const}$, the q-axis rotor voltage equation (4.38), along with the equations for the rotor -d and -q current components (4.54) - (4.55) immediately yield the desired slip:

$$0 = r'_r i^{e}_{qr} + \cancelto{0}{\frac{d\lambda'^{e}_{qr}}{dt}} + (\omega_e - \omega_r)\,\lambda'^{e}_{dr} \Rightarrow \omega^{*}_{e} - \omega_r = -r'_r \frac{r'_r i^{e}_{qr}}{\lambda'^{e}_{dr}} \xrightarrow{(4.54)} \omega^{*}_{sl} = r'_r \frac{L_m}{L_r} \frac{i^{e*}_{qs} - i^{e}_{qi}}{\lambda'^{e*}_{dr}} \tag{4.56}$$

As such, the flux angle is:

$$\theta = \int \omega_e\, dt = \int (\omega_r + \omega_{sl})\, dt = \int \left(\omega_r + r'_r \frac{L_m}{L_r} \frac{i^{e}_{qs} - i^{e}_{qi}}{\lambda'^{e}_{dr}}\right) dt \tag{4.57}$$

Finally, substituting the d-axis rotor current component, as calculated by equation (4.55), in the d-axis rotor voltage equation (4.39), the rotor flux is obtained, from which the desired value of the stator d-axis current component i^{e*}_{ds} can be found:

$$0 = \cancelto{0}{\frac{d\lambda'^{e*}_{dr}}{dt}} - (\omega_e - \omega_r)\cancelto{0}{\lambda'^{e}_{qr}} + r'_r i'_{dr} \Rightarrow \lambda'^{e*}_{dr} = \frac{r'_r L_m}{r'_r + L'_r}\left(i^{e*}_{ds} - i^{e}_{di}\right) \tag{4.58}$$

Beyond the rated speed of the motor, the developed torque rapidly decreases toward its minimum value (which depends on the load torque profile). If it necessary to expand the speed of the machine beyond its rated value, the torque has to be reduced. A common method to achieve the desired torque reduction, is to reduce the magnetizing current of the motor, which produces the magnetizing flux (i.e. to weaken the magnetic field of the machine). In Figure 4.21 this takes place in the field-weakening block, which consists of a look-up table (shown in Figure 4.22) that matches the desired value of the rotor d-axis component flux λ'^{e*}_{dr} to the rotor's speed. For rotational speeds less than the rated speed, λ'^{e}_{dr} is set to be equal to the rated value (a region often called the *constant*

torque area), whereas beyond rated speed the flux reduction is proportional to the rotor's speed increase (*constant power area*), so as the product of torque and rotational speed to remain constant.

Finally, when considering the stator voltage equations (4.35) - (4.36) and flux linkage Equations (4.43) - (4.44) as shown in Equation 4.59, two extra feed-forward terms must be added to the voltage commands of the two PI controllers on the left side of Figure 4.21, so as to increase the performance of the control scheme [Ong, 1998]. This takes place in the voltage compensation block of Figure 4.21.

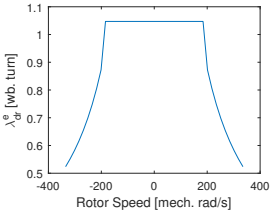

Figure 4.22: Field Weakening.

$$
\begin{aligned}
u_{ds}^{e*} &= r_s i_{ds}^e + \frac{d}{dt}\lambda_{ds}^e - \omega_e \lambda_{qs}^{e*} = r_s i_{ds}^{e*} + \frac{L_{lr}}{L_m} L_s \frac{d}{dt} i_{ds}^{e*} \overbrace{-\omega_e \frac{L_{lr}}{L_m} L_s i_{qs}^{e*} + \frac{L_m^2}{L_r}\frac{d}{dt} i_{ds}^{e*}}^{\text{Voltage compensation extra term}} \\
u_{qs}^{e*} &= r_s i_{qs}^e + \frac{d}{dt}\lambda_{qs}^e + \omega_e \lambda_{ds}^{e*} = r_s i_{qs}^{e*} + \frac{L_{lr}}{L_m} L_s \frac{d}{dt} i_{qs}^{e*} \underbrace{+\omega_e \frac{L_{lr}}{L_m} L_s i_{ds}^{e*} + \frac{L_m^2}{L_r}\frac{d}{dt} i_{ds}^{e*}}_{\text{Voltage compensation extra term}}
\end{aligned}
\tag{4.59}
$$

4.4.3. CALIBRATION RESULTS

The only way to assess the control system for the induction machine, is to examine the machine's response to torque loads and the related voltage modulations along with its efficiency, as shown in Figures 4.23 - 4.24.

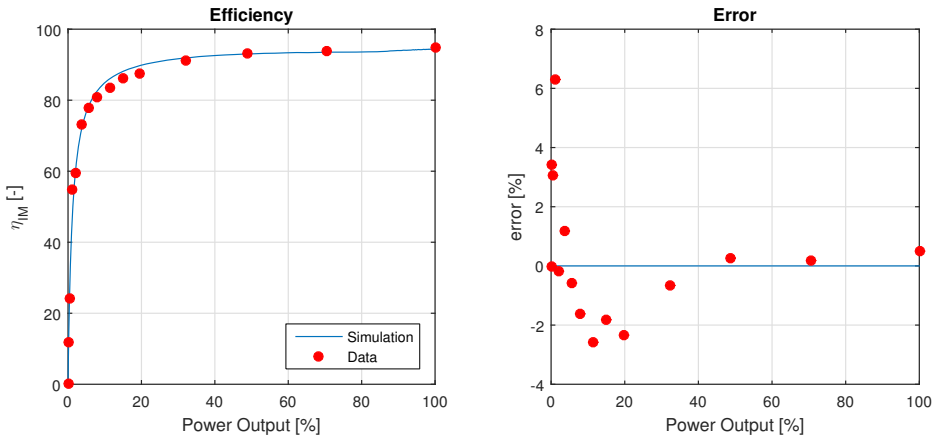

Figure 4.23: Induction Machine Efficiency.

As can be seen from Figure 4.24, the controlled induction machine presents a satisfying torque response in a step load input from zero to rated torque, with a settling time of approximately 0.002 seconds. Note that the lack of overshoot is a characteristic of rela-

tively large (in terms of power) induction motors, in contrast to smaller machines which present oscillatory torque response [Trzynadlowski, 2000]. Moreover, Figure 4.23, shows the efficiency of the induction machine, which is kept relatively high with the control system (higher than 80% for loads higher than 10% of the rated power), and is relatively accurate according to the data, presenting a maximum error of 6.2% for 4% of the machine's rated power output.

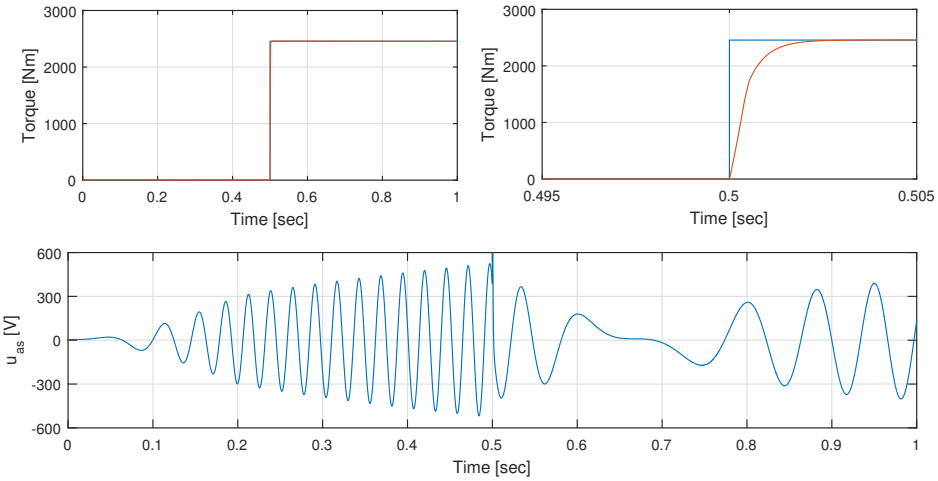

Figure 4.24: Controlled Induction Machine Response.

4.5. GEARBOX

4.5.1. INTRODUCTION

Since the performance of the gearbox is independent of any EMS (the losses will always be the same at a given state of the gearbox), a simple fitted model will be used, able to capture the power/torque losses of the gearbox. As such, the three approaches briefly described in Section 2.4.4 will be examined in more detail, so as to determine which one is able to describe the gearbox behavior most accurately.

4.5.2. MODEL DESCRIPTION

The core of the model is the conservation of energy:

$$\sum_i M_{i,in} = \sum_j M_{j,out} + M_{loss} \tag{4.60}$$

Each of the three different approaches of Section 2.4.4 gives a different equation regarding torque losses, with the nominal state of the gearbox for parameterization. In more detail:

Stapersma Model [Stapersma, 1994]:

$$M_{loss} = P_{loss,nom}\left(\alpha_1 \frac{M_{act}}{P_{nom}} + \alpha_2 \frac{M_{act}}{M_{nom}\omega_{act}} + \alpha_3 \frac{1}{\omega_{nom}}\right) \tag{4.61}$$

Drijver Model [Drijver, 2013]:

$$\frac{M_{loss}}{M_{loss,nom}} = \alpha_1 + \alpha_2 \frac{\omega_{act}}{\omega_{nom}} + \alpha_3 \left(\frac{\omega_{act}}{\omega_{nom}}\right)^2 + \alpha_4 \frac{M_{act}}{M_{nom}} \tag{4.62}$$

Geertsma Model [Geertsma, 2015]:

$$\frac{M_{loss}}{M_{loss,nom}} = \alpha_1 \frac{\omega_{act}}{\omega_{nom}} + \alpha_2 \left(\frac{\omega_{act}}{\omega_{nom}}\right)^2 + \alpha_3 \frac{M_{act}}{M_{nom}} + \alpha_4 \left(\frac{M_{act}}{M_{nom}}\right)^2 + 2\alpha_5 \frac{M_{act}}{M_{nom}} \frac{\omega_{act}}{\omega_{nom}} \tag{4.63}$$

with:

$$P_{loss,nom} = (1 - \eta_{nom}) P_{nom}$$
$$M_{loss,nom} = (1 - \eta_{nom}) M_{nom}$$
$$\sum_{i=1}^{N} \alpha_i = 1, \ \alpha_i \in [0,1]$$

where:

$\eta_{GB,nom}$: Nominal efficiency of the gearbox.
$P_{GB,nom}, M_{GB,nom}$: Nominal power and torque (equal to those of the main engine).

4.5.3. PARAMETER EXTRACTION

The parameters a to d of Equations (4.61) - (4.63) were calculated as the solution to a least-squares fitting problem, with the objective of minimizing the RMS error between torque losses predicted by the model and the measurements.

4.5.4. MODEL COMPARISON & CALIBRATION

The LSE estimation results for all three models can be found in Figure 4.25. It can be seen that the model of Stapersma gives a constant loss estimation with respect to the gearbox's rotational speed. This can be explained by the form of Equation (4.61). It can be seen that only one factor accounts for speed dependent losses $\left(\alpha_2 \frac{M_{act}}{M_{nom}\omega_{act}}\right)$, and it is inversely related to rotational speed. Given the constraint that $\alpha_i \geq 0$, α_2 must be automatically constrained to a zero value, so as not to give an opposite trend with respect to the measurements.

Regarding the last two approaches, both Geertsma's model and the fitted model based on the work of [Drijver, 2013] give approximately equal results, and both could be used for the gearbox simulation. Arbitrarily, the model based on the work of [Drijver, 2013] was chosen. Figure 4.26, shows that a maximum absolute error of 9.4% occurs for a rotational speed of 1400 rpm at 50% of the nominal torque.

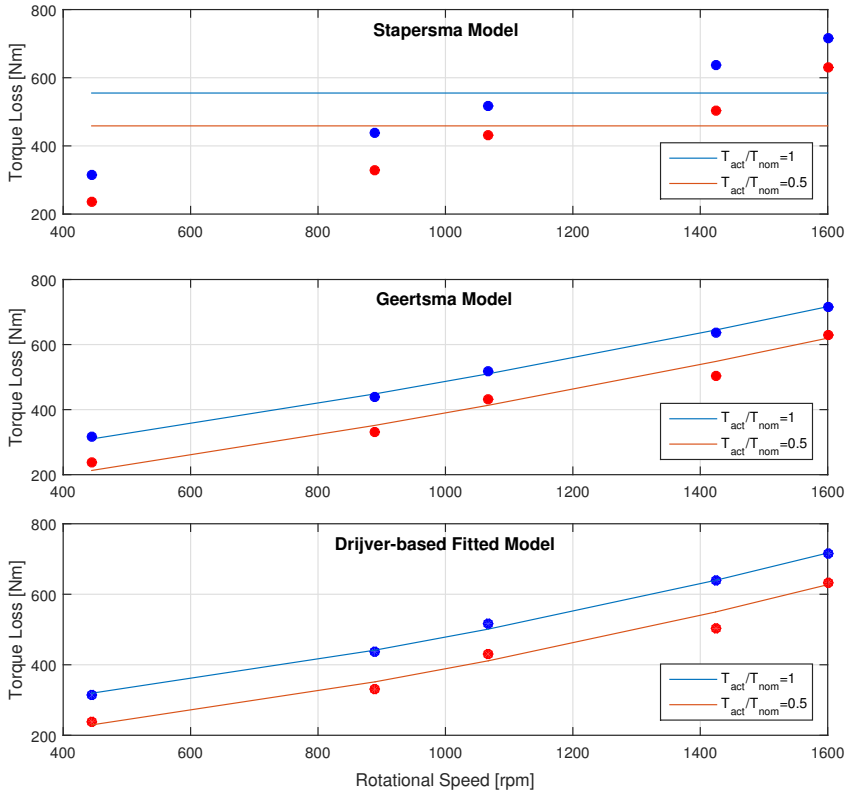

Figure 4.25: Gearbox Loss Models - Best Estimations.

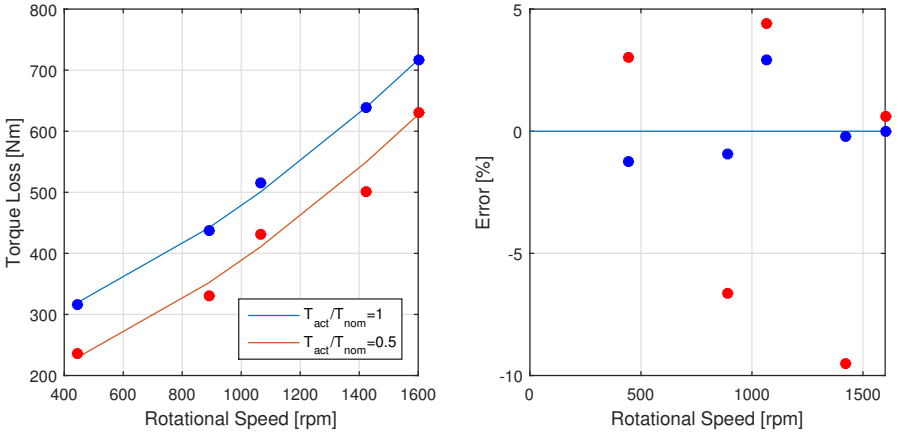

Figure 4.26: Gearbox Model Calibration Results.

4.6. PROPELLER

4.6.1. INTRODUCTION

As stated is Section 2.5.2, the Four-Quadrants diagram will be used for the simulation of the propellers, given in Figure 4.27 for the FPP of the reference tugboat.

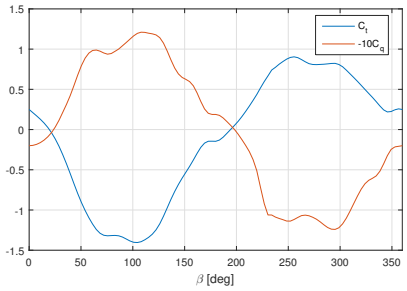

Figure 4.27: Four Quadrants Diagram.

4.6.2. MODEL DESCRIPTION

Based on the hydrodynamic pitch angle β the torque and thrust coefficients of the propeller can be determined from the four quadrants diagram, via the torque and thrust coefficients (C_T^*, C_Q^*) respectively.

Hydrodynamic Pitch Angle:

$$\beta = \arctan\left(\frac{v_A}{0.7\pi n_p D}\right) \tag{4.64}$$

Advance Velocity of the Propeller:

$$v_A = (1-w)\, v_S \tag{4.65}$$

Thrust & Torque Coefficients:

$$C_T^* = \frac{T_{prop}\,(1-t)}{\frac{1}{2}\rho\left(v_A^2 + (0.7\pi n_p D)^2\right)\frac{\pi}{4}D^2} \tag{4.66}$$

$$C_Q^* = \frac{M_{prop}}{\frac{1}{2}\rho\left(v_A^2 + (0.7\pi n_p D)^2\right)\frac{\pi}{4}D^3} \tag{4.67}$$

where:

v_S : Vessel Speed [m/s]
D : Propeller diameter [m]
n_p : Propeller rotational speed [Hz]
w : Wake factor [-]
t : Thrust deduction factor [-]

4.7. SHAFT ROTATIONAL DYNAMICS

The shaft rotational dynamics system is based on the difference between the torque delivered by the prime movers (after the losses on the gearbox have been accounted for) and the torque required by the propulsors. The difference between the two results in the rotational speed of the propeller shaft:

$$\sum_i M_i = I_{tot}\frac{d\omega}{dt} = I_{tot}\, 2\pi\frac{dn}{dt} \Rightarrow n = \int\left(\frac{1}{2\pi}\frac{M_{DE+IM} - M_{prop}}{I_{tot}}\right)dt \tag{4.68}$$

4.8. DIESEL GENERATOR

4.8.1. INTRODUCTION

The Diesel-generator set model consists of the prime mover - Diesel engine and its governor - and the synchronous generator, according to Figure 4.28.

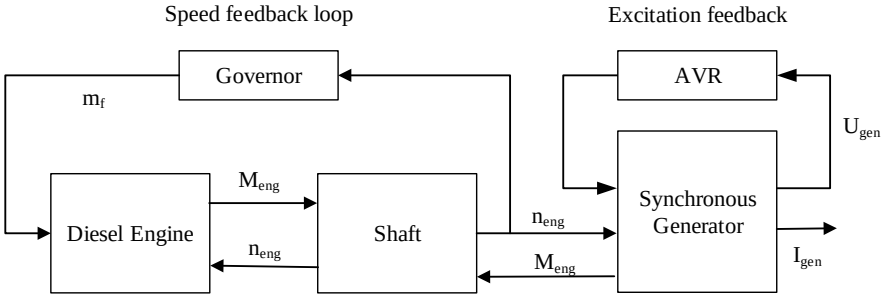

Figure 4.28: Schematic of the Diesel-generator set.

It should be noted that due to the modeling approach of the synchronous generator (steady-state model) the AVR system needs not be modeled.

4.8.2. MODEL DESCRIPTION

Simplified models have been adopted for all the components of the Diesel-generator set, by means of the "Mossel model" for the Diesel engine, a PID controller for its governor, and an equivalent circuit model for the synchronous generator.

4.8.2.1. DIESEL ENGINE & GOVERNOR

Prof. D. Stapersma's "Mossel model" for the Diesel engine allows for a simplified calculation of the torque delivered by the Diesel engine, as a function of its rotational speed and per-cycle fuel injection, according to Equation (4.69), where a,b,c,d and e are the Mossel model parameters that need to be determined [2]:

$$\frac{M}{M_{nom}} = 1 - a\left(1-n^*\right) + b\left(1-n^*\right)^2 - c\left(1-\dot{m}_f^*\right) + d\left(1-\dot{m}_f^*\right)^2 + 2e\left(1-n^*\right)\left(1-\dot{m}_f^*\right) \tag{4.69}$$

Considering that if the synchronous generator is connected to the grid, its operational frequency (which is directly proportional to the rotational speed of the engine) typically varies in the range of ±5% of the rated frequency [Patel, 2012]. As such it has been assumed that the Diesel engine operates approximately at nominal speed. Therefore, Equation (4.69) can be reduced to:

[2] The superscript * in this context denotes normalized values.

$$\left.\frac{M}{M_{nom}}\right|_{n=n_{nom}} = 1 - c\left(1 - \dot{m}_f^*\right) + d\left(1 - \dot{m}_f^*\right)^2 \tag{4.70}$$

Finally, a PID controller has been used to function as the engine's governor.

4.8.2.2. SYNCHRONOUS GENERATOR

For the generator, a steady-state model has been used, based on its per-phase equivalent circuit (Figure 4.29), as the dynamics of the generator are not of importance for the scope of this work. Instead focus will be given on its losses. The state of the generator at any given time is calculated on the basis of current request from the network and the Diesel engine's rotational speed. Through the generator model, these are being converted into a torque demand towards the diesel engine, and the voltage that the generator delivers to the network.

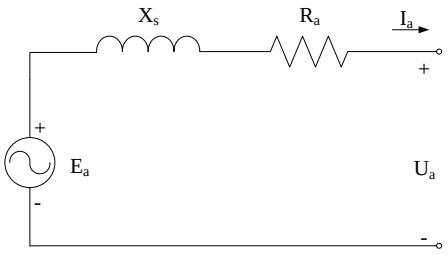

Figure 4.29: Synchronous Generator per-phase Equivalent Circuit [Sen, 2007].

It is assumed that the instantaneous per-phase voltage, and rotational speed can be represented as follows:

$$U_{a,nom} = \frac{U_{line}}{\sqrt{3}} \tag{4.71}$$

$$\omega_{e,nom} = \omega_{m,nom}\frac{p_p}{2} \tag{4.72}$$

$$U_a = U_{a,nom}\frac{\omega_e}{\omega_{e,nom}} = U_{a,nom}\frac{\omega_m}{\omega_{m,nom}} \tag{4.73}$$

where:

p_p : Number of poles of the generator [-]
ω_m : Rotational speed of the Diesel engine [Hz]

Generator losses consist of friction losses and copper losses. As such, the mechanical power input to the generator and the electrical power delivered to the network are calculated as follows:

$$P_{el} = 3U_a I_a \cos(\phi) \tag{4.74}$$

$$P_{loss} = \underbrace{P_{mech,nom}\, c_f}_{\text{Friction Losses}} + \underbrace{|I_a|^2 R_a}_{\text{Copper Losses}} \tag{4.75}$$

$$P_{mech} = P_{el} + P_{loss} \tag{4.76}$$

$$M = \frac{P_{in}}{\omega_m} \tag{4.77}$$

where:

$P_{mech,nom}$: Mechanical power delivered to the generator at nominal conditions [W]
c_f : Friction factor (fraction of nominal power input turned into frictional losses) [-]
M : Torque request towards the Diesel engine [Nm]

4.8.3. PARAMETER EXTRACTION & CALIBRATION RESULTS

4.8.3.1. DIESEL ENGINE

Considering Equation (4.70), from two operating points of the Diesel engine at nominal speed, parameters c and d can be determined algebraically. According to the results (presented in Figure 4.30), maximum error of 4% in fuel consumption occurs for 10% of the nominal engine power output.

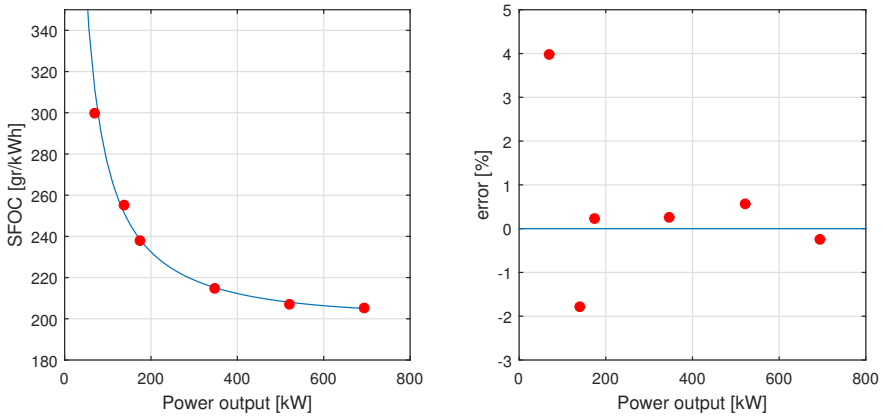

Figure 4.30: Calibration Results: Diesel-Generator Fuel Consumption at Nominal Speed.

4.8.3.2. SYNCHRONOUS GENERATOR

The parameters of the synchronous generator (namely the friction factor c_f and the per-phase stator winding resistance R_a) result from a least-squares error minimization strategy over all the available data, based on Equation (4.78):

$$\eta = \frac{P_{el}}{P_{mech}} \Rightarrow \frac{1}{\eta} - 1 = c_f \frac{1}{\eta_{nom}} + \frac{P_{el}}{\left(U_a cos(\phi)\right)^2} R_a \tag{4.78}$$

Validation results are presented in Figure 4.31. As can be seen the maximum error for the generator efficiency has a value of 0.8% at a power output of about 200 kW for a power factor of 1.

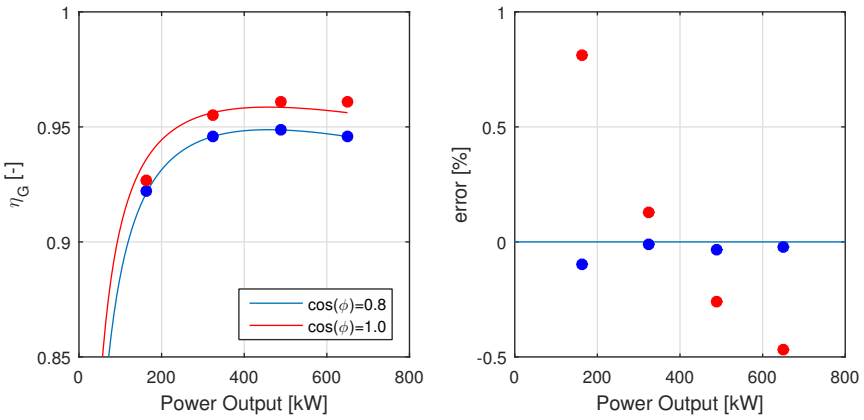

Figure 4.31: Calibration Results: Synchronous Generator Efficiency.

4.9. BATTERY

4.9.1. INTRODUCTION

As stated in section 2.5.2, a dynamic equivalent circuit model will be used (shown in Figure 4.32), able to capture accurately the voltage and current fluctuations depending on the power demand and the state of the battery, so as to obtain accurate predictions regarding the state of charge of the battery packs.

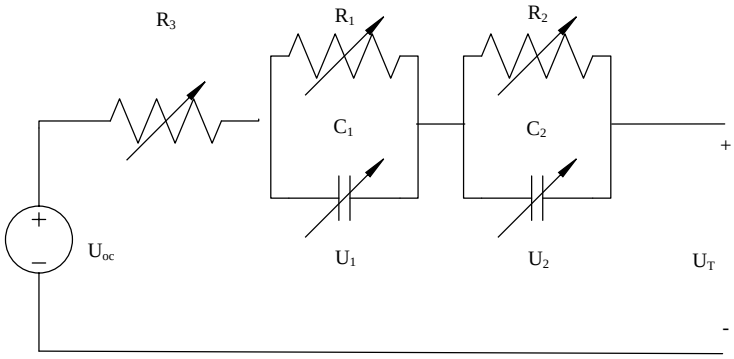

Figure 4.32: Equivalent Circuit Model.

The model consists of a DC voltage source, a series resistance and two resistor-capacitor (RC) parallel networks. The DC source represents the open circuit voltage U_{OC}, the series resistance R_3 represents the internal resistance of the batteries, and the parallel RC networks, although they do not have a physical meaning regarding any properties of the battery (such as the internal resistance, represented by the resistor R_3), they are needed in order to capture both short-time and long-time transient behavior of the battery (the

voltage response curve is known to include both instantaneous and slow voltage drops [Chen and Rincon-Mora, 2006], which can be captured by the parallel RC networks). Finally, the terminal voltage is represented by U_T. Such a model, has a high accuracy and is able to predict the run-time and the current-voltage (I-V) performance of a battery [Chen and Rincon-Mora, 2006, Erdinc et al., 2009, Kakimoto and Goto, 2016].

4.9.2. MODEL DESCRIPTION

The model is a single input (current load), single output (terminal voltage) system, with 16 parameters that need to be defined, as will be explained in the following.

The battery's state of charge is calculated according to Equation (4.79):

$$SOC(t) = SOC(t_0) + \int_{t_0}^{t} -\frac{I_b(\tau)}{Q_b} d\tau \tag{4.79}$$

The electrical behavior of the circuit is given by the following set of equations:

$$\frac{d}{dt} U_i(t) = -\frac{U_i(t)}{C_i R_i} + \frac{I_b(t)}{C_i}, i = 1,2 \tag{4.80}$$

$$U_T(t) = U_{OC}(t) - \sum_{i=1}^{2} U_i(t) - R_3 I_b(t) \tag{4.81}$$

where:

$SOC(t_0)$: Initial SoC of the battery [-]
I_b : Current Load (Positive for discharging conditions) [A]
Q_b : Battery Capacity [Ah]
U_i, C_i, R_i : According to Figure 4.32
U_T : Terminal Battery Voltage [V]
U_{OC} : Open Cell Voltage [V]

The values of the open circuit voltage (U_{OC}), capacitors (C_i) and resistors (R_i) of Figure 4.32 all depend on the state of charge. According to literature [Erdinc et al., 2009, Gao et al., 2002], their values (assumed to be functions of the SoC) can be represented as follows:

$$U_{OC}(SOC(t)) = v_1 e^{-v_2 SOC(t)} + v_3 + v_4 SOC(t) + v_5 SOC^2(t) + v_6 SOC^3(t) \tag{4.82}$$

$$R_i(SOC(t)) = \alpha_{i,1} e^{-\alpha_{i,2} SOC(t)} + \alpha_{i,2}, i = 1,3 \tag{4.83}$$

$$C_i(SOC(t)) = \beta_{i,1} e^{-\beta_{i,2} SOC(t)} + \beta_{i,2}, i = 1,2 \tag{4.84}$$

The values of the constants $\vec{\mathbf{v}} = (v_1, ..., v_6) \in \mathbb{R}^6$ and arrays $\mathbf{A} = (\alpha_{i,j}) \in \mathbb{R}^{3x2}, \mathbf{B} = (\beta_{i,j}) \in \mathbb{R}^{2x2}$ shown in Equations (4.82 - 4.84) are the model parameters that need to be determined.

4.9.3. PARAMETER EXTRACTION

Extracting the values of the parameters constitutes the solution of a least-squares fitting problem: For each SoC value, calculated by Equation (4.79) for a given current load, the circuit parameters are estimated based on the minimization of the modeling RMS error of the terminal voltage.

4.9.4. MODEL CALIBRATION

The resulting parameter values are presented below and the simulation results are shown in Figure 4.32 for charging and discharging characteristics. It can be seen that all the simulation response curves agree with the manufacturer data quite accurately, with the maximum error having a value of around 5.5%, for a discharge rate of 1C.

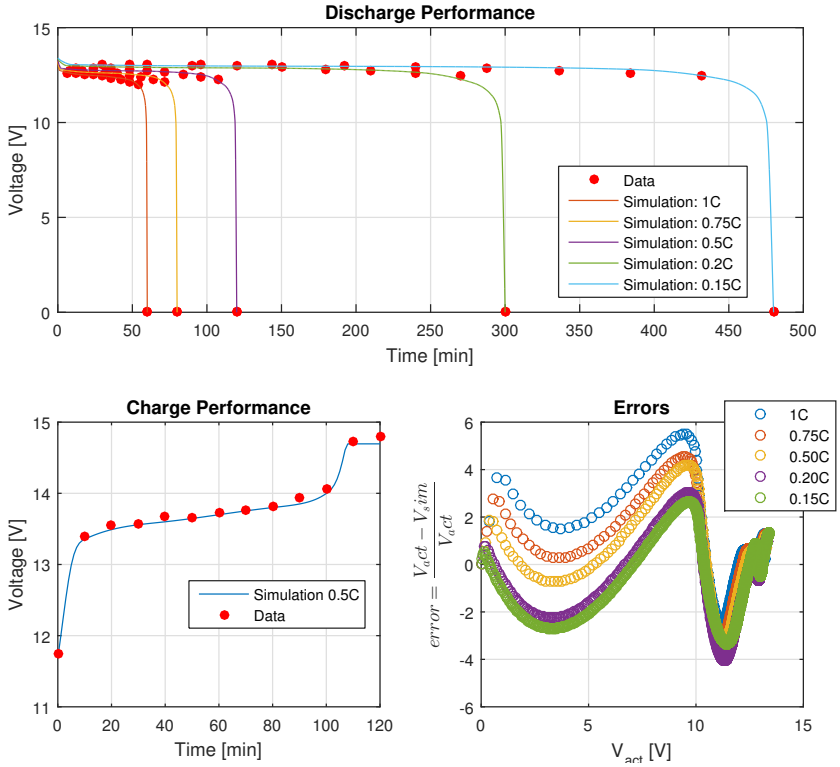

Figure 4.33: Battery Model - Calibration Results.

4.10. POWER ELECTRONICS

4.10.1. INTRODUCTION

To avoid lengthy simulation time, the dynamic response of the converters will be omitted (being in the order of milliseconds [Mohan and Undeland, 2007]). Of importance, for the scope of this work, are power conversion losses.

4.10.2. MODEL DESCRIPTION

As with the gearbox modeling approach, the inverter/rectifier models are based on energy conservation, parameterized by their nominal conditions, according to the following:

$$P_{in} = P_{out} + P_{loss} \tag{4.85}$$

where:

P_{in} : Power demand on the AC (DC) side of the rectifier (inverter) [W]
P_{out} : Power demand on the DC (AC) side of the rectifier (inverter) [W]
P_{loss} : Power Losses [W]

Their values can be calculated according to Equations (4.86)-(4.88) (Equation (4.88) regarding the converter's losses has been taken from the work of [de Waard, 2014]):

$$P_{AC} = \sqrt{3} V_{AC} I_{AC} \cos(\phi) \tag{4.86}$$

$$P_{DC} = V_{DC} I_{DC} \tag{4.87}$$

$$P_{loss} = P_{loss,nom} \left(a + b \frac{I}{I_{nom}} + c \left(\frac{I}{I_{nom}} \right)^2 \right) \tag{4.88}$$

$$\tag{4.89}$$

with:

$$P_{loss,nom} = (1 - \eta_{nom}) P_{nom}$$
$$a + b + c = 1, \quad a, b, c \in [0, 1]$$

where:

a : Constant losses coefficient [-]
b : Conductor losses coefficient [-]
c : Switching losses coefficient [-]
η_{nom} : Nominal inverter/rectifier efficiency [-]

Unless otherwise indicated (due to of lack of measurements/data), the following values have been assumed [de Waard, 2014]: a=0.1, b=c=0.45, η_{nom} = 0.985.

4.11. SWITCHBOARD

In the switchboard all the electric consumers and suppliers are connected with the same voltage. In this work, it has been assumed that this component is ideal, i.e. no power losses are present (in reality switchboards present a high-energy efficiency, with an approximate loss of 0.5% [de Waard, 2014]). As such, power supply is assumed to be equal to power demand:

$$\sum_i P_{i,demand} = \sum_j P_{j,supply} \tag{4.90}$$

4.12. COMPLETE SHIP MODEL VERIFICATION

4.12.1. INTRODUCTION

The total model consists of all the models discussed in this chapter, plus a rule-based control strategy [3]that regulates the operation of the hybrid propulsion plant. In this section, the static and dynamic behavior of the existing model will be verified and partially validated. Unfortunately, due to lack of measurements, proper dynamic validation of the complete model is not possible, but will be performed only for quasi-static maneuvers with respect to total fuel consumption. Furthermore, the verification of the dynamic behavior of the vessel will be limited to straight - line maneuvering (accelerations and decelerations).

4.12.2. QUASI-STATIC MANEUVERING

4.12.2.1. MODEL VERIFICATION

In this section the static working points of the vessel model are verified. The model outputs were calculated as a function of vessel speed for different operating conditions, namely Diesel electric mode, with the main engines turned off, and Diesel direct mode, in which the induction machines are used as shaft generators powered by the main engines. The powers and efficiencies, as a function of the vessel's speed, are represented as a propulsion chain: a chain of powers from ship (demand) to prime mover (supply) linked by the various efficiencies [Woud and Stapersma, 2002]. The propulsion chains for Diesel Electric and Diesel Direct mode are presented in Figures 4.35 - 4.36, and the simulation results in Figures 4.34, 4.37 from which credible trends are observed.

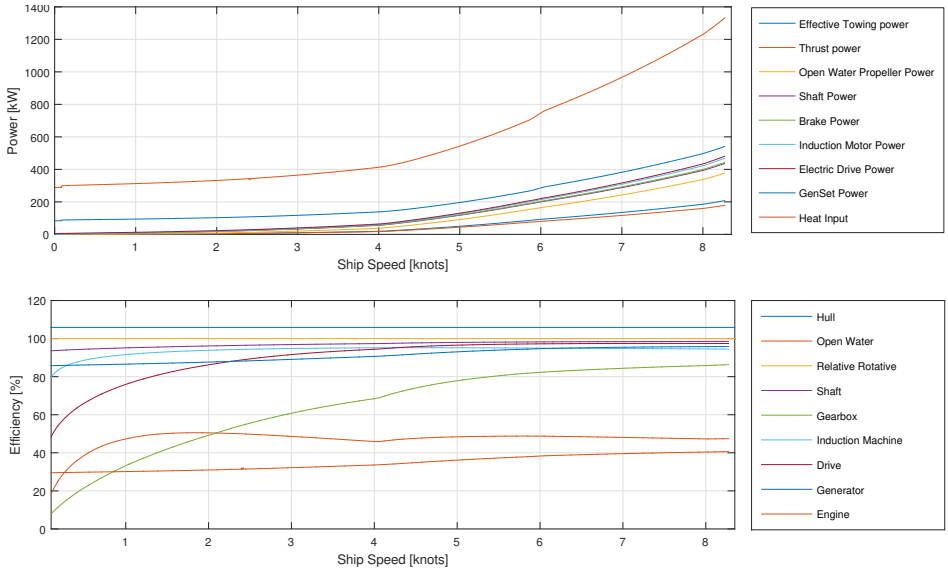

Figure 4.34: Simulation Results - Propulsion Chain, Diesel Electric Mode.

[3]Developed by Damen Shipyards Group.

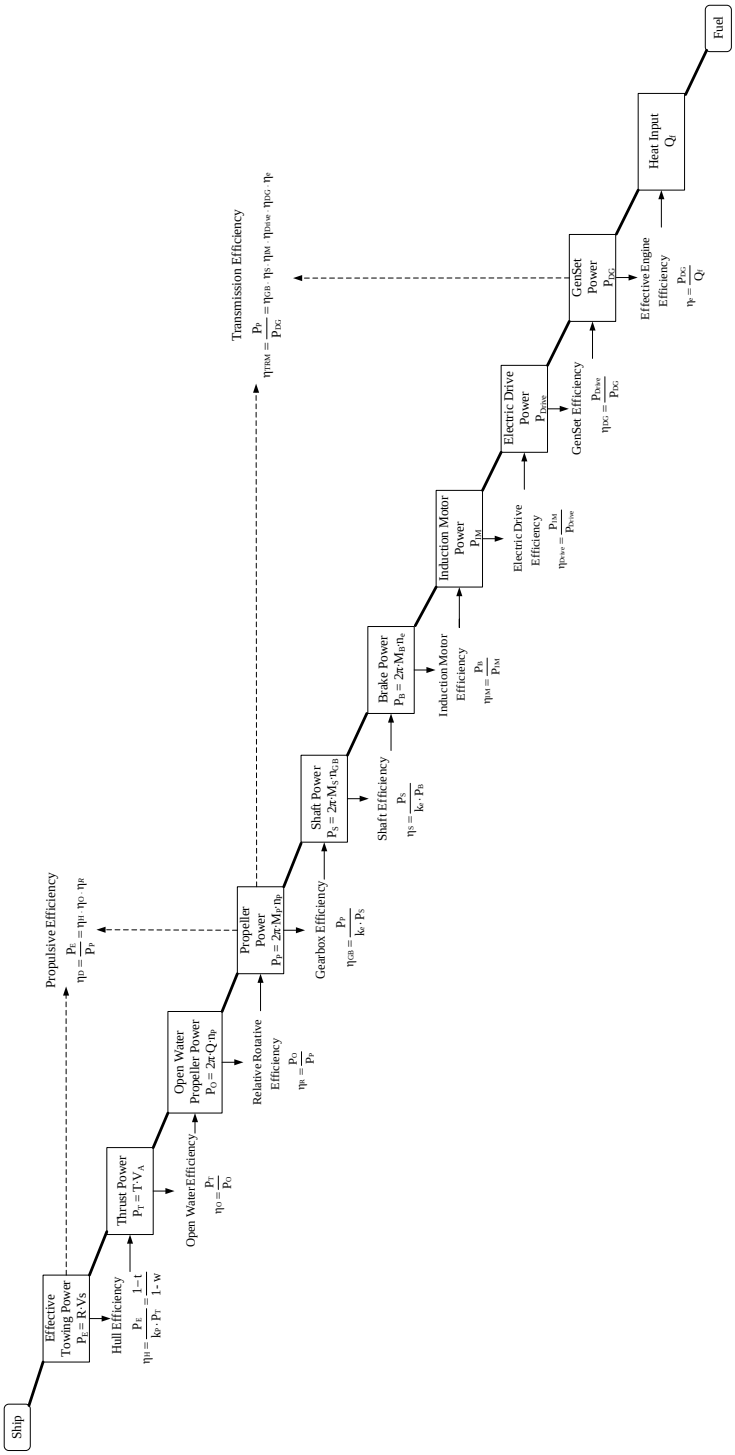

Figure 4.35: Propulsion Chain: Diesel Electric Mode.

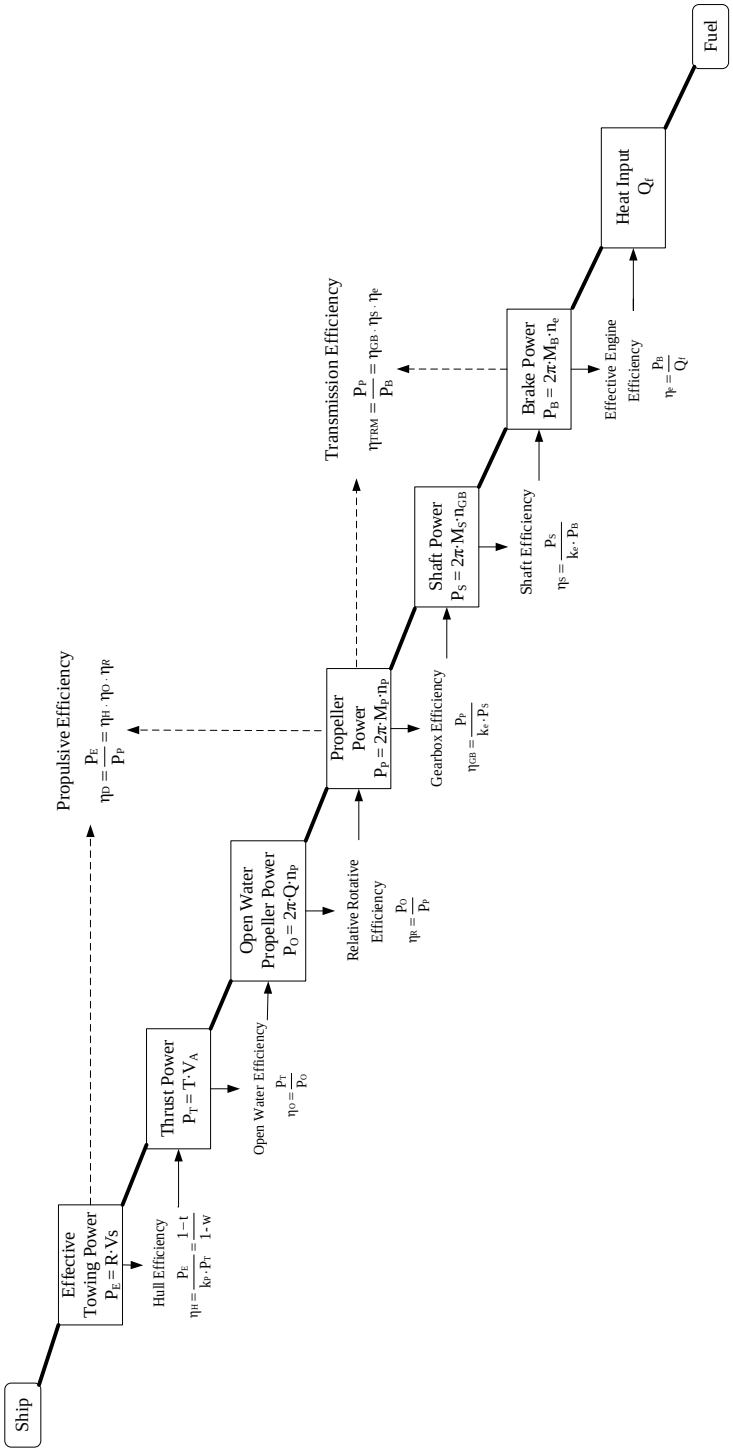

Figure 4.36: Propulsion Chain: Diesel Direct Mode.

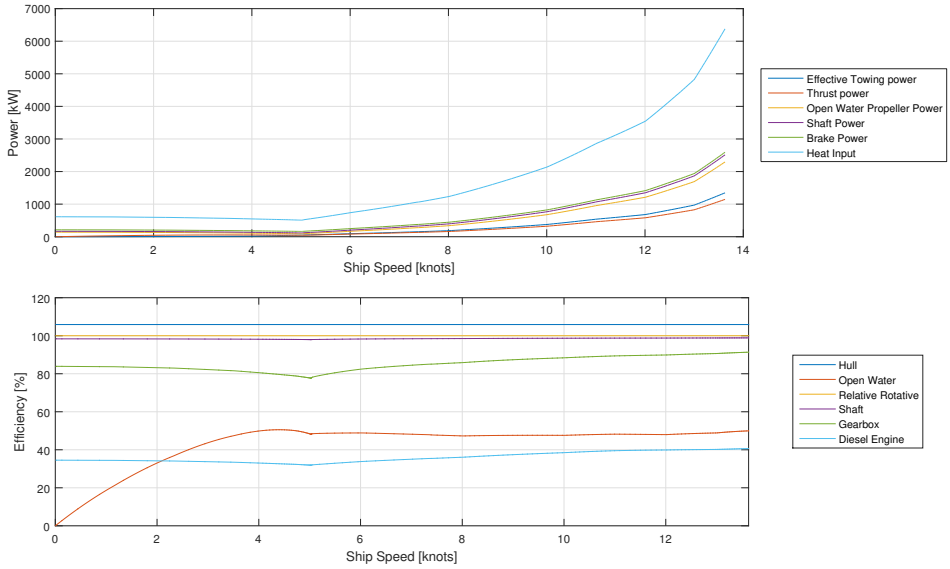

Figure 4.37: Simulation Results - Propulsion Chain, Diesel Direct Mode.

4.12.2.2. MODEL VALIDATION

Regarding the validation process of the model, only the simulated fuel consumption was validated against measurements taken on-board the hybrid tugboat, as in this way the propulsion chain can be validated at once as a whole, from ship level to fuel level (see Figures 4.35 - 4.36). The results for the two operational modes are presented in Figures 4.38 - 4.39.

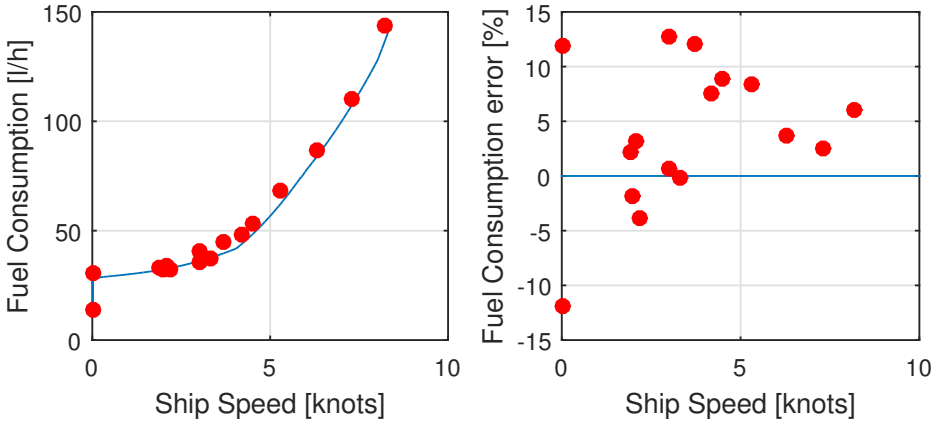

Figure 4.38: Total Ship Model Validation: Diesel Electric Mode.

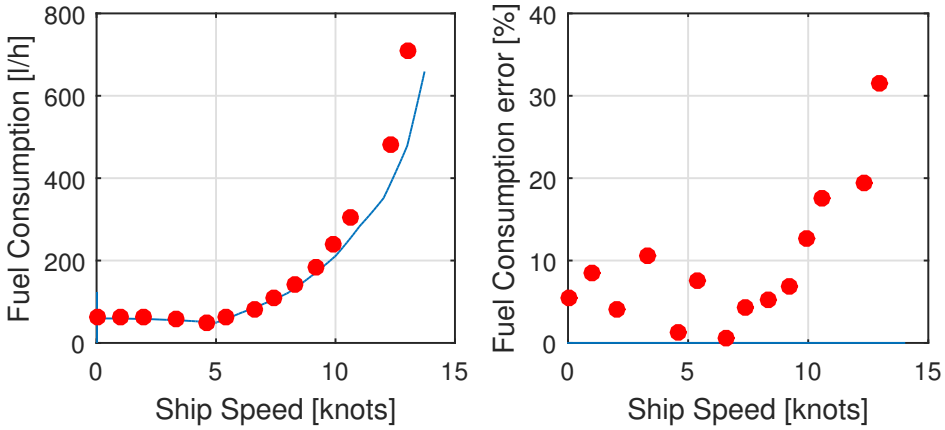

Figure 4.39: Total Ship Model Validation: Diesel Direct Mode.

As can be seen, for lower ship speeds (up to 10 knots) the simulated and measured fuel consumption agree within 12%. However, above 10 knots the relative error increases up to a maximum of 32% for the maximum ship speed. This can be attributed to the resistance curve implemented in the model (calm water resistance), whereas in the measurements a different sea state applies, resulting in a decreased fuel consumption compared to the actual.

4.12.3. DYNAMIC MANEUVERING

The verification of the dynamic behavior of the propulsion plant involves the simulation of a characteristic operating profile of a hybrid tugboat. The results are presented in Figures 4.40 - 4.41. Results are satisfactory, meaning that the observed trends are credible, and that the dynamic behavior of the vessel as observed agrees with the expected behavior of the initial conceptual model.

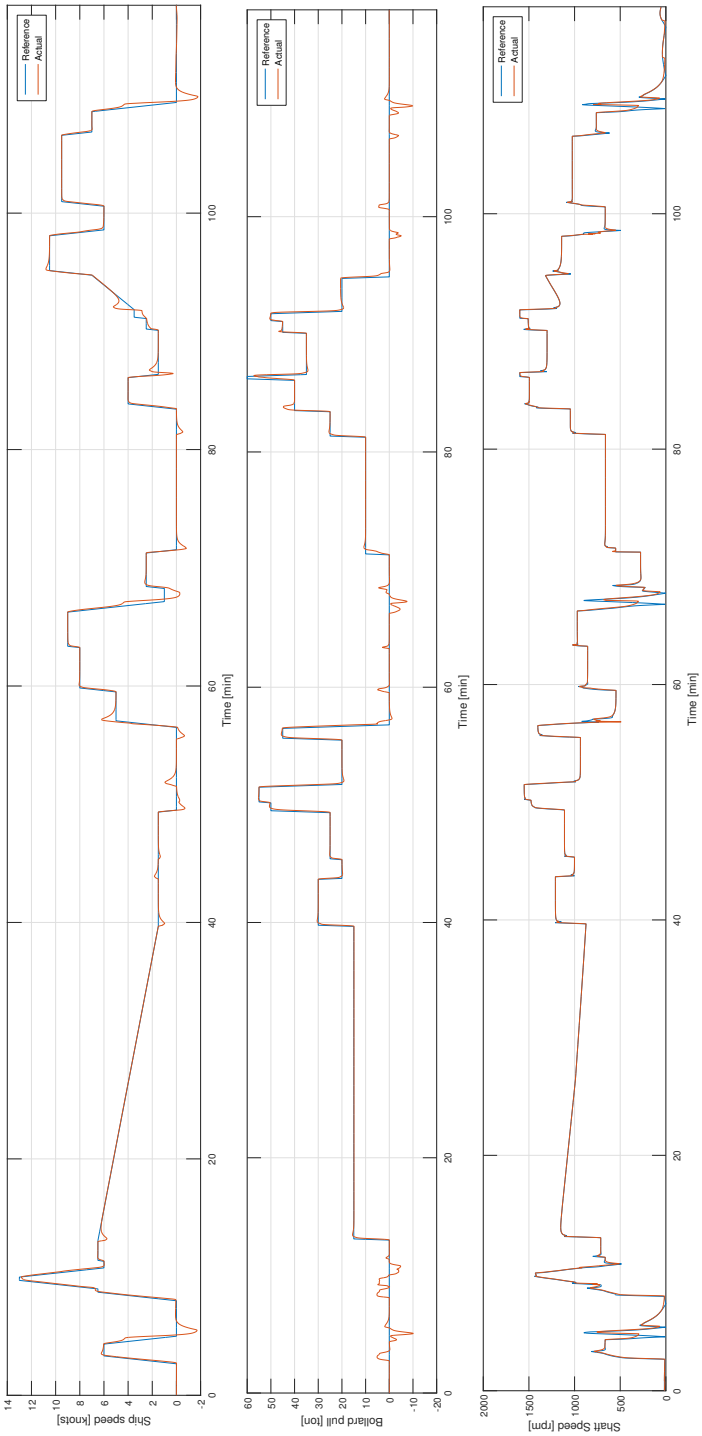

Figure 4.40: Dynamic Verification: Vessel Response.

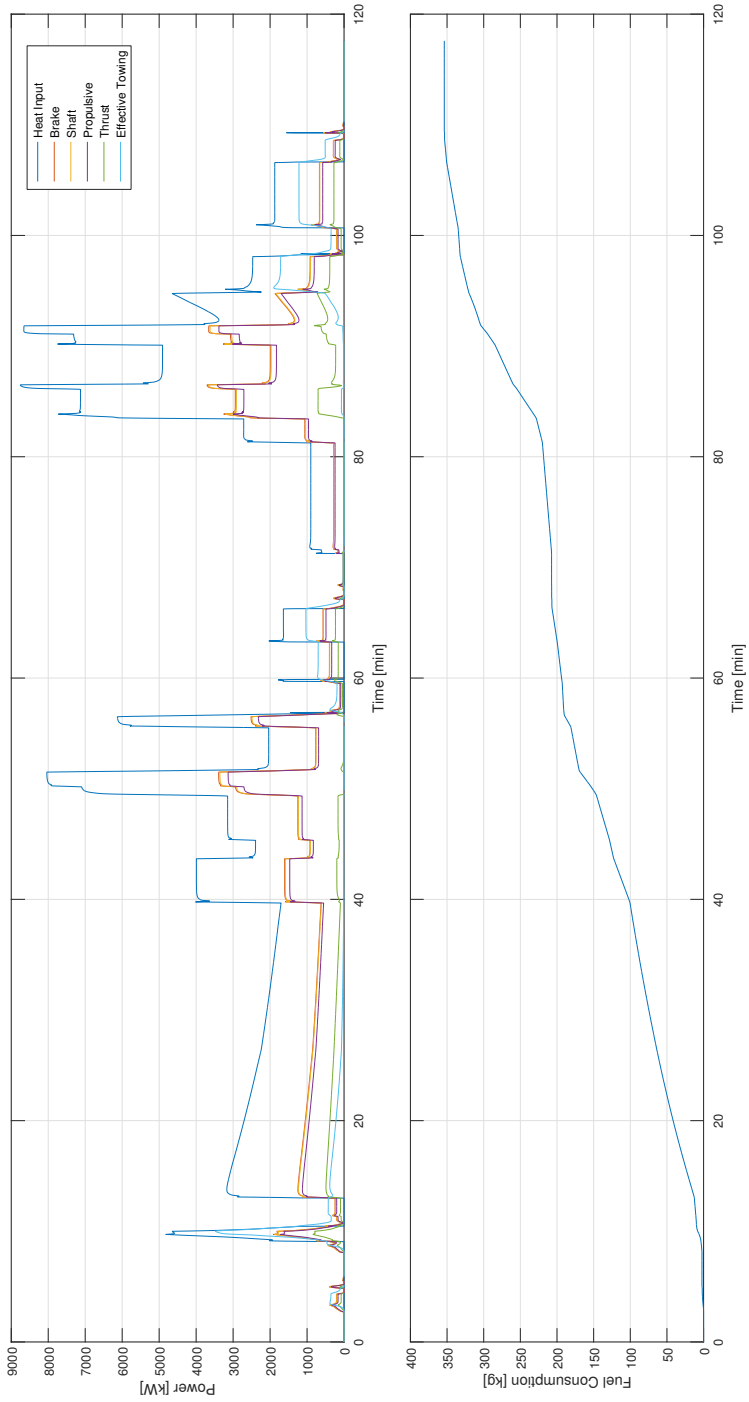

Figure 4.41: Dynamic Verification: Power Output and Fuel Consumption.

5

THE ENERGY MANAGEMENT PROBLEM

"Everything should be made
as simple as possible,
but not simpler."

-Albert Einstein

Energy management in any hybrid vehicle consists of deciding the amount of power delivered at each instant by the energy sources that are present, while meeting several constraints. In this chapter the main features of the energy management controller will be presented, and the problem of designing such a controller will be formalized using optimal control theory.

5.1. INTRODUCTION & GENERAL CONSIDERATIONS

In this work, the problem of managing the on-board energy sources of the vessel will be solved using two different approaches:

1. Variations of a real-time implementable strategy
2. Global (Off-line) optimization, to benchmark the real-time strategy, presented in

An EMS controller deals with making decisions in the best possible manner, a decision-making process that is based on optimization. The solution of an engineering problem using optimization techniques can be broken into three subproblems [Onori et al., 2016]:

1. *Formulate the engineering problem into an optimization problem:* The formulation step involves choosing quantities, typically functions of several variables, one

of which has to be minimized or maximized (the objective function), possibly subject to one or more constraints, described by the remaining functions. In this step, it is important to simplify the objective function and/or the constraints when possible while also taking into consideration the inherent sacrifice in accuracy.

2. *Initialize the optimization algorithm:* Assuming that the engineering problem has been put into a mathematical framework, the properties of the optimization problem that arises are studied, to decide which algorithm will be able to yield the best results, using an acceptable amount of computational power. The initialization deals with the choice of algorithms and with decisions about initial values for the parameters.

3. *Determine the stopping criteria:* Optimization techniques usually involve an iterative scheme, where in each iteration a new, and hopefully better, estimation of the parameter vector x is made. Certain optimization techniques provide the optimal solution in a finite number of steps and the choice of when to stop can be easily determined by the optimality conditions of the previous iteration, whereas other techniques can only find a very good approximation of the optimum. In practice, a stopping criterion consists of several components, usually a mix of (absolute and/or relative) constraints on the objective function value, the current point and the number of iterations, which in turn relates to the desired accuracy of the solution, as determined in step 1.

In the following Sections, the Energy Management problem will be formulated - in a somewhat different way for each approach - its characteristics will be presented, and the theory and rationale behind the different approaches that are considered will be discussed.

5.2. PROBLEM FORMULATION

5.2.1. FORMAL PROBLEM STATEMENT

In this work, the optimal energy management problem consists of finding the control task ($u(t)$) that leads to the minimization of the fuel consumed (m_f) over a trip of length t_f (starting at $t_0 = 0$). This objective can be written as a mathematical optimization problem $\mathscr{P}$, of the form [Jager et al., 2013]:

$$\mathscr{P} = \begin{cases} \underset{u \in \mathbb{U}}{\text{minimize}} & J\big(t, x(t), u(t), r(t)\big) = \displaystyle\int_{t_0}^{t_f} \dot{m}_f\big(t, x(t), u(t), r(t)\big)\, dt \\ \text{subject to:} & \dot{x} = F\big(t, x(t), u(t), r(t)\big), \\ & G\big(x(t), u(t)\big) = 0, \\ & H\big(x(t), u(t)\big) \leq 0, \\ & x, r \in \mathbb{R}^n. \end{cases} \tag{5.1}$$

where:

$\mathbb{U}$	: Set of admissible controls
J	: The control objective (Or Cost Function, or Performance Criterion)
t	: Time index
$x = (x_1, x_2, ..., x_m)$	: State variables
$u = (u_1, u_2, ..., u_n)$	: Control variable vector
$r = (r_1, r_2, ..., r_n)$	: Uncontrolled inputs
F	: Set of dynamic state equations
G	: Set of equality constraints
H	: Set of inequality constraints

The minimization of the performance integral index (J) is subject to constraints related to the physical limitations of the propulsion system's components, limitations in the energy stored in the battery system, and the requirement to maintain the battery's SOC within prescribed limits. This makes the Energy Management problem a constrained, finite-time (mixed integer, as will be shown in later Sections) optimal control problem, in which the objective function must be minimized under a set of both *global* and *local* constraints on the state and control variables. Figure 5.1 gives a schematic representation of the propulsion system and the associated power-flows.

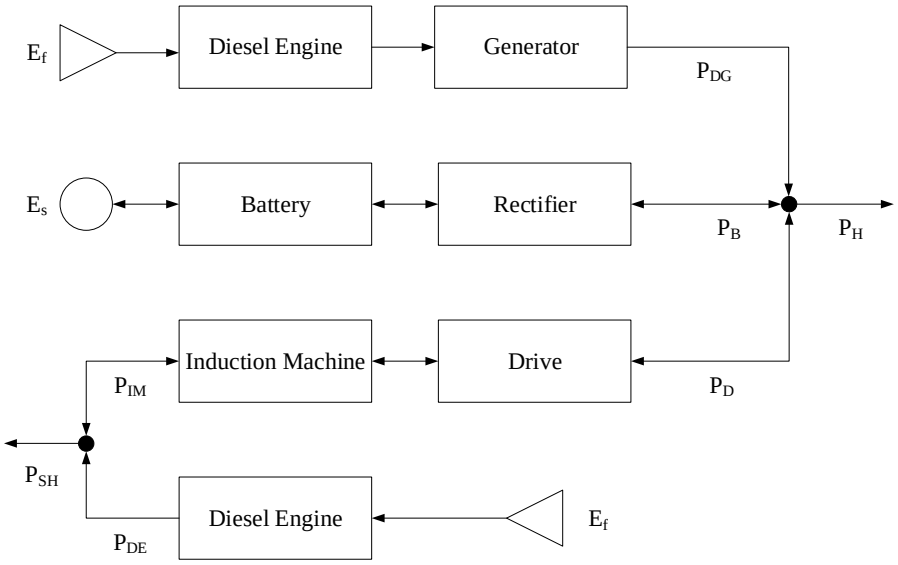

Figure 5.1: Schematic Overview of the propulsion system.

5.3. ECMS-BASED SUPERVISORY CONTROL

ECMS is based on the notion that the electric energy storage system (in this case the batteries) can be seen as an auxiliary reversible fuel tank:

1. Discharging at present implies that at some future time the battery will possibly

need to be recharged, resulting in some additional fuel consumption in the future.

2. In case of charging an extra load is being imposed on the Diesel engines, implying an extra fuel consumption at present, which will be used at a later time in the future to alleviate the engine load required to propel the vessel (through the electric motors), or to meet the electric power requirements.

As explained briefly in section 3.3.2.1, the underlying principle of the ECMS approach is that a cost is assigned to battery energy, so that the use of the stored electrical energy is made equivalent to using (or saving) a certain quantity of fuel. This cost is obviously unknown, as it depends on future states of the system, but this past (or future) fuel consumption, $\dot{m}_{ress}(t)$, can be summed to the present real fuel consumption, $\dot{m}_f(t)$, to obtain the instantaneous fuel consumption $\dot{m}_{f,eqv}(t)$:

$$\dot{m}_{f,eqv}(t) = \sum_i \dot{m}_{f,i}(t) + \dot{m}_{ress}(t) \tag{5.2}$$

$$\dot{m}_{f,i}(t) = \frac{P_{DE,i}(t)}{\eta_{DE,i}(t) Q_{lhv}} = sfoc_{DE,i}(t) P_{DE,i}(t) \tag{5.3}$$

$$\dot{m}_{ress}(t) = sfoc_{eqv}(t) P_{batt}(t) \tag{5.4}$$

The virtual specific fuel consumption $sfoc_{eqv}$ is proportional to an *equivalence factor* (s_t) which differs whether the battery is being charged or discharged. As such, Equation (5.4) can be written as:

$$\dot{m}_{ress} = \frac{s(t)}{Q_{lhv}} P_{Batt}(t) \tag{5.5}$$

Depending on the sign of P_{batt} (i.e., on whether the battery is being charged or discharged), the virtual fuel flow rate can be either positive or negative, therefore making the equivalent fuel consumption higher or lower than the actual fuel consumption.

The equivalence factor is a vector of values, one for charge and one for discharge, $s(t) = [s_{chg}(t), s_{dis}(t)]$. Its task is to assign a cost to the use of electricity, converting electrical power from the battery into equivalent fuel consumption. Practically speaking, it represents the chain of efficiencies through which fuel is transformed into electrical power and vice-versa. As such, it changes for each operational condition of the powertrain. In the original formulation of ECMS [Sciarretta et al., 2004], the equivalence factor is a set of constants which were interpreted as the average overall efficiency of the electric path for each operating mode, and for a specific mission.

However, since the original ECMS formulation, it has been shown [Kirk, 2012] that there is no need for multiple equivalence factors, since the efficiencies along the electrical path (apart from the battery) can be implicitly taken into account on one parameter, the co-state $\lambda(t)$ (a more elaborate analysis is given in Section 5.8.3). The link between the co-state and the vector of equivalence factors is the following:

$$s_{chg}(t) = \lambda(t)\, \eta_{batt}(t) \tag{5.6}$$

$$s_{dis}(t) = \frac{\lambda(t)}{\eta_{batt}(t)} \tag{5.7}$$

Therefore, Equation (5.5) can be simply re-written as:

$$\dot{m}_{ress} = \frac{\lambda(t)}{\eta_{batt}(t)^{sgn(P_{batt}(t))}} \frac{P_{Batt}(t)}{Q_{lhv}} \tag{5.8}$$

Using the co-state λ, ECMS essentially reformulates the global problem of minimizing the total (global) fuel consumption according to Equation (5.1), to a local (instantaneous) problem of minimizing $\dot{m}_{f,eqv}(t)$, given by Equation (5.2):

$$\overbrace{\begin{aligned} \min_{u\in\mathbb{U}} \quad & \int_{t_0}^{t_f} \dot{m}_f\big(t,x(t),u(t),r(t)\big)\,dt \\ \text{s. t.:} \quad & \dot{x} = F\big(t,x(t),u(t),r(t)\big), \\ & G\big(x(t),u(t)\big) = 0, \\ & H\big(x(t),u(t)\big) \le 0, \\ & x, r \in \mathbb{R}^n. \end{aligned}}^{\text{Global}} \Rightarrow \overbrace{\begin{aligned} \int_{t_0}^{t_f} \quad & \min_{u\in\mathbb{U}} \big[\dot{m}_{f,eqv}\big(t,x(t),u(t),r(t)\big)\big]\,dt \\ \text{s. t.:} \quad & \dot{x} = F\big(t,x(t),u(t),r(t)\big), \\ & G\big(x(t),u(t)\big) = 0, \\ & H\big(x(t),u(t)\big) \le 0, \\ & x, r \in \mathbb{R}^n. \end{aligned}}^{\text{Local}}$$

In general, at each time instant t with a time step Δt over the entire duration of operation, the following steps are necessary in order to implement ECMS (of course this is the most simplified / non-sophisticated process):

1. Given the state of the system (required propulsive and electrical power, shaft rotational speed, state of charge of the battery, etc.) the acceptable range of values of the control vector u_t which satisfies the instantaneous constraints (torque limits, etc.) is identified.

2. For each candidate $u(t)$ of the admissible set of control tasks U the equivalent fuel consumption is calculated.

3. The control task which minimizes the equivalent fuel consumption is selected.

An interesting aspect is what discretization time interval Δt should be adopted. This is an important aspect, as the set of admissible control variables are approximated by the nearest available values regarding the system's state, on the so-called *discretization grid*, i.e. at time t_{k-1}. If Δt is relatively large, the actual SOC can reach non-acceptable values in-between two consecutive calls of the optimization process. On the other hand, a small time interval means that there is less time available for the optimization process, therefore the choice of the optimization algorithm becomes highly important. Considerations such as algorithmic efficiency, both in terms of time and space, must be given serious thought.

In any case, the main advantage of this approach is that it has the potential to approximate the global optimal solution [Sciarretta and Guzzella, 2007]. In addition, the instantaneous minimization problem is computationally less demanding than the global problem, usually solved with dynamic programming, and applicable to real-world situations since it does not rely on exact information about future operating conditions. Moreover, if predictions about the future can be made, based on historical data or information about weather conditions, geographical locations etc., they can be easily implemented

in ECMS by adjusting the value of the co-state. This value greatly affects the actual fuel consumption of the system and the SOC of the battery. This is also the main challenge of ECMS, i.e. how to select the most suitable value of the co-state, which should be representative of past, present and future efficiency of the entire drivetrain, to guarantee optimality of the controller's decisions: If the values are too high, an excessive cost is attributed to the use of the battery packs, and therefore the hybridization potential is not realized, on the other hand, if it is too low, the battery is depleted too soon. How the value of the co-state can be calculated and adapted while the system is in operation, is a subject that will be discussed in Section 5.8.3.

5.4. CONSTRAINTS

The problem's constraints can be classified under two different categories, namely state constraints and control input constraints:

The only state variable that is of importance for the EMS is the battery's state of charge. The limitations on the SOC are imposed in order to maintain its cycle life, whose installation incurs a costly investment, which is the main barrier to the growth of HEVs [Vu, 2015]. Based on these limitations, the EMS is called either *charge-sustaining*, in which the SOC at the beginning and the end of the mission is the same, therefore eliminating the need for external recharging, or *charge-depleting*, in which the battery is recharged using an electric outlet, so the final SOC is lower than the initial one. In both cases, inequality constraints are imposed on the SOC, representing the maximum and minimum energy level of the battery, at any given time, which can be either *hard* or *soft*, i.e. whether an additional constraint will be actually implemented in the optimization problem, or whether the objective function will be modified to penalize deviations of the current state of charge $SOC(t)$ from its target value (as shown in Onori et al. [2016]). In this work, a hard constraint will be used, as it guarantees that the SOC will not reach non-admissible values.

Besides the state constraints, input constraints on the control vector $u(t)$ are present. This guarantees that the maximum power-flows through the controlled components remain bounded. Of course, the operating range of the components is always limited, so bounds have to be set on Diesel engine, Diesel-generator and the induction machine's power output. Furthermore, similar bounds are needed for the power flowing in or out of the batteries so as to preserve the battery's health. Finally, constraints are needed so as to ensure that power demand (both propulsive and electric) matches power supply.

5.4.1. DECISION VARIABLES & UNCONTROLLED INPUTS

Uncontrolled inputs include the shaft speed command, along with propulsive power demand, and electric power demand. Continuous decision variables include the power of the induction machine (P_{IM}), battery (P_B), main Diesel engine (P_{DE}), and Diesel - generator (P_{DG}) according to Figure 5.1 (however some of these can be eliminated, as will be explained in Section 5.7). Furthermore, in order to completely define the problem *auxiliary* binary variables (b_i) are needed. These are used to indicate whether a component of the system is operating or not (ON/OFF), and zero out several of the functions that will be presented in the following sections, and eliminate constraints that are non-

applicable anymore. A different one is used for the main Diesel engine, Diesel-generator, induction machine and battery. Depending on the values of these decision variables every operational mode can be identified, and the lower-level control systems can make sure to deliver the power as indicated by the EMS from there on. It should be noted that the following sign conventions shown in Table 5.1 have been used for two of the decision variables (or control inputs):

Table 5.1: Continuous Decision Variables - Sign Conventions

	P_{IM}	P_B
>0	Motor Mode	Discharging
<0	Generator Mode	Charging

5.5. PROBLEM FORMULATION SUMMARY

In the preceding sections, all the elements of the optimization problem were analyzed, and the final forms of the problem (for each control approach) are presented below. More insights on how all these variables and constraints are connected will be given in Section 5.7, after the simplified problem that represents the propulsion system is introduced in the next section.

$$
\mathscr{P} = \begin{cases} \displaystyle\int_{t_0}^{t_f} \min_{u\in\mathbb{U}} \left[\dot{m}_{\text{f,eqv}}\big(t, x(t), u(t), r(t)\big)\right] dt \\ \text{s. t:} \quad x(t) = f(t, x(t), u(t), r(t)) + x(t-1) \\ SOC_{min} \le x(t) \le SOC_{max} \\ x(t_0) = SOC_{max} \\ P_{\text{B,min}} \le P_B(t) \le P_{\text{B,max}} \\ P_d(t) = P_{DE}(t) + P_{IM}(t) \\ P_{DG}(t) + P_B(t) = P_{el}(t) + 2P_D(t) \\ r(t) = (n_{sh}(t), P_d(t), P_{el}(t)) \in \mathbb{R}^3_{>0} \\ u(t) = (P_{DE}, P_{DG}, P_{IM}, P_B) \in \mathbb{R}^4 \ : \begin{cases} [P_{\text{DE,min}}, P_{\text{DE,max}}] \\ [P_{\text{DG,min}}, P_{\text{DG,max}}] \\ [P_{\text{IM,min}}, P_{\text{IM,max}}] \\ [P_{\text{B,min}}, P_{\text{B,max}}] \end{cases} \\ y(t) = (b_{DG}, b_{IM}, b_B, b_{DE}) \in \mathbb{Z}_2^4 \end{cases} \tag{5.9}
$$

5.6. PROPULSION SYSTEM STEADY-STATE MODEL

In any optimization problem, the types of mathematical relationships between the objective, constraints, and decision variables determine how hard it is to solve, define the solution methods or algorithms that can be used for the optimization, and the confidence that the solution is truly optimal. In order to evaluate these relationships a simplified model of the propulsion system is needed from which the total fuel consumption can be predicted. This is the scope of the models that are presented in this Section.

5.6.1. DIESEL ENGINE

Regarding the Diesel engines present in the propulsion system, the fuel consumption $\dot{m}_f$ is needed, as a function of power output and shaft rotational speed. Note that this is not the only option, as an expression about the specific fuel oil consumption, or total engine efficiency could have also be derived, as functions of speed and power (or speed and torque), however the expression $\dot{m}_f = f(n_{sh}, P_b)$ was chosen, as it directly links the inputs of the problem with the desired output, without the need of any conversions in between. In Figure 5.2 the fuel consumption map of the main Diesel engines is presented, as a function of power output and shaft speed. According to this map, an analytical expression was derived based on the Mossel model given by Equation (5.10), with a_i constants to be identified.

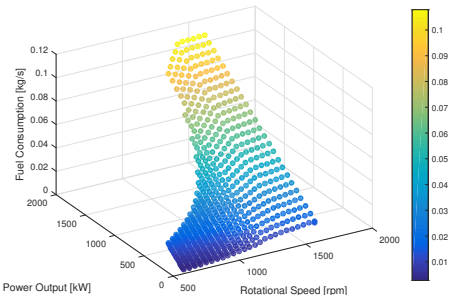

Figure 5.2: Main Diesel Engine Fuel Consumption Map.

$$\frac{\dot{m}_f}{\dot{m}_{f,nom}} = \begin{cases} a_0 + a_1 \frac{n}{n_{nom}} + a_2 \frac{P}{P_{nom}} + a_3 \left(\frac{n}{n_{nom}}\right)^2 + a_4 \left(\frac{P}{P_{nom}}\right)^2 + a_5 \frac{n}{n_{nom}} \frac{P}{P_{nom}}, & 0 < P \leq P_{nom} \\ 0, & P = 0 \end{cases} \tag{5.10}$$

This second-degree polynomial with respect to power output and shaft speed gives an adequate representation of the main engine's fuel consumption. As can be seen from Figure 5.3, the maximum absolute error is around 1%, with an average value of -0.004%, compared to the detailed model of [Geertsma et al.] discussed in Chapter 4.

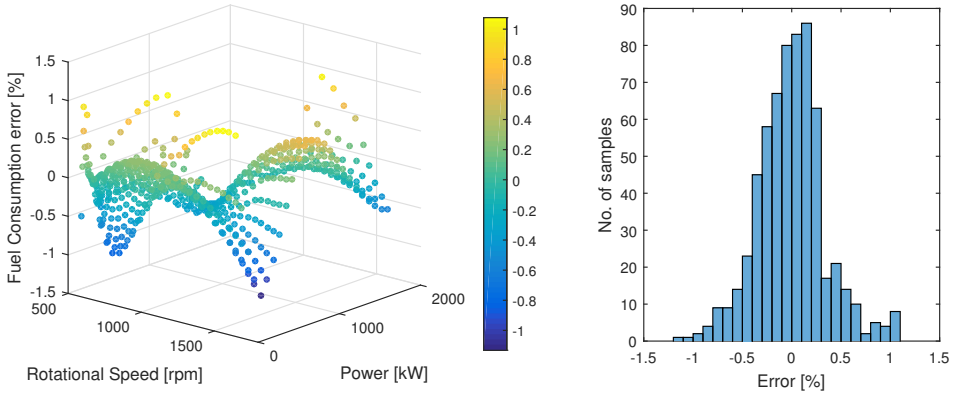

Figure 5.3: Main Diesel Engine Fuel Consumption Map - Fitting Errors.

5.6.2. INDUCTION MACHINE & DRIVE

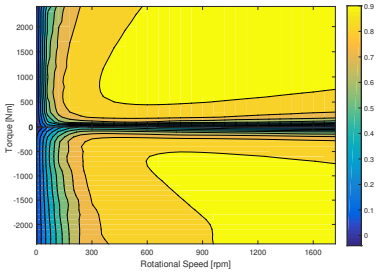

Figure 5.4: Induction Machine & Drive Efficiency Map.

For the induction machine and the electric drive, a function of the power losses as a function of torque and rotational speed was derived, through the components' combined efficiency, shown in Figure 5.4. This was deliberately chosen, as it proved to be much easier to handle the power losses rather than the efficiency in the final form of the objective function, for reasons that will become evident in Section B.3. s for the Diesel engine, a second degree polynomial proved to be adequate for capturing the actual values of the losses. However, due to the asymmetry in the efficiency between motoring and generating conditions, two different sets of coefficients were necessary. In Figure 5.5 the fitting errors are presented, as a percentage of the actual power loss, compared to the models presented in Chapter 4. Although at first sight the fitting does not seem to give an accurate prediction, the higher (in absolute values) errors (> 3%) appear around the zero torque or zero speed region. At these regions the combined efficiency of the two components is practically zero, and the induction machine is not expected to be operated there anyway. Furthermore, the negative error values signify that there is actually an overestimation of the losses in these regions, which will further push the controller to steer the operational points of the machine away from these regions. Still, with these regions included, the average error value is -1.26%.

The general form of the power loss function is given below:

$$\frac{P_{\text{loss}}}{P_{\text{loss,nom}}} = \begin{cases} a_{i1}\frac{n}{n_{nom}} + a_{i2}\frac{M}{M_{nom}} + a_{i3}\left(\frac{n}{n_{nom}}\right)^2 + a_{i4}\left(\frac{M}{M_{nom}}\right)^2 + a_{i5}\frac{n}{n_{nom}}\frac{M}{M_{nom}}, & 0 < M \leq M_{nom} \\ 0, & M = 0 \end{cases} \tag{5.11}$$

with $i = 1,2$ for motor and generator mode respectively. It is interesting to note that all the coefficients are equal in both modes, except form the term a_{i4}.

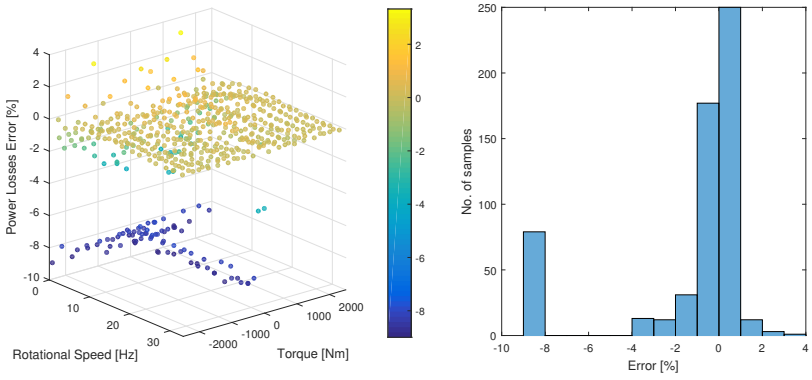

Figure 5.5: Induction Machine & Drive Power Loss Map - Fitting Errors.

5.6.3. DIESEL-GENERATOR SET

For the Diesel-generator set, an expression for the fuel consumption of the Diesel engine was derived (Equation (5.12)) with respect to the generator's power output, as shown in Figure 5.6. Note that, since it has been assumed that the Diesel engine in this case operates at constant speed, this is a one-dimensional fitting problem. Although the fuel consumption (orange curve in Figure 5.6) seems to be a linear function of power output, a quadratic curve was needed in order to provide a fit with seemingly no errors. As can be seen from Figure 5.7, the fitting error reaches absolute values between 0.3% and 2.5% for a power output of less than 4 kW, but after that point the fitting error is practically zero, with an average value of -0.0152%.

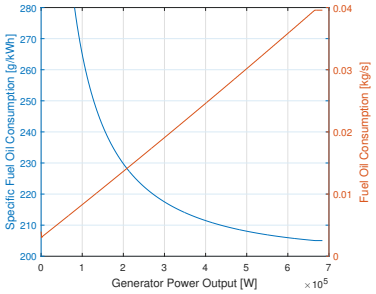

Figure 5.6: Diesel Generator Fuel Consumption.

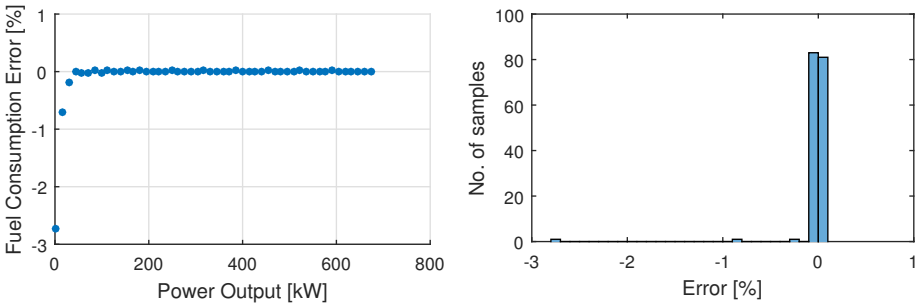

Figure 5.7: Diesel Generator Fuel Consumption - Fitting Errors.

$$\frac{\dot{m}_f}{\dot{m}_{f,nom}} = \begin{cases} a_0 + a_1 \frac{P}{P_{nom}} + a_2 \left(\frac{P}{P_{nom}}\right)^2 & 0 < P \leq P_{nom} \\ 0 & P = 0 \end{cases} \tag{5.12}$$

5.6.4. BATTERY

What is of importance for the optimization process with respect to the battery system, is its efficiency for the objective function, and the SOC and terminal voltage for the constraints. Different approaches were needed in order to determine each one analytically, and they are presented in the following.

5.6.4.1. EFFICIENCY

The efficiency of the battery (not such an obvious concept, since it is an energy storage system) is defined on the basis of a full charge/discharge cycle as the ratio of total energy delivered to the energy that is necessary to charge up the device [Sciarretta and Guzzella,

2007]. This definition however is dependent on the features of the charge/discharge cycle, and more especially whether the battery is charged/discharged at constant current (Peukert test), or at constant power (Ragone test).

The choice was made to evaluate the Ragone efficiency, as it could link directly the decision variable of the optimization problem (power input/output to the battery) to its efficiency, which appears in the formula of the equivalent fuel consumption (5.8). The efficiency as a function of power input to the battery can be seen in Figure 5.8, and was fitted with a quadratic curve with respect to power input/output. The errors of this curve fitting can be seen in Figure 5.9. The maximum error is 0.3% for a power input/output of 125 W, with an average value of 0.0343%.

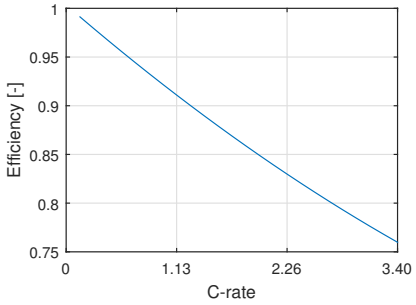

Figure 5.8: Battery Efficiency.

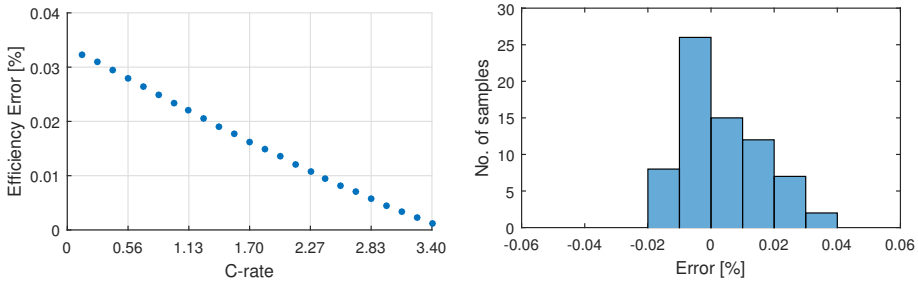

Figure 5.9: Battery Efficiency - Fitting Errors.

5.6.4.2. STATE OF CHARGE

For the estimation of the state of charge and the terminal voltage of the battery, a basic equivalent circuit model was used, shown in Figure 5.10. The open cell voltage U_{OC} is a function of the SOC, as in the model presented in Section 4.9, and a constant resistance has been used, equal to 4.2 $m\Omega$. The state of charge variation can be directly calculated from the terminal power (decision variable in the optimization problem), when semi-empirical data is available from the manufacturer (the same data that was used for the model in Section 4.9). When a current flows in the circuit, according to Kirchoff's law, the following equations apply:

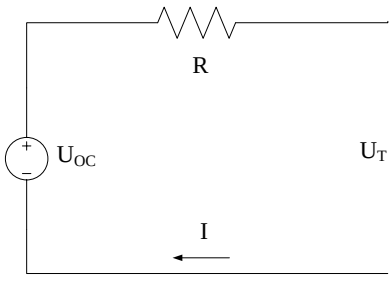

Figure 5.10: Battery Circuit.

$$\left.\begin{aligned} I(t) &= \frac{P(t)}{U_T(t)} \\ U_{OC}\left(SOC(t)\right) - RI(t) &= U_T(t) \end{aligned}\right\} \Rightarrow U_T^2(t) - U_{OC}\left(SOC(t)\right)U_T(t) + P(t)R = 0 \tag{5.13}$$

Solving (5.13) for power yields:

$$P(t) = \frac{-U_T^2(t) + U_T(t)U_{OC}(SOC(t))}{R} \tag{5.14}$$

From Equation (5.14), the upper and lower limits for the battery power can be determined:

$$P_{\max} = \frac{U_{OC}(SOC(t))U_{\mathrm{T,min}} - U_{\mathrm{T,min}}^2}{R} \tag{5.15}$$

$$P_{\min} = -\frac{U_{\mathrm{T,max}}^2 - U_{OC}(SOC(t))U_{\mathrm{T,max}}}{R} \tag{5.16}$$

where $U_{\mathrm{T,min}}$ and $U_{\mathrm{T,max}}$ are the terminal voltage limits that correspond to the minimum and maximum SOC respectively.

The tracking of the SOC of the battery at any time instant (t) can be described by Equation (5.17) [Koot et al., 2005]:

$$SOC(t) = \frac{Q(t)}{Q_b} = \frac{Q(t_0) - \sum_{j_{(t=0)}}^{j_{(t-\Delta t)}} \left(\frac{P_{\mathrm{batt,j}}}{U_{OC}(SOC(t))}\,\Delta t\right)}{Q_b} = SOC_{t-\Delta t} - \frac{P_{\mathrm{batt}}\,\Delta t}{U_{OC}(SOC(t))Q_b} \tag{5.17}$$

with Q_b being the nominal capacity of the battery.

It is evident that a numerical procedure is needed in order to solve the circuit, as the state of charge variation, terminal voltage and open cell voltage are all interconnected via the current state of charge of the battery. Through experimentation with this subroutine, it was clear that two to three iterations were needed for the procedure to converge when it was initiated with the SOC of the previous state. Figure 5.11 shows the different responses between the dynamic model presented in Section 4.9, and the current, steady state model, in terms of terminal voltage (which directly affects the SOC itself). It can be seen that the faster transients in the terminal voltage can no longer be captured, but the overall accuracy is sufficient.

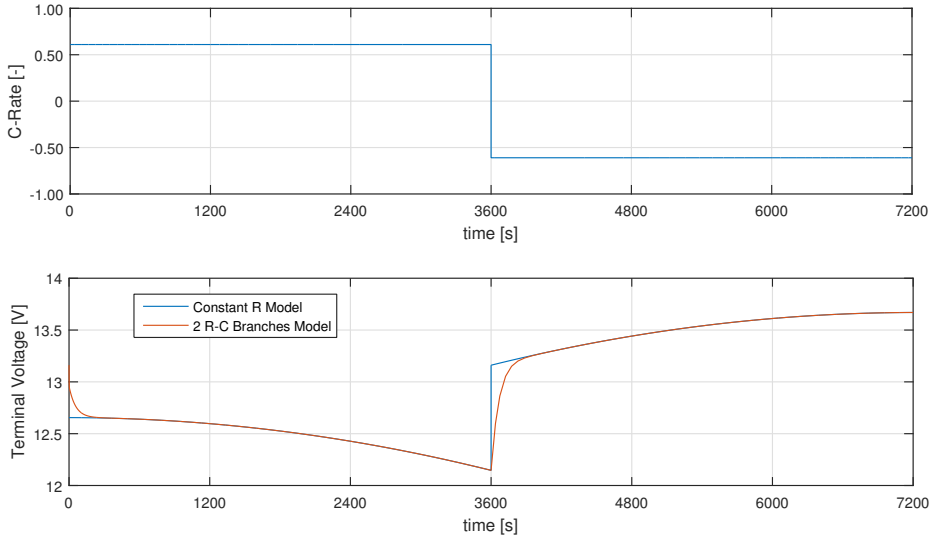

Figure 5.11: Battery System Response: Terminal Voltage.

5.7. ANALYTICAL FORMULATION OF THE OPTIMIZATION PROBLEM

Now that the basic mathematical framework has been introduced, a further analysis of the optimization problem (5.9) can be performed, with the scope of extracting more information on the type of the objective function and/or the constraints, and (if possible) to simplify the problem. In order to proceed, it should first become clear how the objective function is connected with the decision variables. As stated in Section 5.4.1, the uncontrolled inputs to the optimization process are the following:

- P_d: Propulsive power demand [W]
- P_{el}: Electric power demand (hotel loads) [W]
- n_{sh}: Shaft rotational speed [Hz]

with the following decision variables:

- P_{DE}: main Diesel engine power [W]
- P_{DG}: Diesel-generator power [W]
- P_{IM}: Power of the induction machine (rotor) [W]
- P_B: Battery Power [W]

and auxiliary variables:

- b_{DE}: ON/OFF state of the main Diesel engine [binary]

- b_{DG}: ON/OFF state of the Diesel-generator [binary]
- b_{IM}: ON/OFF state of the Diesel-generator [binary]
- b_B: ON/OFF state of the battery system [binary]

As a first step towards reducing the complexity of the optimization problem, it must be noted that some of the decision variables and constraints of the problem can be eliminated or combined with the upper and lower bounds of other decision variables, as will be shown in the following.

Diesel Engine

The decision variable that can be eliminated is the power output of the main Diesel engine. Considering the equality constraint regarding the propulsive power demand, the main Diesel engine power can be directly connected to the power output of the induction machine:

$$P_d = P_{DE} + P_{IM} \Rightarrow \begin{cases} P_{DE} = P_d - P_{IM}, & b_{DE} = 1 \\ P_{DE} = 0, & b_{DE} = 0 \end{cases} \tag{5.18}$$

with the additional constraints on P_{IM}:

$$\begin{cases} 0 \leq P_d - P_{IM} \leq P_{\text{DE,max}}, & b_{DE} = 1 \\ P_d = P_{IM}, & b_{DE} = 0 \end{cases} \tag{5.19}$$

Electric Drive

The power of the electric drive is given by Equation (5.20):

$$P_D = P_{IM} + b_{IM} P_{\text{IM,loss}} \tag{5.20}$$

with $P_{\text{IM,loss}}$ being the piece-wise defined function of the combined losses of the electric machine and drive (Equation (5.11)),

Note that Equation (5.20) is valid regardless of the sign of P_{IM} (i.e. motoring/generating conditons), since $P_{\text{loss}} \geq 0$. Consider the power flows and losses in the following cases:

- $P_{IM} > 0$ (Motoring): $|P_{\text{D}}| \geq |P_{\text{IM}}|$, since $P_{\text{D}} \geq 0$ and $P_{\text{IM}} \geq 0$, then $P_{\text{D}} \geq P_{\text{IM}} \Rightarrow P_{\text{D}} = P_{\text{IM}} + P_{\text{IM,loss}}$
- $P_{IM} < 0$ (Generating): $|P_{\text{D}}| \leq |P_{\text{IM}}|$, since $P_{\text{D}} \leq 0$ and $P_{\text{IM}} \leq 0$, then $P_{\text{D}} \geq P_{\text{IM}} \Rightarrow P_{\text{D}} = P_{\text{IM}} + P_{\text{IM,loss}}$

Diesel Generator

Furthermore, the decision variable regarding the Diesel generator's power can also be eliminated, considering the equality constraint of Equation (5.9), regarding the electric power balance. Note that from the sign conventions of Table 5.1, the battery power is positive for discharging (power supply to the grid) and negative for charging (power demand from the grid). Alternatively, the power of the induction machine (and drive) is

positive when motoring (i.e. when there is power demand from the grid) and negative when generating (i.e., power supply to the grid). Thus, the equality constraint, can be simply solved for the Diesel-generator:

$$\underbrace{P_{DG}+P_{\mathrm{B}}}_{\text{Power supply}} = \underbrace{2P_D+P_{el}}_{\text{Power demand}} \Rightarrow P_{DG}=2P_D+P_{el}-P_{\mathrm{B}} \Rightarrow$$
$$\begin{cases} P_{DG}=2\left(P_{IM}+b_{IM}P_{\mathrm{IM,loss}}\right)+P_{el}-P_{\mathrm{B}}, & b_{DG}=1 \\ P_{DG}=0, & b_{DG}=0 \end{cases} \tag{5.21}$$

with the additional constraints on P_B and P_{IM}:

$$\begin{cases} 0\le P_{DG}\le P_{\mathrm{DG,max}} \Rightarrow 0\le 2\left(P_{IM}+b_{IM}P_{\mathrm{IM,loss}}\right)+P_{el}-P_{\mathrm{B}}\le P_{\mathrm{DG,max}}, & b_{DG}=1 \\ 2\left(P_{IM}+b_{IM}P_{\mathrm{IM,loss}}\right)+P_{el}=P_{\mathrm{B}}, & b_{DG}=0 \end{cases} \tag{5.22}$$

Battery

A constant efficiency for the rectifier η_{REC} has been assumed, equal to 0.97. In a similar way as with the induction machine, the power flow (charging or discharging) depends on the sign of the decision variable P_B (Figure 5.1). The connection between P_B and the power at the battery terminals is given by Equation (5.23).

$$P_{\mathrm{batt}}=\frac{P_B}{\eta_{\mathrm{REC}}^{sgn(P_B)}} \tag{5.23}$$

Binary (auxiliary) variables

At this point it should be noted that with the use of the binary variables, constraints could be imposed on the problem indicating appropriate (possible or impossible) combinations of the individual components. For example, both the induction machine and main Diesel engine cannot be turned off simultaneously, as there will not be any power supply to the shaft (when the shaft speed request is higher than zero). Using a proper set of rules (constraints) like these can somewhat reduce the complexity of the problem by decreasing the search space (and therefore lower the computational cost). a few examples of such a rule-set are presented below:

- At least one energy source must be on always.
- if $P_d > P_{\mathrm{IM,max}}$, then: $b_{DE}=1$

However, such constraints are redundant. The feasibility of all the possible combinations can be explicitly given by constraints (5.19) - (5.22), and the limitations imposed on the SOC of the battery. Equations (5.18) - (5.23), along with the fitted functions for fuel consumption and power losses of the different components, are sufficient to provide an analytical formulation of the objective function and the constraints of the problem presented in Equation (5.9). More specifically, for the objective function the following applies (for DP, the factor corresponding to $\dot{m}_{ress}$ is set to zero):

$$\dot{m}_{f,eqv} = 2\dot{m}_{f,DE} + \dot{m}_{f,DG} + \dot{m}_{ress} =$$
$$= 2b_{DE}\sum_{j=0}^{2}\alpha_j\left(P_d - P_{IM}\right)^j + b_{DG}\sum_{j=0}^{2}\beta_j\left(2P_{IM} + 2b_{IM}\sum_{j=0}^{2}\left(\epsilon_j P_{IM}^j\right) + P_{el} - P_{\mathrm{B}}\right)^j +$$
$$+\gamma\lambda(t)\frac{P_B}{\left(\sum_{j=0}^{2}\delta_j P_B^j\right)^{sgn(P_B)}} \tag{5.24}$$

with constraints:

$$SOC_{min} \le SOC_{t-\Delta t} - \frac{P_B}{\eta_{\mathrm{REC}}^{sgn(P_B)}}\frac{\Delta t}{U_{OC}(SOC(t))Q_b} \le SOC_{max} \tag{5.25}$$

$$0 \le P_d - P_{IM} \le P_{\mathrm{DE,max}}(n_{sh})b_{DE} \tag{5.26}$$

$$0 \le 2\left(P_{IM} + \sum_{j=0}^{2}\epsilon_j P_{IM}^j\right) + P_{el} - P_{\mathrm{B}} \le P_{\mathrm{DG,nom}}b_{DG} \tag{5.27}$$

$$-\frac{U_{\mathrm{T,max}}^2 - U_{OC}(SOC(t))U_{\mathrm{T,max}}}{R} \le \frac{P_B}{\eta_{\mathrm{REC}}^{sgn(P_B)}} \le \frac{U_{OC}(SOC(t))U_{\mathrm{T,min}} - U_{\mathrm{T,min}}^2}{R} \tag{5.28}$$

$$b_{IM}P_{\mathrm{IM,min}} \le P_{IM} \le P_{\mathrm{IM,max}}b_{IM} \tag{5.29}$$

$$b_{DE}, b_{DG}, b_{IM} \in \{0,1\} \tag{5.30}$$

5.8. INPUT & PARAMETER DETERMINATION

It can be seen that in order to solve the optimization problem, the instantaneous propulsive (P_d) and electric (hotel) power demand (P_{el}) must be known beforehand, as they are treated as inputs to the EMS controller. Of course this is not the case for a real-time controller for which the only input is the lever command by the operator, and as such the optimization process must be based only on predictions about these values (noted as $\widehat{P}_d, \widehat{P}_{el}$ respectively). How to predict these values using only past information and the current lever command is the topic of this section.

5.8.1. PROPULSIVE POWER DEMAND

Based on the fact that the lever position is a linear scaling of the desired shaft speed, which in turn is approximately equal to actual shaft speed (neglecting dynamics completely), and by assuming that the propeller law applies, the lever position at time t_k (noted as SLC - Single Lever Command) can be correlated to propulsive power demand:

$$\left.\begin{aligned}\left.\frac{SLC}{SLC_{\mathrm{max}}}\right|_{t_k} &= \left.\frac{n_{\mathrm{sh}}}{n_{\mathrm{sh,max}}}\right|_{t_k}\\ \left.\frac{\widehat{P}_d}{P_{\mathrm{d,max}}}\right|_{t_k} &= \left.\left(\frac{n_{\mathrm{sh}}}{n_{\mathrm{sh,max}}}\right)^3\right|_{t_k}\end{aligned}\right\} \Rightarrow \left.\frac{\widehat{P}_d}{P_{\mathrm{d,max}}}\right|_{t_k} = \left.\left(\frac{SLC}{SLC_{\mathrm{max}}}\right)^3\right|_{t_k} \tag{5.31}$$

Of course this oversimplification provides a very rough estimate of the propulsive power. However, provided that information regarding past lever positions and shaft power are available (with a sampling interval Δt), past estimation errors can be taken into account (while the system is in operation), so as to increase estimation accuracy. As such, Equation (5.31) is modified as follows:

$$\widehat{P}_d|_{t_k} = P_{\text{d,max}} \left(\frac{SLC}{SLC_{\text{max}}} \right)^3 \Bigg|_{t_k} + \mu \sum_{t=0}^{(n-1)\Delta t} \left(P_d|_t - \widehat{P}_d|_t \right) \frac{1}{n-1} \tag{5.32}$$

where μ is a multiplier used to tighten the estimation error tolerances. It's effect, along with the prediction accuracy provided by this correlation can be seen in Figure 5.12 for the simulated operating profile. As can be seen, this method provides accurate estimates (±5%) for the operating profile in consideration.

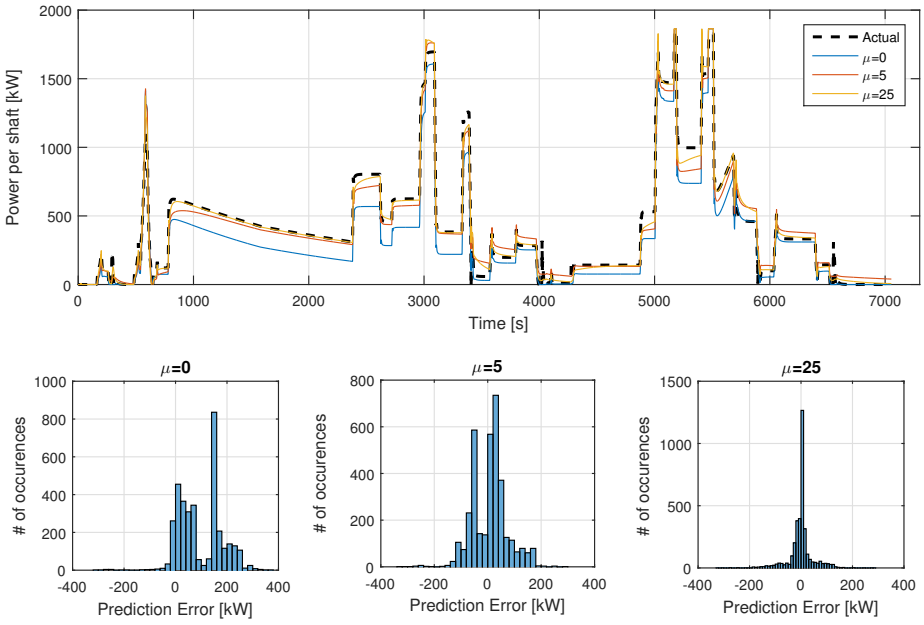

Figure 5.12: Propulsive Power Prediction Accuracy.

5.8.2. ELECTRIC POWER DEMAND

Regarding the electric power demand, it can be estimated from the electric load balance of the vessel, which in this case the total power demand amounts to 75 kW for Diesel electric mode, and 35 kW for Diesel Direct. These values will be used in the optimization process depending on the mode that the vessel operates in.

5.8.3. CO-STATE ADAPTATION

5.8.3.1. OVERVIEW

As discussed in Section 5.3, in ECMS the uncertainty about future operating conditions is transferred to an uncertainty on the correct (optimal) value of the co-state. Various methods have been proposed for the on-line estimation of the co-state, and can be classified into three approaches depending on the information used, namely past, present and future operating conditions:

- *Past operating conditions:* The idea in this case, promising in automotive engineering [Lei et al., 2017, Wei et al., 2016, Zhang and Xiong, 2015, Denis et al., 2016], is to use pattern recognition techniques. Optimal values for the co-state are precalculated off-line for a set of representative operating conditions to form a database, and during real-time operation a neural network periodically decides which representative operating pattern is closest to the current operating conditions. Then the EMS switches to the corresponding value of the co-state.

- *Past and present operating conditions:* A different approach is to constantly adapt the co-state value to the current operating conditions [Tianheng et al., 2015], or simply to the instantaneous deviations of SOC from its target value by means of a P- or PI- controller [Ambuhl et al., 2007, Kessels et al., 2008, Zhang et al., 2016, Khodabakhshian et al., 2013, de Jager and Steinbuch, 2008].

- *Past, present and future operating conditions:* The principle behind this idea is that when no information on future operating conditions is available, optimal fuel economy can not be guaranteed. As such, this family of algorithms aim at using any sort of estimation of future information to feed the ECMS control module with the most suitable values for the co-state. They include an on-the-fly algorithm for the estimation of the equivalence factor based on usually speed prediction (for road vehicles) [Sciarretta and Guzzella, 2007]. Another interesting approach is based on a predictive signal generator combined with a SOC tracking-based controller, which compute the desired battery SOC trajectory as a function of vehicle position using GPS data about the topographic profile of future road segments and the corresponding average traveling speeds [Ambuhl and Guzzella, 2009].

Using an approach based on past and present operating conditions as the ones proposed for land-based HEVs tends to be problematic for the case of a marine-based HEV. First of all, using pattern-recognition techniques requires data that is not readily available, and even if the data can be found, creating a database of optimally-tuned equivalence factors is a challenging and time-consuming task. Note, that this technique has proven to be promising in the automotive industry largely due to the existence of standardized driving cycles that represent conditions of urban, highway (or any variations thereof) driving conditions. As such, data collection or comparison of the actual operating conditions with a reference cycle is much easier.

Moreover, adapting the co-state value using a P- or PI- controller is also a delicate procedure, due to the sensitivity of the method to the co-state value. An extensive sensitivity analysis can be found in [Onori et al., 2016]. Furthermore, adapting the co-state

with a PI- controller based on a constant reference SOC value fails due to the charge-depleting nature of the controller that is being investigated in this work. Indeed, in order to minimize fuel consumption, the battery should be depleted by the end of the mission. One possible solution would be to use a linear, time-varying, SOC reference to adapt the co-state, starting from the maximum SOC at the beginning of the mission, to end up at the minimum SOC at the end of it, however, this fails as well if the end-point is not known.

5.8.3.2. CONSTANT CO-STATE

In this work, two different approaches have been used. Firstly, a constant co-state has been considered, its value (2.36) representing the nominal fuel consumption of the main Diesel engines. The rationale behind these choices is that the battery system will be used in such a way so as to discourage low engine loading, therefore increasing the overall efficiency of the propulsion plant. As indicated in [Yuan et al., 2016b, Dedes, 2013], when the load demand falls within the inefficient, low-loading, region of the engine, the value of the specific fuel oil consumption of the main engine will be higher than that of the battery system, therefore the controller will be forced to use the batteries entirely, or increase the loading of the engines toward a more efficient operating point and use the excess power to charge the batteries if the SOC is lower than its maximum value. However, after the results were obtained (see the relevant discussion in Section 6.3.2.3), it was clear that the value 2.16, representing the nominal fuel consumption of the main engines, corrected for the nominal efficiency of the components between the battery and the shaft (i.e. the battery's rectifier, the electric drive, and the induction machine) gives results close to the optimum.

The idea of a constant co-state has been suggested in several studies, as a means to simplify computations during simulation [Delprat et al., 2002, Guzzella and Onder, 2009, Sciarretta and Guzzella, 2007]. However it should be stressed that, considering the equivalence between ECMS and PMP, a constant co-state is not always correct from a mathematical point of view: It only applies in cases where the battery usage is limited to a relatively narrow SOC range so that the voltage and resistance do not vary so much with the operating conditions [Kim et al., 2011]. However, after a relatively straightforward analysis (see Appendix C), it was concluded that it can be applied in this case as well.

5.8.3.3. ADAPTATION BASED ON OPERATING LOAD ESTIMATION

Furthermore, an adaptive strategy has also been implemented which does not require tuning or modifying any control parameters, but numerically estimates the co-state value using measurement data. This strategy is based on a propulsive load prediction scheme, introduced in [Vu et al., 2014] and extended in [Vu, 2015], which only requires information regarding the general operational characteristics of the vessel. With those, it is able to forecast - to a certain degree of accuracy - the load demand at a given time instant using historical data obtained since the beginning of each mission. Note that in [Vu et al., 2014, Vu, 2015] this scheme is used to predict the power demand that the controller optimizes for, i.e. the equivalent of Section 5.8.1 (but over a longer prediction horizon), however in this work it will be used as a means to estimate co-state values.

Using available data from 28 operating profiles of tugboats operating in the port of

Rotterdam, the probability distribution of Figure 5.13 arises. It can be observed that on average the vessels operate on low load ($P_d^* \leq 20\%$) for 80% of the time, medium loads ($20\% < P_d^* \leq 50\%$) for 15%, and high load ($P_d^* > 50\%$) for only 5% of the total profiles' duration, as indicated in Figure 5.14. Based on this data, the power prediction scheme works as follows (for a more detailed description, the reader is referred to [Vu et al., 2014, Vu, 2015]):

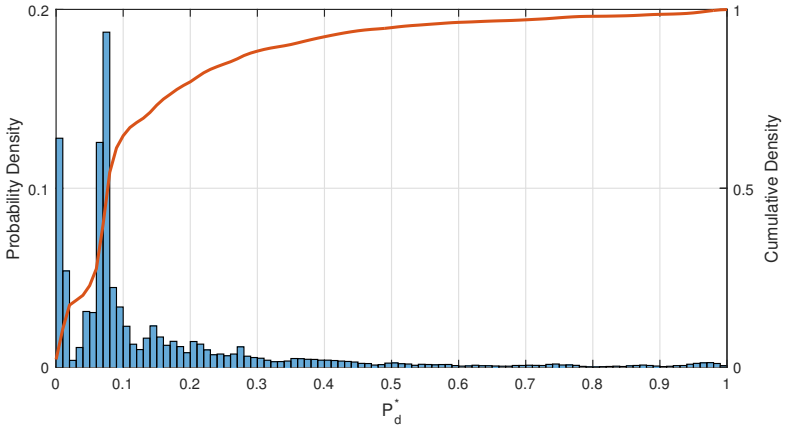

Figure 5.13: Measured Power Demand Distribution.

In the period $[0, n\Delta t]$, with n being a positive integer, and a sampling time Δt, let a_n, b_n, c_n be the percentages of time in which the vessel operates in low, medium, and high load respectively, with $a_n + b_n + c_n = n$. Let $k > 1$ be an integer, and ϵ a real number, such that $\frac{1}{k} < \epsilon < 1$. The integers a_{kn}, b_{kn}, c_{kn} can be estimated as:

$$\frac{a_{kn}}{kn} - a \approx \epsilon\left(\frac{a_n}{n} - a\right) \tag{5.33}$$

$$\frac{b_{kn}}{kn} - b \approx \epsilon\left(\frac{b_n}{n} - b\right) \tag{5.34}$$

$$\frac{c_{kn}}{kn} - c \approx \epsilon\left(\frac{c_n}{n} - c\right) \tag{5.35}$$

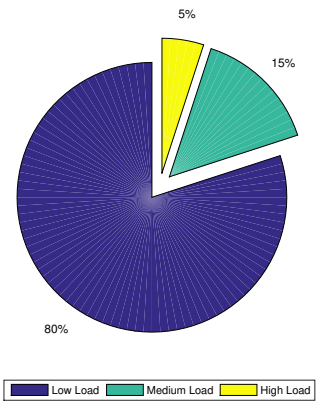

Figure 5.14: Operating Load Regions.

with a, b, c being the percentage of time in which the vessel operates in low, medium, and high load respectively. Finally, the total time percentage in the duration $[n\Delta t, kn\Delta t]$ that the vessel operates in each load demand region can be identified as: $(i_{kn} - i_n)$, $i = a, b, c$.

Figure 5.15 gives a comparison between the actual and predicted power demand for different sampling times Δt. As can be seen, the difference between the predictions and

the actual power demand is quite substantial. Although a decreasing sampling time allows the prediction scheme to track the changes in the load measurement, therefore giving sharper predictions, it can not capture peak or near-zero load conditions. It should be noted that a higher number of operating load regions was also used - six instead of the usual three (low, medium and high load) - but it did not affect the predicted results in any way, and neither did a different choice for the power limits over which the load regions are categorized (20% and 50% of the maximum power output per shaft).

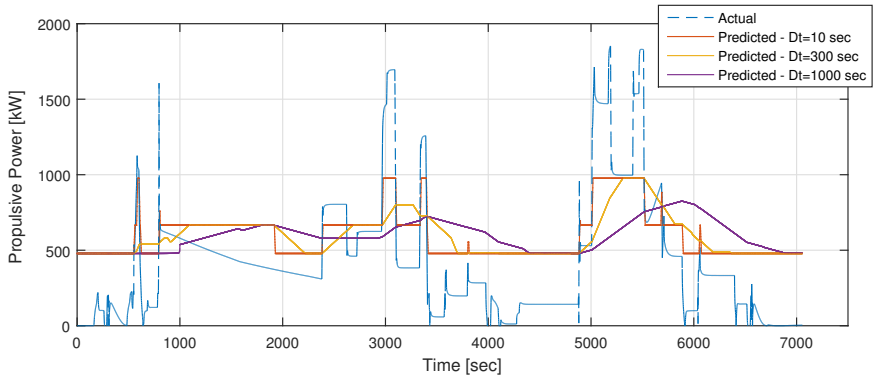

Figure 5.15: Comparison between load prediction and actual load demand.

It should be taken into account that, although a lower sampling time seems to give a better prediction, it does so with an inherent sacrifice in the prediction horizon (smaller time intervals of prediction). For this reason a sampling time equal to 300 seconds has been used, which as can be seen by Figure 5.15, shows a favorable trade-off between future time horizon - prediction accuracy.

Now, the co-state value is updated as follows: Following the notion of ECMS that using the battery *now* will result in an extra load *in the future*, whether or not the extra load will be imposed on the Diesel engines, Diesel generator, or the grid via shore connection, is of no consequence as far as the controller is concerned), the efficiency of the battery system is assumed to be equal to the efficiency of the main Diesel engine at the complementary percentage of the predicted power demand at nominal speed. Now, the co-state value is set to the inverse product of the chain efficiency between the battery and the shaft, according to Figure 4.2 (battery - rectifier - electric drive - induction motor). Note that the term $max(:)$ is used primarily for the induction motor and its electric drive, to fix their combined efficiency equal to its nominal value in case the predicted power demand is higher than the nominal power output of the motor:

$$\lambda = \left(\prod_{i=1}^{4} \max\left(\eta_{i,nom}, \eta_i (1 - \widehat{P}_d^*)\right) \right)^{-1} \tag{5.36}$$

The rationale behind Equation (5.36) can be easily understood using the following example. Based on intuition, the co-state's value gives an indication of the inefficiency of the battery (remember that a higher value for the co-state biases the controller not to

use the battery). Now, given a time instant, for simplicity and without loss of generality assume $n\Delta t$, and a predicted power demand over the next time interval $[n\Delta t, kn\Delta t]$ equal to $\widehat{P}_d^* = 0.3P_{d,nom}$ - a not so efficient operational condition for the Diesel engines - the following process is triggered: The 'efficiency' of the battery system, which is equal to $\eta_B = \eta_{DE}\left((1-0.3)P_{d,nom}\right) > \eta_{DE}\left(0.3P_{d,nom}\right)$, is combined with the efficiencies of its rectifier, induction motor and electric drive to form the total efficiency from battery to shaft $\eta_{B\to sh} = \prod_{i=1}^{4}\max\left(\eta_{i,nom}, \eta_i(1-\widehat{P}_d^*)\right)$. If the total efficiency is marginally higher than the efficiency of the Diesel engine, the value assigned to the co-state will indicate a lower specific fuel consumption for the battery compared to the Diesel engine. As such, the controller will be inclined to either turn the engines off and supply the propulsive power by operating the electric motors either using the battery or the Diesel generator, or increase the load of the Diesel engine (up to a maximum of $(1-\widehat{P}_d^*)P_{d,nom}$), and charge the battery system, again taking into consideration the efficiencies of all the components in-between. On the other hand, boost mode (Diesel engine and induction machine motoring in parallel) will only be enabled if the predicted power demand can not be satisfied by the Diesel engine at the reference shaft speed, therefore improving somewhat the system's response to abrupt accelerations.

5

Furthermore, regarding the choice of whether or not to supply energy to the induction motor by the battery system or the Diesel - generator, it is a matter of comparison between the efficiency of the Diesel - generator set and the battery, since all the other components between them and the shaft are the same. Given the fact that the Diesel engine, and the Diesel-generator set present approximately the same specific fuel consumption at nominal speed (this can be easily verified from Sections 4.2, 4.8), a fair 'weighing' between the two is also ensured from Equation 5.36. Note though that the maximum charging / discharging limits for the battery correspond to a power flow of 240kW, whereas the Diesel - generator has a much higher rated power output (650kW), therefore the comparison between the two is only valid for an inefficient operating region of the Diesel - generator, at about one third of its nominal power. If the electric power can be supplied by the battery only, it would always be preferable to switch the Diesel - generator off.

Finally, in order to bias the adaptive controller not to charge or discharge the battery when the SOC is near the upper or lower bounds respectively, the co-state value is modified by using an appropriately constructed multiplication factor $\mu(SOC)$, as follows:

$$\mu(SOC) = \begin{cases} 1 - \left(\dfrac{SOC(t) - SOC_\alpha}{\dfrac{SOC_{max} - SOC_{min}}{2}}\right)^\alpha, & \text{for } SOC(t) < SOC_\alpha \\ 1, & \text{for } SOC_\alpha \le SOC(t) \le SOC_\beta \\ 1 - \left(\dfrac{SOC(t) - SOC_\beta}{\dfrac{SOC_{max} - SOC_{min}}{2}}\right)^\alpha, & \text{for } SOC(t) > SOC_\beta \end{cases} \tag{5.37}$$

where:

$$\begin{aligned} SOC_{\alpha} &= 0.35 \\ SOC_{\beta} &= 0.85 \\ SOC_{max} &= 1.00 \\ SOC_{min} &= 0.20 \\ \alpha &= 3 \end{aligned}$$

The effect of this function can be seen in Figure 5.16. The multiplication factor has a unitary value if SOC $\in [SOC_{\alpha}, SOC_{\beta}]$, otherwise it increases (decreases) the co-state value by a maximum of 8% if the SOC is close to the lower (upper) bound.

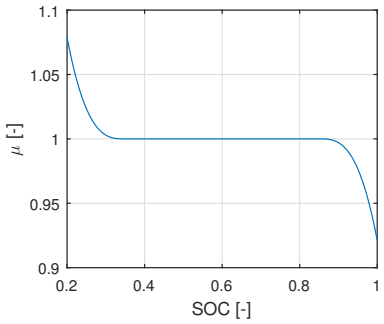

Figure 5.16: Multiplication factor to correct for SOC deviation.

5.9. PROBLEM TYPE IDENTIFICATION

Note that the following sections of this chapter refer only to ECMS, unless otherwise indicated.

5.9.1. OVERVIEW

The optimization problem belongs to the category of mixed-integer non-linear programming (MINLP) , as it combines both discrete variables, non-linear objective function, and non-linear constraints (Equations (5.27)-(5.28)). These optimization problems are very complex and mathematically classified as NP-hard, because the time needed to reach a solution increases exponentially with respect to the number of dimensions.

Most solution methods for MINLP include the application of *heuristic search methods*, or *deterministic methods*. Both approaches have advantages and disadvantages. As opposed to exact methods, which guarantee to give an optimum solution of the problem, heuristic methods only attempt to yield a good, but not necessarily optimum solution. Nevertheless, the time taken by an exact method to find an optimum solution to a difficult problem, is in a much greater order of magnitude than the heuristic one (sometimes taking so long that in many cases it is inapplicable). Key factors in determining the time required to solve a MIP problem are *the number of integer variables* and whether the problem has some *special structure* that can be exploited.

Luckily, for this specific application, the optimization problem does not involve a large number of discrete variables, so as to require a prohibitive amount of search trees. In fact, with $n = 3$ variables there are at most $2^n = 8$ solutions to be considered (as usually some of them can be readily discarded because they violate the functional constraints). Furthermore, the continuous relaxation of this optimization problem is also *Convex* (a proof of this is presented in Appendix B), which greatly simplifies the search for an optimal solution. As such, exact methods should not require an excessive amount of time to reach a solution that is indeed the optimal.

5.9.2. DETERMINISTIC METHODS FOR CONVEX MINLP

Exact methods for solving Convex MINLP can be classified into two broad categories, each with its own algorithms:

- Single-tree methods:
  - Nonlinear branch-and-bound
  - Branch-and-cut
- Multi-tree methods:
  - Outer approximation
  - Generalized Benders decomposition
  - Extended cutting-plane method

The most efficient class of methods however are of the hybrid type, which combine the strengths of both classes. An in-depth analysis of all these algorithms and combinations thereof, can be found in the work of [Belotti and Kirches, 2013]. Furthermore, since the continuous relaxations of the problem that are generated are convex, the subproblems can be readily solved by the following algorithms [Boom and De Schutter, 2015, Ben-Tal and Nemirovski, 2001]:

- Cutting-plane methods
- Ellipsoid method
- Interior-point methods

In this work, since the number of trees that need to be generated is not large (only $2^3 = 8$ as stated earlier) there is no need for a highly sophisticated multi-tree method, so as to reduce the search space, and as such, the classic *BIP branch-and-bound algorithm* will be used. Furthermore, all the convex methods mentioned above have been well-researched and seem to present similar characteristics in terms of complexity and computational time [Ben-Tal and Nemirovski, 2001]. As such, the subproblems created by the branch-and-bound method will be solved using an *interior-point method*.

5.9.3. BRANCH & BOUND - INTERIOR POINT ALGORITHMIC FRAMEWORK

To provide a better understanding regarding the solution process of the optimization problem, the branch-and-bound and interior point algorithms will be briefly discussed.

5.9.3.1. THE BRANCH & BOUND ALGORITHM

The basic concept underlying the branch-and-bound technique is to *divide and conquer*. Since the original problem is too difficult to be solved directly, it is divided into smaller and smaller subproblems, until these subproblems can be conquered. The dividing (*branching*) is done by partitioning the entire set of feasible solutions into smaller and smaller subsets. The conquering (*fathoming*) is done partially by *bounding* how good the best solution in the subset can be and then discarding the subset if its bound

indicates that it cannot possibly obtain an optimal solution for the original problem [Hillier, 2012]. The three basic steps - branching, bounding, and fathoming - are illustrated in Algorithm 1.

Algorithm 1: BIP Branch & Bound Method

Initialization: Set $U = +\infty$, and initialize the heap of open problems $\mathcal{H} = \emptyset$
Add the continuous relaxation of the problem: $(NLP|_{x_0 \in [0,1]})$ to the heap:
  $\mathcal{H} = \mathcal{H} \cup \{NLP|_{x_0 \in [0,1]}\}$, $i = 0$
while $\mathcal{H} \neq \emptyset$ **do**
  Select and remove a subproblem $(NLP|_{x_i \in [0,1]})$ from the heap
    $\mathcal{H} = \mathcal{H} - \{NLP|_{x_i \in [0,1]}\}$
  Solve the problem $NLP|_{x_i \in [0,1]}$, and let its solution be $x_i^{[0,1]}$
  if $NLP|_{x_i \in [0,1]}$ *is infeasible* **then**
    Fathoming: No further search is needed along this branch
  else if $f(x_i^{[0,1]}) > U$ **then**
    Fathoming: No further search is needed along this branch
  else if $x_i^{[0,1]} \in \{0,1\}$ **then**
    Fathoming: No further search is needed along this branch
    Update incumbent solution: $U = f(x_i^{[0,1]})$, $x^\star = x_i^{[0,1]}$
  else
    Branching: Set $i = i + 1$
    Add the subproblems $NLP|^{x_{i-1}=0}_{x_i \in [0,1]}$ and $NLP|^{x_{i-1}=1}_{x_i \in [0,1]}$ to the heap:
      $\mathcal{H} = \mathcal{H} \cup \left\{NLP|^{x_{i-1}=0}_{x_i \in [0,1]}, NLP|^{x_{i-1}=1}_{x_i \in [0,1]}\right\}$
end

One question that can be raised at this point is how to select for which subproblem to solve for, after the initialization. In this work, the simple *depth first search strategy* will be employed, in which all nodes at one level of the search tree are processed before any node at the next level. Understandably, this is the most basic algorithm of the branch-and-bound method, but since the number of trees in our problem is limited, it is sufficient. More advanced and sophisticated algorithms, in terms of selecting the branching variable, or choosing which branch to solve for first also exist. The interested reader is referred to [Belotti and Kirches, 2013] for further details.

5.9.3.2. INTERIOR POINT METHOD

The subproblems created by Algorithm 1 will be solved using an interior point method[1].

Consider a general problem:

$$\min_x f(x) \quad \text{subject to: } g_i(x) \leq 0, \quad i = 1, ..., m \tag{5.38}$$

with f, g_i convex functions.

Interior point methods solve problem 5.38 by applying Newton's method to a sequence of equality constrained problems, using the following procedure (an extensive analysis can be found in [Boyd and Vandenberghe, 2004]):

[1] Matlab Optimization Toolbox™was used for this.

1. Introduce slack variables ($w_i > 0$) to turn all inequality constraints into equality constraints.

2. Replace non-negativity constraints of the slack variables with logarithmic barrier terms (barrier functions) $\left(\sum_{i=1}^{m} log(w_i)\right)$ in the objective function. Note that the slack variables are restricted to positive values to keep the barrier functions bounded.

3. Incorporate the new equality constraints into the objective function using Lagrange multipliers (y_i). At this point the original problem, has been transformed to the following:

$$\min_{x,y} L(x,y) = f(x) - \mu \sum_{i=1}^{m} log(w_i) + y^{\intercal}\left(g(x) + w\right)$$

where $\mu > 0$ is a parameter that sets the accuracy of the approximation. As $\mu \to 0$ the approximation becomes more accurate.

4. Apply the Karush–Kuhn–Tucker conditions, which for convex problems are necessary and sufficient conditions for optimality.

5

5.10. RESULTING CONTROLLER LAYOUT

To conclude, now all the relevant information about the EMS controller's structure has been presented, the overall layout of the controller can be presented:

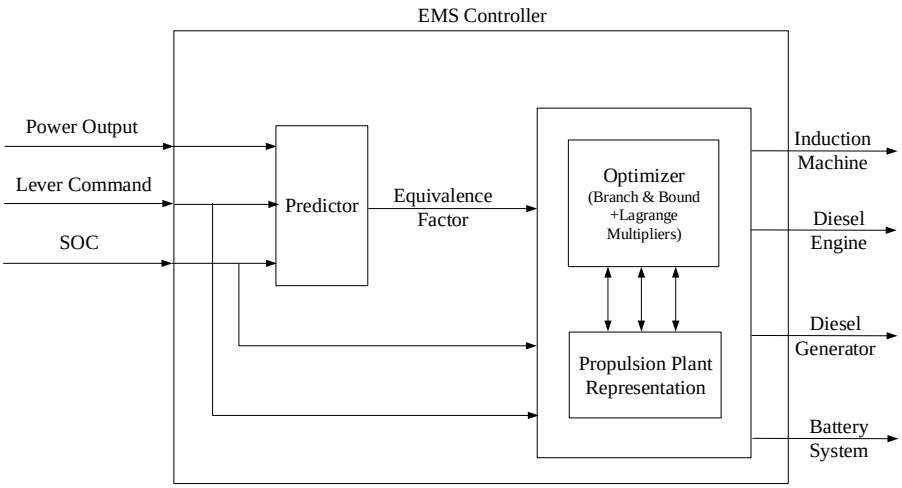

Figure 5.17: Schematic overview of the EMS controller.

The inputs to the controller include the lever command, a data buffer that tracks the total power output that the vessel products from the beginning of the mission up to the last call of the EMS controller, and a feedback regarding the SOC of the batteries. Its outputs indicate whether each component of the propulsion system is operating or not.

Internally, it consists of a predictor, for the adaptive strategy only, and an optimizer. The predictor is responsible for adjusting the co-state value, according to Section 5.8.3. Based on its value, the optimizer, using the simplified components' models that were introduced in this Chapter, runs the optimization algorithm according to Section 5.7.

6

CONTROLLER EVALUATION

"Negative results are just what I want.
They're just as valuable to me as positive results.
I can never find the thing that does the job best until I find the ones that don't."

-Thomas Edison

Different case studies are used to illustrate the concept of the supervisory control algorithm introduced in Chapter 5. Details about the response of the propulsion system will be presented, and the behavior (decisions) and robustness of the strategies will be analyzed. Detailed results for each case (profile) are presented in Appendix D.

6.1. INTRODUCTION

Different operating profiles have been used to test the performance of the proposed control algorithm, in terms of fuel consumption reduction. To give a well-founded indication about the 'quality' of the EMS, the results have been compared with the existing rule-based controller, and the global optimum obtained with Dynamic Programming. These simulations will indicate whether or not it is worthwhile to develop this control strategy further and/or implement it in a real vessel. Throughout the section 'DP' refers to Dynamic Programming, 'ECMS' implies constant co-state value throughout the profile, in contrast to 'A-ECMS' which includes the adaptive algorithm presented in Section 5.8.3.3, 'RB' refers to the rule-based controller, and the notation 'RB-CD' has been used for the rule-based controller for which the rule-set used to recharge the battery has been removed.

Before moving on with the results and the comparison, it should be pointed out that the results obtained with Dynamic Programming, being the global optimum in terms of fuel consumption, have been used as a benchmark for the real-time strategies, and also

to provide usable insights regarding control decisions. On the other end of the spectrum is the rule-based controller, which has been designed to be *charge-sustaining*. Its results have been included in this section as an upper bound in terms of fuel consumption.

6.2. MODE SELECTION

Firstly, a simulation for straight-line quasi-static maneuvers was performed, in order to compare mode selection between the different controllers. The power output of each component and total fuel consumption, with respect to vessel speed are given in Figure 6.1.

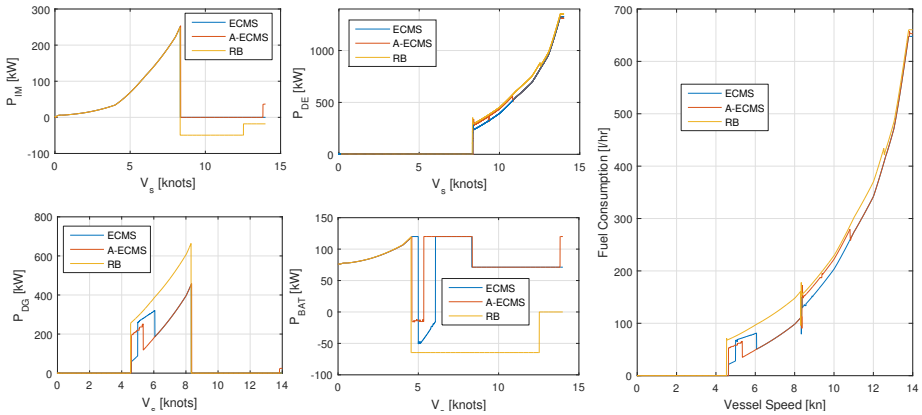

Figure 6.1: Fuel Consumption in quasi-static maneuvers.

The following remarks can be made:

- $v_s \in [0-4.5)$ kn: All controllers present the same behavior, that is discharging the batteries to propel the vessel with the induction machines.
- $v_s \in [4.5-8.5)$ kn: With the rule-based controller, the Diesel-generator is used to power the induction machines and recharge the battery. The ECMS-based controllers also switch on the Diesel-generator to power the induction motors, however they recharge the batteries at lower C-rates and not for the whole speed range. For speeds above 6 knots, both controllers operate the induction machines combining batteries, which are discharged at the upper bound, and the Diesel - generator as well.
- $v_s \in [8.5-14]$ kn: All controllers switch off the Diesel-generator, operating with the main engines. The difference is that the rule-based controller, using the main engine, keeps recharging the battery up to a speed of around 13 knots while also providing power for the hotel loads. On the other hand, the ECMS-based controllers use the main engines to propel the vessel, and the batteries to provide power for hotel loads. Finally, just before reaching 14 knots, A-ECMS operates switches to boost mode, using the batteries to provide power both for the hotel loads, and induction motors.

It should be noted that there is also an inherent time-dependency on the ECMS-based controllers' decisions, coming from the SOC time-dependent trajectory. This implies that, given a different simulation time, the recharging of the batteries might occur at a different operating point, or not at all. Regardless of that, the operation of the Diesel-generator and main engines is roughly the same, as both controllers switch them on/off depending on the power demand. The most significant difference is observed in the way the batteries are being operated.

6.3. STANDARD OPERATIONAL PROFILES

The only goal of the proposed control algorithms is to reduce fuel consumption. As such, the scope of these simulations is to evaluate the control decisions in terms of total fuel used for the mission, analyze them, and identify the potential for further improvements.

In Figure 6.2 the different operating profiles used for the simulations are presented. It should be noted that, in order to have missions that are representative of the actual operating conditions of a tugboat, all the profiles are variations of the original profile (Profile 1) as measured by Damen Shipyards Group - which implies that the overall power demand approximates the distribution presented in Figure 5.13. Note that, the controllers have also been tested for two profiles with radically different power demand distributions, compared to the profiles presented here. The relevant discussion can be found in Section 6.4.3.

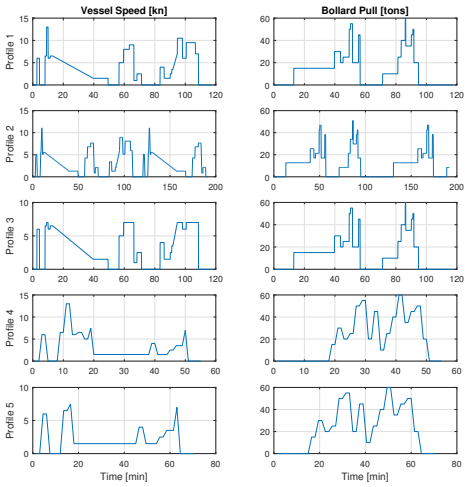

Figure 6.2: Simulated Operating Profiles.

- Profile 2 is a repeating sequence (1.5 times) of the original profile, with a constant 15% decrease in bollard pull and vessel speed.
- In profile 3, the speed profile is the same as the original, but restricted to a maximum of 7 knots, bollard pull has not been altered.
- Profile 4, statistically speaking, is the same as the original, however it has been modified to include only 1 (longer) towing job, as can be seen in the bollard pull graph.
- Profile 5 is a 50% time elongation of profile 4, with a maximum speed of 7 knots.

6.3.1. COMPARATIVE RESULTS

In Tables 6.1 - 6.2, the results of these simulations are presented. It should be noted that the controller referred to as 'ECMS-2', comes from the discussion of Section 6.3.2.3, the results are also presented here for the sake of completeness.

Table 6.1: Comparative Results - Fuel Consumption, Efficiency, Running Hours.

	EMS	Fuel		$\bar{\eta}$			C-rate	SOC	$t_{\text{ICE,ON}}$	
		m_f [kg]	Savings [%] RB	DE	DG [%]	vessel	[-]	[%]	DE [%]	DG of t_{end}
Profile 1	DP	336	7.7	35.0	37.6	35.5	0.49	20	68	41
	RB	364	-	35.9	38.1	36.0	0.31	94	69	28
	RB-CD	361	0.8	35.7	37.8	35.3	0.30	69	69	28
	ECMS	345	5.3	36.0	36.9	35.8	0.39	42	68	36
	A-ECMS	343	5.7	36.0	36.2	35.8	0.35	36	68	36
	ECMS-2	340	6.6	35.7	36.9	35.6	0.37	31	68	38
Profile 2	DP	551	5.6	36.4	36.7	36.1	0.43	20	69	30
	RB	584	-	37.6	38.2	36.0	0.32	99	69	29
	RB-CD	569	2.6	36.7	38.9	35.2	0.29	61	69	29
	ECMS	567	3.0	38.1	34.6	35.4	0.31	58	68	39
	A-ECMS	566	3.2	38.2	35.0	35.3	0.30	56	68	44
	ECMS-2	558	4.4	38.1	35.6	35.10	0.32	41	69	38
Profile 3	DP	311	8.8	34.0	37.0	35.8	0.44	20	65	50
	RB	341	-	34.9	38.4	36.3	0.30	94	65	40
	RB-CD	338	0.9	34.7	38.2	35.3	0.20	78	64	40
	ECMS	329	3.5	35.0	34.9	35.6	0.32	58	64	50
	A-ECMS	323	5.6	35.0	35.3	35.7	0.30	42	65	50
	ECMS-2	316	7.3	34.8	35.7	35.7	0.32	29	65	44
Profile 4	DP	239	11.2	36.4	36.7	37.2	0.49	27	64	62
	RB	269	-	35.9	38.1	37.5	0.29	100	64	45
	RB-CD	267	0.8	35.8	38.8	37.0	0.20	86	64	45
	ECMS	259	3.9	36.8	37.2	37.0	0.28	66	65	63
	A-ECMS	250	7.3	36.8	37.5	37.2	0.32	45	65	60
	ECMS-2	243	9.6	36.6	37.1	37.1	0.32	33	65	58
Profile 5	DP	470	4.8	37.8	36.9	37.3	0.47	20	75	55
	RB	494	-	39.6	38.3	37.9	0.30	100	75	35
	RB-CD	489	1.0	39.2	38.1	37.4	0.20	69	74	35
	ECMS	483	2.2	38.1	36.2	37.4	0.32	53	75	48
	A-ECMS	479	3.0	38.2	36.3	37.1	0.34	45	75	45
	ECMS-2	475	3.8	38.0	36.4	37.3	0.32	38	75	49

ECMS: $\lambda = 2.36$, ECMS-2: $\lambda = 2.16$.

From Table 6.1, it can be seen that the total fuel consumption is consistently lower with the ECMS-based controllers by an average of 3.5% (ECMS), 5.0% (A-ECMS) and 6.3% (ECMS-2), with respect to the existing control strategy, and the solutions obtained with Dynamic programming give average fuel savings of 8%. It is interesting to note that ECMS-2, for which the most appropriate *constant* co-state has been used, gives an extra fuel consumption of around 1-2% compared to the DP solution. This implies that, in

order to obtain this additional 1-2%, a time-varying function is needed for the co-state.

Table 6.2: Comparative Results - Operating Modes.

	EMS	Propulsive Power			Electric Power			
		DE	IM	Hybrid	DG	BAT	IM	Hybrid
		[%] of mission duration						
Profile 1	DP	47	32	21	-	43	12	45
	RB	70	30	-	28	06	66	-
	RB-CD	70	30	-	28	06	66	-
	ECMS	55	35	10	05	62	-	32
	A-ECMS	56	33	11	02	63	-	34
	ECMS-2	50	34	16	04	48	11	37
Profile 2	DP	10	70	24	23	04	22	51
	RB	70	30	-	26	07	67	-
	RB-CD	70	30	-	26	07	67	-
	ECMS	42	39	17	08	02	48	42
	A-ECMS	24	53	19	29	19	29	24
	ECMS-2	21	50	29	26	08	18	19
Profile 3	DP	38	45	17	01	34	14	50
	RB	58	42	-	39	06	55	-
	RB-CD	58	42	-	39	06	55	-
	ECMS	29	56	14	36	14	29	21
	A-ECMS	57	35	08	48	07	-	45
	ECMS-2	30	50	20	12	43	26	19
Profile 4	DP	26	34	60	-	26	-	74
	RB	64	36	-	42	10	49	-
	RB-CD	64	36	-	42	10	49	-
	ECMS	30	42	28	44	23	10	23
	A-ECMS	28	42	30	34	26	08	32
	ECMS-2	27	28	45	-	26	09	20
Profile 5	DP	29	22	49	-	32	08	59
	RB	75	25	-	33	12	55	-
	RB-CD	75	25	-	33	12	55	-
	ECMS	27	31	42	31	36	08	24
	A-ECMS	23	33	44	24	33	08	35
	ECMS-2	28	20	52	-	26	09	65

Hybrid: Use of more than one component for power production.

In terms of efficiency, the RB controller (the one including battery recharging) could not be surpassed, and is followed closely by the DP solution, and then the ECMS-based controllers. This implies that fuel consumption is reduced primarily because of the increased use of the batteries, rather than the increased efficiency of the propulsion

plant, which can also be seen by Table 6.1 quite clearly, considering the inversely proportional relation between fuel savings and final SOC. This implies that, a charge-sustaining ECMS-based controller would result in fuel consumptions comparable to those obtained with the RB controller. Regarding the average C-rate used by each controller, it can be seen that DP exhibits the 'heaviest' use of the batteries, with an average C-rate close to the limit. The ECMS controllers are not so aggressive as DP, and RB controllers are the most conservative.

Considering the running hours of the ICEs (last two columns of Table 6.1), it can be seen that the operation of the main engines is approximately constant for the same profile regardless of the solution method. This indicates that all the controllers, along with the DP solution operate the main engines as a last resort, only when the power demand can not be satisfied by the other components. Regarding the Diesel-generator sets, the RB controllers operate them the least. Increased running hours are observed for all the other controllers, with the DP algorithm to operate them the most. This hints that parallel operation of more than one energy sources is necessary in order to reduce fuel consumption, as Table 6.2 also indicates. The question at which operating points parallel operation is preferable, is the discussion of Section 6.3.2.2. The DP solution shows the highest (in terms of time) use of hybrid modes, followed by the ECMS-based controllers. On the other hand, the rule-based controllers have not been designed to operate on hybrid modes.

6.3.2. CONTROLLER BEHAVIOR ANALYSIS

In the following, the decisions of the ECMS controllers and DP solution will be analyzed, to identify sources of poor decisions and reflect on how these can be improved.

6.3.2.1. DIESEL ENGINE LOADING & EFFICIENCY

The main question that all controllers try to answer is when it is most efficient to charge or discharge the battery in the typical two-to-three hour operating profile. Starting with the DP solution, it was found that batteries should also be discharged at peak load conditions, as the operating mode chosen is boost mode, including battery discharge. Consider that the peak power delivered by the Diesel engines is lower for all the profiles by 240kW, power that is supplied by the induction motors. Although it seems counter-intuitive from an efficiency point of view, in terms of total fuel consumption it is reasonable: According to Figure 6.3, reducing the load of two Diesel engines by $240/P_{DE,nom} \approx 13\%$, results in a fuel consumption reduction of about $2 \times 75 = 150\ l/h$. On the other hand, loading the third engine (DG) at $\left(2 \times 240/\eta_{\text{IM+D}} - P_{\text{bat,max}}\right)/P_{\text{DG,nom}} \approx 60\%$ results in an increase of about $100\ l/h$.

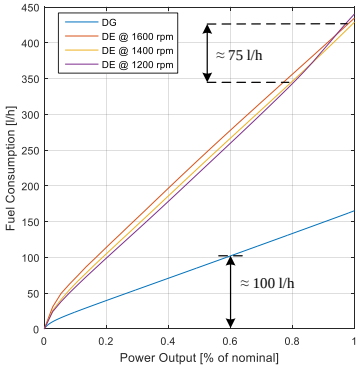

Figure 6.3: Fuel Consumption of ICEs.

This fact however, was not identified by neither of the ECMS-based controllers. In

fact, both of them operate with the Diesel engines only, and use the batteries and/or Diesel-generator for hotel loads. This choice indicates ill-defined co-state values. The values that have been chosen are relatively high (which is also reflected on the final SOC), penalizing heavy use of the batteries. Without the batteries to supply part of this extra load, the Diesel - generator must be loaded to around 90% of the nominal point (including the hotel loads) it can be verified from Figure 6.3, that by loading the Diesel-generator at around this value, is exactly the same (in terms of total fuel consumption) as operating the two main engines to supply the requested power. In fact, the choice of the co-state values are so high that the ECMS-based controllers decide that it is better to generate part of the electric load with the induction machines to recharge the batteries (note that in the objective function - Equation (5.24) - the artificial fuel consumption of the batteries gets negative values if the batteries are being charged). To give a perspective about the subtle differences in fuel consumption, Figure 6.4 presents the actual fuel consumption for the three different choices of the controllers, for operating profile 1 while the vessel is assisting. For the RB and ECMS-based controllers the fuel consumption is practically the same, whereas the DP solution, gives a decrease of about 0.02 kg/sec.

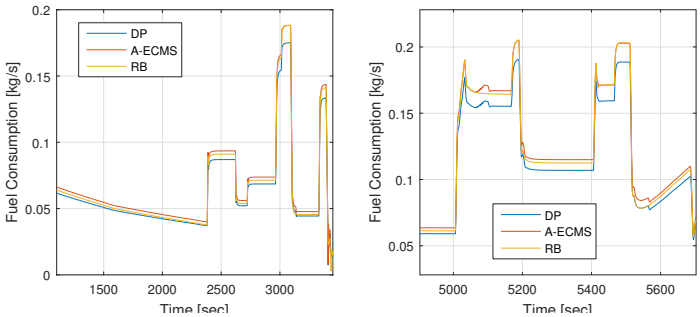

Figure 6.4: Fuel Consumption while towing - Profile 1.

The lower loading of the ICEs compared to the other components is also reflected on their efficiency drop. Considering the rest of the components the efficiency difference is negligent, for example the combined efficiency of the induction machine and the electric drive stays very close to its nominal value of 0.93. The same also applies to the battery system, for which the maximum efficiency variation was found to be equal to 1.7%. However, regarding the main engines, the ECMS-based controllers operate them most efficiently, followed by the RB controllers. In Figure 6.5, the main engines' operation points for three out of the five different

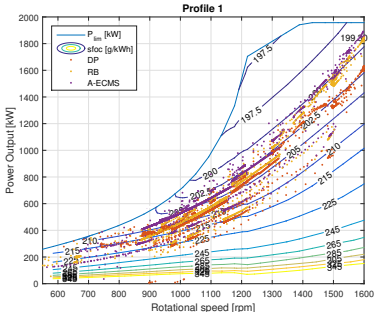

Figure 6.5: Operational Points of the Diesel engines - Profile 1.

controllers are shown for profile 1. Note that the difference between the two RB and the two ECMS-based controllers is not substantial, therefore the operational points are not shown here. Small differences can be found in the region between 900 and 1200 rpm, in which the A-ECMS controller has chosen slightly higher loads, making the operation of the engine somewhat more efficient. On the other hand, the DP solution is clearly lowering the engine load, especially above 1400 rpm. The behavioral differences of the controllers regarding the engines is clearer for Profiles 4 and 5, as shown in Figure 6.6. At lower speeds (< 1000 rpm) with the A-ECMS controller, the main engines are clearly more efficient due to higher loading, however at higher rotational speeds the difference between A-ECMS and the RB controller diminishes. The reverse is observed for the DP solution. At low speeds there is no significant distinction between the operating points of the RB controller and the DP solution, however at high speeds the lower loading of the engines is notable.

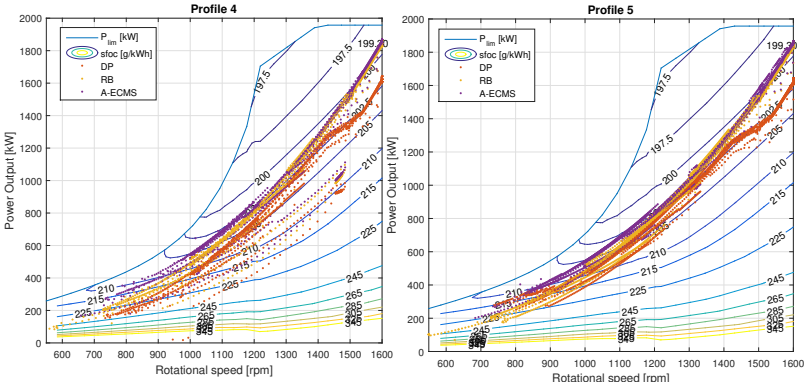

Figure 6.6: Operational Points of the Diesel engines - Profiles 4 and 5.

On the other hand, the Diesel-generators are most efficient with the RB controller, whereas ECMS and A-ECMS fail to operate them at such efficient points. Finally, the DP solution gives the lowest average efficiency of all the controllers with an average drop of about 1.6% and 6.5% respectively, due to the low loading of the ICEs, both in terms of propulsive and electric power production. This, of course, indicates that hybrid operational modes are heavily used by the DP solution, while not so for the rest of the controllers. This can also be seen in Table 6.2, where it is evident that the degree of hybridization is relatively higher for DP compared to the other controllers, both in terms of propulsive, as well as electric power production.

6.3.2.2. DECISION VARIABLES

Apart from identifying and comparing the behavior of the propulsion system with each controller, a key component of this analysis is to determine which factors affect the control variables, especially for the DP solution (for the ECMS-based controllers, this has been discussed in Section 5.8.3, regarding the co-state). First of all, at very low shaft speeds all of the controllers present the very same behavior, which is using the batteries as a power source for the induction machines, in order to propel the vessel. However, at

higher speeds (when the maximum battery power alone is not able to satisfy the power demand via the induction motors), the behavior of each controller is different.

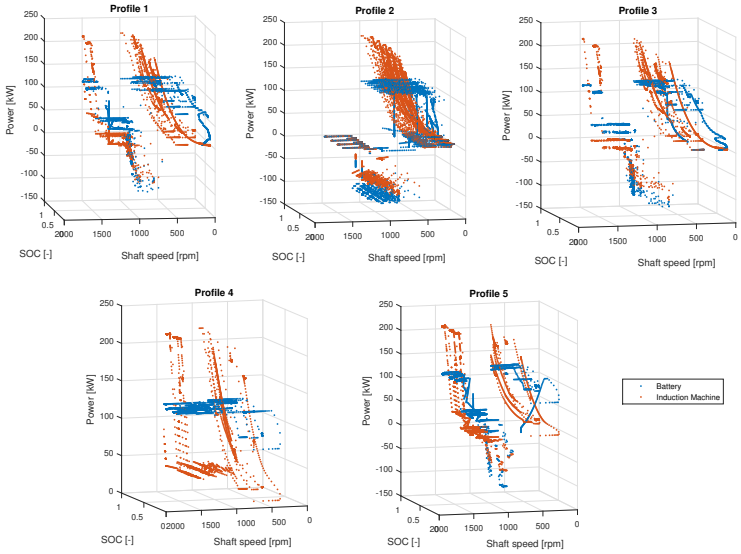

Figure 6.7: DP Solution - Control Decisions.

For the DP solution, there is a trend regarding the battery and induction machine power outputs. This can be seen in Figure 6.7, in which both control variables are depicted as a function of SOC and shaft speed. Regardless of profile or SOC the following behavior is observed:

- $n \in [0, 400]$ rpm: The induction machines are propelling the vessel supplied by the batteries, which also provide power for the hotel loads. The maximum discharging current for the batteries is reached at around 400 rpm.
- $n \in (400, 800]$ rpm: The induction machines keep their motoring operation up to around 800 rpm, powered by both batteries and Diesel-generator, the latter needed due to the C-rate limitations imposed on the battery, which can no longer provide the necessary power to the induction machines on their own.
- $n \in (800 - 1000]$ rpm: In this region, the induction machines are generating power to recharge the batteries at the maximum allowable current. Exception here is profile 4, in which the batteries are still being discharged as in the previous region. This occurs due to the low duration of this profile (3300 sec) compared to the rest of the profiles whose duration ranges between 5500 - 11500 sec.
- $n \in (1000 - 1400]$ rpm: The induction machines are turned off, with the batteries providing power for the hotel loads. However, in profile 4 it seems that the induction machines keep motoring in parallel with the Diesel engines, using the maximum available power from the batteries, which also provide power for the hotel

loads. Furthermore, different behavior is also observed for profile 2, in which both batteries and induction machines are turned off. This is due to the extended operation of the vessel at relatively low loads, considering that profile 2 is essentially a 50% extension of profile 1, with the vessel speed and towing force equal to 85% of the values used in profile 1 (Figure 6.2 provides a visualization).

- $n \in (1400 - 1600]$ rpm: Once more, apart from profile 2, for which the same behavior as in the previous region is observed, maximum discharging occurs for the batteries, with the induction machines motoring to the limit. Taking also into account the fact that the Diesel generator is also turned on (see Section 6.3.2.1), this indicates that the parallel operation of all three energy sources on board is preferable.

Although the pattern that emerges is relatively straightforward, the ECMS-based controllers failed to identify it, and they do not exhibit the same behavior. Of course, as stated earlier, this can be translated into a wrong co-state value. Considering Figures 6.8 - 6.9, there is no discernible pattern regarding the decisions of the controllers. The only safe remark is that the control decisions seem to be mostly SOC dependent, with just a weak relation to shaft speed.

Furthermore, there does not seem to be any noticeable difference between ECMS and A-ECMS apart from profiles 3 and 4 (see Table 6.1), which suggests that there is either no added-value in investing into a more complicated algorithm to adapt the co-state, or possibly, that the prediction horizon considered in this work is not sufficient. Comparing graphs 6.8 - 6.9 for each profile, it can be seen that the adaptive strategy tends to be more aggressive with the batteries, which is reflected in the lower SOC at the end of each profile, as shown in Table 6.1.

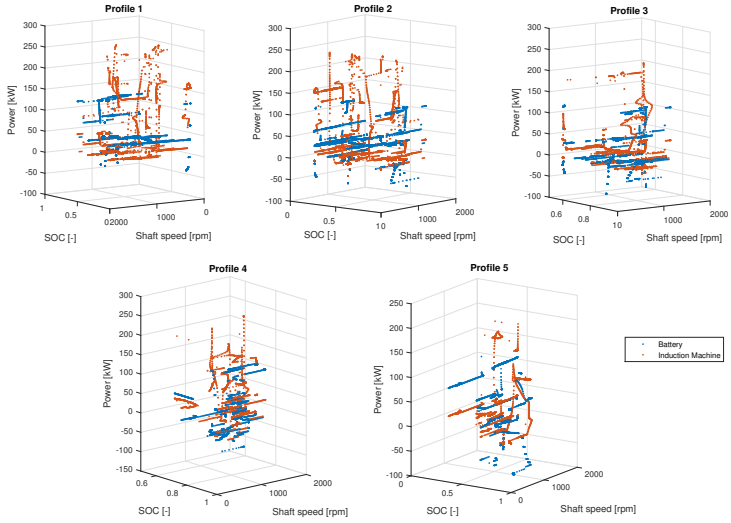

Figure 6.8: ECMS - Control Decisions.

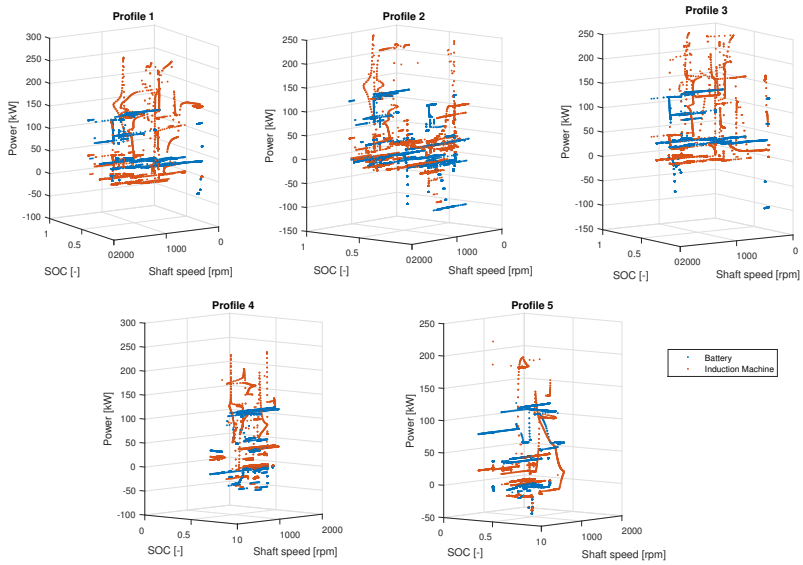

Figure 6.9: A-ECMS - Control Decisions.

6.3.2.3. CO-STATE TRAJECTORIES

A quantitative view of the optimality of the solution obtained with the two ECMS-based controllers can be given, by calculating the optimal co-state value (or its trajectory) using the DP solution, following the discussion of Appendix C.

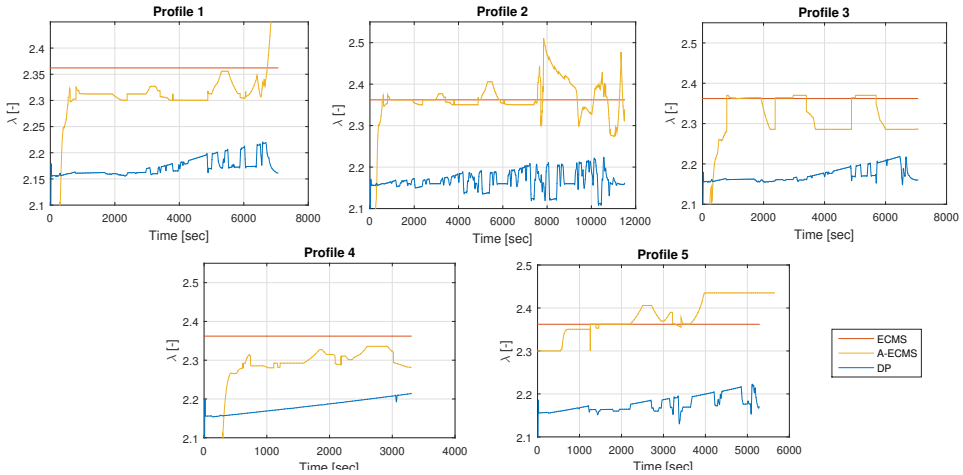

Figure 6.10: Co-state trajectories - Profiles 1 to 5.

Figure 6.10 shows the co-state trajectories of each solution. Of course, since the tra-

jectories of the ECMS-based controllers do not follow the path indicated by the DP solution, both of them result in sub-optimal solutions. What is of importance though, is that the average value of the optimal co-state is on average equal to 2.16, which corresponds to a fuel consumption of 182 g/kWh. For A-ECMS on the other hand, the co-state trajectory is again too high, and far for optimal. Finally, regarding the optimal co-state itself, it should be noted that these graphs also validate that the co-state is indeed more volatile at lower SOC values, as Figure C.12 also indicates.

The same value for the most suitable *constant* co-state can also be verified by Figure 6.11, which shows the total battery energy used as a function of fuel savings for all five operating profiles. From this graph, two important conclusions can be drawn: First of all, there is an almost linear relationship between the two variables, and secondly, the gradient of this line shows that for these 'average' tugboat profiles, i.e. profiles which approximate the power demand distribution of Figure 5.13, the equivalent fuel consumption of the battery can be assumed equal to 182 g/kWh ($\lambda = 2.16$).

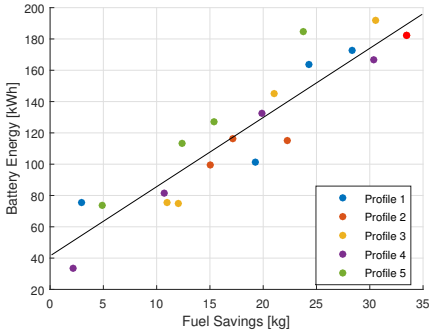

Figure 6.11: Battery energy as a function of achieved fuel savings.

Interesting is the fact that this value can be easily traced back to the nominal fuel consumption of the main engine - equal to 199 g/kWh - applying a correction for the efficiency of the components that are in-between the shaft and the battery. i.e. the battery's rectifier, with a nominal efficiency $\eta_{REC} = 0.98$ (assumed to be constant), and the induction machine and electric drive, with a nominal efficiency $\eta_{IM+D} = 0.93$, which is indeed roughly constant. As stated in Section 6.3.2.1, the average efficiency of the induction machine and the drive system for all the profiles was found to be equal to 0.929. Therefore: $\text{sfoc}_{BAT} = \text{sfoc}_{DE} \times \eta_{REC} \times \eta_{IM+D} = 181.368$ g/kWh $\Rightarrow \lambda = \frac{\text{sfoc}_{BAT}\ Q_{\text{lhv}}}{3.6\ 10^6} = 2.151$.

6.4. SENSITIVITY ANALYSIS

Apart from the simulations presented in the previous section, a sensitivity analysis has been performed with respect to the value of the co-state, the operating profiles and the batteries' power limitations.

6.4.1. EFFECT OF CO-STATE VALUE

At first, the sensitivity of ECMS - in terms of resulting fuel consumption - was investigated, with respect to the co-state value. The remark that ECMS is very sensitive to this parameter has been pointed out in several studies, and is also identified as its main disadvantage [Sciarretta and Guzzella, 2007]. Multiple simulations were performed on the original profile (Profile 1 in Figure 6.2), with different (constant) co-state values, to provide an indication of how the solution changes depending on this value.

The resulting SOC trajectories and fuel consumption are shown in Figure 6.12. It

can be seen that an increasing co-state indeed penalizes the use of the batteries, as the final SOC keeps increasing with higher co-state values. On average 10% increase of the co-state results in about 35% increase on the final SOC. However, the most important observation is that the lowest fuel consumption is observed for a co-state value equal to 2.16, which agrees with the discussion of Section 6.3.2.3. Furthermore, using this value results in a total fuel consumption of 340 kg. Considering Table 6.1, the solution obtained with DP for profile 1 (with an average co-state equal to 2.16), results in 336 kg in total. This shows that in order to reduce the 4 kg difference between the two solutions, it would be necessary to transition from a constant co-state to a time-varying value, as indicated in Appendix C.

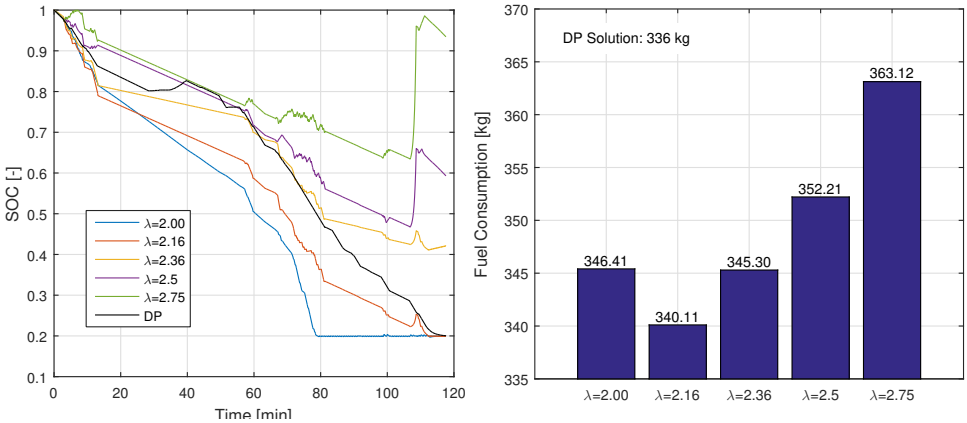

Figure 6.12: SOC trajectories and fuel consumption for different co-state values.

6.4.2. EFFECT OF INCREASED BATTERY POWER LIMITS

The scope of the simulations in this case is twofold: To identify the potential of the proposed controllers for further fuel savings when the battery's maximum charge and discharge current are increased, and furthermore to see what effects the increased limits have on them, i.e. check their robustness. As such, the C-rate limits have been increased from 0.5 to 2, and new simulations for profile 1 of Section 6.3 have been performed for the two ECMS-based controllers, and the new optimal solution has been found using Dynamic Programming.

Comparative results for both the initial and the new C-rate limits, are given in Tables 6.3 - 6.4, at the end of this Section. The resulting SOC trajectories and total fuel consumption for all the controllers, are presented in Figure 6.13. First of all, the new DP solution results in a fuel consumption of 324.8 kg, 11.3 kg less than with the previous C-rate limits. On the other hand ECMS has not been affected by the increased limits at all. If this limit relaxation has not resulted in a different solution - better or worse - it means that the existing control decisions of ECMS for this profile can not be further improved with this co-state value. Finally, A-ECMS shows a highly different behavior for this new case. In terms of fuel consumption, a reduction of around 4 kg has been achieved, from

340.2 kg down to 336.1 (equal to the DP solution for profile 1 with the original battery limits).

Considering the highly different SOC trajectory obtained with A-ECMS in this case [1], the following conclusions can be drawn: To begin with, the improved solutions obtained with A-ECMS (compared to a constant co-state) for the standard operating profiles (Section 6.3) may be attributed more to the relatively narrow constraints (the algorithm was hitting the power's lower bound, which prevented the early discharging), rather than the correct load prediction and timely adjustment of the co-state. Secondly, considering the SOC trajectories of DP and A-ECMS, the only important difference lies in the recharging of the battery. Figure 6.13 shows that both of them do recharge the battery between 25-60 minutes of operation, however A-ECMS fails to recognize that a high charging current is preferable, which indicates a relatively low co-state value. The right graph on Figure 6.14 also validates this.

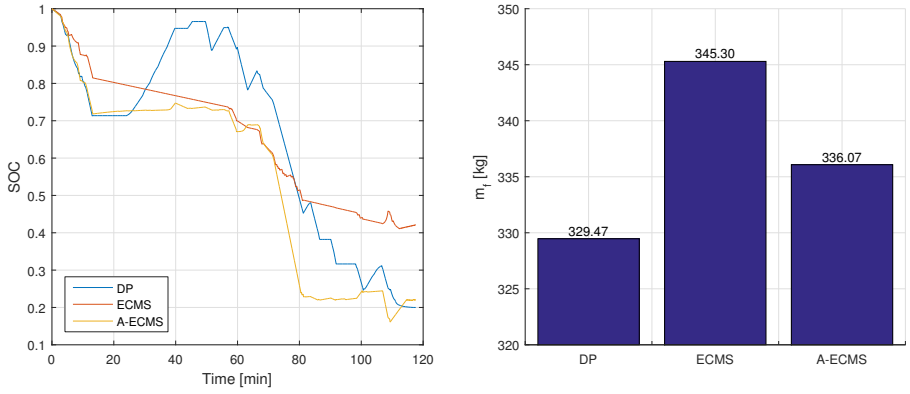

Figure 6.13: SOC trajectories and fuel consumption for increased C-rate limitations.

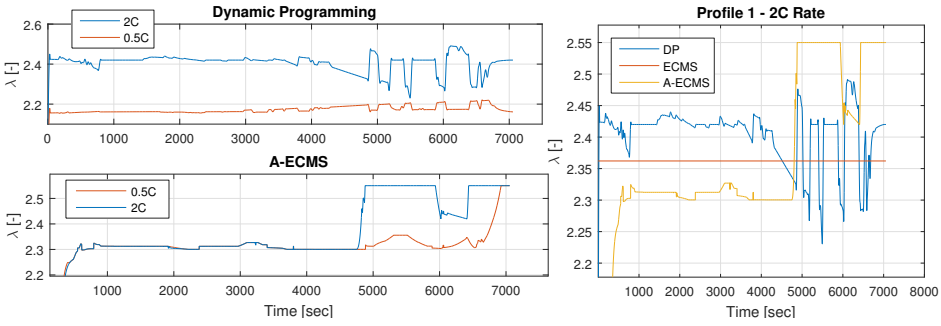

Figure 6.14: Co-state trajectories for initial and increased battery limits.

[1] All SOC trajectories can be found in Appendix D.

Furthermore, Figure 6.14 shows that the increased battery limits have a substantial influence on the optimal co-state. First and foremost, the average value has increased from 2.16 to 2.4. Moreover, its values seem to be more volatile as the SOC decreases. On the other hand, in A-ECMS the only changes appear at the second half of the profile when the battery has been depleted. Considering that the power demand is exactly the same in both cases, the power prediction algorithm of Section 5.8.3.3 does not alter the values of the co-state. As such the changes can be traced back to the SOC feedback that has been introduced to the adaptive co-state (see Equation (5.37) of Section 5.8.3.3).
Considering the effects on the other components that the new C-rate brings about, a slightly more efficient operation of the Diesel engine has been observed, especially for the DP solution, as Table 6.3 indicates. This occurs due to the shifting of the engines' operating points to high efficiency regions, mostly at low load. According to Figure 6.15, the operating points chosen by the DP algorithm are more efficient than before. On the contrary, at peak load conditions, the engines operate at even lower loads, resulting in lower fuel consumption (a comparison between Figures 6.5 and 6.15 gives an impression of the difference). Finally, the efficiency of the Diesel - generator has increased slightly, as the controllers are able to increase their load even higher when recharging the batteries.

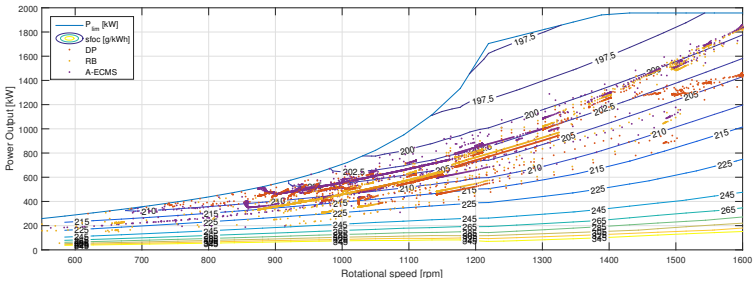

Figure 6.15: Main engines' operating points for the increased C-rate limitations.

Regarding the decision variables, the most notable difference in the optimal solution obtained by DP, is the more aggressive use of the batteries both in terms of charging and discharging. This can also be seen by the increased average C-rate, in Table 6.3. However, the pattern of the solution is still the same (see the discussion in Section 6.3.2.2), and a visualization is given in Figure 6.16.

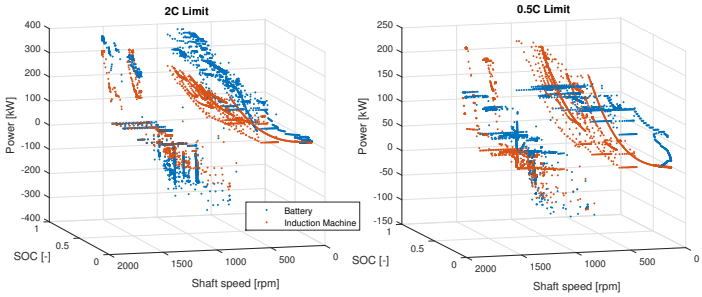

Figure 6.16: Effect on decision variables obtained with Dynamic Programming.

Table 6.3: Increased C-Rate Comparative Results - Fuel Consumption, Efficiency, Running Hours.

EMS	Fuel		$\bar{\eta}$						C-rate		SOC		$t_{\text{ICE,ON}}$			
	m_f [kg]		DE		DG		vessel		[-]		[%]		DE [%] of t_{end}		DG [%] of t_{end}	
	0.5C	2C	0.5C	2C	0.5C	2C	0.5C	2C	0.5C	2C	0.5C	2C	0.5C	2C	0.5C	2C
DP	336	325	35.0	35.6	37.6	38.5	36.5	36.9	0.49	1.41	20	20	62	61	41	65
ECMS	345	345	36.0	36.0	36.9	36.9	35.6	35.6	0.39	0.39	42	42	64	64	37	37
A-ECMS	343	336	36.0	36.6	36.2	36.9	35.8	36.4	0.30	1.28	36	21	64	65	36	51

Table 6.4: Increased C-Rate Comparative Results - Operating Modes.

EMS	Propulsive Power						Electric Power							
	DE		IM		Hybrid		DG		BAT		IM		Hybrid	
	[%] of mission duration													
	0.5C	2C	0.5C	2C	0.5C	2C	0.5C	2C	0.5C	2C	0.5C	2C	0.5C	2C
DP	47	38	32	42	21	20	-	23	43	03	12	23	45	51
ECMS	55	55	35	35	10	10	05	05	62	62	-	-	32	32
A-ECMS	56	21	33	50	11	29	02	26	63	23	-	21	34	30

Hybrid: Use of more than one component for power production.

6.4.3. EFFECT OF OPERATING PROFILE

Finally, the effect of the operating profile was studied as well. All the operating profiles of Section 6.3 are based on the power demand distribution that was measured by Damen Shipyards, and has been given in Figure 5.13. In order to get an indication of the sensitivity of the proposed control algorithms to the changes on this power distribution, two more profiles were composed and studied: One extremely busy profile, consisting of mostly towing operations, and one idle profile, in which the vessel is mostly free-sailing at low speeds, with only two extremely small towing jobs. The time distributions between stand-by, free-sailing and assisting modes are presented in Figure 6.17, and the two profiles along with the original profile (profile 1 of Section 6.3) for comparison, are shown in Figure 6.18

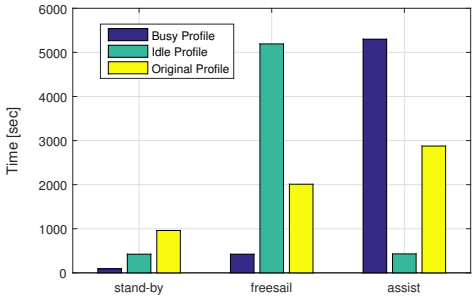

Figure 6.17: Operational time in each mode for the three different profiles.

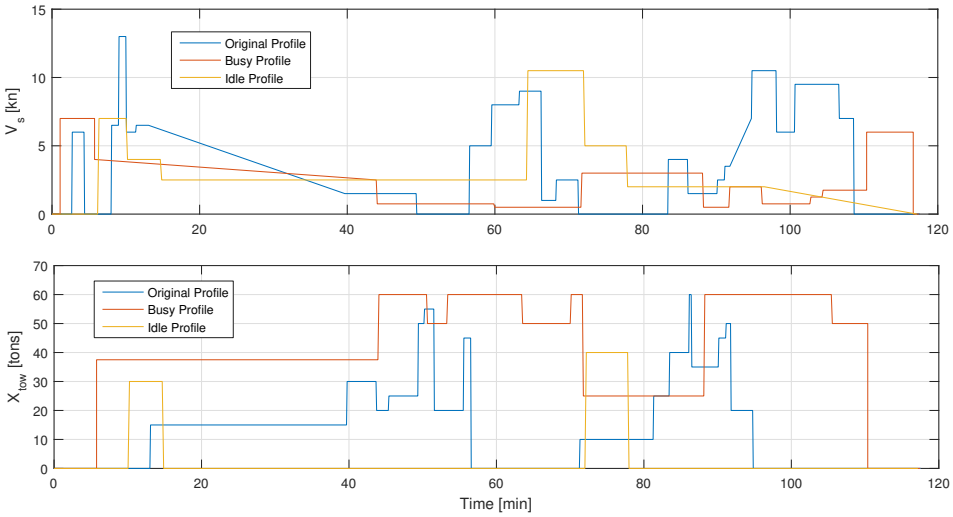

Figure 6.18: Original, Idle and Busy Operating Profiles.

Comparative results of the simulations can be found in Tables 6.5 - 6.6, from which the following conclusions can be drawn:

- ECMS-based controllers still outperform the rule-based ones in terms of fuel consumption, even though the power demand distribution is significantly different

Table 6.5: Comparative Results - Fuel Consumption, Efficiency, Running Hours.

	EMS	Fuel		$\bar{\eta}$			C-rate	SOC	$t_{\text{ICE,ON}}$	
		m_f [kg]	Savings [%] RB	DE	DG [%]	total	[-]	[%]	DE [%]	DG of t_{end}
Idle	DP	224	16.1	38.4	35.8	35.8	0.43	20	15	92
	RB	267	-	39.5	38.1	34.2	0.30	99	15	84
	RB-CD	265	0.8	39.4	38.1	33.8	0.21	85	15	79
	ECMS	234	12.3	39.2	35.3	34.6	0.38	20	17	88
	A-ECMS	235	12.3	39.2	35.2	34.6	0.38	20	17	88
	ECMS-2	239	10.5	37.9	34.3	34.3	0.40	20	16	85
Busy	DP	1039	3.5	39.6	38.0	38.9	0.45	20	92	89
	RB	1077	-	40.9	39.4	38.6	0.29	95	92	06
	RB-CD	1073	0.4	40.9	39.2	38.3	0.22	61	92	06
	ECMS	1048	2.7	40.4	37.9	38.5	0.21	38	92	34
	A-ECMS	1046	2.8	40.5	37.3	38.5	0.21	33	92	29
	ECMS-2	1047	2.7	40.2	37.7	38.7	0.36	37	29	38

than the assumed one (see Section 5.8.3.3), which of course affects the power prediction algorithm.

- The advantages are much higher for the idle profile, whereas they diminish for the busy one. Of course, this also occurs because the optimization algorithm is less restricted on the idle profile, whereas for the busy one the main engines must be in operation most of the time.
- The decreased fuel consumption occurs due to the increased use of the batteries, rather than the higher overall efficiency of the plant, as the average total efficiency of the plant reveals.
- The utilization of the batteries for the ECMS-based controllers is significantly sub-optimal, as for the busy profile the final SOC is between 30-40 %, whereas for the idle profile, the SOC reaches its lower bound halfway through the mission (see Figures D.18-D.20). Note that, for the optimal DP solution, the battery is also being depleted too early.
- Once more, the DP algorithm indicates that the use of boost mode at high power demand is preferable. This is reflected on the main engines' efficiency drop.
- Heavy use of the batteries can be observed for the DP solution, which operates the batteries close to the imposed limitations, followed by the ECMS-based controllers, and finally by the RB controllers.
- Hybrid modes are preferred by the DP solution, whereas the ECMS-based controllers are more conservative, especially in terms of electric power production. The same can be inferred by the combined operational time of the ICEs on board.

Table 6.6: Comparative Results - Operating Modes.

	EMS	Propulsive Power			Electric Power			
		DE	IM	Hybrid	DG	BAT	IM	Hybrid
		[%] of mission duration						
Idle	DP	06	72	23	24	-	06	70
	RB	15	85	-	79	10	11	-
	RB-CD	15	85	-	79	10	11	-
	ECMS	06	77	17	54	09	-	38
	A-ECMS	05	77	18	54	11	-	36
	ECMS-2	05	71	25	54	10	-	36
Busy	DP	48	05	47	30	05	-	65
	RB	92	08	-	15	48	37	-
	RB-CD	92	08	-	15	48	38	-
	ECMS	35	03	61	05	59	02	34
	A-ECMS	31	03	65	-	63	-	37
	ECMS-2	40	08	52	-	62	-	38

- Figure 6.19 shows the effect of the different power demand distribution on the co-state trajectory. It can be seen that the values assigned to the co-state in A-ECMS differ significantly with its optimal values (obtained with DP), especially for the idle profile, and the first half of the busy profile.

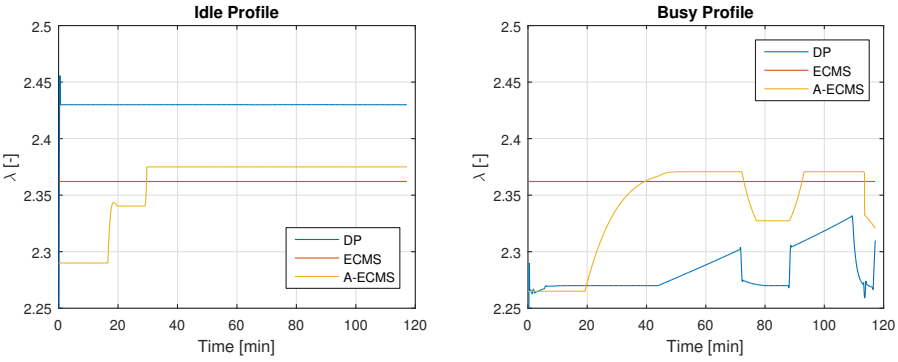

Figure 6.19: Co-state trajectories, Busy and Idle profiles.

6.5. CONCLUSIONS

From the analysis presented thus far, it is clear that the rule-based controller and ECMS have different goals: ECMS splits the power between the different components trying to consume the least possible amount of fuel, whereas the rule-set views the battery as a means of increasing the overall plant efficiency. As such, it was natural - and expected

- that the proposed control algorithms would decrease the overall fuel consumption of the vessel, but the main question was by how much. On average, fuel savings of around 7% can be expected by making the transition from the existing rule-set, to an optimization based-algorithm such as the proposed EMS. Considering that the *theoretical* upper bound (given by the DP solution) is around 8%, ECMS does provide very good results.

Important insights were also obtained by the sensitivity analysis that was performed, as it led to several useful conclusions: First and foremost, it revealed that the quality of the solution obtained with the real-time strategies is highly sensitive to the values used for the artificial fuel consumption of the battery (co-state). Although this is not a new remark, as it has been mentioned in several studies [Sciarretta and Guzzella, 2007], it was shown (Section 6.4.1), that by sizing the 'fuel consumption' of the battery appropriately, results with only 1.15% deviation from the global optimum can be achieved with a constant co-state.

Finally, through the use of highly different profiles than the ones the adaptive strategy was based on, the robustness of the proposed algorithm was tested, and benchmarked with respect to the existing control algorithm and the optimum solution. The results indicate that, even if the assumptions, based on which the adaption of the battery's equivalent fuel consumption is estimated are wrong, an ECMS-based algorithm can still provide satisfactory solutions, with an average of 12.5% and 1.5% fuel economy for an idle, and an extremely busy operating profile respectively.

7

CONCLUSIONS & RECOMMENDATIONS

"Life can only be understood backwards;
but it must be lived forwards."

-Soren Kierkegaard

This work focuses on improving the fuel economy of a hybrid propulsion plant, through the design of an optimization-based control strategy. This strategy determines the instantaneous optimal power distribution between primary and secondary power sources while the vessel is in operation. A general discussion regarding the potential and limitations of this work will be given in the following, along with the author's general recommendations for further research on this field.

7.1. CONCLUSIONS

Returning to the research objectives of Section 1.5, the following conclusions can be drawn:

What is the fuel savings potential of the proposed control strategy?
This constitutes the main goal of this work. In order to provide a well-founded comparison, the proposed EMS has been compared with the existing heuristic strategy used in the hybrid tugboats of Damen Shipyards, and the global optimum, obtained with an exhaustive search method. Five different profiles were studied, the results shown in Table 7.1.

It can be seen that the proposed strategies result in significantly lower fuel consumption compared to the existing control solution used today. ECMS and A-ECMS result in

Table 7.1: Fuel savings potential of each EMS.

	m_f [kg] (% of RB-EMS)				
	RB	RB-CD	ECMS_{opt}	A-ECMS	DP
Profile 1	364	361 (-0.8)	340 (-6.6)	343 (-5.7)	336 (-7.7)
Profile 2	584	569 (-2.6)	558 (-4.4)	566 (-3.2)	551 (-5.6)
Profile 3	341	338 (-0.9)	316 (-7.3)	323 (-5.6)	311 (-8.8)
Profile 4	269	267 (-0.8)	243 (-9.6)	250 (-7.3)	239 (-11.2)
Profile 5	494	489 (-1.0)	475 (-3.8)	479 (-3.0)	470 (-4.8)
Profile 6	1077	1073 (-0.4)	1046 (-2.8)	1046 (-2.8)	1039 (-3.5)
Profile 7	267	265 (-0.8)	239 (-10.5)	235 (-12.3)	224 (-16.1)

Profiles 6 - 7: Busy and idle profiles of Section 6.4.3.
ECMS_{opt}: $\lambda = 2.16$.

6.4% and 5.7% fuel savings, with the theoretical limit (i.e. under the assumption of perfect information) being around 8.3%.

How can the propulsion plant be modeled to allow for the evaluation of energy management strategies?
In order to develop and test a new control strategy a valid simulation model of the propulsion plant is needed. Building the simulation model used in this work proved to be a time-consuming task, with relatively difficult choices regarding complexity, structure and desired accuracy. In this project a forward-facing model has been used, in accordance with the modeling approach used in TU Delft. The simulation model had to be capable of capturing the physics of the hybrid propulsion drivetrain accurately enough, to act as a validation to the control decisions. As such, the prediction of power losses for all the components is of primary importance, both in nominal and part-load conditions, as well as the fuel consumption of the main engines and the Diesel-generator set, and the state of charge of the battery. Regarding dynamics, surely the slower dynamic effects should be taken into account, i.e. hull dynamics, and possibly the ICEs' dynamic behavior, so as to provide a realistic representation of reality. In this work however, the dynamics of the battery and the induction machine have also been considered, the former to increase the accuracy of SOC estimation, the latter mostly for the completeness of the approach. Furthermore, a full dynamic model may be of help to further research Energy Management Strategies that incorporate the transient behavior of propulsion components (i.e. fast acceleration requirements, etc.)

How can operating constraints, such as direct availability of full bollard pull, and discrete decisions (ON/OFF), be taken into account in the EMS?
In order to deal with discrete decisions in the control strategy, the use of binary variables was deemed necessary, in order to regulate the on/off switch of the induction machines and the ICEs on board. From a complexity point of view, this can cause problems, as we are effectively seeking the *real-time* solution of a Mixed Integer Non-Linear Programming - NP-Hard - problem. In this case however, the introduction of these *few* binary

variables helped with the optimization, as the original problem was broken down to eight convex subproblems, the solution of which can be found in polynomial time.

Most operational constraints of the components were handled in the traditional way, as with any optimization problem. These include the operating envelope of the ICEs, for which a polynomial function with respect to shaft speed and power output, and the envelope of the induction machines, handled in the same way. Regarding the direct availability of bollard pull, a constraint was introduced in the optimization algorithm, which in essence forced the main engines to be turned on if the towing force is higher than zero. Note that a constraint preventing the frequent on/off of the ICEs was not necessary, as the controller would only switch on the Diesel-generator if power demand can not be met with the batteries, and in turn the main engines were turned on only when the Diesel-generator itself could not provide sufficient power to meed the demand.

Which optimization strategy presents the highest potential and ability to identify the optimal power split between the existing, distinct types of power sources?
In this project Equivalent Consumption Minimization Strategy (ECMS) has been used, as it provides a favorable trade-off between simplicity and optimality. A relatively simple optimization process is the core of the controller, based on the equivalent fuel consumption of the battery. Although this strategy provides satisfactory results - after all it can reach the global optimum within 1-2% - it is clear from this project that any sort of future information certainly can help to achieve even better control decisions. In the case of ECMS this means estimating on-line, or using pre-configured values, of the equivalent fuel consumption of the battery. Considering this, it is possible that a more suitable strategy may have been Model Predictive Control (MPC) instead of ECMS, in which future system states are inherently taken into account in the controller's decisions. Of course, it can not be stated with certainty that MPC will give better results for these profiles than the proposed EMS, it is the author's belief that it would result in a more robust controller, free of the sensitivity of ECMS to the co-state value.

7.2. RECOMMENDATIONS FOR FURTHER WORK

The main focus of this work was to assess the fuel savings potential of an optimization-based EMS. Although the preliminary results are indeed promising, several recommendations can be given as future research directions:

1. All the components of the propulsion system have been calibrated individually, based on actual measurements of Damen Shipyards Group. However, to improve the reliability of the simulation results, it would desirable to also validate the dynamic behavior of the components of the propulsion system, and properly asses the validity of the simulation model (uncertainty analysis etc.). The relevant discussion - with very helpful references - can be found in the introductory sections of Chapter 4.

2. Considering individual components, extra consideration must be given to the battery. The model used to simulate its behavior *must* be extended with information regarding battery wear, as their aging may influence the decisions of a supervisory control system.

3. Special attention must be given in the main engine's model as well, as the difference between data and measurements at low loads is not by any means negligible. Note that, for the scope of this work, it is equally important to have accurate predictions at part-load conditions as well. It is exactly at these low loads that the control strategy must decide which combination of components will provide the requested power, as at high loads there is really no choice - the only components capable of producing the required power are the main engines.

4. Thus far, a frequent ICE on/off switching is not penalized by the strategies presented in this work, as the ECMS-based controllers would only operate on the main engines as a last resort, and only at high power demands, therefore it was not really an issue. However, in other implementations this might be an important set-back. The inclusion of an extra hard constraint, or the use of an additional penalty function in the control objective could be used in order to prevent this problem.

5. Considering the very distinct pattern regarding the control decisions of the DP solution for all the profiles, the translation of its behavior into a rule-set, according to the discussion of Section 6.3.2.2 would also be of interest. Another point worth of attention, is that the derivative of the co-state with respect to time seems to be only a function of mission duration, SOC and battery power (see discussion of Appendix C). Under the assumption that the end-point of the mission is known - the operator could provide an estimation at the beginning of each job for example - it would be worth investigating whether the expression that has been derived in this work (Equations (C.10) - (C.11) of Appendix C) can be used in real-time.

6. Moreover, emission limitations could be imposed on the existing strategy as well. This however implies additional states on the problem, i.e. extra co-states (one for each constrained type of emissions) to be included in the control objective, resulting in a multiple-times more complicated problem - that still needs to be solved on-line. In terms of algorithmic efficiency, a solution-method-proposal would be very interesting.

7. By introducing a CPP, an extra control degree of freedom could be incorporated, namely the propeller pitch angle. Additional constraints could then be imposed on the operation of the propulsion plant, such as the overloading of the main engines. It would be of interest to explore the feasibility of including these ideas in an optimal control oriented approach, applicable to the control solutions presented in this work.

8. Finally, as stated in the previous section, during the development of the controller, it became abundantly clear that any sort of future estimations can benefit the decisions of the EMS controller. As such, an interesting approach would be to apply Model Predictive Control to the energy management problem, and assess the benefits of that control approach.

9. In this work, the EMS controller was designed to take decisions without the end-point of the profile. However, if the duration of the operating profile is known, an

SOC reference trajectory can be drawn with respect to time - a straight-line between the points $(t_0, SOC_0), (t_f, SOC_f)$- and by means of a PI controller the actual SOC of the battery can be forced to follow the predefined reference trajectory.

A

DYNAMIC PROGRAMMING

In the following, an introduction to the principles of Dynamic Programming is given.

A.1. INTRODUCTION

When developing causal suboptimal controllers, it is an advantage if the optimal controller is known, even if this controller is not causal. In many cases, such optimal controllers can be found using a Dynamic Programming (DP) algorithm, introduced in [Bellman, 1957]. Of course, this optimal controller can only be found if all future disturbances and reference inputs are known *a priori*, i.e. only if perfect future information is available. Nevertheless, the optimal solution is useful as it can be used as a benchmark to which all other causal controllers can be compared to. In the remainder of this section, a brief discussion on the main characteristics of DP will be given. For the interested reader, a detailed discussion on DP theory can be found in the textbooks of [Bellman, 1957, Bertsekas, 1995], and a brief overview on the history of DP in [Bellman and Lee, 1984].

Dynamic programming is a numerical method for solving multistage decision-making problems [Bertsekas, 1995]. It is capable of providing the optimal solution to problems of any complexity level, however it is non-causal and only implementable in a simulation environment, as it requires a priori knowledge of the operating profile. In DP, use is made of *Bellman's Principle of Optimality*, according to which [Bellman, 1957]:

> An optimal policy has the property that whatever the initial state and initial decision are, the remaining decisions must constitute an optimal policy with regard to the state resulting from the first decision.

This implies that, given a problem in discrete time, it is sufficient to find the optimal trajectories for state and for control inputs in going from any state at sample time k to any other state at sample time $k+1$. By concatenating those optimal solutions for all instants, a globally optimum solution arises. Understandably, in order to keep the set

A

of possible instants - and the set of possible states and control inputs at each instant - finite, time is discretized and the state and control inputs are quantized. As such, the globally optimal solution can be found in finite time, by an exhaustive search procedure. Of course, the size of quantization and discretization intervals determine the accuracy of the solution and the computational burden of the algorithm, which scales linearly with the problem time (N), the number of discretized state values, and the number of discretized control inputs.

A.2. APPLICATION TO THE ENERGY MANAGEMENT PROBLEM

Consider Problem (5.1) of Section 5.2.1, reformulated in a discretized form:

$$\mathscr{P} = \begin{cases} \underset{u\in\mathbb{U}}{\text{minimize}} & J\big(k, x_k, u_k, r_k\big) = \Delta t \sum_{k=0}^{N-1} \Delta \dot{m}_f\big(k, x_k, u_k, r_k\big) + \phi(x(t_f)) \\ \text{subject to:} & x_{k+1} = f\big(k, x_k, u_k, r_k\big) + x_k, \;\; x_0 = SOC_{max} \\ & G\big(x_k, u_k\big) = 0, \\ & H\big(x_k, u_k\big) \leq 0, \\ & k = 0, 1, ..., N-1, \\ & N = \dfrac{t_f - t_0}{t_s} + 1, \end{cases} \tag{A.1}$$

where Δm_f is the fuel mass consumption at each time step t_s, and $\phi(x(t_f))$ is a penalty function that can be added to the performance index, in order to represent any constraints that may apply on the final state of the system.

DP uses the above definition of the performance index J, but it extends this definition to any point of the time-state space by defining the cost-to-go function (denoted as $\Gamma(t,x)$) as the performance index J of the optimal trajectory from any point (t,x) to the point $(t_f, x(t_f))$. By definition, the value $\Gamma(0,x(0))$ is equal to the optimal value of the performance index J^* that is sought [Guzzella and Onder, 2009]. Figure A.1 presents the basic DP algorithm applied to the Energy Management problem. Although the process is rather straightforward, numerical problems can arise when implementing the algorithm, which if not treated, can have a major impact on the final result. Firstly, the state values that arise as a solution of the minimization process may not match any of the possible points of the grid, therefore the corresponding values of the optimal control inputs, and the resulting cost-to-go function, need to be interpolated from the values calculated for the closest points of the grid. An overview of interpolation methods, including advantages and disadvantages can be found in [Guzzella and Onder, 2009].

Furthermore, in order for the algorithm to handle infeasible state values or control inputs, a penalty cost on the function Γ must be assigned. Choosing a very high (infinite) value as a penalty in combination with an interpolation scheme, it will cause the infinite value to propagate backwards in the grid, resulting in feasible states near the boundary of the feasible state region, to be treated as infeasible as well. In numerous applications this does not cause any serious problems, but in cases where the optimal solution lies close to the boundaries, which occurs relatively often in managing the energy of HEVs, the algorithm will result in suboptimal solutions. Several techniques have been used to

overcome this problem, for example using large enough, but finite, values as a penalty, or to calculate exactly the boundaries between feasible and infeasible states. In this work, the DP algorithm introduced in [Sundstrom and Guzzella, 2009], and extended in [Elbert et al., 2013, Sundstrom et al., 2010] is used, as has been developed with special focus on the optimal control of non-linear, time-variant, constrained, discrete approximations of of continuous-time dynamic models, and includes special methods to treat the aforementioned problems.

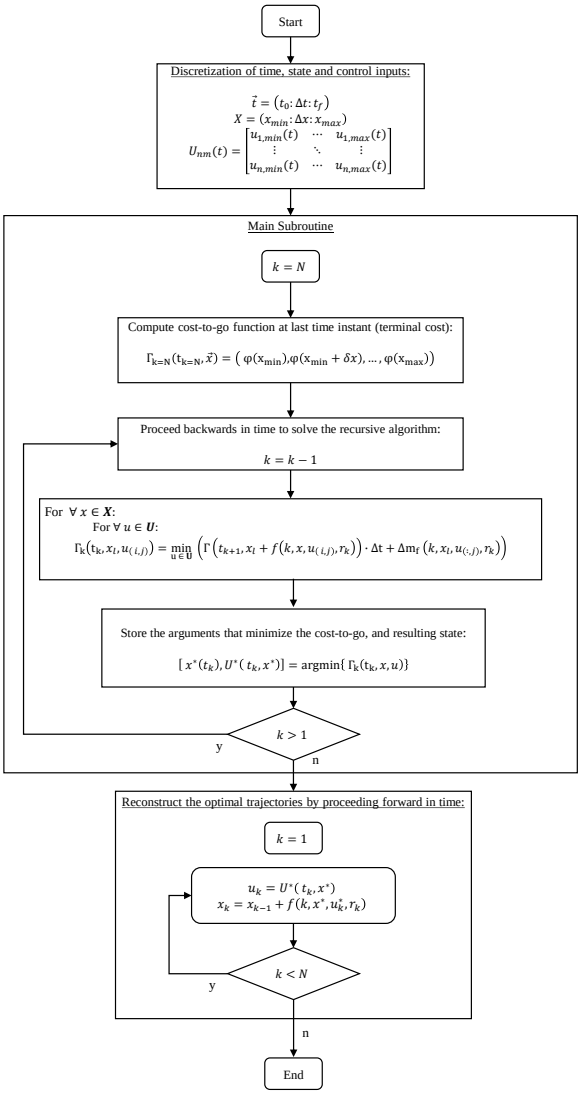

Figure A.1: Dynamic Programming Flowchart.

B

CONVEXITY OF THE ENERGY MANAGEMENT PROBLEM

In the following, a mathematical proof that the continuous relaxation of the Energy Management problem belongs to the class of Convex Programming will be presented.

B.1. IMPORTANCE OF CONVEXITY

Requirements for classifying an optimization problem in the class of *Convex programming* are the following:

1. For minimization (maximization) problems, the objective is a convex (concave) function.
2. The feasible region is a convex set.

A convex set is simply a set of points such that, for each pair of points in the collection, the entire line segment joining these two points is also in the collection. In general, the feasible region for a non-linear programming problem is a convex set whenever all of the constraints are convex functions. What is of importance here is that these two characteristics are necessary and sufficient conditions to ensure that any local optimum is also a global optimum, i.e. that there can only be one optimal solution to the problem [Hillier, 2012], a property which greatly simplifies the search for the optimum.

B.2. DEFINITIONS & THEOREMS

Before going into details it would be prudent to give a list of all the definitions and theorems that will be used throughout this section. It should be noted that everything presented here can be found in the textbook of [Boyd and Vandenberghe, 2004].

Definition 1 (Convexity) *A function f is convex if **dom** f is a convex set and if for all $x,y \in$ **dom** f, and θ with $0 \leq \theta \leq 1$ we have:*

$$f\left(\theta x + (1-\theta)\, y\right) \leq \theta f(x) + (1-\theta) f(y)$$

B

Definition 2 (Positive semi-definite matrix) *A symmetric $n \times n$ real matrix M is said to be positive semi-definite if the scalar $z^T Mz$ is non-negative for every non-zero column vector z of n real values.*

Theorem 1 (First-order conditions) *Supposing f is differentiable (i.e., its gradient ∇f exists at each point in **dom** f, which is open). Then f is convex if and only if **dom** f is convex and:*

$$f(y) \geq f(x) + \nabla f(x)^{\mathsf{T}}(y - x)$$

for all $x, y \in \operatorname{dom} f$

Theorem 2 (Second-order conditions) *Supposing f is twice differentiable, that is, its Hessian or second derivative $\nabla^2 f$ exists at each point in **dom** f. Then f is convex if and only if **dom** f is convex and its Hessian is positive semidefinite.*

Theorem 3 (Convexity preservation: Non-negative weighted sums) *If $f_1, f_2, \ldots f_n$ are convex function and $w_1, w_2, \ldots w_n \geq 0$, then the weighted sum of convex functions,*

$$f = w_1 f_1 + \ldots + w_n f_n$$

is convex.

Theorem 4 (Convexity preservation: Composition) *Given the functions g in **dom** g and h in **dom** h, function f defined by:*

$$f(x) = (h \circ g)(x) \text{ with } \textbf{dom} f = \left\{x \in \textbf{dom}\ g \mid g(x) \in \textbf{dom}\ h\right\}$$

is convex when one of the following statements is valid:

- *h is convex, $\tilde{h}$ is non-decreasing, and g is convex.*
- *h is convex, $\tilde{h}$ is non-increasing, and g is concave.*

*where $\tilde{h}$ denotes the extended-value extension of function h, which assigns the value $+\infty$ ($-\infty$) to points not in **dom** h for h convex (concave).*

B.3. CONVEXITY OF THE PROBLEM

In order to assist the readability of this section, new notation will be used to address each function and the decision variables, according to Table B.1. Note, that only the case in which all the components of the system are in operation will be considered, being the most general case. However, as will become apparent in the following, convexity holds for any combination of components.

Table B.1: Notation used in this Section.

Reference	New symbol
M_{IM}	x
P_B	y
$\dot{m}_{\text{f,eqv}}(M_{IM})$	$f(x)$
$\dot{m}_{f,DE}(M_{IM})$	$f_1(x)$
$\dot{m}_{f,DG}(M_{IM},P_B)$	$f_2(x,y)$
$\dot{m}_{ress}(P_B)$	$f_3(y)$
$P_{\text{IM,loss}}(M_{IM})$	$q(x)$

The objective function can be written as follows:

$$f(x,y) = 2f_1(x) + f_2(x,y) + f_3(y)$$

As such, according to Theorem 3, proving that f is convex, is equivalent to proving that each f_i, $i = 1,2,3$ is convex. One complication that arises immediately, is that Theorem 3 refers to functions defined on the same domain, whereas f_1 and f_3 are defined on different domains. It can be proven that Theorem 3 also applies in this case. Let $f(x)|x \in \mathbb{F}$ be convex, and $g(y)|y \in \mathbb{G}$ also convex. Then $h(x,y) = f(x) + g(y)$ is also convex in the domain $\{x \in \mathbb{F}|y \in \mathbb{G}\}$, considering Definition 1:

Let $z_1 = (x_1, y_1)$ and $z_2 = (x_2, y_2)$, then:

$$\begin{aligned} h(\theta z_1 + (1-\theta)z_2) = h\left(\theta x_1 + (1-\theta)x_2, \theta y_1 + (1-\theta)y_2\right) = \\ = f(\theta x_1 + (1-\theta)x_2) + g\left(\theta y_1 + (1-\theta)y_2\right) \leq \theta f(x_1) + (1-\theta)f(x_2) + \\ + \theta g(y_1) + (1-\theta)g(y_2) = \theta h(z_1) + (1-\theta)z_2 \end{aligned}$$

which proves that $h(x,y)$ is indeed convex.

B.3.1. MAIN DIESEL ENGINE FUEL CONSUMPTION

Function $f_1(x)$ can be written as a scaler composition of two functions g and h and its convexity of f_1 will be proven using Theorem 4. Here $g(x)$ refers to the normalized main engine's power output, as a function of the induction machine's torque, according to Equation (5.18), and $h(g(x))$ refers to fuel consumption, which is a function of the engine's power output and shaft speed, from Equation (5.10). Therefore:

$$\begin{aligned} &f_1(x) = (h \circ g)(x), \text{ with } \mathbf{dom} f_1 = \{x \in \mathbf{dom}\ g \mid g(x) \in \mathbf{dom}\ h\} \\ &h(z) = c_0 + c_1 z + c_2 z^2, z \in (0, +\infty) \\ &\text{where:} \quad c_0 = b_{DE}\dot{m}_{f,nom}\left(a_0 + a_1 \frac{n_{sh}}{n_{\text{DE,nom}}}\right) \\ &\qquad\quad c_1 = b_{DE}\dot{m}_{\text{f,nom}}\left(a_2 + a_5 \frac{n_{sh}}{n_{\text{DE,nom}}}\right) \\ &\qquad\quad c_2 = b_{DE}a_4\dot{m}_{\text{f,nom}} \end{aligned}$$

$$g(x) = c_3 - c_4 x,\ x \in [M_{\text{IM,min}}, M_{\text{IM,max}}]$$
$$\text{where:}\quad c_3 = P_p$$
$$c_4 = 2\pi n_{sh}$$

Furthermore, $z = \frac{P_{\text{DE}}}{P_{\text{DE,nom}}}$ is only meaningful when $z \in [0,1]$ i.e within the operating envelope of the engine. The fact that the fuel consumption (function h) has values outside this domain, is just a useful extension of the function to help prove its convexity.

Now, the following apply:

- g is linear, therefore it is both convex and concave, and no further analysis is needed.
- h is continuous and twice differentiable, with a positive second derivative $\frac{d^2h}{dz^2} = c_2 = a_4 \dot{m}_{\text{f,nom}}$. Therefore it is convex and non-decreasing in $\mathbb{R}_{++}$.

Since g is both convex and concave, h is convex, and non-decreasing, then f_1 is convex.

B.3.2. DIESEL - GENERATOR FUEL CONSUMPTION

Following the same procedure as in the previous section, $f_2(x)$ can be written in the form of $(h \circ g)(x,y)$. Here $g(x,y)$ refers to the normalized diesel generator's power output, as a function of the induction machine's torque and battery power, according to Equation (5.7), and $h(g(x,y))$ refers to fuel consumption, which is a function of power output (constant shaft speed has been assumed for the Diesel generator), from Equation (5.12). Therefore:

$$f_2(x) = (h \circ g)(x,y), \text{ with } \mathbf{dom} f_2 = \{(x,y) \in \mathbf{dom}\ g \mid g(x,y) \in \mathbf{dom}\ h\}$$
$$h(z) = b_{DG}\left(a_0 + a_1 z + a_2 z^2\right), z \in (0,1]$$
$$\text{where: } a_i > 0,\ i = 0,1,2 \text{ are given in Equation (5.12)}$$
$$g(x,y) = c_0 x + c_1 q(x) - y + c_2,\ x \in [M_{\text{IM,min}}, M_{\text{IM,max}}], y \in [P_{\text{B,min}}, P_{\text{B,max}}]$$
$$\text{where:}\quad c_0 = b_{IM} 4\pi n_{sh}, c_1 = 2b_{IM}, c_2 = P_h b_{IM}$$
$$q(x) = c_{00} + c_{01} x + c_{02} x^2$$

$$\text{with:}\quad c_{00} = P_{\text{IM,loss nom}}\left(a_{i1}\frac{n_{sh}}{n_{\text{IM,nom}}} + a_{i3}\left(\frac{n_{sh}}{n_{\text{IM,nom}}}\right)^2\right)$$
$$c_{01} = \frac{P_{\text{IM,loss nom}}}{M_{\text{IM,nom}}}\left(a_{i2} + a_{i5}\frac{n_{sh}}{n_{\text{IM,nom}}}\right)$$
$$c_{02} = P_{\text{IM,loss nom}}\frac{a_{i4}}{M^2_{\text{IM,nom}}}$$
$$a_{ij},\ i = 1,2\ \&\ j = 1,2...5 \text{ constants}$$

The fact that h is convex and non-decreasing can be proven in the same way as before. Only the proof that $g(x,y)$ is convex will be given.

g is twice differentiable for $\forall x, y \in \{\text{dom } g | x \neq 0\}$. For $x = 0$, the following apply:

$$\left.\begin{array}{l}\lim\limits_{x\to 0^-}\big(g(x,y)\big) = c_1 c_{00} + c_2 - y \\ \lim\limits_{x\to 0^+}\big(g(x,y)\big) = c_1 c_{00} + c_2 - y\end{array}\right\} \begin{array}{c}\text{Since } c_{00} = f(a_{i1}, a_{i3}) \text{ is the same both for motoring} \\ \text{and generating conditions, then:} \\ \lim\limits_{x\to 0^-}\big(g(x,y)\big) = \lim\limits_{x\to 0^+}\big(g(x,y)\big)\ \forall y \in \text{dom } g\end{array}$$

$$\lim_{\epsilon\to 0}\left(\frac{g(0+\epsilon, y) - g(0,y)}{\epsilon}\right) = \lim_{\epsilon\to 0}(c_0 + c_{01} + c_{02}\epsilon) = c_0 + c_{01}$$

$$\lim_{x\to 0^-}\left(\frac{dg(x,y)}{dx}\right) = \lim_{x\to 0^+}\left(\frac{dg(x,y)}{dx}\right) = c_0 + c_1 c_{01}$$

$$\lim_{\epsilon\to 0}\left(\frac{\frac{dg(0+\epsilon,y)}{dx} - \frac{dg(0,y)}{dx}}{\epsilon}\right) = \lim_{\epsilon\to 0}(c_0 + c_{01} + c_{02}\epsilon) = 2c_{02}$$

Since $c_{02} = f(a_{i4})$ changes value around $x = 0$ the first derivative of g is not differentiable. Therefore, in order to prove that g is indeed convex, the first order conditions will be used (Theorem 1).

Let $z_1 = (x_1, y_1)$ and $z_2 = (x_2, y_2)$, then:

$$\left.\begin{array}{c} g(z_2) \geq g(z_1) + \nabla^{\mathsf{T}} g(z_1)(z_2 - z_1) \\ \nabla g(z) = \begin{bmatrix} \frac{dg(z)}{dx} \\ \frac{dg(z)}{dy} \end{bmatrix} = \begin{bmatrix} c_0 + c_1(c_{01} + 2x c_{02}) \\ -1 \end{bmatrix}\end{array}\right\} \Rightarrow$$

$$c_0 x_2 + c_1 q(x_2) - y_2 + c_2 \geq c_0 x_1 + c_1 q(x_1) - y_1 + c_2 +$$
$$+ (c_0 + c_1(c_{01} + 2x_1 c_{02}))(x_2 - x_1) - (y_2 - y_1) \Rightarrow$$
$$\Rightarrow c_1 c_{02}(x_1 - x_2)^2 \geq 0$$

which is true for $\forall x_1, x_2 \in \text{dom } g$, taking into account that:

- $c_1 = 2 > 0$
- $c_{02} = f(a_{i4}) > 0$ for both motoring and generating conditions, since $a_{i4} > 0,\ i = 1, 2$.

Therefore g is convex. As h is both convex and non-decreasing, we conclude that f_2 is convex.

B.3.3. BATTERY EQUIVALENT FUEL CONSUMPTION

f_3 is a function of y of the following form:

$$f_3(y) = c_1 \frac{y}{\left(c_{00} + c_{01}|y| + c_{02}|y|^2\right)^{\text{sgn}(y)}},\ y \in [P_{\text{B,min}}, P_{\text{B,max}}]$$

where:
$$c_1 = \eta_{\text{REC}} \frac{\lambda}{Q_{\text{lhv}}}$$
$$c_{00} = a_0$$
$$c_{01} = \frac{a_1}{n_s n_p}$$
$$c_{02} = \frac{a_2}{\left(n_s n_p\right)^2}$$
with $a_i,\ i = 0, 1, 2$ constants

f_3 is differentiable for $\forall y \in \{\text{dom } f_3 \mid y \neq 0\}$. For $y = 0$, the following apply:

$$\lim_{y\to 0^-}\left(f_3(y)\right) = \lim_{y\to 0^+}\left(f_3(y)\right) = 0$$

$$\left.\begin{aligned} \lim_{\epsilon\to 0^+}\left(\frac{f_3(0+\epsilon) - f_3(0)}{\epsilon}\right) &= \frac{c_1}{c_{00}} \\ \lim_{\epsilon\to 0^-}\left(\frac{f_3(0+\epsilon) - f_3(0)}{\epsilon}\right) &= c_1 c_{00} \end{aligned}\right\} \quad \begin{aligned} &\text{Since } c_{00} = a_0 = 1, \text{ then:} \\ &\lim_{\epsilon\to 0^+}\left(\tfrac{f_3(0+\epsilon)-f_3(0)}{\epsilon}\right) = \lim_{\epsilon\to 0^-}\left(\tfrac{f_3(0+\epsilon)-f_3(0)}{\epsilon}\right) = c_1 \end{aligned}$$

Therefore, f_3 is differentiable for $\forall y \in \text{dom } f_3$, with:

$$\frac{df_3}{dy} = \frac{1}{\left(c_{00} + c_{01}|y| + c_{02}|y|^2\right)^{\text{sgn}(y)}} - y\left(\text{sgn}(y)\frac{c_{01}\text{sgn}(y) + 2c_{02}|y|\text{sgn}(y)}{\left(c_{00} + c_{01}|y| + c_{02}|y|^2\right)^{\text{sgn}(y)+1}}\right)$$

The function's convexity can be proven using the first order conditions, according to Theorem 1:

$$f_3(y_2) \geq f_3(y_1) + \frac{df_3}{dy}(y_1)(y_2 - y_1) \Rightarrow f_3(y_2) - f_3(y_1) - \frac{df_3}{dy}(y_1)(y_2 - y_1) \geq 0 \tag{B.1}$$

Due to the complexity of the functions involved, this inequality was not solved analytically, but rather plotted over the whole range of (y_1, y_2), and is shown in Figure B.1. It can be seen that Equation (B.1) holds for $\forall y \in \text{dom } f_3$.

Since all $f_1,\ f_2,\ f_3$ are convex, it is concluded that $f(x, y)$, being $\dot{m}_{\text{f,eqv}}$, is convex. Furthermore, the constraints of the problem $P_{DE} \leq P_{\text{DE,nom}}$, $P_{DG} \leq P_{\text{DG,nom}}$ are also convex.

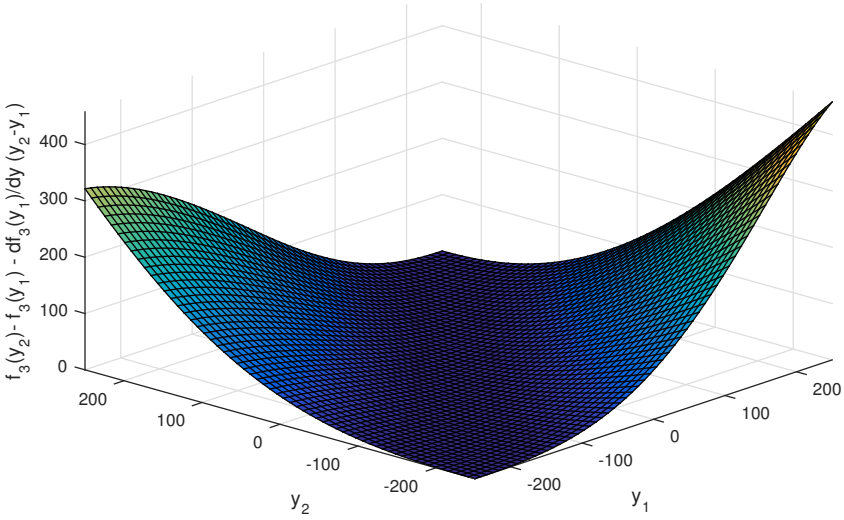

Figure B.1: Left hand-side of Equation (B.1).

The power to the main Diesel engine is a linear function of the power of the induction machine, therefore it is both convex and concave. The same applies to the constraint for the state of charge of the battery, which is a linear function of the battery power. Finally, regarding the power of the Diesel generator, it has already been shown that it is convex as well (see function $g(x, y)$ of Section B.3.2).

Since all the constraints of the problem, along with the objective function are convex variables, it is concluded that the optimization problem is convex.

C

PONTRYAGIN'S MINIMUM PRINCIPLE

In the following, a brief introduction on Pontryagin's Minimum Principle (PMP) will be given, and will be shown that a constant co-state can be considered for this optimal control problem. For a detailed analysis of the concepts presented here, the reader is referred to [Zak, 2003, Kirk, 2012].

PMP is another approach that can be used to solve finite horizon optimal control problems. It redefines the problem in terms of local conditions that must apply, expressed by a set of first-order differential equations, and an instantaneous minimization. Consider a dynamic system with the following state equation (a system with only one state will be considered here for the sake of simplicity):

$$\dot{x} = f(t, x(t), u(t)),\ x(t_0) = x_0$$

where x is the state of the system and u the control input(s). A performance index J is defined over a fixed time interval, $t \in [t_0, t_f]$ that drives the system from the initial state state x_0 to the final state x_f:

$$J(t_0, x(t_0), u) = \int_{t_0}^{t_f} F(\tau, x(\tau), u(\tau))\, d\tau \tag{C.1}$$

The problem is to find the optimal control input $u^*(t),\ t \in [t_0, t_f]$ that minimizes the objective function F, resulting in the optimal performance index J^* with state trajectory $x^*(t)$[1]

Define the Hamiltonian function as:

$$H(t, x(t), u(t), r(t)) = L(t, x(t), u(t), r(t)) + \lambda f(t, x(t), u(t)) \tag{C.2}$$

where:

[1] In this context, the symbol $(^*)$ is used to denote *optimal* values.

$x = (x_1, x_2, ..., x_m)$: State variables
$u = (u_1, u_2, ..., u_n)$: Control variable vector
$r = (r_1, r_2, ..., r_n)$: Uncontrolled inputs
$\lambda = -\frac{dJ^*}{dx}, \lambda \neq 0$: Co-state

According to Bellman's Principle of Optimality (see Section **??**), the following equation holds:

$$\frac{dJ^*(t, x(t), u(t), r(t))}{dt} + \min_{u(t)} H(t, x(t), u(t), r(t)) = 0 \tag{C.3}$$

C

This partial differential equation is known as *Hamilton-Jacobi-Bellman* (HJB) Equation, and its solution provides the optimal control input. This indicates that searching for the optimal control input can be done by minimizing the Hamiltonian:

$$u^*(t) = \underset{u(t) \in \mathscr{U}}{\operatorname{argmin}} H(t, x(t), u(t), r(t)) \tag{C.4}$$

U being the set of admissible control values. Altogether, this can be used to derive necessary, *but not sufficient*, conditions for optimality on u and λ, the set of which is described by PMP:

$$\dot{x}^*(t) = \left.\frac{dH}{d\lambda}\right|_{u^*(t)} = f\left(t, x^*(t), u^*(t)\right) \tag{C.5}$$

$$\dot{\lambda}^*(t) = -\left.\frac{dH}{dx}\right|_{u^*(t)} = -\frac{dL}{dx}\left(u^*(t), t\right) - \lambda^*(t)\frac{df}{dx}\left(x^*(t), u^*(t), t\right) \tag{C.6}$$

$$H\left(t, u^*(t), x^*(t), \lambda^*(t)\right) \leq H\left(t, u(t), x^*(t), \lambda^*(t)\right), \ \forall u(t) \in U(t), \ \forall t \in \left[t_0, t_f\right] \tag{C.7}$$

$$x(t_0) = x_0, \ x(t_f) = x_{\text{final}} \tag{C.8}$$

In the case of the Energy Management problem, L is the instantaneous cost, i.e. the fuel consumption at each time instant (note that it is independent from the SOC), only one state variable $x = SOC$ exists (therefore only one co-state as well), and f represents the right hand side of the system's dynamic Equation (C), which will be derived in the following.

Considering the simple battery model of Section 5.6.4, the state of charge variation is given by Equation (C.9):

$$\begin{aligned}\dot{x}^*(t) = \frac{dSOC^*}{dt} &= -\frac{1}{\eta_{\text{bat}}^{sgn(I(t))}}\frac{I(t)}{Q_{nom}} = \\ &= -\frac{1}{Q_{nom}\eta_{\text{bat}}^{sgn(P^*_{bat}(t))}}\left(\frac{U_{OC}(x)}{2R} - \sqrt{\left(\frac{U_{OC}(x)}{2R}\right)^2 - \frac{P^*_{bat}(t)}{n_s n_p R}}\right)\end{aligned} \tag{C.9}$$

where the open cell voltage U_{OC} is given by Equation (4.82) - and the battery efficiency is a quadratic curve with respect to battery power, as stated in Section 5.6.4. They are shown again below for completeness:

$$U_{OC}(x(t)) = v_1 e^{-v_2 x(t)} + v_3 + v_4 x(t) + v_5 x^2(t) + v_6 x^3(t)$$
$$\eta_{bat} = a_2 P_{bat}^2(t) + a_1 P_{bat}(t) + a_0$$

Therefore:

$$\frac{d\dot{x}^*(t)}{dx} = \frac{df}{dx}\left(x^*(t), u^*(t), t\right) = -\frac{1}{Q_{nom}\eta_{\text{bat}}^{sgn(P^*_{bat}(t))}} \frac{d}{dx}\left(\frac{U_{OC}(x)}{2R} - \sqrt{\left(\frac{U_{OC}(x)}{2R}\right)^2 - \frac{P^*_{bat}(t)}{n_s n_p R}}\right)$$
$$= \frac{4\left(n_p n_s\right)^{\sigma_2} P^*_{bat}(t)\left(\frac{v_4}{2} + x^*(t)v_5 + \frac{\sigma_3}{2} + \left(v_4 + 2x^*(t)v_5 + \sigma_3\sigma_1\right)\frac{\sigma_5}{2\sigma_4} + \frac{\sigma_1}{2}\right)}{Q_{nom}\left(a_0 n_s^2 n_p^2 + a_1 n_s n_p P^*_{bat}(t) + a_2 P^{*2}_{bat}(t)\right)^{sgn(P^*_{bat}(t))}} \times$$
$$\times \frac{1}{\left(v_3 + x^*(t)v_4 + \sigma_6 + x^*(t)^2 v_5 + x^*(t)^3 v_6 + \sigma_4\right)^2} \tag{C.10}$$

with:

$$\sigma_1 = v_1 v_2 e^{v_2 x}$$
$$\sigma_2 = 2sgn(P^*_{bat}(t)) - 1$$
$$\sigma_3 = 3x^2 v_6$$
$$\sigma_4 = \sqrt{\sigma_5^2 - \frac{4RP^*_{bat}(t)}{n_s n_p}}$$
$$\sigma_5 = v_3 + x v_4 + \sigma_6 + x^2 v_5 + x^3 v_6$$
$$\sigma_6 = v_1 e^{v_2 x}$$

Now, according to Equation (C.6):

$$\dot{\lambda}^*(t) = -\left.\frac{dH}{dx}\right|_{u^*(t)} = -\cancelto{0}{\frac{dL}{dx}} - \lambda^*(t)\frac{df}{dx} \Rightarrow \frac{\dot{\lambda}^*(t)}{\lambda^*(t)} = -\frac{df}{dx} \tag{C.11}$$

The value of the right hand side of Equation (C.11), given in analytical form by Equation (C.10), is shown in Figure C.1, for various combinations of SOC and battery power. As can be seen, its variation is relatively small, compared to the absolute value of the co-state for the entire operating profile (the value corresponding to the nominal fuel consumption of the main Diesel engines is approximately 2.36). Therefore it would be reasonable to assume that the optimal co-state could be approximated by a constant value:

$$\frac{\dot{\lambda}^*(t)}{\lambda^*(t)} = -\frac{df}{dx} \approx 0 \Rightarrow \lambda^*(t) = \text{const} \tag{C.12}$$

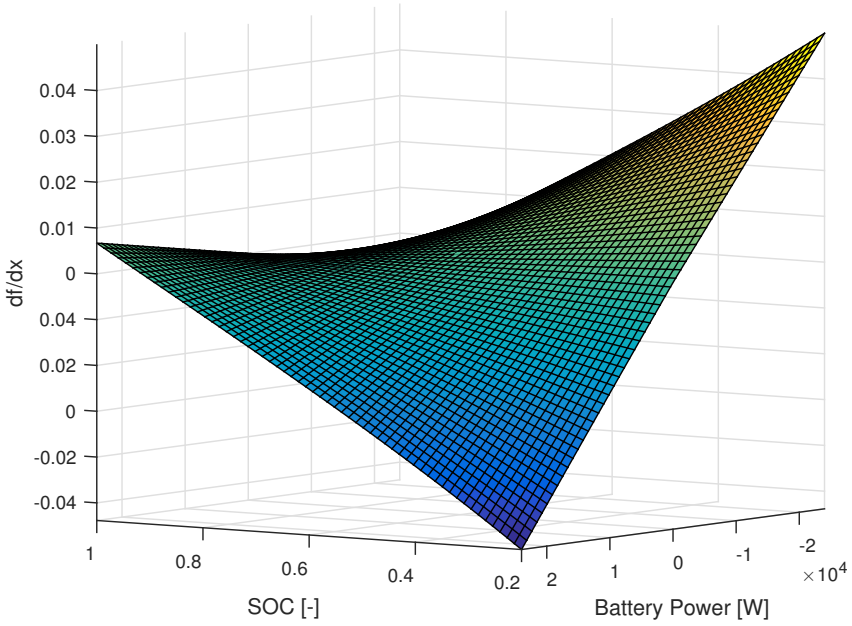

Figure C.1: Right hand-side of Equation (C.11).

D

Controller Evaluation: Results

In the following, detailed results of the case studies discussed in Chapter 6 are presented.

D.1. Quasi-static Maneuvering

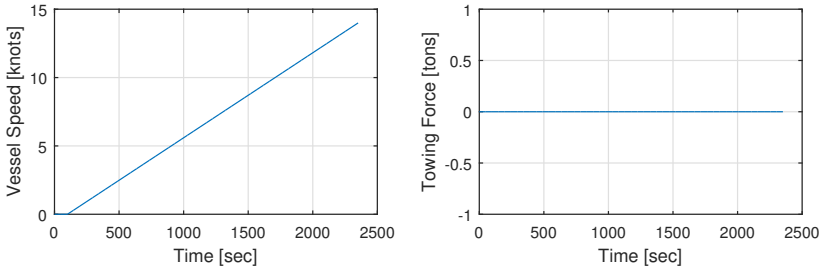

Figure D.1: Reference vessel speed and towing force.

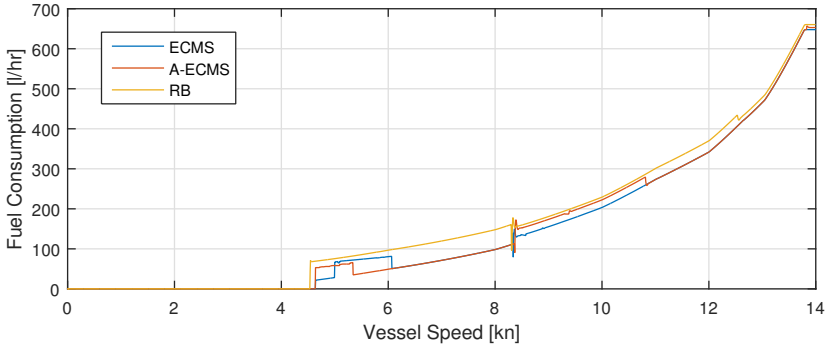

Figure D.2: Resulting Fuel Consumption.

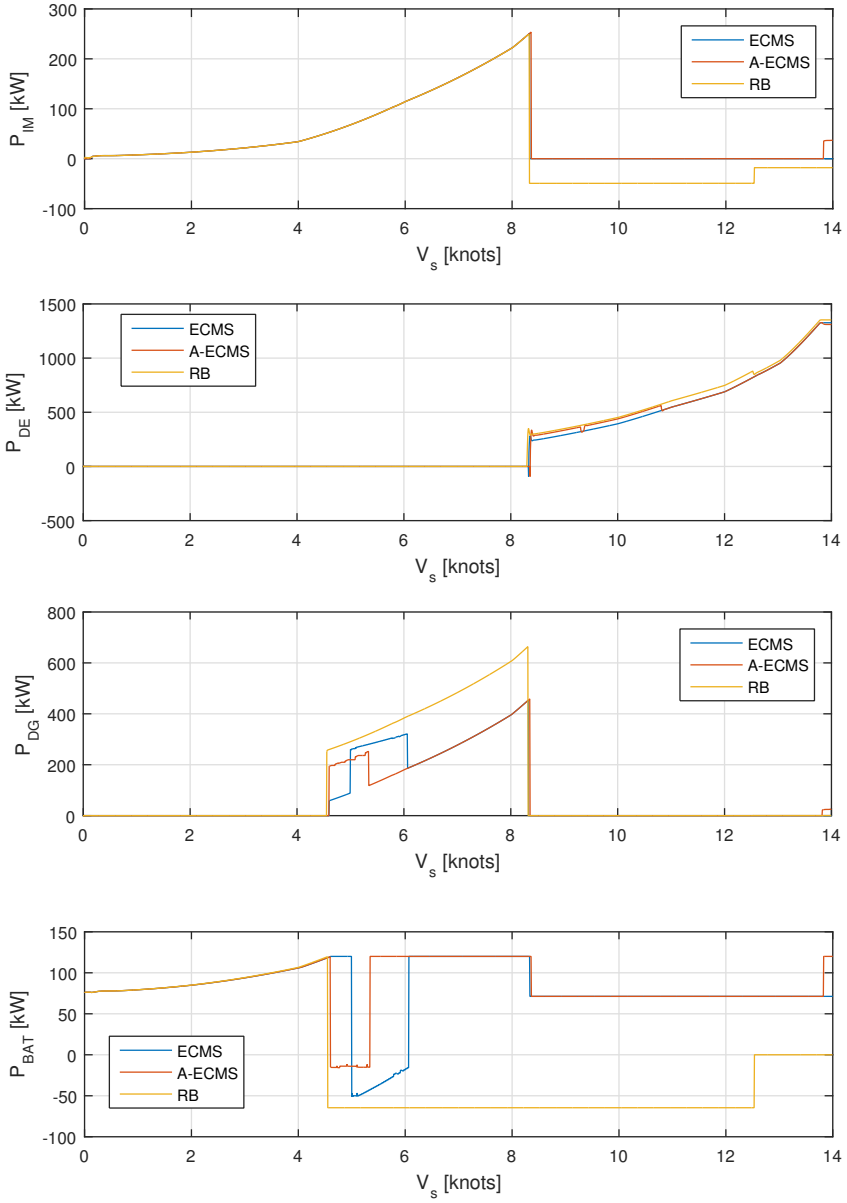

Figure D.3: Power Output of each component.

D.2. STANDARD OPERATIONAL PROFILES

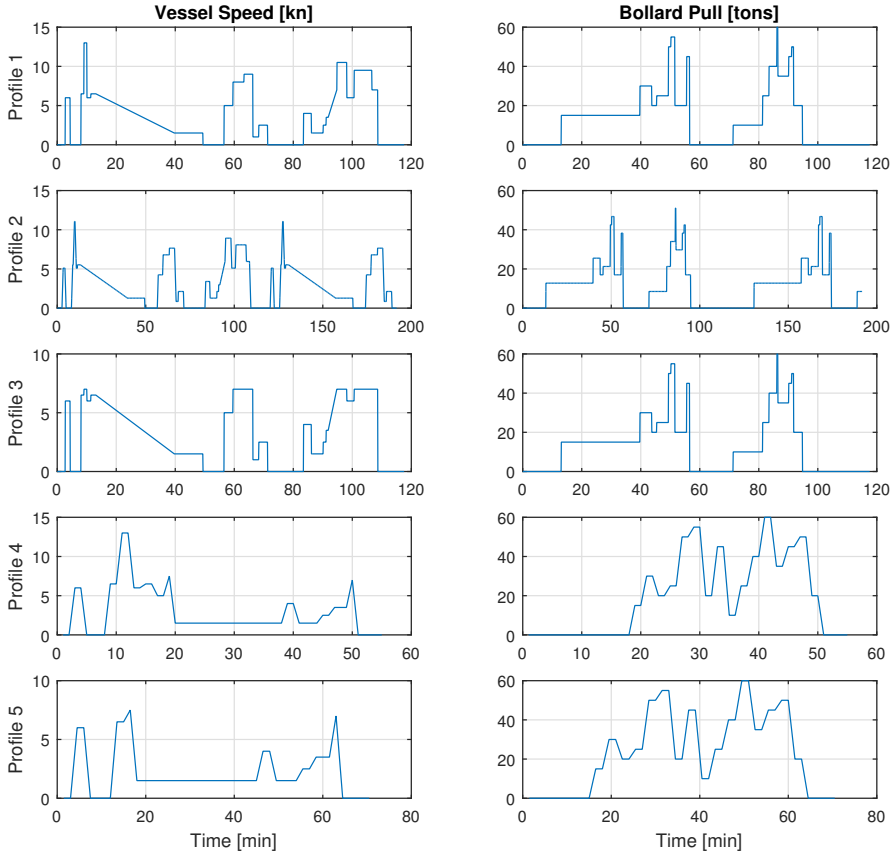

Figure D.4: Reference vessel speed and towing force.

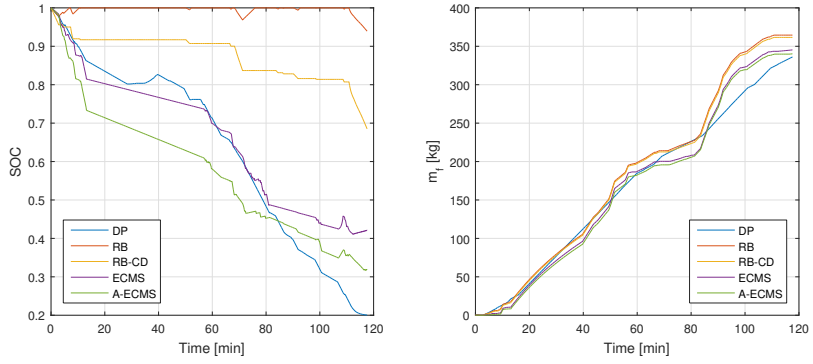

Figure D.5: Fuel Consumption and SOC trajectories - Profile 1.

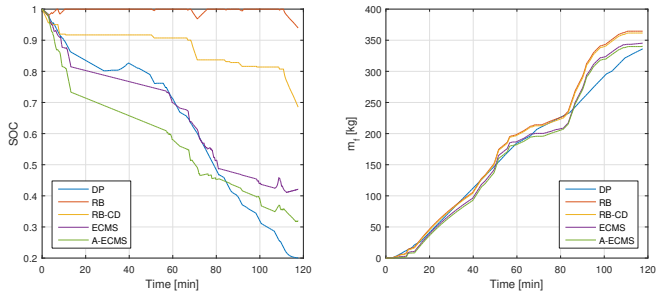

Figure D.6: Fuel Consumption and SOC trajectories - Profile 2.

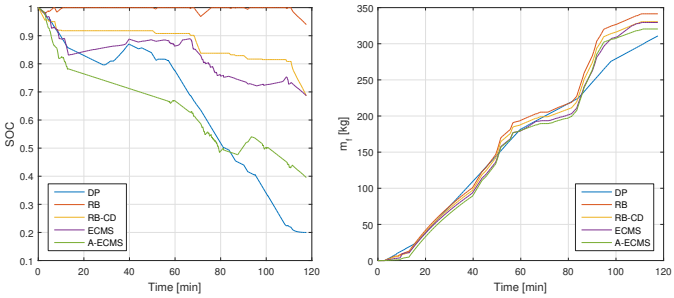

Figure D.7: Fuel Consumption and SOC trajectories - Profile 3.

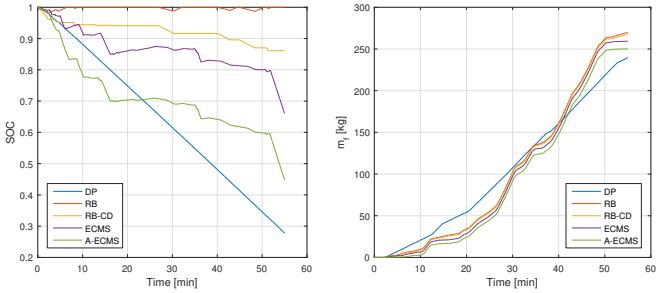

Figure D.8: Fuel Consumption and SOC trajectories - Profile 4.

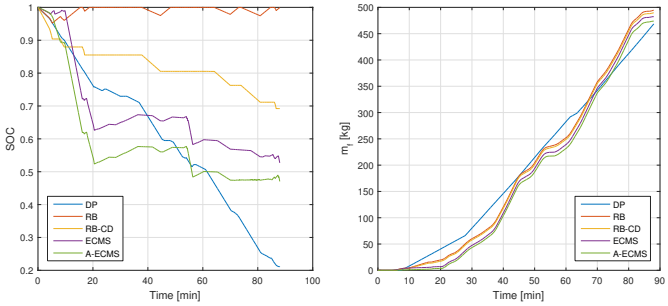

Figure D.9: Fuel Consumption and SOC trajectories - Profile 5.

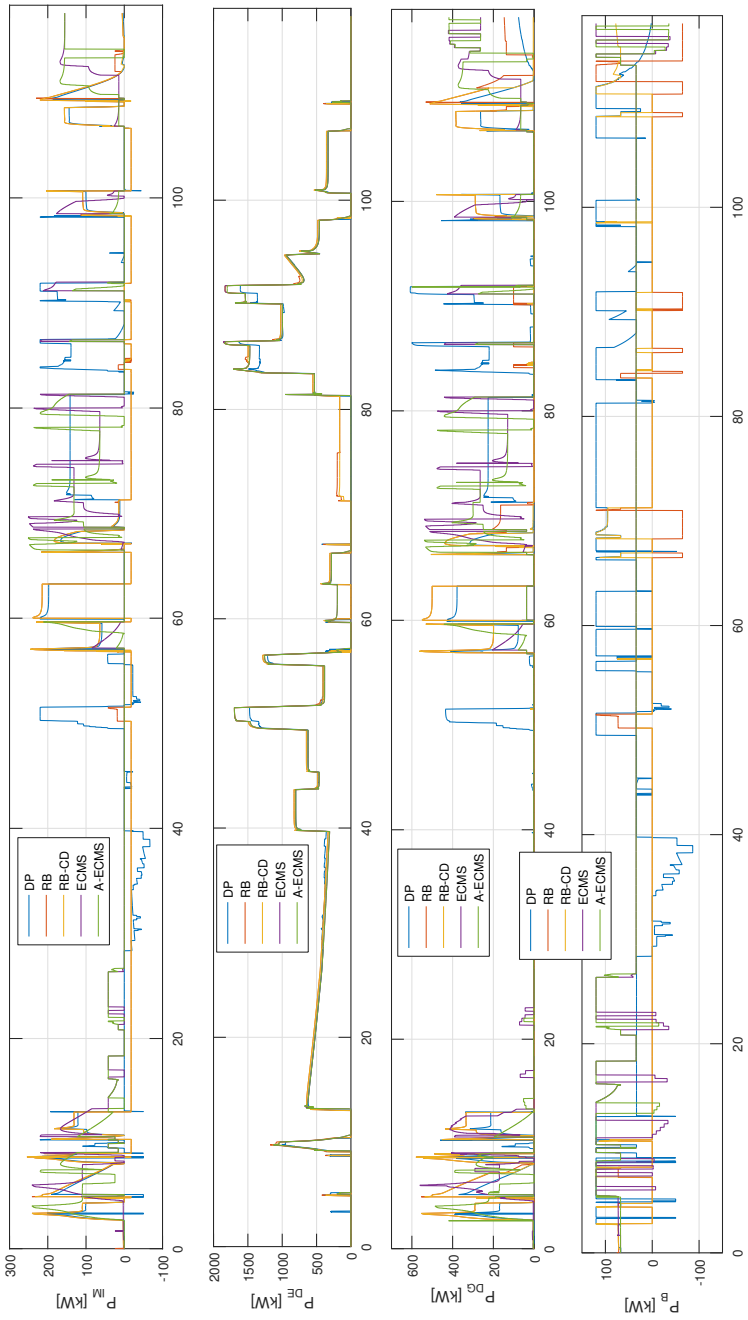

Figure D.10: Power Output of each component - Profile 1.

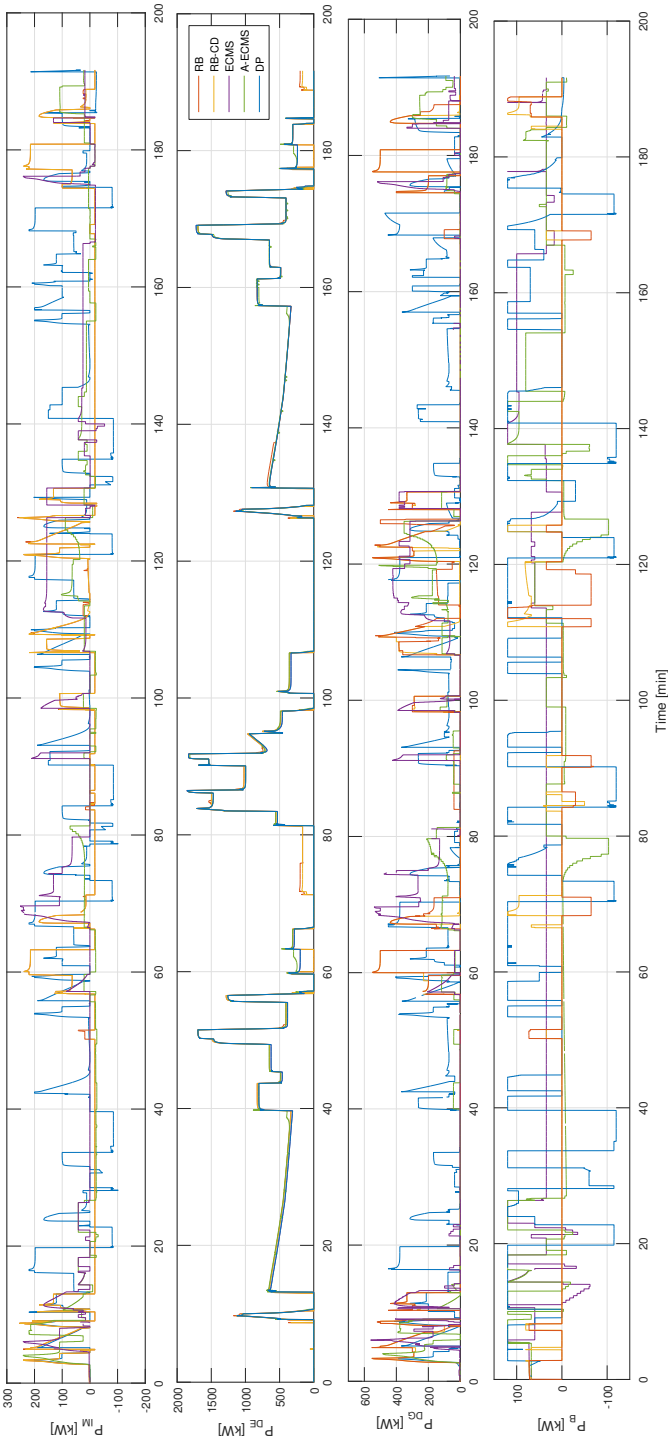

Figure D.11: Power Output of each component - Profile 2.

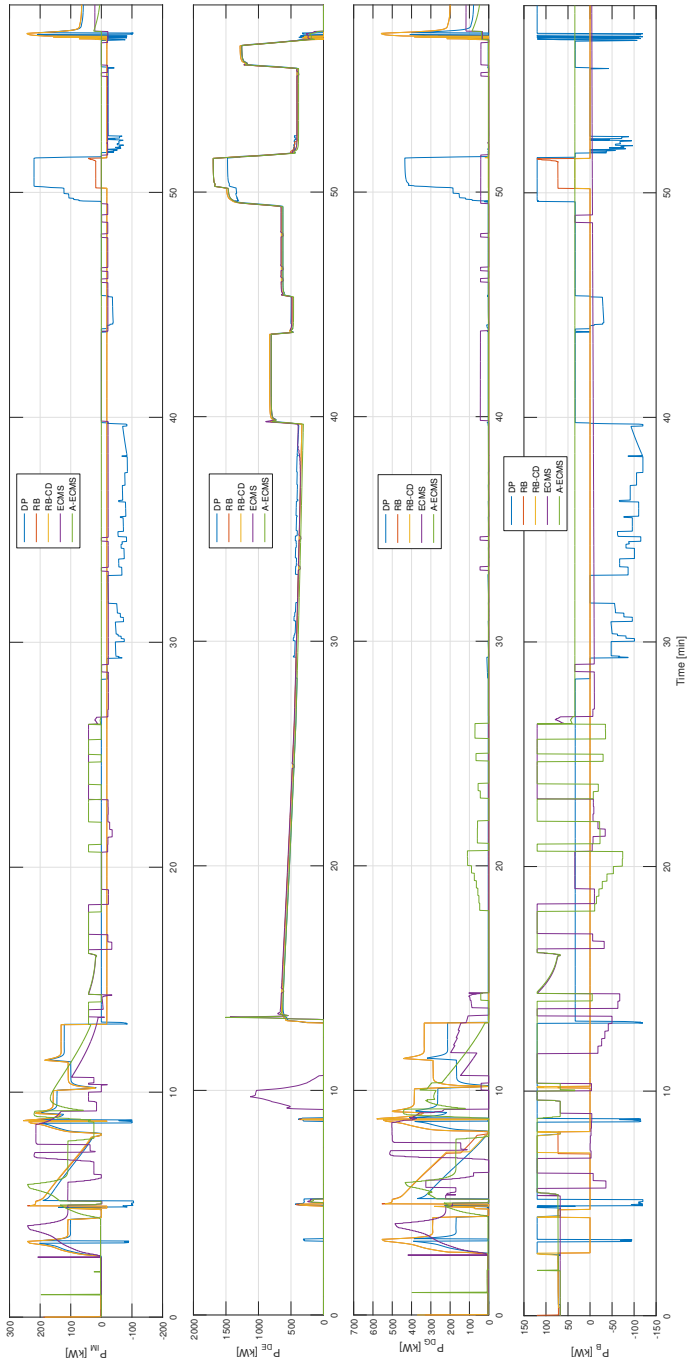

Figure D.12: Power Output of each component - Profile 3.

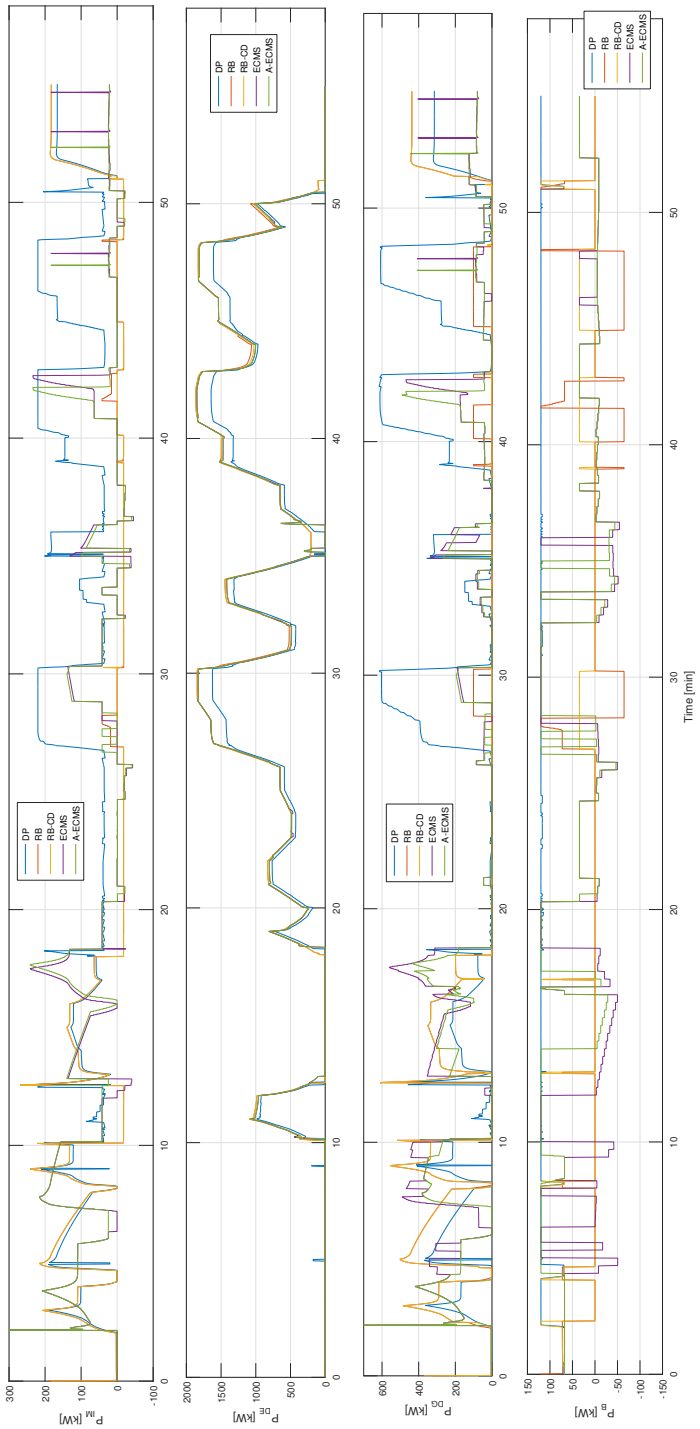

Figure D.13: Power Output of each component - Profile 4.

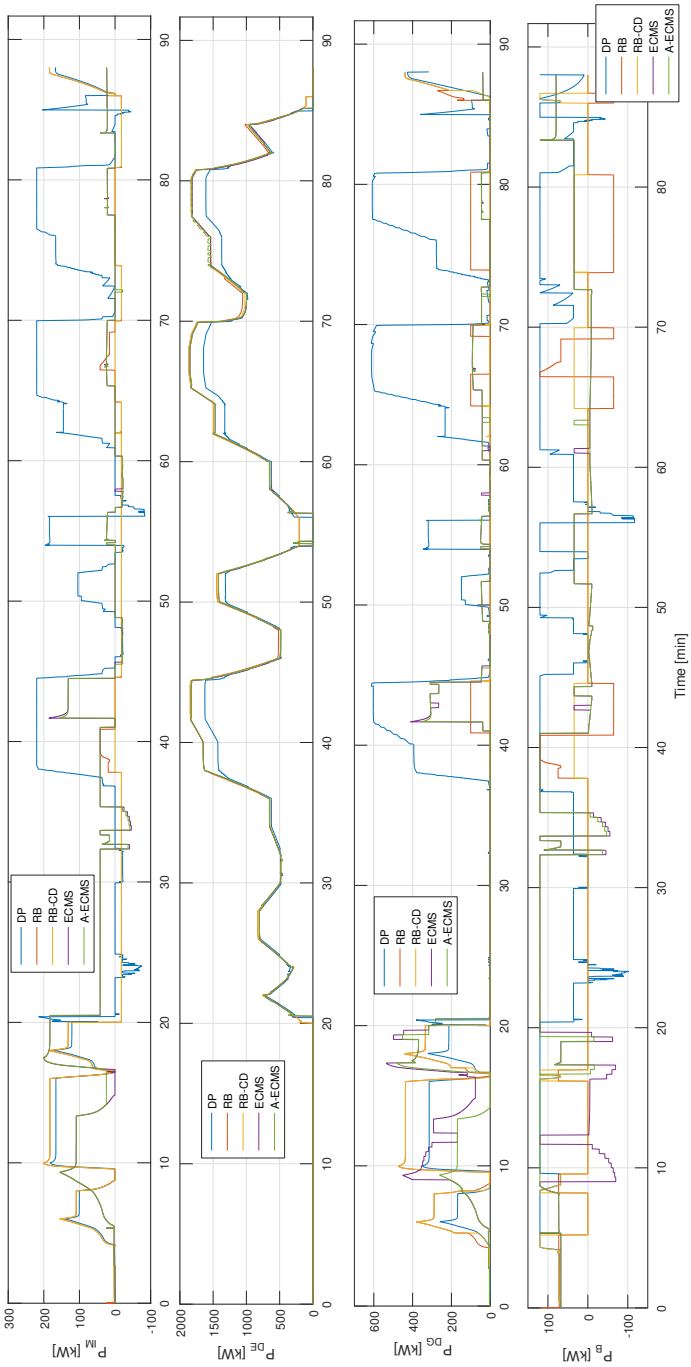

Figure D.14: Power Output of each component - Profile 5.

D

D.3. SENSITIVITY ANALYSIS

D.3.1. EFFECT OF BATTERY POWER LIMITS

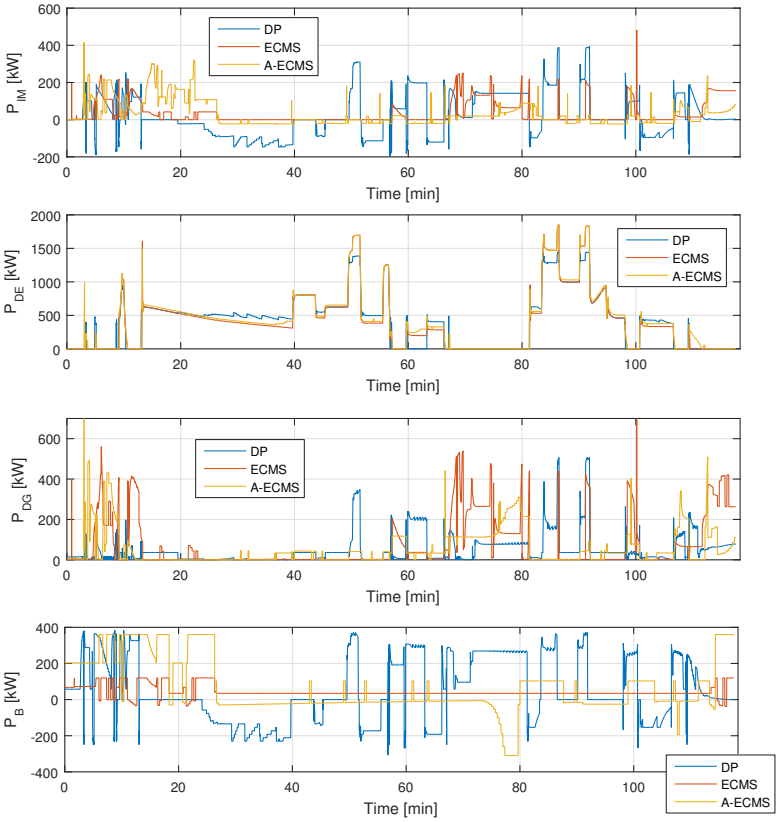

Figure D.15: Power output of each component for 2-C rate battery limits - Profile 1.

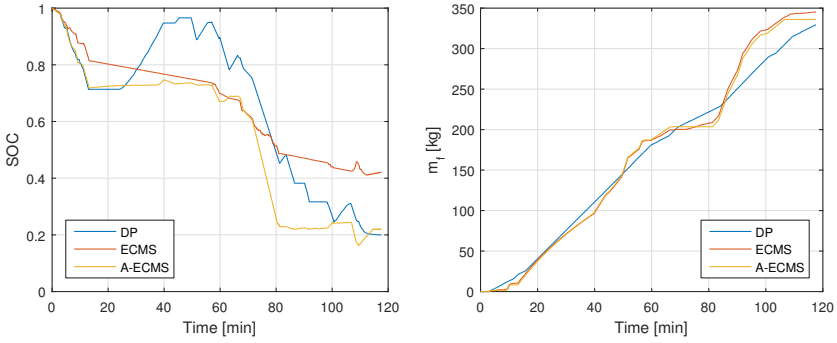

Figure D.16: Fuel consumption and SOC trajectory for 2-C rate battery limits - Profile 1.

D.3.2. EFFECT OF OPERATING PROFILES

D.3.2.1. IDLE PROFILE

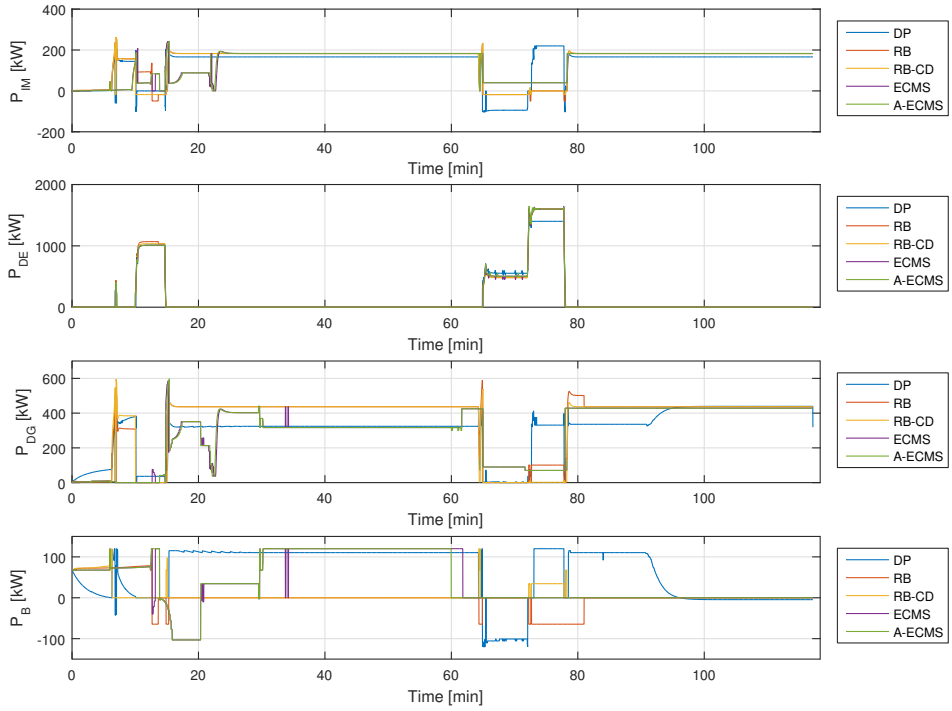

Figure D.17: Power output of each component - Idle Profile.

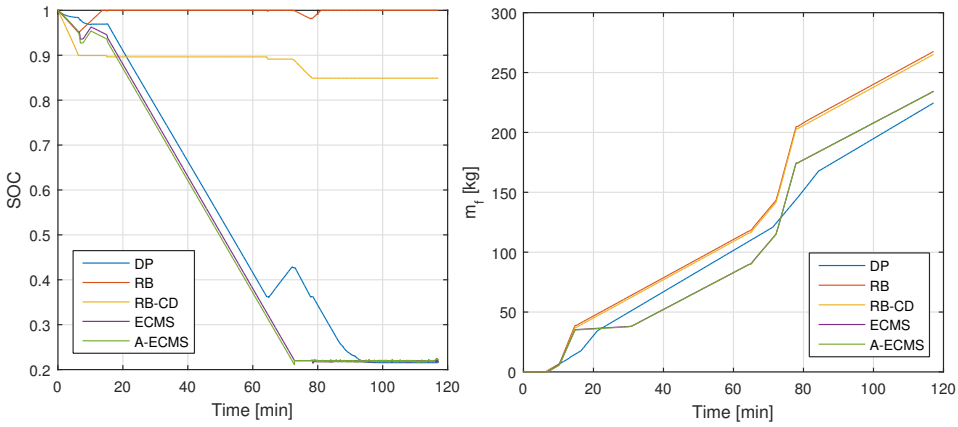

Figure D.18: Fuel consumption and SOC trajectory - Idle Profile.

D.3.2.2. BUSY PROFILE

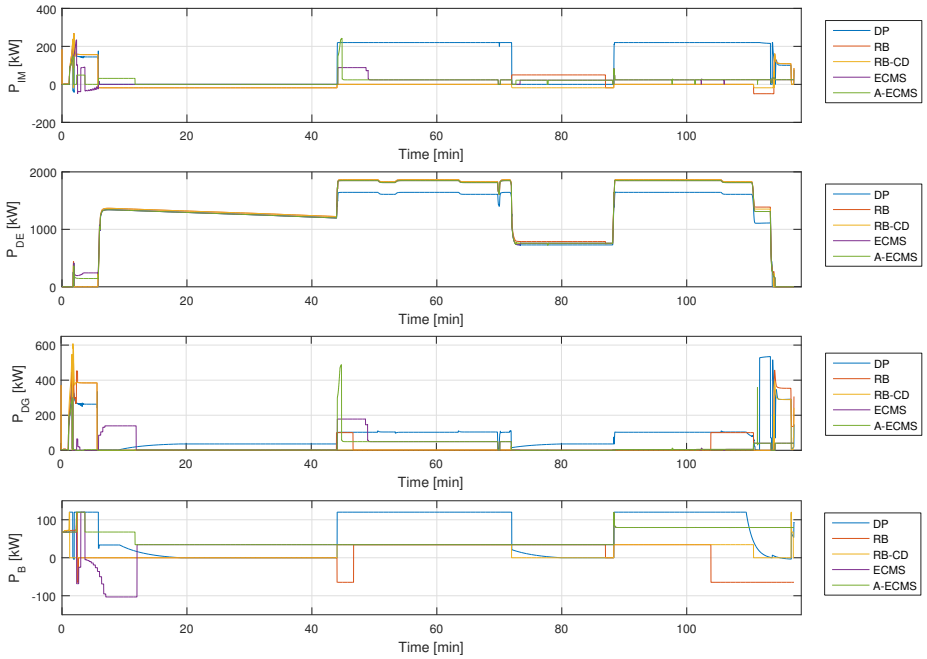

Figure D.19: Power output of each component - Busy Profile.

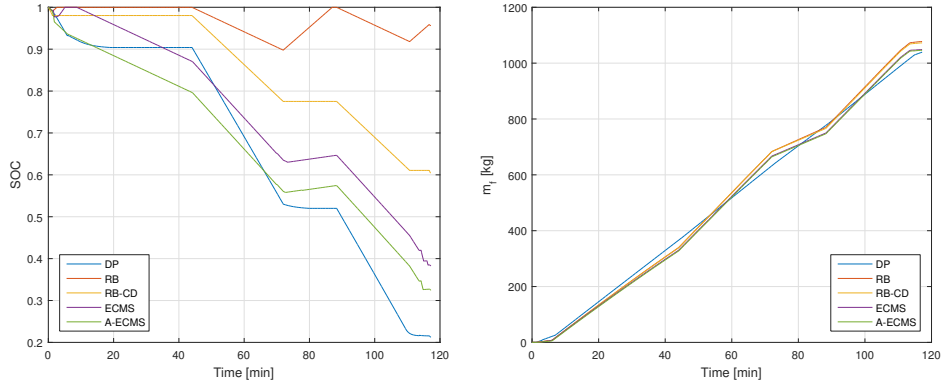

Figure D.20: Fuel consumption and SOC trajectory - Busy Profile.

REFERENCES

Crude oil historical data. http://www.tradingeconomics.com.

D. Ambuhl and L. Guzzella. Predictive reference signal generator for hybrid electric vehicles. *IEEE Transactions on Vehicular Technology*, 58(9):4730–4740, Nov 2009. doi: 10.1109/TVT.2009.2027709.

D. Ambuhl, A. Sciarretta, C. Onder, et al. A Causal Operation Strategy for Hybrid Electric Vehicles based on Optimal Control Theory. In *Hybrid vehicles and energy management : 4th symposium, 14th and 15th February 2007, Stadthalle Braunschweig*, pages 317–331, Braunschweig, 2007. GZVB.

W.J.D. Annand et al. Heat transfer in the cylinders of reciprocating internal combustion engines. *Proceedings of the Institution of Mechanical Engineers*, 177(1):973–996, 1963.

K. B. Ariyur and M. Krstic. *Real-time optimization by extremum-seeking control*. John Wiley & Sons, 2003.

I. Arsie, C. Pianese, G. Rizzo, and M. Santoro. A model for the energy management in a parallel hybrid vehicle. In *Proceedings of the 3rd International Conference on Control and Diagnostics in Automotive Applications*. Citeseer, 2001.

S. Bacha, I. Munteanu, A. I. Bratcu, et al. Power electronic converters modeling and control. *Advanced Textbooks in Control and Signal Processing.—London: Springer*, 454, 2014.

F. Baldi. *Modelling, analysis and optimization of ship energy systems*. PhD thesis, Chalmers University of Technology, Gothenburg, Sweden, 2016.

F. Baldi, U. Larsen, and C. Gabrielii. Comparison of different procedures for the optimisation of a combined diesel engine and organic rankine cycle system based on ship operational profile. *Ocean Engineering*, 110, Part B:85 – 93, 2015a.

F. Baldi, G. Theotokatos, and K. Andersson. Development of a combined mean value–zero dimensional model and application for a large marine four-stroke diesel engine simulation. *Applied Energy*, 154:402 – 415, 2015b. doi: http://dx.doi.org/10.1016/j.apenergy.2015.05.024.

B. M. Baumann, G. Washington, B. C. Glenn, et al. Mechatronic design and control of hybrid electric vehicles. *IEEE/ASME Transactions on Mechatronics*, 5(1):58–72, Mar 2000. doi: 10.1109/3516.828590.

R. Bellman. Dynamic programming. *Princeton, USA: Princeton University Press*, 1(2):3, 1957.

R. Bellman and E. Lee. History and development of dynamic programming. *IEEE Control Systems Magazine*, 4 (4):24–28, November 1984. ISSN 0272-1708. doi: 10.1109/MCS.1984.1104824.

P. Belotti and C. Kirches. Mixed-integer nonlinear optimization. *Acta Numerica*, 22:1–131, 005 2013. doi: 10.1017/S0962492913000032.

A. Ben-Tal and A. Nemirovski. *Lectures on modern convex optimization: analysis, algorithms, and engineering applications*. SIAM, 2001.

M. Berecibar, I. Gandiaga, I. Villarreal, et al. Critical review of state of health estimation methods of li-ion batteries for real applications. *Renewable and Sustainable Energy Reviews*, 56:572 – 587, 2016. doi: http://dx.doi.org/10.1016/j.rser.2015.11.042.

D.P. Bertsekas. *Dynamic programming and optimal control*, volume 1. Athena Scientific Belmont, MA, 1995.

C. Beverelli et al. Oil prices and maritime freight rates: An empirical investigation. Technical report, United Nations Conference on Trade and Development (UNCTAD), Geneva, Switzerland, April 2010.

I. Bloom, B.W. Cole, J.J. Sohn, S.A. Jones, E.G. Polzin, et al. An accelerated calendar and cycle life study of li-ion cells. *Journal of Power Sources*, 101(2):238 – 247, 2001. doi: http://dx.doi.org/10.1016/S0378-7753(01)00783-2.

T. Boom and B. De Schutter. *Optimization in Systems and Control*. Delft Center for Systems and Control, Mekelweg 2, Delft, the Netharlands, August 2015.

H.J. Boonen. Development of a hybrid propulsion simulation model. In *13th international naval engineering conference and exhibition*, Hamburg, Germany, April 2016.

S. Boyd and L. Vandenberghe. *Convex optimization*. Cambridge university press, 2004.

M. Broussely, S. Herreyre, P. Biensan, P. Kasztejna, K. Nechev, and R.J. Staniewicz. Aging mechanism in li ion cells and calendar life predictions. *Journal of Power Sources*, 97–98:13 – 21, 2001. doi: http://dx.doi.org/10.1016/S0378-7753(01)00722-4. Proceedings of the 10th International Meeting on Lithium Batteries.

A. E. Bryson. Optimal control-1950 to 1985. *IEEE Control Systems*, 16(3):26–33, 1996.

F. Burel, R. Taccani, and N. Zuliani. Improving sustainability of maritime transport through utilization of liquefied natural gas (lng) for propulsion. *Energy*, 57:412 – 420, 2013. doi: http://dx.doi.org/10.1016/j.energy.2013.05.002.

S. D. Cairano, D. Bernardini, A. Bemporad, et al. Stochastic mpc with learning for driver-predictive vehicle control and its application to hev energy management. *IEEE Transactions on Control Systems Technology*, 22(3):1018–1031, May 2014. ISSN 1063-6536. doi: 10.1109/TCST.2013.2272179.

P. Cariou. Is slow steaming a sustainable means of reducing co_2 emissions from container shipping? *Transportation Research Part D: Transport and Environment*, 16(3):260–264, 2011. doi: 10.1016/j.trd.2010.12.005.

C.J. Carpenter. Magnetic equivalent circuits. *Electrical Engineers, Proceedings of the Institution of*, 115(10):1503–1511, 1968.

P. Casoli, A. Gambarotta, N. Pompini, et al. Development and validation of a "crank-angle" model of an automotive turbocharged engine for hil applications. *Energy Procedia*, 45:839 – 848, 2014. ISSN 1876-6102. doi: http://dx.doi.org/10.1016/j.egypro.2014.01.089.

C. C. Chan, A. Bouscayrol, and K. Chen. Electric, hybrid, and fuel-cell vehicles: Architectures and modeling. *IEEE Transactions on Vehicular Technology*, 59(2):589–598, February 2010. doi: 10.1109/TVT.2009.2033605.

S. Chapman. *Electric machinery fundamentals*. Tata McGraw-Hill Education, 2005.

K.T Chau, Y.S Wong, and C.C Chan. An overview of energy sources for electric vehicles. *Energy Conversion and Management*, 40(10):1021 – 1039, 1999. doi: http://dx.doi.org/10.1016/S0196-8904(99)00021-7.

M. Chen and G. A. Rincon-Mora. Accurate electrical battery model capable of predicting runtime and i-v performance. *IEEE Transactions on Energy Conversion*, 21(2):504–511, June 2006. doi: 10.1109/TEC.2006.874229.

S. K. Chen and P. F. Flynn. Development of a single cylinder compression ignition research engine. Technical report, SAE Technical Paper, 1965.

Z. Chen, C. C. Mi, J. Xu, et al. Energy management for a power-split plug-in hybrid electric vehicle based on dynamic programming and neural networks. *IEEE Transactions on Vehicular Technology*, 63(4):1567–1580, May 2014. ISSN 0018-9545. doi: 10.1109/TVT.2013.2287102.

L. W. Chong, Y. W. Wong, R. Kumar, et al. Hybrid energy storage systems and control strategies for stand-alone renewable energy power systems. *Renewable and Sustainable Energy Reviews*, 66:174–189, 2016. doi: http://dx.doi.org/10.1016/j.rser.2016.07.059.

J.J. Corbett and J. Winebrake. The impacts of globalization on international maritime transport activity: Past trends and future perspectives. Technical report, Organization for Economic Cooperation and Development, Paris, France, November 2008.

R. De Doncker, D. Pulle, and A. Veltman. *Advanced electrical drives: analysis, modeling, control*. Springer Science and Business Media, 2010.

T. K. B. de Jager and M. Steinbuch. An adaptive sub-optimal energy management strategy for hybrid drivetrains. *IFAC Proceedings Volumes*, 41(2):102 – 107, 2008. ISSN 1474-6670. doi: http://dx.doi.org/10.3182/20080706-5-KR-1001.00017.

R. de Jong, I. Rollema, R. Schillings, et al. Geardrive: Gearbox power loss models and validation in hybrid propulsion configurations. Master's thesis, Delft University of Technology, Delft, the Netherlands, June 2015.

D.S. de Waard. Parameterization of ship propulsion drives. Master's thesis, Delft University of Technology, Delft, the Netherlands, June 2014.

E. Dedes. *Investigation of hybrid systems for diesel powered ships*. PhD thesis, University of Southampton, 2013.

E. Dedes, D. A. Hudson, and S. R. Turnock. Assessing the potential of hybrid energy technology to reduce exhaust emissions from global shipping. *Energy Policy*, 40:204 – 218, 2012. doi: 10.1016/j.enpol.2011.09.046.

S. Delprat, T. M. Guerra, and J. Rimaux. Control strategies for hybrid vehicles: optimal control. In *Proceedings IEEE 56th Vehicular Technology Conference*, volume 3, pages 1681–1685 vol.3, 2002. doi: 10.1109/VETECF.2002.1040502.

N. Denis, M. R. Dubois, R. Dube, et al. Blended power management strategy using pattern recognition for a plug-in hybrid electric vehicle. *International Journal of Intelligent Transportation Systems Research*, 14(2):101–114, 2016. doi: 10.1007/s13177-014-0106-z.

C. Dextreit and I. V. Kolmanovsky. Approaches to energy management of hybrid electric vehicles: Experimental comparison. In *UKACC International Conference on Control*, pages 1–6, Sept 2010. doi: 10.1049/ic.2010.0294.

C. Dextreit and I. V. Kolmanovsky. Game theory controller for hybrid electric vehicles. *IEEE Transactions on Control Systems Technology*, 22(2):652–663, March 2014. ISSN 1063-6536. doi: 10.1109/TCST.2013.2254597.

E. Dinccmen, I. Uygan, B. A. Guvenc, et al. Powertrain control of parallel hybrid electric vehicles via extremum seeking algorithm. In *ASME 2010 10th Biennial Conference on Engineering Systems Design and Analysis*, pages 147–156. American Society of Mechanical Engineers, 2010.

DNV-GL. Prevention of air pollution from ships: Assessment of imo efficiency measures for the control of ghg emissions from ships. Technical report, London, UK, July 2011.

D. Dochain, M. Perrier, and M. Guay. Extremum seeking control and its application to process and reaction systems: A survey. *Mathematics and Computers in Simulation*, 82(3):369 – 380, 2011. ISSN 0378-4754. doi: http://dx.doi.org/10.1016/j.matcom.2010.10.022. 6th Vienna International Conference on Mathematical Modelling.

J. Drijver. Evaluation of transmission losses, heat flows and temperatures of propulsive drive lines. Master's thesis, Delft University of Technology, Delft, the Netherlands, June 2013.

X. Du and W. Chen. Efficient uncertainty analysis methods for multidisciplinary robust design. *AIAA journal*, 40(3):545–552, 2002.

M. Ehsani and A. Emadi. *Modern electric, hybrid electric, and fuel cell vehicles: fundamentals, theory, and design*. CRC press, 2009.

P. Elbert, S. Ebbesen, and L. Guzzella. Implementation of dynamic programming for n- dimensional optimal control problems with final state constraints. *IEEE Transactions on Control Systems Technology*, 21(3):924–931, May 2013. ISSN 1063-6536. doi: 10.1109/TCST.2012.2190935.

O. Erdinc, B. Vural, and M. Uzunoglu. A dynamic lithium-ion battery model considering the effects of temperature and capacity fading. In *Clean Electrical Power, 2009 International Conference on*, pages 383–386. IEEE, 2009.

L. Eriksson and L. Nielsen. *Modeling and control of engines and drivelines*. John Wiley & Sons, 2014.

R. Galeazzi, Mo. Blanke, L. P. Perera, et al. Identification of optimal trim configurations to improve energy efficiency in ships. *IFAC-PapersOnLine*, 48(16):267 – 272, 2015. doi: http://dx.doi.org/10.1016/j.ifacol.2015.10.291.

L. Gao, S. Liu, and R. A. Dougal. Dynamic lithium-ion battery model for system simulation. *IEEE transactions on components and packaging technologies*, 25(3):495–505, 2002.

W. Gao and S. K. Porandla. Design optimization of a parallel hybrid electric powertrain. In *2005 IEEE Vehicle Power and Propulsion Conference*, pages 6 pp.–, Sept 2005. doi: 10.1109/VPPC.2005.1554609.

R. Geertsma. Extensive quadratic fit model. Unpublished, 2015.

R. D. Geertsma, R. R. Negenborn, K. Visser, and J. J. Hopman. Pitch control for ships with mechanical and hybrid propulsion: Modeling, validation and performance quantification. Unpublished.

R. D. Geertsma, R. R. Negenborn, K. Visser, and J. J. Hopman. Design and control of hybrid power and propulsion systems for smart ships: A review of developments. *Applied Energy*, (194):30–54, 2017. doi: http://dx.doi.org/10.1016/j.apenergy.2017.02.060.

J. M. German. Hybrid powered vehicles. Technical report, SAE Technical Paper, 2003.

M. Godjevac, J. Drijver, L. de Vries, et al. Evaluation of losses in maritime gearboxes. *Proceedings of the Institution of Mechanical Engineers, Part M: Journal of Engineering for the Maritime Environment*, 2015.

A. Gomez-Exposito, A. Conejo, and C. Canizares. *Electric energy systems: analysis and operation*. CRC Press, 2016.

H. Grimmelius, E. Mesbahi, P. Schulten, and D. Stapersma. The use of diesel engine simulation models in ship propulsion plant design and operation. *CIMAC International Council on Combustion engines*, pages 1–12, 2007.

H. Grimmelius et al. Control of hybrid ship drive systems. In *10th international conference on computer and IT applications in the maritime industries*, Hamburg, Germany, 2011.

C. Guan, G. Theotokatos, P. Zhou, et al. Computational investigation of a large containership propulsion engine operation at slow steaming conditions. *Applied Energy*, 130:370 – 383, 2014. doi: http://dx.doi.org/10.1016/j.apenergy.2014.05.063.

C. Guardiola, B. Pla, D. Blanco-Rodriguez, and P. O. Calendini. Ecu-oriented models for nox prediction. part 1: a mean value engine model for nox prediction. *Proceedings of the Institution of Mechanical Engineers, Part D: Journal of Automobile Engineering*, pages 185–206, 2014.

Y. Gurkaynak, A. Khaligh, and A. Emadi. State of the art power management algorithms for hybrid electric vehicles. In *2009 IEEE Vehicle Power and Propulsion Conference*, pages 388–394, Sept 2009. doi: 10.1109/VPPC.2009.5289823.

G. Gutmann. Hybrid electric vehicles and electrochemical storage systems — a technology push–pull couple. *Journal of Power Sources*, 84(2):275 – 279, 1999. doi: http://dx.doi.org/10.1016/S0378-7753(99)00328-6.

L. Guzzella and C. Onder. *Introduction to modeling and control of internal combustion engine systems*. Springer Science & Business Media, Berlin, Germany, 2009.

L. Guzzella, A. Sciarretta, et al. *Vehicle propulsion systems: Introduction to Modeling and Optimization*, volume 1. Springer, Berlin, Germany, 2007.

J. B. Heywood et al. *Internal combustion engine fundamentals*, volume 930. McGraw-hill New York, 1988.

F. S. Hillier. *Introduction to operations research*. Tata McGraw-Hill Education, 2012.

K. Honkura, K. Takahashi, and T. Horiba. Capacity-fading prediction of lithium-ion batteries based on discharge curves analysis. *Journal of Power Sources*, 196(23):10141 – 10147, 2011. doi: http://dx.doi.org/10.1016/j.jpowsour.2011.08.020.

X. Hu, S. Asgari, S. Lin, S. Stanton, and W. Lian. A linear parameter-varying model for hev/ev battery thermal modeling. In *2012 IEEE Energy Conversion Congress and Exposition (ECCE)*, pages 1643–1649, Sept 2012. doi: 10.1109/ECCE.2012.6342616.

F. Huang and C. Yang. Hull form optimization of a cargo ship for reduced drag. *Journal of Hydrodynamics, Ser. B*, 28(2):173 – 183, 2016. doi: http://dx.doi.org/10.1016/S1001-6058(16)60619-4.

I. Husain. *Electric and hybrid vehicles: design fundamentals*. CRC press, Florida, USA, 2011.

International Chamber of Shipping. Shipping, world trade and the reduction of $c0_2$. Technical report, Geneva, Switzerland, April 2010.

International Council on Clean Transportation. Air pollution and greenhouse gas emissions from ocean-going ships: Impacts, mitigation options and opportunities for managing growth. *Maritime Studies*, (153):3–10, 2007. doi: 10.1080/07266472.2007.10878845.

International Maritime Organization. Third IMO GHG study: Prevention of air pollution from ships. Technical report, International Maritime Organization, London, UK, June 2014.

B. D. Jager, T. V. Keulen, and J. T. B. A. Kessels. *Optimal control of hybrid vehicles*. Springer, 2013.

J. Jaguemont, D. Yves, L. Boulon, and F. Martel. Thermal management of a hybrid electric vehicle in cold weather. *IEEE Transactions on Energy Conversion*, (99):1–1, 2016. doi: 10.1109/TEC.2016.2553700.

K. Johnson, K. Mollenhauer, and H. Tschoke. *Handbook of diesel engines*. Springer Science & Business Media, Berlin, Germany, 2010.

N. Kakimoto and K. Goto. Capacity-fading model of lithium-ion battery applicable to multicell storage systems. *IEEE Transactions on Sustainable Energy*, 7(1):108–117, 2016.

J. T. B. A. Kessels, M. W. T. Koot, P. P. J. van den Bosch, and D. B. Kok. Online energy management for hybrid electric vehicles. *IEEE Transactions on Vehicular Technology*, 57(6):3428–3440, Nov 2008. ISSN 0018-9545. doi: 10.1109/TVT.2008.919988.

M. Khodabakhshian, L. Feng, and J. Wikander. Improving fuel economy and robustness of an improved ecms method. In *2013 10th IEEE International Conference on Control and Automation (ICCA)*, pages 598–603, June 2013. doi: 10.1109/ICCA.2013.6564946.

F. Khoucha, M. Benbouzid, and A. Kheloui. An optimal fuzzy logic power sharing strategy for parallel hybrid electric vehicles. In *2010 IEEE Vehicle Power and Propulsion Conference*, pages 1–5. IEEE, 2010.

U. Kiencke and L. Nielsen. *Automotive control systems: for engine, driveline, and vehicle*. Springer Science & Business Media, Berlin, Germany, 2005.

K. Kijima and Y. Nakiri. On the practical prediction method for ship maneuvering characteristics. 2003.

C. Kim, E. N. Goongand, S. Lee, et al. Fuel economy optimization for parallel hybrid vehicles with cvt. Technical report, SAE Technical Paper, 1999.

N. Kim, S. Cha, and H. Peng. Optimal control of hybrid electric vehicles based on pontryagin's minimum principle. *IEEE Transactions on Control Systems Technology*, 19(5):1279–1287, Sept 2011. doi: 10.1109/TCST.2010.2061232.

D. Kirk. *Optimal control theory: an introduction*. Courier Corporation, 2012.

I.V. Kolmanovsky, L. Lezhnev, and T.L. Maizenberg. Discrete-time drift counteraction stochastic optimal control: Theory and application-motivated examples. *Automatica*, 44(1):177 – 184, 2008. doi: http://dx.doi.org/10.1016/j.automatica.2007.06.002.

M. Koot, J. T. B. A. Kessels, B. de Jager, W. P. M. H. Heemels, P. P. J. van den Bosch, and M. Steinbuch. Energy management strategies for vehicular electric power systems. *IEEE Transactions on Vehicular Technology*, 54 (3):771–782, May 2005. ISSN 0018-9545. doi: 10.1109/TVT.2005.847211.

P. C. Krause, O. Wasynczuk, S. D. Sudhoff, et al. *Analysis of electric machinery and drive systems*, volume 75. John Wiley & Sons, 2013.

P. R. Krugman. Increasing returns, monopolistic competition, and international trade. *Journal of International Economics*, 9(4):469–479, 1979. doi: 10.1016/0022-1996(79)90017-5.

R. Latorre. Ship hull drag reduction using bottom air injection. *Ocean engineering*, 24(2):161–175, 1997.

H.D. Lee, E.S. Koo, S.K. Sul, et al. Torque control strategy for a parallel-hybrid vehicle using fuzzy logic. *IEEE Industry Applications Magazine*, 6(6):33–38, Nov 2000. doi: 10.1109/2943.877838.

Z. Lei, D. Qin, Y. Liu, et al. Dynamic energy management for a novel hybrid electric system based on driving pattern recognition. *Applied Mathematical Modelling*, 45:940 – 954, 2017. ISSN 0307-904X. doi: http://doi.org/10.1016/j.apm.2017.01.036. URL http://www.sciencedirect.com/science/article/pii/S0307904X17300422.

L. Li, S. You, and C. Yang. Multi-objective stochastic mpc-based system control architecture for plug-in hybrid electric buses. *IEEE Transactions on Industrial Electronics*, 63(8):4752–4763, Aug 2016. ISSN 0278-0046. doi: 10.1109/TIE.2016.2547359.

R. Li, Y. Huang, G. Li, K. Han, et al. Calibration and validation of a mean value model for turbocharged diesel engine. *Advances in Mechanical Engineering*, 5:579–583, 2013.

C. C. Lin, H. Peng, J. W. Grizzle, and J.M. Kang. Power management strategy for a parallel hybrid electric truck. *IEEE Transactions on Control Systems Technology*, 11(6):839–849, Nov 2003. ISSN 1063-6536. doi: 10.1109/TCST.2003.815606.

V.T. Long and N.V. Nhan. Bees-algorithm-based optimization of component size and control strategy parameters for parallel hybrid electric vehicles. *International Journal of Automotive Technology*, 13(7):1177–1183, 2012.

R. Lu, O. Turan, E. Boulougouris, et al. A semi-empirical ship operational performance prediction model for voyage optimization towards energy efficient shipping. *Ocean Engineering*, 110, Part B:18 – 28, 2015. doi: http://dx.doi.org/10.1016/j.oceaneng.2015.07.042.

E. R. Lwithwaite. Magnetic equivalent circuits for electrical machines. *Electrical Engineers, Proceedings of the Institution of*, 114(11):1805–1809, November 1967. ISSN 0020-3270. doi: 10.1049/piee.1967.0344.

A. A. Malikopoulos. Stochastic optimal control for series hybrid electric vehicles. In *2013 American Control Conference*, pages 1189–1194, June 2013. doi: 10.1109/ACC.2013.6579997.

MAN B & W. G-type engine: Revolutionary ultra-long stroke. Technical report, May 2012. URL https://marine.man.eu/docs/librariesprovider6/technical-papers/5510-0104-01pp_low.pdf?sfvrsn=12.

J. F. Manwell and J. G. McGowan. Lead acid battery storage model for hybrid energy systems. *Solar Energy*, 50 (5):399–405, 1993.

J. F. Manwell and J. G. McGowan. Extension of the kinetic battery model for wind/hybrid power systems. In *Proceedings of EWEC*, pages 284–289, 1994.

F. Maroteaux and C. Saad. Combined mean value engine model and crank angle resolved in-cylinder modeling with {NOx} emissions model for real-time diesel engine simulations at high engine speed. *Energy*, 88:515 – 527, 2015. doi: http://dx.doi.org/10.1016/j.energy.2015.05.072.

C. Mi, B. Li, D. Buck, and N. Ota. Advanced electro-thermal modeling of lithium-ion battery system for hybrid electric vehicle applications. In *2007 IEEE Vehicle Power and Propulsion Conference*, pages 107–111, Sept 2007. doi: 10.1109/VPPC.2007.4544108.

C. Mi, M. A. Masrur, and D. W. Gao. *Hybrid electric vehicles: principles and applications with practical perspectives*. John Wiley & Sons, 2011.

N. Mohan and T. M. Undeland. *Power electronics: converters, applications, and design*. John Wiley & Sons, 2007.

M. Montazeri, A. Poursamad, and B. Ghalichi. Application of genetic algorithm for optimization of control strategy in parallel hybrid electric vehicles. *Journal of the Franklin Institute*, 343(4–5):420 – 435, 2006. ISSN 0016-0032. doi: http://dx.doi.org/10.1016/j.jfranklin.2006.02.015. Modeling, Simulation and Applied Optimization.

M. R. Motley, M. N., and Y. L. Young. Integrated probabilistic design of marine propulsors to minimize lifetime fuel consumption. *Ocean Engineering*, 45:1 – 8, 2012. doi: http://dx.doi.org/10.1016/j.oceaneng.2012.01.032.

S. J. Moura, H. K. Fathy, D. S. Callaway, et al. A stochastic optimal control approach for power management in plug-in hybrid electric vehicles. *IEEE Transactions on Control Systems Technology*, 19(3):545–555, May 2011. doi: 10.1109/TCST.2010.2043736.

Y. L. Murphey, J. Park, Z. Chen, et al. Intelligent hybrid vehicle power control - part i: Machine learning of optimal vehicle power. *IEEE Transactions on Vehicular Technology*, 61(8):3519–3530, Oct 2012. ISSN 0018-9545. doi: 10.1109/TVT.2012.2206064.

Y. L. Murphey, J. Park, L. Kiliaris, et al. Intelligent hybrid vehicle power control - part ii: Online intelligent energy management. *IEEE Transactions on Vehicular Technology*, 62(1):69–79, Jan 2013. ISSN 0018-9545. doi: 10.1109/TVT.2012.2217362.

C. Musardo, G. Rizzoni, Y. Guezennec, et al. A-ecms: An adaptive algorithm for hybrid electric vehicle energy management. *European Journal of Control*, 11(4):509–524, 2005.

A. Neffati, M. Guemri, S. Caux, and M. Fadel. Energy management strategies for multi source systems. *Electric Power Systems Research*, 102:42 – 49, 2013. doi: http://dx.doi.org/10.1016/j.epsr.2013.03.008.

M. Nelson, D.W. Temple, J.T. Hwang, et al. Simultaneous optimization of propeller – hull systems to minimize lifetime fuel consumption. *Applied Ocean Research*, 43:46 – 52, 2013. doi: http://dx.doi.org/10.1016/j.apor.2013.07.004.

R. F. Nielsen, F. Haglind, and U. Larsen. Design and modeling of an advanced marine machinery system including waste heat recovery and removal of sulphur oxides. *Energy Conversion and Management*, 85:687–693, 2014. doi: http://dx.doi.org/10.1016/j.enconman.2014.03.038.

K. Nikzadfar and A. H. Shamekhi. An extended mean value model (emvm) for control-oriented modeling of diesel engines transient performance and emissions. *Fuel*, 154:275 – 292, 2015. doi: http://dx.doi.org/10.1016/j.fuel.2015.03.070.

W. L. Oberkampf, T. G. Trucano, and C. Hirsch. Verification, validation, and predictive capability in computational engineering and physics. *Applied Mechanics Reviews*, 57(5):345–384, 2004.

K. Oh, J. Min, D. Choi, and H. Kim. Optimization of control strategy for a single-shaft parallel hybrid electric vehicle. *Proceedings of the Institution of Mechanical Engineers, Part D: Journal of Automobile Engineering*, 221(5):555–565, 2007.

L. Olatomiwa, S. Mekhilef, M.S. Ismail, and M. Moghavvemi. Energy management strategies in hybrid renewable energy systems: A review. *Renewable and Sustainable Energy Reviews*, 62:821–835, 2016. ISSN 1364-0321. doi: http://dx.doi.org/10.1016/j.rser.2016.05.040.

C. M. Ong. *Dynamic simulation of electric machinery: using MATLAB/SIMULINK*, volume 5. Prentice Hall Publishing House, 1998.

S. Onori, L. Serrao, and G. Rizzoni. *Hybrid Electric Vehicles: Energy Management Strategies*. Springer, Berlin, Germany, 2016.

G. Paganelli, T.M. Guerra, S. Delprat, et al. Simulation and assessment of power control strategies for a parallel hybrid car. *Proceedings of the Institution of Mechanical Engineers, Part D: Journal of Automobile Engineering*, 214(7):705–717, 2000.

A. Panday and H. O. Bansal. A review of optimal energy management strategies for hybrid electric vehicle. *International Journal of Vehicular Technology*, 2014, 2014. doi: http://dx.doi.org/10.1155/2014/160510.

J. Park, Z. Chen, L. Kiliaris, et al. Intelligent vehicle power control based on machine learning of optimal control parameters and prediction of road type and traffic congestion. *IEEE Transactions on Vehicular Technology*, 58(9):4741–4756, Nov 2009. ISSN 0018-9545. doi: 10.1109/TVT.2009.2027710.

M. R. Patel. *Introduction to electrical power and power electronics*. CRC Press, 2012.

M. Petit, E. Prada, and V. Sauvant-Moynot. Development of an empirical aging model for li-ion batteries and application to assess the impact of vehicle-to-grid strategies on battery lifetime. *Applied Energy*, 172:398 – 407, 2016. doi: http://dx.doi.org/10.1016/j.apenergy.2016.03.119.

G. Pistoia. *Electric and Hybrid Vehicles - Power Sources, Models, Sustainability, Infrastructure and the Market*. Elsevier, New Jersey, USA, 2010.

P. Pisu and G. Rizzoni. A supervisory control strategy for series hybrid electric vehicles with two energy storage systems. In *2005 IEEE Vehicle Power and Propulsion Conference*, pages 8 pp.–, Sept 2005. doi: 10.1109/VPPC.2005.1554534.

C. D. Rahn and C. Wang. *Battery systems engineering*. John Wiley & Sons, 2013.

D. Rakhmatov, S. Vrudhula, and D. Wallach. Battery lifetime prediction for energy-aware computing. In *Proceedings of the 2002 international symposium on Low power electronics and design*, pages 154–159. ACM, 2002.

D. Rakhmatov, S. Vrudhula, and D. A Wallach. A model for battery lifetime analysis for organizing applications on a pocket computer. *IEEE Transactions on Very Large Scale Integration (VLSI) Systems*, 11(6):1019–1030, 2003.

D. N Rakhmatov and S. Vrudhula. An analytical high-level battery model for use in energy management of portable electronic systems. In *Proceedings of the 2001 IEEE/ACM international conference on Computer-aided design*, pages 488–493. IEEE Press, 2001.

V. Rao, G. Singhal, A. Kumar, et al. Battery model for embedded systems. In *18th International Conference on VLSI Design held jointly with 4th International Conference on Embedded Systems Design*, pages 105–110, Jan 2005. doi: 10.1109/ICVD.2005.61.

J. Reb, C. Sturzebecher, C. Bohn, et al. A diesel engine model including exhaust flap, intake throttle, lp-egr and vgt. part i: System modeling. *IFAC-PapersOnLine*, 48(15):52 – 59, 2015. doi: http://dx.doi.org/10.1016/j.ifacol.2015.10.008.

G. Ripaccioli, D. Bernardini, S. Di Cairano, et al. A stochastic model predictive control approach for series hybrid electric vehicle power management. In *Proceedings of the 2010 American Control Conference*, pages 5844–5849, June 2010. doi: 10.1109/ACC.2010.5530504.

S. Risse and K. Buchmann. New turbochargers for modern large engines with low emissions and high performance. In *Proceedings of The 23rd International Council on Combustion Engines*, Shanghai, China, May 2013.

G. Rizzoni, L. Guzzella, and B. M. Baumann. Unified modeling of hybrid electric vehicle drivetrains. *IEEE/ASME Transactions on Mechatronics*, 4(3):246–257, September 1999. ISSN 1083–4435. doi: 10.1109/3516.789683.

M.F. M. Sabri, K.A. Danapalasingam, and M.F. Rahmat. A review on hybrid electric vehicles architecture and energy management strategies. *Renewable and Sustainable Energy Reviews*, 53:1433 – 1442, 2016. doi: http://dx.doi.org/10.1016/j.rser.2015.09.036.

E. Sarasketa-Zabala, E. Martinez-Laserna, M. Berecibar, et al. Realistic lifetime prediction approach for li-ion batteries. *Applied Energy*, 162:839 – 852, 2016. doi: http://dx.doi.org/10.1016/j.apenergy.2015.10.115.

C. Schlegel, A. Hosl, and S. Diel. Detailed loss modelling of vehicle gearboxes. In *Proceedings of the 7th International Modelica Conference*, number 043, pages 434–443, Como, Italy, September 2009. Linkoping University Electronic Press.

S. Schlesinger et al. Terminology for model credibility. *Simulation*, 32(3):103–104, 1979.

N. J. Schouten, M. A. Salman, and N. A. Kheir. Fuzzy logic control for parallel hybrid vehicles. *IEEE Transactions on Control Systems Technology*, 10(3):460–468, May 2002. doi: 10.1109/87.998036.

P. Schulten and D. Stapersma. A study of the validity of a complex simulation model. *Journal of Marine Engineering & Technology*, 6(2):67–77, 2007.

A. Sciarretta and L. Guzzella. Control of hybrid electric vehicles. *IEEE Control systems*, 27(2):60–70, 2007.

A. Sciarretta, M. Back, and L. Guzzella. Optimal control of parallel hybrid electric vehicles. *IEEE Transactions on Control Systems Technology*, 12(3):352–363, May 2004. ISSN 1063-6536. doi: 10.1109/TCST.2004.824312.

E. Sciberras, Bashar Z., David A., et al. Electric auxiliary propulsion for improved fuel efficiency and reduced emissions. *Proceedings of the Institution of Mechanical Engineers, Part M: Journal of Engineering for the Maritime Environment*, 229(1):36–44, 2015.

P. C. Sen. *Principles of electric machines and power electronics*. John Wiley & Sons, 2007.

A. Shafiei, A. Momeni, and S. S. Williamson. Battery modeling approaches and management techniques for plug-in hybrid electric vehicles. In *2011 IEEE Vehicle Power and Propulsion Conference*, Sept 2011. doi: 10.1109/VPPC.2011.6043191.

A. M. Shamekhi and A. H. Shamekhi. A new approach in improvement of mean value models for spark ignition engines using neural networks. *Expert Systems with Applications*, 42(12):5192 – 5218, 2015. doi: http://dx.doi.org/10.1016/j.eswa.2015.02.031.

W. Shao et al. Development of a novel forward dynamic programming method for weather routing. *Journal of Marine Science and Technology*, 17(2):239–251, 2012. doi: 10.1007/s00773-011-0152-z.

L. Shaohua, D. Changqing, Y. Fuwu, et al. A rule-based energy management strategy for a new bsg hybrid electric vehicle. In *2012 Third Global Congress on Intelligent Systems*, pages 209–212, Nov 2012. doi: 10.1109/GCIS.2012.63.

C. M. Shepherd. Design of primary and secondary cells i. effect of polarization and resistance on cell characteristics. *Journal of the Electrochemical Society*, 112(3):252–257, 1965a.

C. M. Shepherd. Design of primary and secondary cells ii. an equation describing battery discharge. *Journal of the Electrochemical Society*, 112(7):657–664, 1965b.

K. Shiraishi, S. Minami, K. Kobayashi, et al. Development of a hybrid tugboat propulsion system. *MTZ industrial*, 3(2):36–43, 2013. doi: 10.1007/s40353-013-0097-2.

W. Shuaiyu, H. Kaisheng, J. Zhenhua, and P. Yuanyuan. Parameter optimization of control strategy for parallel hybrid electric vehicle. In *2007 2nd IEEE Conference on Industrial Electronics and Applications*, pages 2010–2012, May 2007. doi: 10.1109/ICIEA.2007.4318762.

E. Silvas, T. Hofman, N. Murgovski, et al. Review of optimization strategies for system-level design in hybrid electric vehicles. *IEEE Transactions on Vehicular Technology*, PP(99):1–1, 2016. ISSN 0018-9545. doi: 10.1109/TVT.2016.2547897.

D. V. Singh and E. Pedersen. A review of waste heat recovery technologies for maritime applications. *Energy Conversion and Management*, 111:315 – 328, 2016. doi: http://dx.doi.org/10.1016/j.enconman.2015.12.073.

G. Sitkei. Beitrag zur theorie des warmeuberganges im motor. *Konstruktion*, 14(2):67, 1962.

G. Y. Sizov, D. M. Ionel, and N. A. O. Demerdash. Modeling and parametric design of permanent-magnet ac machines using computationally efficient finite-element analysis. *IEEE Transactions on Industrial Electronics*, 59(6):2403–2413, June 2012. doi: 10.1109/TIE.2011.2163912.

C. Stanislovaitis. A systematic approach to hybrid electric vehicle modeling. Master's thesis, The Ohio State University, Ohio State, USA, 2015.

D. Stapersma. The importance of (e) mission profiles for naval ships. In *Conference on Cost Effective Maritime Defense*, London, UK, September 1994.

D. Stapersma. *Diesel Engines A: Part I - Performance Analysis and Turbocharging, Volume 2*. Delft University of Technology, Delft, the Netherlands, 8th edition, January 2010.

M. Stopford. *Maritime Economics*. Routledge, London, UK, 3rd edition, December 2008.

C. Sturzebecher, J. Reb, C. Bohn, et al. A diesel engine model including exhaust flap, intake throttle, lp-egr and vgt. part ii: Identification and validation. *IFAC-Papers OnLine*, 48(15):60 – 65, 2015. doi: http://dx.doi.org/10.1016/j.ifacol.2015.10.009.

O. Sundstrom and L. Guzzella. A generic dynamic programming matlab function. In *2009 IEEE Control Applications, (CCA) Intelligent Control, (ISIC)*, pages 1625–1630, July 2009. doi: 10.1109/CCA.2009.5281131.

O. Sundstrom, L. Guzzella, and P. Soltic. Optimal hybridization in two parallel hybrid electric vehicles using dynamic programming. *IFAC Proceedings Volumes*, 41(2):4642–4647, 2008.

O. Sundstrom, D. Ambuhl, and L. Guzzella. On implementation of dynamic programming for optimal control problems with final state constraints. *Oil & Gas Science and Technology*, 65(1):91–102, 2010.

Y. K. Tan, J. C. Mao, and K. J. Tseng. Modelling of battery temperature effect on electrical characteristics of li-ion battery in hybrid electric vehicle. In *Power Electronics and Drive Systems (PEDS), 2011 IEEE Ninth International Conference on*, pages 637–642, Dec 2011. doi: 10.1109/PEDS.2011.6147318.

J. Tang, L. Guo, B. Gao, et al. Energy management of a parallel hybrid electric vehicle with cvt using model predictive control. In *2016 35th Chinese Control Conference (CCC)*, pages 4396–4401, July 2016. doi: 10.1109/ChiCC.2016.7554036.

C.F. Taylor. The internal combustion engine in theory and practice, 1960.

B. H. Thacker, S. W. Doebling, F. M. Hemez, et al. Concepts of model verification and validation. Technical report, Los Alamos National Lab., Los Alamos, NM (US), 2004.

G. Theotokatos. On the cycle mean value modelling of a large two-stroke marine diesel engine. *Proceedings of the Institution of Mechanical Engineers, Part M: Journal of engineering for the maritime environment*, 224 (3):193–205, 2010.

F. Tianheng, Y. Lin, G. Qing, H. Yanqing, Y. Ting, and Y. Bin. A supervisory control strategy for plug-in hybrid electric vehicles based on energy demand prediction and route preview. *IEEE Transactions on Vehicular Technology*, 64(5):1691–1700, May 2015.

J. P. Trovao, P. G. Pereirinha, H. M. Jorge, et al. A multi-level energy management system for multi-source electric vehicles – an integrated rule-based meta-heuristic approach. *Applied Energy*, 105:304 – 318, 2013. doi: http://dx.doi.org/10.1016/j.apenergy.2012.12.081.

A. M. Trzynadlowski. *Control of induction motors*. Academic press, 2000.

California University of Berkeley. Fortran programs for the simulation of electrochemical systems. http://www.cchem.berkeley.edu/jsngrp/fortran.html.

A. Veltman, D. Pulle, and R. De Doncker. *Fundamentals of electrical drives*. Springer, 2007.

R. Vettor and C. G. Soares. Development of a ship weather routing system. *Ocean Engineering*, 123:1 – 14, 2016. doi: http://dx.doi.org/10.1016/j.oceaneng.2016.06.035.

I. Vlaskos, D. Gagliardi, et al. Analysis and evaluation of innovative hybrid powertrain architectures combining gas engines and electric propulsion for tugboats. In *CIMAC Congress, Shanghai*, 2013.

A. Vrijdag. Estimation of uncertainty in ship performance predictions. *Journal of Marine Engineering & Technology*, 13(3):45–55, 2014.

A. Vrijdag, D. Stapersma, and T. Van Terwisga. Systematic modelling, verification, calibration and validation of a ship propulsion simulation model. *Journal of Marine Engineering & Technology*, 8(3):3–20, 2009.

T. L. Vu. Power management for electric tugboats through operating load estimation. *IEEE Transactions on Control Systems Technology*, 23(6):2375–2382, 2015.

T. L. Vu et al. Optimal power management for electric tugboats with unknown load demand. In *2014 American Control Conference*, pages 1578–1583, Oregon, USA, June 2014. IEEE.

Y. Wang, R. Chen, Tao Chen, et al. Emerging non-lithium ion batteries. *Energy Storage Materials*, 4:103 – 129, 2016. doi: http://dx.doi.org/10.1016/j.ensm.2016.04.001.

Z. Wang, B. Huang, Y. Xu, et al. Optimization of series hybrid electric vehicle operational parameters by simulated annealing algorithm. In *2007 IEEE International Conference on Control and Automation*, pages 1536–1541, May 2007a. doi: 10.1109/ICCA.2007.4376618.

Z. Wang, W. Li, and Y. Xu. A novel power control strategy of series hybrid electric vehicle. In *2007 IEEE/RSJ International Conference on Intelligent Robots and Systems*, pages 96–102, Oct 2007b. doi: 10.1109/IROS.2007.4399024.

Z. Wei, Z. Xu, and D. Halim. Study of {HEV} power management control strategy based on driving pattern recognition. *Energy Procedia*, 88:847 – 853, 2016. ISSN 1876-6102. doi: http://doi.org/10.1016/j.egypro.2016.06.062. URL http://www.sciencedirect.com/science/article/pii/S1876610216301266. {CUE} 2015 - Applied Energy Symposium and Summit 2015: Low carbon cities and urban energy systems.

M. Wen, S. Ropke, H.L. Petersen, R. Larsen, and O.B.G. Madsen. Full-shipload tramp ship routing and scheduling with variable speeds. *Computers & Operations Research*, 70:1 – 8, 2016. ISSN 0305-0548. doi: http://dx.doi.org/10.1016/j.cor.2015.10.002.

T. Wildi et al. *Electrical machines, drives and power systems, 6/E*. Pearson Education India, 2007.

S. G. Wirasingha and A. Emadi. Classification and review of control strategies for plug-in hybrid electric vehicles. *IEEE Transactions on Vehicular Technology*, 60(1):111–122, Jan 2011. doi: 10.1109/TVT.2010.2090178.

J. Se. Won and R. Langari. Fuzzy torque distribution control for a parallel hybrid vehicle. *Expert Systems*, 19(1):4–10, 2002.

J.S. Won, R. Langari, and M. Ehsani. An energy management and charge sustaining strategy for a parallel hybrid vehicle with cvt. *IEEE Transactions on Control Systems Technology*, 13(2):313–320, March 2005. ISSN 1063-6536. doi: 10.1109/TCST.2004.838569.

G. Woschni. Beitrag zum problem des warmeuberganges in verbrennungsmotor. Technical Report 4, M.T.Z., April 1965.

H. K. Woud and D. Stapersma. *Design of propulsion and electric power generation systems*. The Institute of Marine Engineering, Science and Technology, London, UK, 2002.

J. Wu, C. H. Zhang, and N.X. Cui. Pso algorithm-based parameter optimization for hev powertrain and its control strategy. *International Journal of Automotive Technology*, 9(1):53–59, 2008.

X. Wu, G. Guo, J. Xu, et al. Application of parallel chaos optimization algorithm for plug-in hybrid electric vehicle design. *International Journal of Bifurcation and Chaos*, 24(01):1450001, 2014.

G. Xie. Optimal preliminary propeller design based on multi-objective optimization approach. *Procedia Engineering*, 16:278–283, 2011. doi: 10.1016/j.proeng.2011.08.1084.

J. Yang and G. G. Zhu. Model predictive control of a power split hybrid powertrain. In *2016 American Control Conference (ACC)*, pages 617–622, July 2016. doi: 10.1109/ACC.2016.7524982.

M. Yilmaz. Limitations/capabilities of electric machine technologies and modeling approaches for electric motor design and analysis in plug-in electric vehicle applications. *Renewable and Sustainable Energy Reviews*, 52:80 – 99, 2015. doi: http://dx.doi.org/10.1016/j.rser.2015.07.033.

L. C. Yuan et al. Equivalent consumption minimization strategy for hybrid all-electric tugboats to optimize fuel savings. In *2016 American Control Conference (ACC)*, pages 6803–6808. IEEE, 2016a.

L. C. W. Yuan, T. Tjahjowidodo, G. S. G. Lee, et al. Equivalent consumption minimization strategy for hybrid all-electric tugboats to optimize fuel savings. In *2016 American Control Conference (ACC)*, pages 6803–6808, July 2016b. doi: 10.1109/ACC.2016.7526743.

L. A. Zadeh. Fuzzy sets. *Information and control*, 8(3):338–353, 1965.

B. Zahedi and L. E. Norum. Efficiency analysis of shipboard dc power systems. In *Industrial Electronics Society, IECON 2013-39th Annual Conference of the IEEE*, pages 689–694. IEEE, 2013.

B. Zahedi, L. E. Norum, and K. B. Ludvigsen. Optimized efficiency of all-electric ships by dc hybrid power systems. *Journal of power sources*, 255:341–354, 2014.

S. H. Zak. Systems and control. 2003.

F. Zhang, J. Xi, and R. Langari. An adaptive equivalent consumption minimization strategy for parallel hybrid electric vehicle based on fuzzy pi. In *2016 IEEE Intelligent Vehicles Symposium (IV)*, pages 460–465, June 2016. doi: 10.1109/IVS.2016.7535426.

L. Zhang, C. Lin, and X. Niu. Optimization of control strategy for plug-in hybrid electric vehicle based on differential evolution algorithm. In *2009 Asia-Pacific Power and Energy Engineering Conference*, pages 1–5, March 2009a. doi: 10.1109/APPEEC.2009.4918574.

L. Zhang, C. Lin, and X. Niu. Optimization of control strategy for plug-in hybrid electric vehicle based on differential evolution algorithm. In *2009 Asia-Pacific Power and Energy Engineering Conference*, pages 1–5. IEEE, 2009b.

P. Zhang, F. Yan, and C. Du. A comprehensive analysis of energy management strategies for hybrid electric vehicles based on bibliometrics. *Renewable and Sustainable Energy Reviews*, 48:88 – 104, 2015. doi: http://dx.doi.org/10.1016/j.rser.2015.03.093.

R. Zhang and Y. Chen. Control of hybrid dynamical systems for electric vehicles. In *American Control Conference, 2001. Proceedings of the 2001*, volume 4, pages 2884–2889. IEEE, 2001.

S. Zhang and R. Xiong. Adaptive energy management of a plug-in hybrid electric vehicle based on driving pattern recognition and dynamic programming. *Applied Energy*, 155:68 – 78, 2015. ISSN 0306-2619. doi: http://doi.org/10.1016/j.apenergy.2015.06.003. URL http://www.sciencedirect.com/science/article/pii/S0306261915007485.